PLEISTOCENE ENVIRONMENTAL CHANGE THROUGH LAKE-LEVEL CHANGE: SEQUENCE STRATIGRAPHIC MODELLING OF THE KBS MEMBER, KOOBI FORA FORMATION, OMO GROUP

Bukho Charles

Student Number: G19C8395

MASTER OF SCIENCE

(GEOLOGY)

2025

Supervised by:

Dr. Silindokuhle Mavuso

A dissertation submitted to the Faculty of Science, Rhodes University, in partial fulfilment of the requirements for the Degree of Master of Science (MSc) in Geology.

Department of Geology

Rhodes University

P.O. Box 94, Makhanda, South Africa, 6140

DECLARATION

I, Bukho Charles, hereby declare that this thesis is my own work, unaided work, unless otherwise noted in the text. It is being submitted for a Master of Science (MSc) degree in Geology at Rhodes University, Makhanda (Grahamstown), South Africa. This work has not been submitted to any other university.

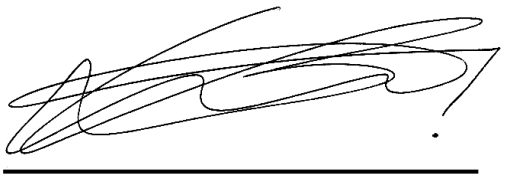

(Signature of candidate)

Bukho Charles

On the 14th of February 2025 in Makhanda (Grahamstown), Eastern Cape, South Africa

ABSTRACT

The Turkana Basin, Omo Group, in northern Kenya, has been a region of numerous palaeontological, archaeological, and geological investigations in eastern Africa due to its recognised prehistoric repository of biotic evolution, cultural history, and rift valley geology. These significant records are archived by the Plio-Pleistocene volcaniclastic deposits of the Koobi Fora Formation, which includes one of the eight consequential stratigraphy intervals, the Kay Behrensmeyer Site (KBS) Member time-interval deposits. Numerous palaeontological, archaeological, and geological research have been conducted in these deposits; however, there have been limited investigations in understanding source areas, punctuation, and influence of the palaeoenvironmental change in relation to noted lake level fluctuations and how they drove biotic evolution (including hominin adaptation). This study investigates the palaeoenvironmental dynamics of the KBS Member that have shaped its observed stratigraphic succession. This geological study provides comprehensive basin analysis, grounded in extensive fieldwork, through depositional lithofacies and palaeoenvironmental distribution across the KBS Member in space, offering a more detailed palaeogeographical interpretation. The research identifies extensive palaeoenvironmental heterogeneity across the formation's three subregions, with a significant predominance of meandering fluvial channel patterns defined by distributive fluvial systems. Additionally, the sandstones are derived from two primary source rocks: The basement Precambrian Ethiopian outcrops east of the basin; The Kenyan Cenozoic volcano-sedimentary rocks extending north of the basin. Furthermore, with the adoption of sequence stratigraphic modelling, two parasequences that reflect two low-frequency transgressive-regressive cycles are established; this revealed that the origins of these fluctuations primarily originate from climatic-related factors with some tectonic- and volcanic-related forcings. This suggests that ancient Lake Turkana (Paleolake Lorenyang, 2–1.6 Ma) expanded asynchronously in the rift, resulting in variable depositional slopes in times of flooding. The study integrates sedimentary facies analysis and provenance studies to provide a better understanding of the depositional history and stratigraphic controls in the basin. This study contributes to existing work on the region, offering understanding of biotic evolution and the adaptive strategies of organisms (including hominins) in response to changing environmental conditions during the Pleistocene epoch.

ACKNOWLEDGEMENTS

This thesis is a conclusive work of a Master of Science (MSc) in Geology at Rhodes University (Geology Department). Submitting a thesis of this nature would not have been possible without numerous individuals and organisations' wholehearted support, guidance, and encouragement. For this reason, I cannot go any further without expressing my sincere appreciation to my supervisor, Dr. Silindokuhle Mavuso, for his support and guidance throughout my entire MSc duration, from training and mentoring to offering academic resources, giving me good scientific writing tips, and organising field trips; it is highly regarded and appreciated. Your perseverance and trust in me have been invaluable. Lastly, you introduced me to the field of research and allowed me to finish both my Bachelor of Science Honours (BSc Hons) thesis and my MSc degree. I cannot thank you enough; I could not have done this without you.

My gratitude extends to the Rhodes University (RU) Geology Department, Professor Stephen A. Prevec (HoD) and staff, who have inspired and motivated me throughout my time at RU, providing me with opportunities and facilities to complete this research; I have had excellent years being with you all. Specifically, I would like to thank our secretary, Nkanyi Maqanda, for her support and assistance with all financial administration related to my MSc, as well as our principal technical officer, Pelele Lehloenya, for helping in the department. My thanks are also extending to everyone in the Geography Department for allowing me to use their Geographic Information Systems (GIS) and remote sensing laboratory. Additionally, Dr. Sinenhlanhla Memela and Philippa Irvine from the Geography Department (Rhodes University) deserve special mention for their support, which provided invaluable mentorship through inspirational discussions and a willingness to help.

Funding was also a crucial component of this project's success. Therefore, I am very grateful to Environmental Resources Management (ERM), Turkana Basin Institute (TBI), and Palaeontological Scientific Trust (PAST Africa) for their financial support and for bringing my project to completion—also, a special thanks to National Museums of Kenya (NMK) for inviting me as an affiliate.

A heartfelt thank you to Kathryn Ranhorn from Arizona State University (AUS) for organising the Turkana Basin field trips and her field teaching in human evolution. I

would also like to thank Molatelo Chokoe (BSc Hons) for your immense assistance and support during field and laboratory work, together with Emmanuel Galo Khalibwa and Christine Adhiambo from NMK during fieldwork. My sincerest gratitude also goes to the TBI staff and drivers, and special thanks go to Apolo Longaye and Richard Loki Salle as TBI field assistants in the first and second field seasons, respectively.

To Sithabile Sigwebela, Siyasanga Dyan, Akimu Adam Rajab, Sinazo Makasi, Siphiwo Gumbi, and Kabelo Sopeletsile, thanks for your unwavering support and being a constant source of strength, either being your professional and emotional support, and the continual reminder that I need to stop "over-thinking"; Hi Sithabile. Thank you for your ongoing support and understanding. This also applies to friends and everyone I know at RU.

Most importantly, I would like to express my sincere gratitude to God for His grace in caring for me throughout this journey. I also want to acknowledge and thank myself for staying dedicated and overcoming challenges to achieve this objective.

Last but far from least, I want to express my profound gratitude to my family. To my parents, Thembinkosi and Phumla Pamela Charles, you are my source of energy, motivation, direction, and affirmation. Thank you for being there for me and supporting my career decisions; this is all for you. Without a doubt, you are the best parents in the world. I hope I am making both of you proud. To my siblings, Vuyolwethu, Inathi, and Ayabulela, as well as my niece and nephew, Singalakha and Mihlali, I have learned from you. Thank you for your patience and support; you are all always appreciated. To all of you, I cannot thank you enough; also, I could not have done this without you. I am who I am because of your efforts and sacrifices.

To my niece, Singalakha Charles, I dedicate this work to you.

Uyabulela kakhulu uNdlovu!

Thank you all.

CONTENTS

LIST OF FIGURES

Figure 6: *Terminology of sedimentary rocks based on percentages of sand, mud, and gravel ratio (Folk, 1954).*

Figure 7: ***(A)*** *Terminology of degree of rounding of detrital grains (Powers, 1953).* ***(B)*** *Classification regarding the degree of sorting (Compton, 1962).*

Figure 8: *Comparison chart for porosity estimations in percentages (Terry and Chilingar, 1955).*

Figure 9*: Composite stratigraphic section of the KBS Member as an illustration demonstrating the origin and internal organisation of a lacustrine continental rift depositional sequence generated during lake-level fluctuations. A high-resolution version of this figure is found in the Appendices section (Appendix F).*

Figure 10: *Representative lithofacies found in the KBS Member of the Koobi Fora Formation.* ***(A)*** *Interlaminated silt and clay (Fl).* ***(B)*** *Massive mud (Fm) with gastropod fossil hash assemblages and collapsed Fl-lithofacies on the surface.* ***(C)*** *Gradational depositional contact between the Fl-lithofacies and the underlying Fm-lithofacies. Photographs A, B, and C were taken and measured at Area 102 in the Base Camp subregion.* ***(D)*** *Horizontally bedded sandstone (Sh) overlying KBS Tuff. The photograph was taken and measured at Area 105 in the Karari subregion.* ***(E)*** *Horizontally bedded sandstone (Sh) overlying reworked KBS Tuff in an erosional depositional contact, with an assemblage of ripple cross-laminated sandstone. The photograph was taken and measured at Area 104 in the Base Camp subregion.* ***(F)*** *Trough cross-bedded sandstone (St). The photograph was taken and measured at Area 9 in the Ileret subregion.* ***(G)*** *St-lithofacies interbedded between Fm-lithofacies in erosional depositional contacts with silt or clay with pedogenic structures (Pv) as minor facies on the overlying bed. The photograph was taken and measured at Area 12 in the Ileret subregion.* ***(H)*** *Ripple cross-laminated sandstone (Sr). The photograph was taken and measured at Area 13 in the Ileret subregion.* ***(I)*** *Sr-lithofacies overlying Pv-facies in an erosional depositional contact. The photograph was taken and measured at Area 10 in the Ileret subregion.* ***(J)*** *Planar cross-bedded sandstone (Sp). The photograph was taken and measured at Area 6A in the Ileret subregion.* ***(K)*** *Sp-lithofacies alongside other sandstone facies (Sr and Sh), consisting of rhizoliths and bioturbation (burrowing). The photograph was taken and measured at Area 10 in the*

Ileret subregion. ***(L)*** *Various lithofacies (Sp, Sr, Pv, Bm) in close association overlying a reworked KBS Tuff. The photograph was taken and measured at Area 13 in the Ileret subregion.* ***(M)*** *Matrix-supported stratified gravel (Gms) overlying Pv-lithofacies that overlie reworked KBS Tuff, all in erosional depositional contacts.* ***(N)*** *Planar-cross bedded gravel (Gp) overlying the pedogenic carbonate lithofacies (Pcc) in an erosional depositional contact. Photographs M and N were taken and measured at Area 8A in the Ileret subregion.* ***(O)*** *Pcc-lithofacies with calcareous nodules underlying Sh-lithofacies. The photograph was taken and measured at Area 105 in the Karari subregion.* ***(P)*** *Molluscan carbonate – siliceous bioclastic carbonate (Bm) dominated by bivalve shells, alongside Pcc-lithofacies.* ***(Q)*** *Exposure of the Bm-lithofacies dominated by gastropod shells, alongside Pcc-lithofacies. Photographs P and Q were taken and measured at Area 10 in the Ileret subregion. This figure corresponds with Table 3 above.*

Figure 11: *Example of the KBS meandering fluvial lithofacies association (FA1) from the study locality. The FA1 exposure is defined by lateral accretion with erosive base and upward fining sequence and FA2 underlying an erosional contact of FA1. Scale: 178 cm.*

Figure 12: *FA2 pedogenic carbonates in a mudstone (Fm) underlying an erosional contact with FA1 that is defined by Sh, Gp and Gms.*

Figure 13: ***(A)*** *Example of the marginal lacustrine lithofacies association (FA3) from study locality. The FA3 is defined by sedimentary sequences that are heterolithic with the exception of well-packed bioclastic sandstones and are distinguished by a heterogeneous assortment of lithofacies.* ***(B)*** *The white circle represents a scale of 172cm.*

Figure 14: *FA3 outcrop defined by Fm, Pcc, Pv* as locally prevalent surface lags and as carbonate nodule inclusions *and some bioclastic units (Bm) protruding.*

Figure 15: *Example of the prodeltaic and delta front lithofacies association (FA4) from study locality. The FA4 is defined by fine-grained clastics that are frequently planar laminated (Fl) with weakly developed asymmetrical and wavy lamination in coarser upward-fining units, poorly developed fine sandy sequences (St, Sr) with*

carbonate grains that are always thin and invariably planar laminated, and sand-silt sequences interbeds that are capped by sands and silts that have been bioturbated or massive fine-grained sequences (Fm) with carbonate concretions and desiccation cracks. Scale: 193 cm.

Figure 16: ***(A)*** *Example of the crevasse splay lithofacies association (FA5) from study locality. The FA5 is defined by thin rippling sand sections (Sr) that are coarsening upwards, representing by soft sediment deformation erosive contact, with laminated silts (Fl) and clays that display poorly developed pedogenic overprints (Pv). Geologic hammer (red circle) as scale.* ***(B)*** *A closeup of Figure 16A.*

Figure 17: *Spatially correlated (measured) KBS Member stratigraphic sections. See locations in Figure 1B. Lithologies and sedimentary structures allowed the interpretation of five depositional environments. A high-resolution version of this figure is found in the Appendices section (Appendix H).*

Figure 18: *Examples of KBS Member palaeocurrent indicators observed in the field that were used as vector measurements for palaeocurrent analysis.* ***(A)*** *Planar cross-bedded sandstone deposits.* ***(B)*** *Ripple cross-laminated sandstone deposits, displaying rib-and-furrow structures. Red arrow shows palaeocurret direction.*

Figure 19: *Rose diagrams showing palaeocurrent directions of the KBS Member palaeo-fluvial systems that were measured in the field. This includes vector mean azimuths and statistical data of the KBS Member deposits within the KFF sub-regions (Ileret, Karari and Base Camp). See Appendix C for comprehensive raw palaeocurrent data.*

Figure 20: *Map showing mean palaeocurrent vector directions demonstrated by the KFF KBS Member deposits.*

Figure 21: *Photomicrographs showing quartz as primary framework grain mineralogy in the KBS Member sandstones, indicated by arrows; yellow arrows indicate monocrystalline quartz (Qm), whereas the red arrows indicate polycrystalline quartz (Qp).* ***(A)*** *XPL and* ***(B)*** *PPL.*

Figure 22: *XPL photomicrographs showing feldspar as primary framework grain mineralogy in the KBS Member sandstones.* ***(A)*** *Plagioclase feldspar (P; albite).* ***(B)*** *Potassium feldspar (K; microcline).* ***(C)*** *The yellow arrows indicate plagioclase feldspar, whereas the red arrows indicate potassium feldspar in the total rock components.*

Figure 23: *Photomicrographs showing primary framework grain mineralogy of volcanic lithic fragments* ***(A)*** *and* ***(B)****, and sedimentary lithics* ***(C)*** *and* ***(D)****. Photomicrographs* ***(A)*** *and (****C)*** *are XPL, and photomicrographs* ***(B)*** *and* ***(D)*** *are PPL, respectively.*

Figure 24: *Photomicrographs showing accessory minerals as primary framework grain mineralogy in the KBS Member sandstones; tabular biotite, chlorite, amphibole, and opaque minerals (hematite).* ***(A)*** *XPL and* ***(B)*** *PPL.*

Figure 25: *XPL photomicrographs showing the primarily calcite cement and grain-contact types in the KBS Member sandstones; long contacts (1), concavo-convex closely packed (2), tangential (3), and sutured contacts (4).*

Figure 26: *Ternary diagram (after Garzanti, 2019) for rock classification of the twenty-nine KBS Member sandstones used in this study, together with relevant petrographic parameters. This figure corresponds with Table 6 below.*

Figure 27: *Spatially correlated (measured) KBS Member stratigraphic sections with QFL mineralogical proportions plotted in positions of sample collection. See Appendix F for high resolution. A high-resolution version of this figure is found in the Appendices section (Appendix I).*

Figure 28: *Thin section photomicrographs showing the Iler et subregion sandstones, represented under XPL (Left) and PPL (Right). Photomicrographs* ***(A)*** *and* ***(B)*** *represent immature sandstones, and photomicrographs* ***(C)*** *and (****D)*** *represent submature sandstones. Photomicrograph* ***(E)****and* ***(F)*** *represent biogenic materials as lithic fragment components; molluscan shell fragments, identified as cross sections.*

Figure 29: *Thin section photomicrographs showing the Karari subregion sandstone, representing submature sandstone. Under XPL (Left) and PPL (Right).*

Figure 35: ***(A)*** *Overview diagram illustrating the timing of global eccentricity cycles (eccentricity), shaded in red, in association with the KBS Member time interval (1.87–1.6 Ma), shaded in blue, as well as pelagic lakes and tectonic episodes in the Omo-Turkana Basin. Acquired and modified after Gathogo (2017).* ***(B)*** *KBS Member time interval (1.87–1.60 Ma) climate proxy records based on marine deposits from the Mediterranean Sea in association with the eccentricity cycles in Figure 35A. the estimated palaeolake level fluctuation periods are indicated. Acquired and modified after Gathogo (2017). This figure is in accordance with the produced lake level model presented in Figure 34.*

Figure 36: *KBS Member sandstone QFL ternary diagram coinciding with that of Garzanti (2016) on East African Rift modern sediments in relation to climate-related weathering, denoting that the East African Rift Basins experience intermediate to tropical dry seasons. Acquired and modified after Garzanti (2016).*

LIST OF TABLES

CHAPTER 1: INTRODUCTION

The East African Rift System (EARS) is renowned for its dynamic geological history, associated with various ecological transitions in a continental rift basin setting (Feibel, 2011). This history is well-documented in the Turkana Basin, located between the Ethiopian and East-Africa (Kenyan) Domes, extending from south-western Ethiopia to north-western Kenya (Baker *et al.*, 1972; Fitch *et al.*, 1976; Burggraf & Vondra, 1982; Feibel, 2011) (Figures 1 and 2). It is defined as a Cenozoic volcano-sedimentary basin that is hydrologically confined and occupied by a saline-alkaline lake, Lake Turkana. The Turkana Basin has been a region of numerous palaeontological, archaeological, and geological studies due to its recognised preservation of biotic evolution, cultural history, and rift valley geology records, mostly from its Plio-Pleistocene sedimentary deposits (Ebinger *et al.*, 2000; Quinn *et al.*, 2007; Lepre, 2009; Mathisen & Vondra, 1983; Feibel, 2011).

These deposits have been acclaimed as sources of significant vertebrate fossils and archaeological site discoveries, with chronologic and palaeogeographic dispersal patterns that serve as complex contributions to understanding the hominin evolution in eastern Africa (Arambourg & Wolff, 1969; White *et al.*, 1981; Vrba *et al.*, 1995; Wood, 1996; Wood & Strait, 2004; Wood, 2009; Wood & Baker, 2011; Wood & Leakey, 2011). The discoveries include fossils such as *Homo ergaster* (Groves & Mazak, 1975), *Homo rudolfensis* (Alexeev, 1986), *Australopithecus anamensis* (Leakey *et al.*, 1995), *Kenyanthropus platyops* (Leakey *et al.*, 2001), some non-hominin taxonomically distinctive fossils (*e.g.* cercopithecoids, bovids, rhinocerotids, equids, giraffids, suids, and snakes) (Harrison & Harris, 1996; Bobe & Leakey, 2009; Bobe *et al.*, 2011; Hakala, 2012; Rannikko *et al.*, 2017; Hammond *et al.*, 2021), as well as numerous stone artefacts (tools), including the oldest examples of Acheulean and Lomekwian stone tool technologies (Isaac *et al.*, 1971; Harris, 1972; Roche *et al.*, 1999; Delagnes & Roche, 2005; Braun *et al.*, 2010; Lepre *et al.*, 2011; Harmand *et al.*, 2015).

In addition, the Turkana Basin Plio-Pleistocene sedimentary deposits also act as significant stratigraphic markers for climate, environmental and faunal changes, with

temperature declines, grassland expansions, and aridification on regional and global scales, influencing Turkana Region palaeoenvironments (Cerling *et al.*, 1988; Bobe & Behrensmeyer, 2004; Bobe, 2006; Quinn *et al.*, 2007; Lepre, 2009, 2014; Halaka, 2012; Nutz *et al.*, 2020; Crete, 2021; Quinn *et al.*, 2021; Yost, *et al.*, 2021; Lepre & Quinn, 2022). However, there are considerable uncertainties regarding the onset, timing, and duration of these palaeoenvironmental changes (Behrensmeyer *et al.*,1997; Lepre, 2014). Numerous hypotheses have been proposed to reflect equally considerable disagreements regarding how global climate change influenced the evolution of palaeoenvironments and hominins in eastern Africa (Lepre, 2014). These hypotheses encompass the early stages and intensification of the Northern Hemisphere glaciation, orbital shifts, the ending of Indonesian and Central American seaways, and cyclical orbital shifts (Milankovitch cycles) (Quinn *et al.*, 2007). Nevertheless, depending on the topography, size, tectonic and depositional regime, and water supply of basins, different environments within basins respond to climate change with various sensitivities and thresholds (Withjack *et al.*, 2002; Quinn *et al.*, 2007).

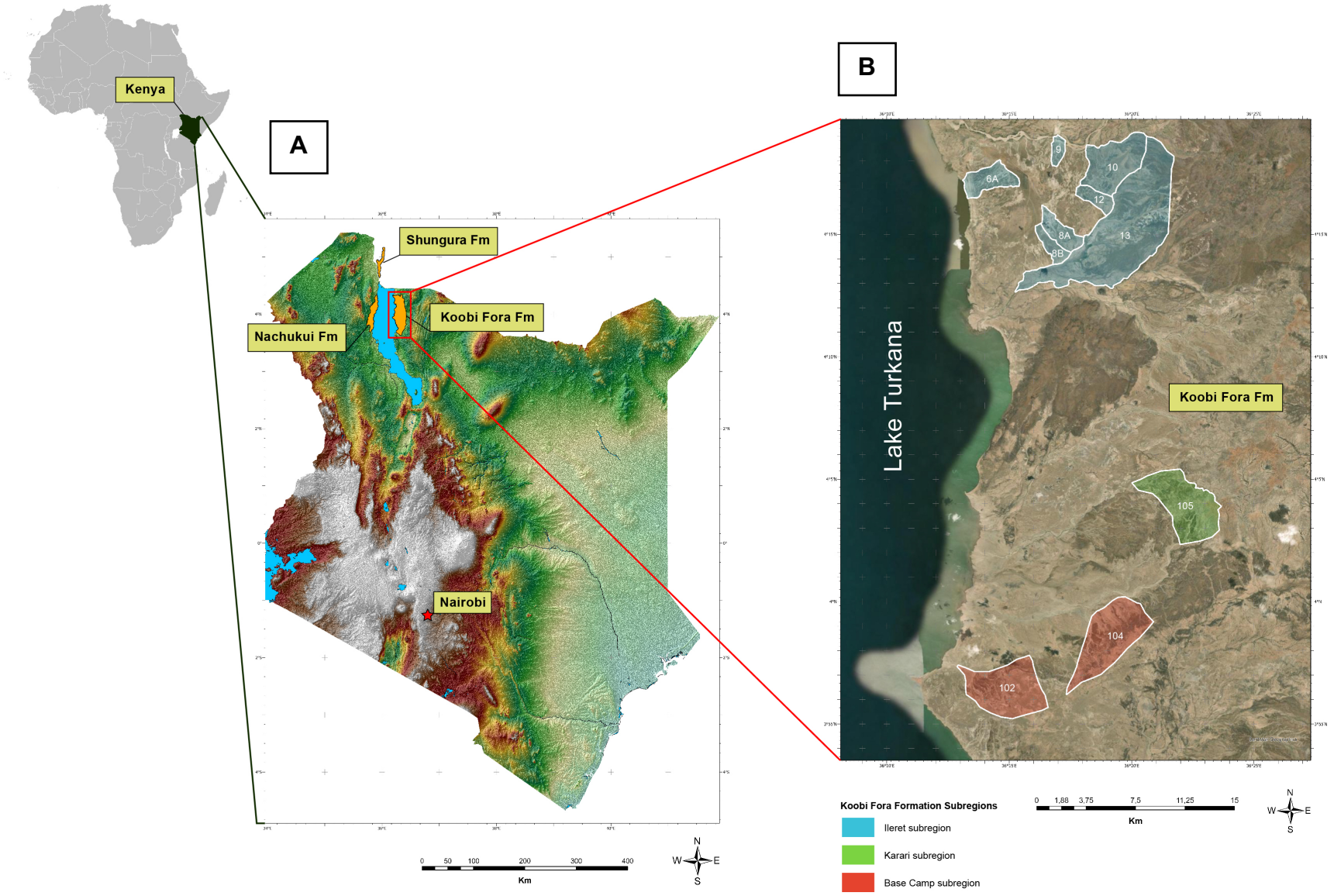

Figure 1: ***(A)*** *Digital elevation model (DEM) map showing the East African Turkana Basin, Kenya, with the Koobi Fora (Red Box), Nachukui and Shungura Formations. The DEM data was acquired from the World Resources Institute.* ***(B)*** *Satellite image of the Koobi Fora Region (formation) with Lake Turkana in the western end of the image, showing the formations' subregions and collection areas (represented by white numerals) from which the KBS Member sandstone and supplemented datasets were derived: Ileret (Blue), Karari (Green) and Base Camp (Red) subregions. A high-resolution version of this figure is found in the Appendices section (Appendix A).*

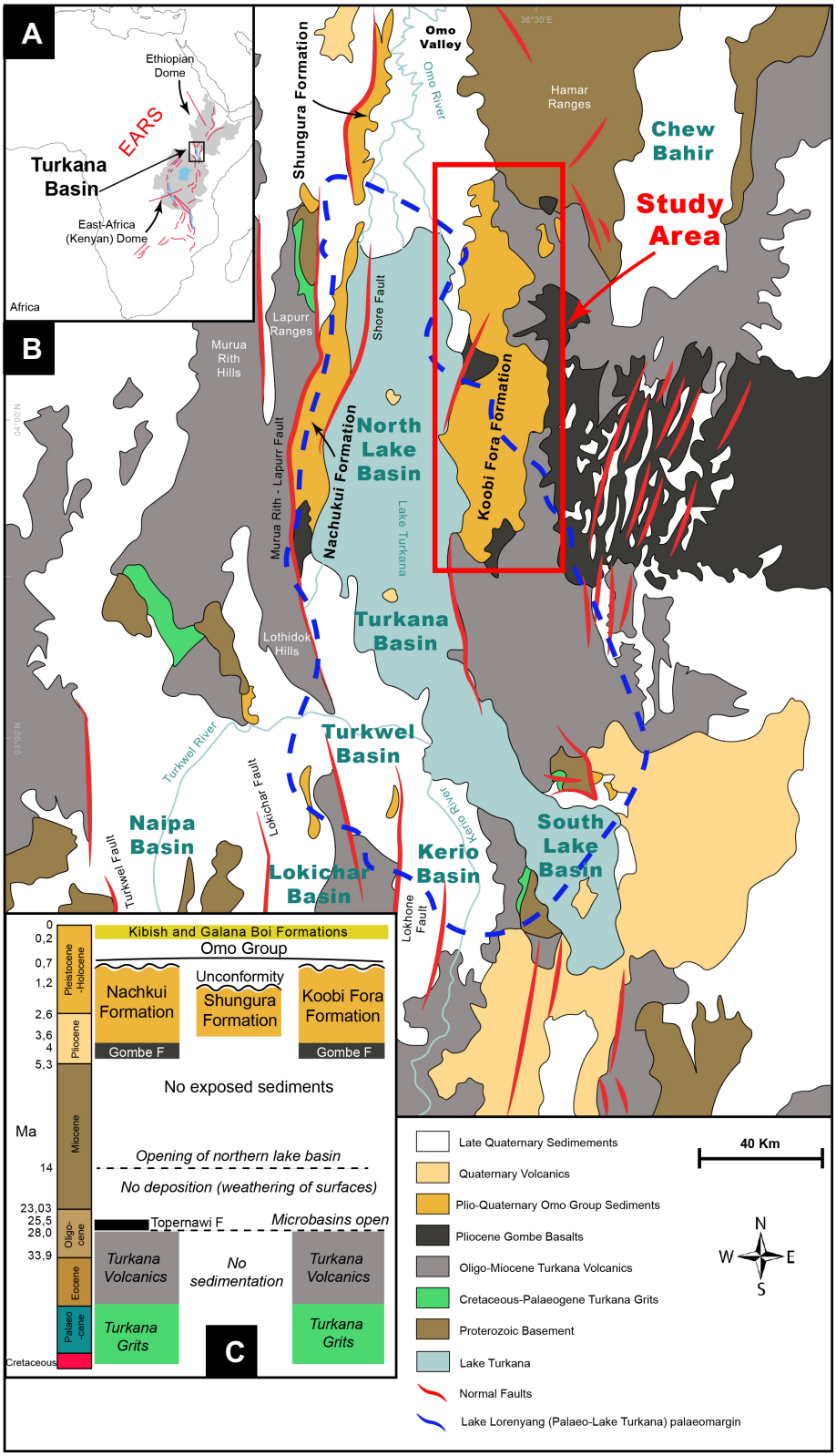

Figure 2: *Map showing the geological setting of the Turkana Basin.* ***(A)*** *Position of the Turkana Basin within the East African Rift System (EARS), between the Ethiopian and Kenyan domal uplifts.* ***(B)*** *Geological map of the Turkana Basin compiled from Ragon et al. (2019), Nutz et al. (2020), and Renault and Owen (2023). The study area is located east of the Northern Lake Basin (Koobi Fora Formation); shown by a red block, together with the palaeomargin of Lake Lorenyang (2-1.6 Ma) in reference to the present Lake Turkana; shown by the navy-blue dotted lines, after Brown and Feibel (1991).* ***(C)*** *Stratigraphic and geologic chart of the Turkana Basin; after Renault and Owen (2023). A high-resolution version of this figure is found in the Appendices section (Appendix B).*

The need to comprehend the context of the aforementioned Turkana Basin discoveries has led to extensive geologic research in the region, including on the north-eastern shores of Lake Turkana, the Koobi Fora Formation (KFF) (Mathisen & Vondra, 1983; Gathogo, 2017; Lepre, 2010) (Figures 1 and 2). The geologic explorations in KFF were initiated in 1969, providing context for palaeontological and archaeological interpretations of the basin through comprehensive stratigraphic, petrographic and palaeoenvironmental studies (Leakey *et al.,* 1970; Vondra *et al.*, 1971; Bowen & Vondra, 1973; Bowen, 1974; Findlater, 1976; Vondra & Bowen, 1976; 1978; Vondra *et al.*, 1978; Vondra & Burggraf, 1978; Burggraf *et al.*, 1981; White *et al.*, 1981; Brown & Cerling, 1982; Burggraf & Vondra, 1982; Cerling & Brown, 1982). However, these studies lacked adequate data to interpret the primary provenance of these fossiliferous Plio-Pleistocene sediments (Mathisen & Vondra, 1983; Brown & Feibel, 1986).

Amalgamating the KFF valley geology with palaeontological and archaeological records, mammalian fossils discovered in the formation represent periods of profound palaeoenvironmental changes, with distinct ecosystems (rivers, deltas, and lake margins) coexisting as a result of tectonic processes, rift-related volcanism, and climate change (Gathogo & Brown, 2006; Lepre, 2009; Halaka, 2012). These make the north-eastern Turkana Basin recognised as a crucial region for understanding the relationship between palaeoenvironmental changes and human evolution (Maslin & Trauth, 2009; Potts & Faith, 2015). Moreover, the composite stratigraphic section and type sections of the KFF are categorised into eight members, delimited by layers of dateable volcanic ash (Brown & Feibel, 1986) (Figures 3 and 4). Nearly all of the Plio-Pleistocene sedimentary strata in the Koobi Fora Formation can be classified within these members using lithostratigraphic and biostratigraphic attributions, with extensive tuffs serving as bounding marker horizons (Brown & Feibel, 1986). Consequently, a precise chronostratigraphic framework can be applied to position the sedimentary sequence and related faunal records (Cerling & Brown, 1982).

Due to abundant resistant lithologies, delaying erosion, and highly variable exposures, the Kay Behrensmeyer Site (KBS) Member can be studied more comprehensively compared to other members of the formation (Feibel, 1988) (Figures 3 and 4). This study attempts to constrain the sediment provenance of the KBS Member sandstones using framework petrography and paleocurrent analysis to depict the source areas'

palaeohydrological conditions during their deposition, coupled with sedimentary facies analysis and sequence stratigraphic modelling to synthesise the occurrence, timing and influence of palaeoenvironmental changes and palaeogeographic variability across the KFF (KBS Member), with an emphasis in developing a high-resolution palaeoenvironmental reconstruction for the Pleistocene period, and produce a basin analysis model that will serve as an environmental control setting in understanding biotic evolution and hominin adaptation at the onset of this period.

The KBS Member is also interesting as it encompasses a time frame of 1.8–1.7 Ma, which is considered to have experienced increased aridity and grassland expansion in eastern Africa, potentially as a result of climate change on a regional and global scale (Cerling, 1992; Bobe & Behrensmeyer, 2004; Lepre *et al.*, 2007). Moreover, this provenance approach will serve to improve our understanding of the KBS Member depositional history and stratigraphic controls and produce a detailed palaeoenvironmental reconstruction of the landscape and its recognised driving forces in the Koobi Fora Formation palaeogeography of the fossil record.

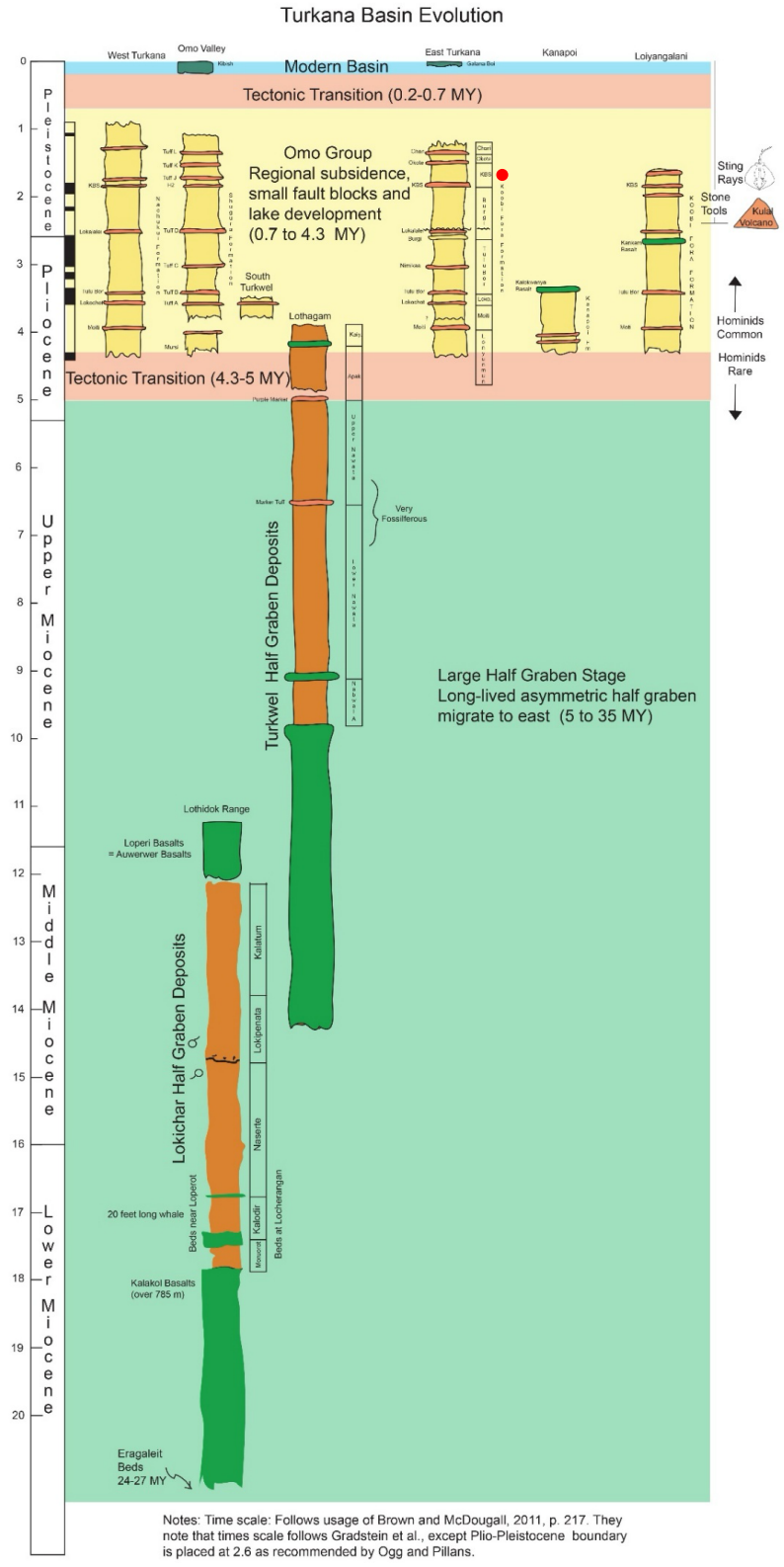

Figure 3*: Stratigraphic chart of the Turkana Basin Evolution. The red circle indicates the stratigraphic position of the KBS Member. Retrieved from: https://www.turkanastratigraphy.org/strat-chart/main-strat-chart.*

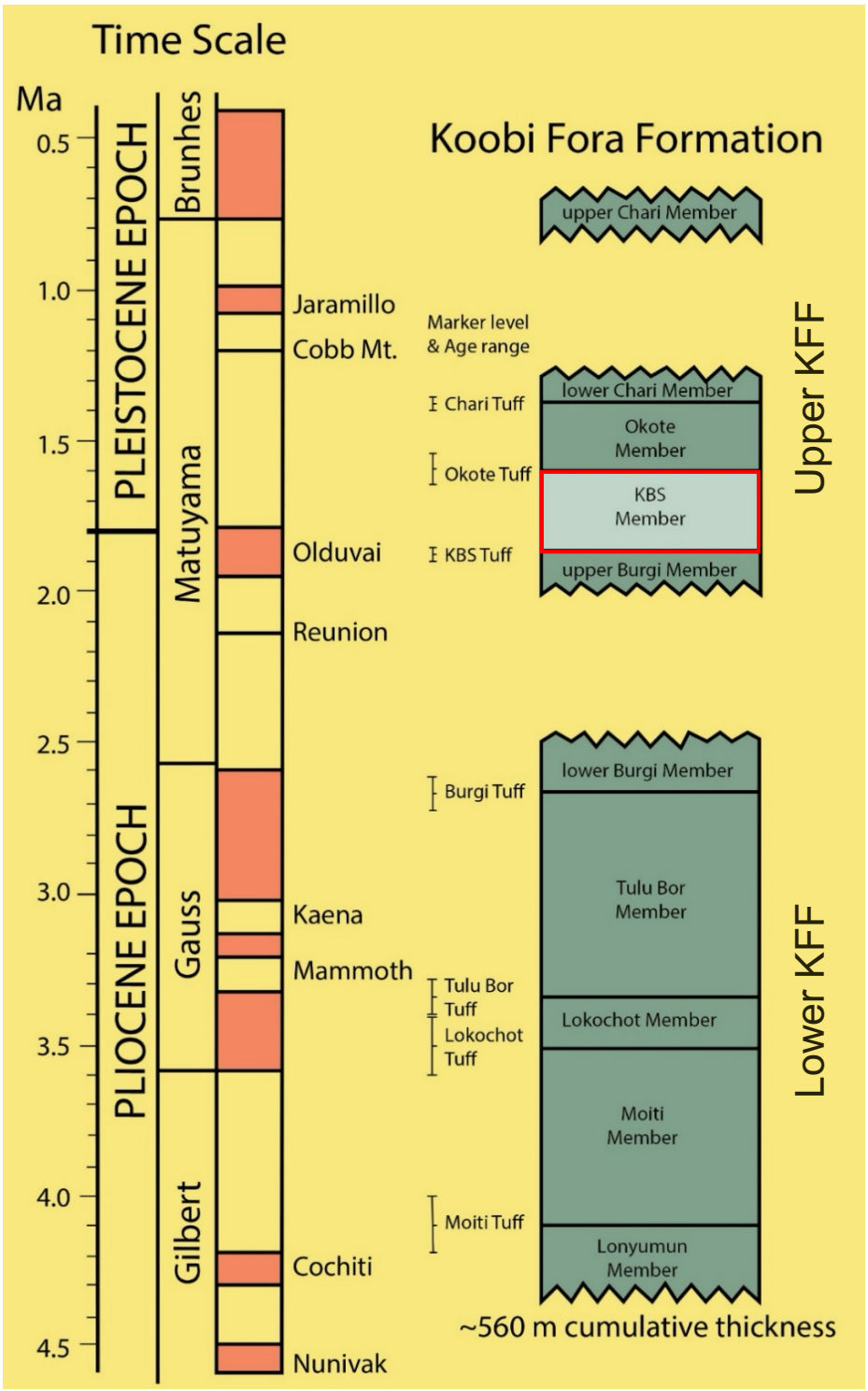

Figure 4: *Diagram showing chronostratigraphic sequence of the Plio-Pleistocene Koobi Fora Formation (KFF) of the Omo Group, and its eight stratigraphic members. The red block indicates the chronostratigraphic position of the KBS Member. Redrawn after Lepre and Kent (2010).*

CHAPTER 2: LITERATURE REVIEW

2.1. Turkana Basin

2.1.1. Physical geography

The Turkana Basin is a low-lying geographic and hydrographic depression region situated in the eastern zone of the East African Rift System (EARS), spanning about 131,000 km^2 from northwestern Kenya to southwestern Ethiopia (Ebinger *et al.,* 2000; Lepre, 2009; Feibel, 2011) (Figure 1). The basin is currently hydrologically confined and occupied by the saline-alkaline Lake Turkana, formerly known as Lake Rudolf, which receives most of its water from the perennial Omo River, draining from the Ethiopian Highlands to the north and the Tuckwell-Kerio drainage region, southwest of the basin (Yuretich, 1979; Feibel, 1988; Quinn, 2007; Levin, 2008; Lepre, 2009; Dondeyne *et al.*, 2024) (Figure 2). The lake is characterised as a systematically closed water system with a basin drainage elevation that ranges from approximately 365 m to 4,000 m at lake level, and a lake surface that encompasses coverage of about 7,000 km^2 with a catchment area of approximately 143,000 km^2 (Gathogo, 2017; Dondeyne *et al.*, 2024). However, according to lake level fluctuation and zoogeography data, the basin was once connected to the White Nile River, and its water outlet was on its north-western end (Kolding, 1992). Overall, Lake Turkana is acknowledged as the world's largest alkaline lake, permanent desert lake and Africa's third-largest lake (Dondeyne *et al.*, 2024; Halaka, 2012).

The Turkana Basin is geographically defined by varying intra-seasonal variations; where the northern region (Ethiopian Highlands) is characterised by a tropical climate with summer rains and deciduous forests, the central region (Kenya) is characterised by transitional semi-arid climate and savanna vegetation, and the southern region (Kenya) is characterised by very arid climate and semi-desert vegetation (Walter, 1970; Fernández & Vrba, 2006; Pratt *et al.*, 1966). These intra-seasonal variations are attributed to rainfall and temperature abnormalities as functions of the Intertropical Convergence Zone (ITCZ) biannual equatorial passages (Fazzini *et al.*, 2015); however, when it comes to Africa's equatorial areas; there are uncertainties

(Nicholson, 2017). Nevertheless, mesoscale convective systems are well-documented as primary functions of intra-seasonal variations, moving westward and passing through different equatorial latitudes, or are attributed to vertical cells over the Indian Ocean and Madden-Julian oscillations (Nicholson, 2018).

2.1.2. Geological Setting

The Turkana Basin is situated between the Kenyan and Ethiopian domal uplifts in the eastern zone of the EARS, namely the Kenya Rift/Gregory Rift to the south and the Main Ethiopian Rift to the north, respectively (Ebinger & Ibrahim, 1994; Mechie *et al.*, 1997; Ebinger *et al.*, 2000; Rooney *et al.*, 2022) (Figure 2). Its initiation emerged during the early Cenozoic as apparent through crustal extension and drift-related volcanism (Ebinger *et al.*, 2000), making the basin a tectonic anomaly region that is characterised by extensional tectonic systems (rifting and magmatism) that have taken place for more than 30 Ma, and playing a principal role in forming the region's various topographies and affecting its hydrology and ecosystems (Baker & Wohlenberg, 1971; Cerling & Powers, 1977; Morley *et al.*, 1992, 1999; Haileab *et al.*, 2004; Furman *et al.*, 2004, 2006; Rooney, 2017; Nutz *et al.*, 2022 Beck *et al.*, 2024).

The basin is divided into three sub-basins based on morphological and structural characteristics, namely the Northern, Centre (Turkwel), and Southern sub-basins (Ragon *et al.*, 2019). This division is characterised by a host of N/S normal faulting systems (50–150 km) (and NE/SW transfer faulting) within the Cenozoic EARS, encompassing approximately 3,500 km from Mozambique to the Afar Triple Junction (Rooney *et al.*, 2022; Kidney, 2012). The basin is further characterised by a complex of north-south oriented half-graben structural entities with a flexural margin to the east and a faulted (normal) escarpment margin to the west (Frostick & Reid, 1990), from the middle-upper Eocene to the present, namely the Turkana, Kibish, Usno and Omo Rift systems (Feibel, 1988; Morley *et al.*, 1999) (Figure 2). These structural entities are hypothesised to have resulted from crustal thinning approximately 5 Ma (Feibel, 1988; Morley *et al.*, 1999). The Northern sub-basin coincides with a single N/S oriented half-graben, unit approximately 80 km wide and 4 km deep, referred to as the North Lake Basin (Dunkelman *et al.*, 1989; Morley *et al.*, 1992; Olago & Odada, 2000; Nicholson,

2016). This half-graben unit resulted from the EARS second pulse extension, approximately 14 Ma (Nutz *et al.*, 2020). In contrast, the Turkwel and South Sub-Basins coincide with a series of juxtaposed N/S half-graben units that are approximately 200 km wide, namely, Naipa, Lokichar, Turkwel, Kerio, and South Lake Basins (Dunkelman *et al.*, 1989; Buck, 1991; Morley *et al.*, 1992; Olago & Odada, 2000). The Naipa and Lokichar Basins began approximately 15–40 Ma during the Cenozoic EARS-related extension, followed by Turkwell and Kerio Basins, which opened during the early Miocene (23–15 Ma) due to surface rupture, and lastly, the South Lake Basin, which began earlier than 10 Ma (V'etel & Le Gall, 2006).

In the framework of rifting and magmatism, the basin indicates the earliest rifting event to its northwest section, representing Eocene volcanism (McDougall & Brown, 2008; Nutz *et al.*, 2022). The rifting extended northwest to the Ethiopian Rift system during the early Oligocene, and by the Late Oligocene to Middle Miocene, half-graben units extended west of Lake Turkana (Ebinger *et al.*, 2000). During the Middle-Late Miocene, rifting extended southward, resulting in the development of N-S trending normal faults and volcanism in the basin's centre region before extending eastward, and this extension continued until the end of the Pliocene period (Kidney, 2012). This extension was due to transient eruptions of basaltic material known as the Gombe basalts of the Gombe Group (6–4 Ma), representing the current initial phase of rift pulsing (Haileab *et al.*, 2004; Kidney, 2012; Watkins, 1986). These basaltic materials are overlain by Plio-Pleistocene deposits of the Omo Group (4–1 Ma), which are volcano-sedimentary sequences, representing the later stage of the current rift event (Behrensmeyer, 1970; Bowen & Vondra, 1973; McDougall, 1985; Watkins, 1986; Brown & Feibel, 1986; Feibel, 2011) (Figure 2).

The Omo Group sedimentary strata preserve windows into earlier periods of the region's geological history and significant palaeontological evidence, crucial for comprehending African evolutionary trends (Feibel, 2011). These sedimentary strata are subdivided into three formations: the Nachukui Formation, west of modern Lake Turkana; the Shungura Formation in the Lower Omo Valley; and the Koobi Fora Formation, east of modern Lake Turkana (Rogers *et al.*, 1994; deHeinzelin, 1983; Brown & Feibel, 1986; Harris *et al.*, 1988) (Figure 2). Overall, due to significant fossil records preserved in these sediments, there has been considerable interest in

establishing the environmental context for human evolution, which fuelled the primary aim of this research, which is to reconstruct Pleistocene palaeogeography and paleoenvironments using the Koobi Fora Formation deposits.

2.2. Koobi Fora Formation (KFF)

Situated in the northeast of Lake Turkana, the Koobi Fora Formation (KFF) is a sedimentary formation with relatively complete Plio-Pleistocene sequences that are discontinuously exposed for over 1,200 km^2, extending from Ileret (north) to Jarigole (south) (Feibel, 1988). The formation is acknowledged for preserving prehistoric localities with renowned rift valley geological, palaeontological, and archaeological records (Gathogo & Brown, 2006; Gathogo *et al.*, 2008; Levin, 2008). Its potential significance was first identified by R.E.F. Leakey in 1967 due to its abundant fossil and archaeological discoveries (McDougall, 1985), and that fuelled the formation as the subject site of numerous studies in eastern Africa with considerable interest in establishing aspects considering rift basin palaeoenvironmental changes and human evolution during the Plio-Pleistocene time-period (Feibel, 1983; Brown & Feibel, 1991; Quinn *et al.*, 2007; Lepre, 2009). Furthermore, the stratigraphic and geochronologic records of the KFF are based on its geographic subregions, Ileret, Karari, and Koobi Fora Ridge (Base Camp), which are subdivided into numbered paleontological and archaeological collecting localities due to the formation's rift valley geology, palaeontology, and archaeology contents (Brown & Feibel, 1986; Quinn *et al.*, 2007) (Figure 1B).

2.2.1. KFF palaeontological and archaeological records

The KFF encompasses a critical period in hominin evolution as well as preserves vast assemblages of vertebrate, invertebrate, and flora fossils that date back approximately 5 Ma (Feibel *et al.*, 1989; Wood, 1992). The most significant recoveries in the formation are the over 250 hominin specimens that date back to approximately 4–3 Ma, constituting the earliest species of *Australopithecus anamensis and A. afarensis* to a period of high diversity in hominin between 2 Ma and 1.4 Ma which may have been coexisted in highly variable and dynamic environments (Bobe and Carvalho, 2019; Patterson *et al.*, 2019), represented by synchronous *Paranthropus* fossil assemblages (*Paranthropus boisei*) — conceptualising hominin family tree branching structures, *Homo rudolfensis, H. habilis* fossils — earliest representatives of our genus, and *Homo erectus* (or *ergaster*) skeletons and footprints — demonstrating speciation events

within the east Omo-Turkana ecosystem (Leakey *et al.*, 1964; Leakey, 1970; Leakey, 1973, 1976; Day *et al.*, 1976; Leakey and Leakey, 1978; Behrensmeyer and Laporte, 1981; Kimbel, 1988; Wood, 1991, 1992; Leakey *et al.*, 2012; Quinn, 2006; Spoor *et al.*, 2007; Wood and Leakey, 2011; Hammond *et al.*, 2021). Consequently, these discoveries enable biostratigraphic correlations within the formation and accurate conceptualisation of hominin speciation, migration and extinction through high-resolution radiometric and paleomagnetic dating (Quinn, 2006; Sier *et al.*, 2017; Villaseñor *et al.*, 2023). The formation further archives behavioural indicators synchronous with numerous *Homo* species' brain-size evolution in discrete spatial-temporal paleoenvironmental systems, and these include dietary trends, social dynamics, and stone tool production techniques during the Plio-Pleistocene (Isaac & Harris, 1976; Issac, 1978; Brown and Feibel, 1985; Feibel *et al.*, 1989; Bunn, 1994; McDougall & Brown, 2006; Lepre, 2009; Patterson *et al.*, 2019).

2.2.2. KFF stratigraphic succession

The KFF stratigraphic succession was initially defined by Brown and Vondra (1973) and further thoroughly revised by Cerling (1982), Brown and Feibel (1986), and Gathogo and Brown (2006). The formation comprises a Precambrian metamorphic basement (i.e., quartzites, gneisses, schists, and granitoids) that is overlain by fine pebble conglomerates, calcite-cemented sandstones, and mudstones (Gathogo & Brown, 2006; Quinn, 2006). Its composite-type stratigraphic sections attain an overall thickness of 560 m (Feibel, 1988). These stratigraphic sections are referred to as composite sequences because the formation has no complete sequences accessible in single sections (Feibel, 1988). In this instance, there are no contradictions between biostratigraphic and lithostratigraphic attributes, and nearly all of the Plio-Pleistocene sequences can be subdivided into eight stratigraphic members based on widespread chemically distinct tuff layers that are expressed as bounding marker horizons (Feibel, 1988) (Figures 3 and 4).

Each KFF stratigraphic member comprises sediments up to the base of the next bounding tuff. These sediments are classified by the eight primary basal tuff layers, from which the members' names are derived (Brown & Feibel, 1986; Feibel, 1988;

Gathogo, 2017) (Figures 3 and 4). These tuff layers are hypothesised to be primarily sourced from explosive volcanic eruptions of the volcanic centres within the axial zone of the Main Ethiopian Rift (WoldeGabriel *et al.*, 2005; Feibel, 2011; Phillips *et al.*, 2023); however, the precise provenance of these volcanic centres has not yet been determined (Phillips *et al.*, 2023). However, there have been reports of periodic ashfall deposition directly from the volcanic source as well as deposition through fluvial transportation (redeposition/reworking), aeolian reworking, and volcanic mudflows (McDougall and Brown 2006, 2008; Feibel, 2011). Furthermore, the basal contacts between the volcanic tuffs and the underlying stratigraphic members suggest a short time interval between the volcanic eruptions and subsequent depositions in the basin (Brown 2006, 2008; Phillips *et al.*, 2023).

The stratigraphically lowest volcanic tuff unit of the formation occurs within Lonyumum Member sediments (4.4 Ma to 3.97 Ma), which are subsequently overlain by the Moiti (3.97 Ma to 3.60 Ma), Lokochot (3.60 Ma to 3.44 Ma), Tulu Bor (3.44 Ma to 2.26 Ma), Burgi (2.62 Ma to 1.87 Ma), KBS (1.87 Ma to 1.60 Ma), Okote (1.60 Ma to 1.38 Ma) and Chari (1.38 Ma to Middle Pleistocene) Members, in ascending order (Feibel, 1988) (Figures 3 and 4). Stratigraphically, Pliocene sedimentary deposits are presented by the lowest four members and the Burgi Member below the Lokalalei Tuff (Gathogo, 2017) (Figures 3 and 4); in contrast, Pleistocene sedimentary deposits are presented by the remaining three members, with a 2.6 Ma boundary between these Epochs (Gathogo, 2017) (Figures 3 and 4). Moreover, the KFF stratigraphic succession control has been derived from geomagnetic polarity stratigraphy, tuff radiometric dating, tuff correlation, and aerial extensive bioclastic lacustrine bed markers (Quinn *et al.*, 2007).

Despite the well-defined continuous deposition of these stratigraphic members, the KFF consists of two significant unconformities due to extensive structural instabilities and erosional processes (Feibel, 1988) (Figure 4). The first unconformity subdivides the Burgi Member into the lower and upper sections, representing approximately 500,000 years of missing segment throughout the 2.5–2.0 Ma period, and this is the basis for the informal subdivision of the formation into lower and upper KFF (Feibel, 1988; McDougall & Brown, 2008; Baldes *et al.*, 2024) (see Figure 4). This unconformity is one of the three aspects demonstrating tectonic activity during the KFF deposition period (Feibel, 1988; McDougall & Brown, 2008) and is hypothesised to have formed

due to regional uplift in southern Ethiopia and related down-warping of the Turkana Basin (Feibel, 1988; Brown & Feibel, 1991). The second unconformity subdivides the Chari Member into lower and upper members; however, its origin is poorly understood compared to the one within the Burgi Member (Feibel, 1988; Lepre, 2009). Moreover, due to abundant resistant lithologies, delaying erosion, exposures for each member are highly variable; however, the KBS Member can be studied more comprehensively compared to other members of the formation (Feibel, 1988).

2.3. KBS Member (~1.87–1.60 Ma)

Interest in Lake Turkana's eastern shores was piqued as early as the late 1880s when the first European explorers arrived at the lake in 1888 (Harris *et al.*, 2006). The geological significance of the shores was pronounced by the French expedition of Bourg de Bozas, who discovered its palaeontological significance through the recovery of Plio-Pleistocene vertebrate fossils in 1902 and 1903 (Harris *et al.*, 2006) and the discovery of the first archaeological site with artefacts in volcanic tuff in 1968, known as the Kay Behrensmeyer Site (KBS) (Lavin, 2010). The chronologic and palaeogeographic dispersal patterns of these discoveries serve as complex contributions to the comprehensive understanding of hominin evolution, and fundamental to these dispersal patterns are the fossil-bearing outcrops of the KBS Member in the north-eastern Turkana Basin (Lepre, 2010). Additionally, the KBS Member deposits are an essential source for some of the world's oldest remains of the genus *Homo* (Leakey & Leakey, 1978; Feibel *et al.*, 1989; Wood, 1991; Lavin, 2010).

As mentioned above, the KBS Member time deposits are classified as one of the eight KFF Plio-Pleistocene stratigraphic members (upper KFF) (Figure 4) and are exposed over a larger area compared to any other members of the formation (Brown & Feibel,1986; Gathogo & Brown, 2006). These deposits are exposed in collection areas 6, 6A, 8, 8A, 8B, 9, 10, 11, 12, 13, 14, 15, 40, 41, and 42 within the Ileret subregion. In the central part of the Koobi Fora subregions (*e.g.,* Karari and Base Camp), these deposits are exposed in collection areas 100, 101, 102, 103, 104, 105, 106, 107, 109, 110, 112, 118, 119, 120, 121, 123, 124, 125, 127, 128, 129, 130, 131, 133, and 200 (Feibel, 1988) (Figure 1).

Sedimentation of the KBS Member is hypothesised to mark the beginning of a significant high lateral variability phase observed by lateral changes in sedimentary facies and depositional environments (Feibel, 1988). This phase is estimated to have spanned approximately 270,000 years, particularly evident in the later members of the KFF (Feibel, 1988; Phillips *et al.*, 2023). The deposits of this member range from upward-finning, interbedded detrital clastic and bioclastic depositional units to coarser and more homogeneous detrital clastic depositional units with pedogenic carbonate accumulations (Feibel *et al.***,** 1989; Feibel, 1988; Brown, 1995; Lepre *et al.***,** 2007). These represent a variety of complex fluvial systems along with marginal lacustrine

settings, defined by a high degree of temporal and geographic heterogeneity in depositional settings compared to other KFF members (Feibel, 1988). This characteristic heterogeneity results from the interaction between periodic astronomical climatic forcing and tectonic activities (Brown, 1995; Gathogo & Brown, 2006; Lepre *et al.*, 2007; Nutz *et al.*, 2017; Boes *et al.*, 2019; Nutz *et al.,* 2020; Nutz *et al.*, 2022).

The stratigraphy of the KBS Member is described and interpreted synthetically by White *et al.* (1981), Burggraf *et al.* (1981), Burggraf and Vondra (1982), Feibel (1983), Brown and Feibel (1986), and Gathogo and Brown (2006). According to these authors, the Plio-Pleistocene sediments comprise beds of arenaceous bioclastic carbonate (ABC), terrigenous clastic, and volcaniclastic deposits from marginal lacustrine depositional settings. The ABC beds comprise mollusc packstones, stromatolites, and associated sand deposits. The terrigenous clastic deposits are dominated by fine- to coarse-grained sandstones, siltstones, and claystones. Lastly, volcaniclastics mainly consist of rhyolitic tuffs (Cerling & Brown, 1982). Additionally, Brown and Feibel (1986) defined the KBS Member deposits as sediments that are stratigraphically delineated by two radiometrically dated volcanic tuffs, namely the KBS Tuff (~1.879 Ma) at the base and the Okote Tuff (~1.67 Ma) at the top of the member (Feibel *et al.*, 1991; McDougall & Brown, 2006; Brown *et al.*, 2006; Braun & Harris, 2009; Braun *et al.*, 2009) (Figure 4).

2.3.1. KBS Tuff

The initial sedimentation pattern of the KBS Member is relatively straightforward and can be distinctly observed due to the spatial distribution complexity of the KBS Tuff (Feibel, 1988). These widespread KBS Tuff deposits are significant markers for hominin discoveries, archaeological sites, and geological basin dynamics (Brown & Feibel, 1991; Isaac, 1997), together with crucial calibration positions for orbital tuning of palaeo-climate proxy records, illuminating complex interactions between palaeo-climate and geological sedimentation drivers (Phillips *et al.*, 2023).

The KBS Tuff serves as the initial bounding marker bed to emerge before the KBS Member deposits (McDougall & Brown, 2008). Its spatial depositional timing and

palaeoenvironment vary with the geography of the basin. The KBS tuff was deposited in fluvial environmental sequences in the Shungura and Koobi Fora Formations. In contrast, the KBS Tuff is amidst lacustrine deposits in the Nachukui Formation (Harris *et al.*, 1988). The tuff occurs discontinuously as thinner, tabular, fine-grained deposits frequently altered into secondary minerals and as lenticular, relatively coarse tuff with pumice deposits (Feibel, 1988) (Figure 5). The majority of the tuff is additionally enclosed by mudstones containing palaeo-vertisol overprints (White *et al.*, 1981). The finer-grained sequences are locally identified through thin pumice lines. These deposits have been hypothesised to represent the meandering river channel fill and discontinuous floodplain blanket resulting from swale fill accumulations (White *et al.*, 1981). However, in some areas of the Koobi Fora Formation, the tuff occurs in deltaic facies that locally consist of molluscan fossil assemblages and in lacustrine facies as a reworked tuff in a fluvial deposit (Feibel, 1988) (Figures 10E, 10L, and 10M).

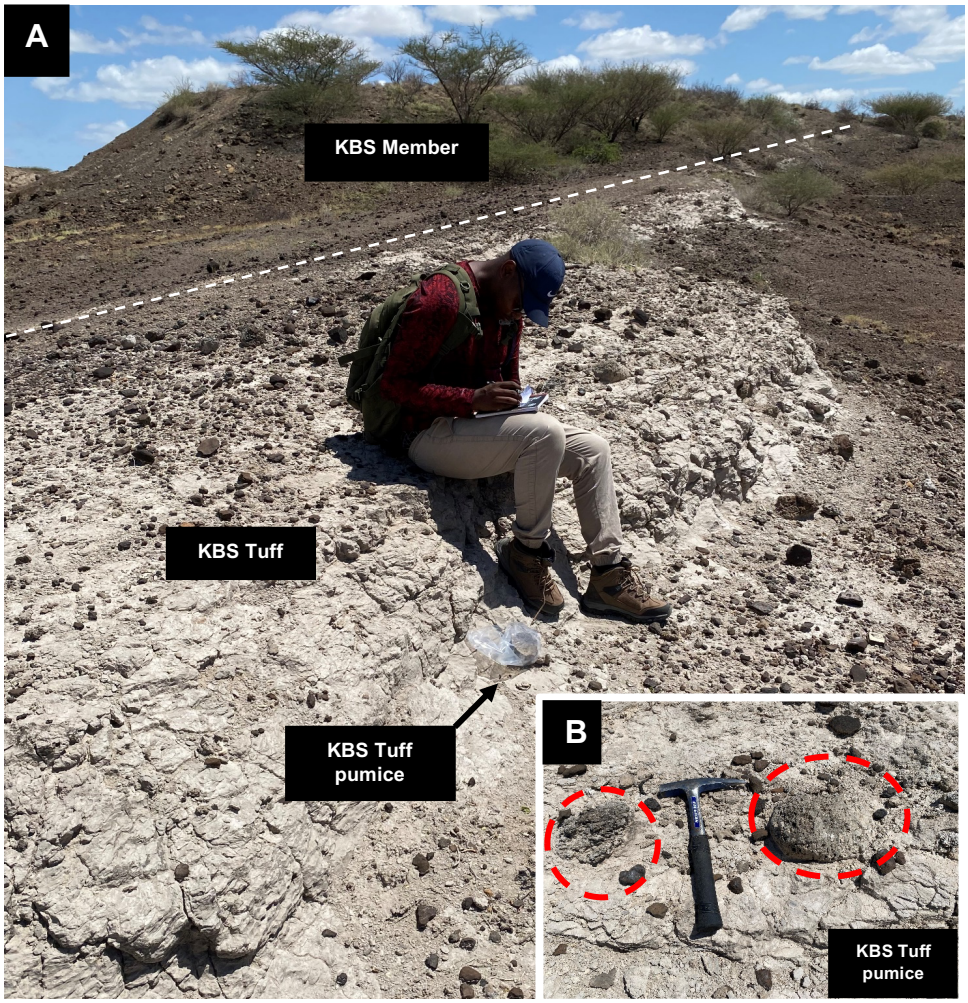

Figure 5: ***(A)*** *The discontinuous distribution of the KBS Tuff as thinner, tabular, fine-grained deposits frequently altered into secondary minerals and as lenticular, relatively coarse tuff.* ***(B)*** *KBS Tuff pumice deposits (red circles).*

Radiometric ages of the KBS Tuff have been controversial, primarily due to its significance in determining the hominin skull KNM-ER-1470 (*Homo rudolfensis*) upper age limit with its corresponding vertebrate fauna and ancient artefacts embedded within the tuff (Hay, 1980; Drake *et al.*, 1980; Gleadow, 1980). Fitch and Miller (1970) initially applied the K–Ar and $^{40}Ar/^{39}Ar$ step-heating method to date feldspar from the tuff, and the results suggested that the tuff was 2.6 ± 0.26 Ma. This age estimate was questioned concerning dated faunas at Olduvai Gorge in the Shungura Formation since it was inconsistent with the existing biostratigraphic markers, leading to a debate on the validity of the KBS Tuff's radiometric age (Bishop & Miller, 1972; Hay, 1980).

In 1974, Brook and Isaac studied the palaeomagnetic stratigraphy of the Koobi Fora Formation by contrasting their polarity to the Fitch and Miller (1970) polarity time scale. The KBS tuff date of 2.6 Ma was consistent with one of the two possible fits they discovered with their polarity scale. Curtis (1975) pronounced the controversy by proposing K–Ar dates of 1.60 Ma and 1.82 Ma. In 1976, Hurford *et al.* (1976) used the fission-track approach as an additional geochemical analysis to determine the age of KBS Tuff zircons, and the results produced an age of 2.44 ± 0.08 Ma. After analysing Hurford *et al.* (1976) step-heating data, Fitch *et al.* (1976) suggested 2.42 Ma as an ideal K–Ar age. Hillhouse *et al.* (1977), Harris and White (1977), and Cerling *et al.* (1979) obtained the same KBS Tuff age of about 1.7–1.85 Ma in subsequent palaeomagnetic investigations of the Koobi Fora Formation.

In 1980, Hay proclaimed that the controversy over the age of the KBS Tuff was settled after Drake *et al.* (1980) and Gleadow (1980) produced dating results of 1.89 ± 0.01 Ma, supporting geochemical analyses of Hillhouse *et al.* (1977), Harris and White (1977), and Cerling *et al.* (1979). The 1.89 ± 0.01 Ma was the standard age until McDougall *et al.* (1980) proposed their conclusions on the KBS Tuff age and generated an age of 1.87 ± 0.04 Ma and 1.89 ± 0.01 Ma through K–Ar dating of feldspar and fission-tracking dating, respectively. Additionally, based on single-dating, McDougall and Brown (2006 and 2008) estimated the age of the KBS Tuff to be 1.869 ± 0.021 Ma until Phillips *et al.* (2023) reviewed several statistical methods and produced astronomically calibrated Bayesian age estimations of 1879.1 ± 0.6 ka; including external errors of ±2.4 ka. Moreover, the KBS Member deposits consist of multiple small-scale tuffaceous strata; however, these horizons are not laterally continuous, making it challenging to determine a more accurate chronology (Brown *et al.,* 2006; Braun *et al.*, 2009).

2.3.2. KBS Member palaeontological and archaeological significance

The French expedition of Bourg de Bozas initiated the palaeontological significance of the Koobi Fora Formation by recovering Plio-Pleistocene vertebrate fossils in 1902 and 1903 (Harris *et al.*, 2006). The KBS Member time deposits are renowned for their high abundance of mammalian fossils, particularly in the Ileret and Base Camp

subregions, where the deposits are extensively exposed compared to other Koobi Fora Formation members (Harris *et al.*,1988). Leakey and Leakey (1978), Feibel *et al.* (1989), Wood (1991), Antón and Swisher (2004), and Bobe and Carvalho (2019) document some *Paranthropus boisei* fossils and some of the earliest African *Homo* species; *H. habilis, H. rudolfensis, and H. erectus/ergaster* fossils preserved in these deposits.

The first archaeological significance of the Koobi Fora Formation was discovered during a geological and palaeontological survey in 1969, where *in situ* Oldowan-type artefacts were yielded from volcanic ash in Area 105 (Braun & Harris, 2009). The geologist excavating at the time, Kay Behrensmeyer, inspired the site's name, and the site was named Kay Behrensmeyer Site (KBS). Today, the site is referred to as FxJj-1 and the volcanic tuff underlying it is referred to as the KBS tuff (Leakey, 1970; Isaac, 1997; Braun & Harris, 2009). The FxJj-1 discoveries included detached artefact assemblages, with only five in situ and seven surface finds. Many of the fragments demonstrate evidence of the exterior surfaces of cobbles sourced from fluvial settings (Braun & Harris, 2009), and this led Isaac (1997) to hypothesise that the artefacts and fossils at the site underwent minimal post-depositional water transportation due to the low frequency of refitting pieces and the absence of small flaking debris.

The KBS excavation occurred from 1969 to 1972, yielding approximately 138 *in situ* artefacts. These archaeological horizons' fine-grained deposits record floodplain settings that are an aspect of a delta prograding southward because these deposits are situated directly below the bend of a palaeo-channel extensively filled by tuffaceous sediment (Braun & Harris, 2009). The KBS excavations also produced several faunal specimens, which provide essential data on early Pleistocene hominin carcass processing techniques (Bunn, 1981, 1997; Pobiner *et al.*, 2008). These findings support the hypothesis that hominins systematically butchered various mammals during this period (Pobiner *et al.*, 2008).

Furthermore, the macro-mammal fossils are dominated by reduncine bovids (*e.g.*, waterbucks and reedbucks), reflecting wetland settings nearby (Braun & Harris, 2009). The discovery of fish, hippopotamus and crocodile fossils indicates perennial water sources and records the earliest evidence of aquatic resource exploitation by hominins in eastern Africa (Braun *et al.*, 2010). However, alcelaphine bovids (*e.g.*, hartebeests

and wildebeests) and hypsodont suids (*Metridiochoerus*) were also discovered, indicating that grasslands were adjacent to the site (Braun & Harris, 2009). Overall, the KBS records significant changes in hominin land-use and tool discard patterns due to its *in-situ* hominin artefacts preserved in palaeo-wet settings that were potentially seasonally inundated, with extensive ground cover (Patterson, 2016).

The behavioural relationship between the artefacts and fossils has never been established through bone surface modifications. However, their stratigraphic relationship suggests that some fossils represent hominin food refuse (Bunn, 1997). Early research centred on comprehending stone tool production and discard (Keely & Toth, 1981; Harris & Isaac, 1976), the paleogeographic framework (Isaac & Behrensmeyer, 1997), and site formation processes (Schick, 1987) of archaeological sites. Although East Turkana's archaeological sites significantly contributed to our knowledge regarding eastern African hominin behaviour between 2.0 and 1.4 Ma, they can still be used to gather more data that could assist in determining how hominin behaviour corresponds to the ecosystem (Patterson, 2016).

2.3.3. KBS Member palaeoecosystem in response to palaeoclimate: Insights from previous studies

The KBS Member deposits are also recognised for encompassing a period (1.8 and 1.7 Ma) which is hypothesised to have experienced extensive global climate change in eastern Africa through Plio-Pleistocene palaeosol stable isotope measurements and palaeoprecipitation estimates (Cerling, 1992; Bobe & Behrensmeyer, 2004; Wynn, 2004; Fernández & Vrba, 2006). These provided high-resolution records of increased aridity and grassland growth, which led to an increased proportion of open habitats and ecosystem spatial negentropy and heterogeneity.

Studies by Bowen (1974), Tindall (1986), Feibel (1988), Lepre (2014), and O'Brien *et al.* (2020) identify sedimentary facies successions in the deposits, which archive data regarding lake-level fluctuations in relation to palaeoenvironments, resulting in the rise in significant habitat reorganisation. These authors emphasise that multiple facies variations exhibit predictable patterns, which indicates a cyclical depositional influence

similar to Milankovitch's climatic forcing. Brown (1995) examines the applications of KBS Member deposits to comprehend the interactions between climate change and palaeoenvironmental changes. Lepre *et al.* (2007) analysed KBS Member facies environments to determine the development of hominin habitats in the north-eastern Turkana Basin lake margin. Through sedimentary sequences, this study examines the member's offshore and nearshore lacustrine, alluvial channel, and floodplain environments to produce detailed correlation data between palaeoenvironmental changes and orbital and marine climate records. This study concludes that the KBS Member facies environments from the Koobi Fora Ridge provide evidence of the lake-margin hominin habitats and that environmental changes in these habitats may be influenced by monsoonal rainfall oscillations that arise from orbital insolation or glacial forces. Therefore, facies environmental characteristics also provide data on the hydro-sedimentary dynamic changes of lake margins and climatic controls (Lepre *et al.*, 2007). Lavin (2010) also integrates palaeoecological research methods with landscape-scale archaeological collections to determine whether behavioural changes in hominins result from palaeoecological changes through KBS Member time deposits.

CHAPTER 3: RESEARCH PROBLEM AND AIMS

3.1. Research rationale and problem

Lake Turkana has experienced varying lake level fluctuations marked by distinctive geological features that developed over time, representing various palaeoenvironments and depositional periods that define the refinement of the KFF stratigraphic sequence (Nutz *et al.*, 2017). As mentioned, Turkana Basin's geological history is hypothesised to be a dynamic landscape responding to environmental factors, such as climate change and/or tectonism and volcanism, resulting in lake-level fluctuations (Nutz *et al.*, 2020; Boës *et al.*, 2019). In the context of the EARS, the most significant Pleistocene hominin evolutionary events have been attributed to environmental dynamics (climate, tectonics, and volcanism), which also affected the hominin environments in the past (MacLatchy *et al.*, 2010). However, the interplay and punctuation of these factors are poorly understood; thus, further research and clarifications are needed (Maslin & Christensen, 2007).

Most studies in the Turkana Basin employ environmental reconstructions through lithostratigraphic investigations for palaeogeographic and tectonic interpretations of the region (Vondra & Bowen, 1976; Feibel, 1988; Brown & Feibel, 1991). However, more recent research in other hominin sites in eastern Africa (e.g., Olduvai and Olorgesailie) has adopted environmental reconstructions through sequence stratigraphic modelling to comprehend the timing of landscape changes and the evolution of hominids (Blumenschine *et al.*, 2009; Behrensmeyer *et al.*, 2018). In the Turkana Region, studies by Nutz *et al.* (2017), Boës *et al.* (2019), Nutz *et al.* (2020), and Nutz *et al.* (2022) adopted sequence stratigraphic approaches as tools to represent reconstructions of palaeo-Lake Turkana levels, providing comprehensive records of palaeohydrology during the Mio-Plio-Pleistocene, with implications for understanding hominin evolution, using the West Turkana Basin (Nachukui Formation) as a study area. In contrast, this study will focus on the East Turkana Basin (KFF) using the Pleistocene KBS Member stratigraphic sequence, which is known to yield a large number of hominin specimens, presenting an opportunity to examine early human evolution over time.

In addition, this stratigraphic sequence also preserves extensive bounding surfaces that can be correlated due to their chronostratigraphic confines, spatial and temporal variability in depositional settings and consists of extensive exposures in the Koobi Fora Region compared to other members of the formation (Feibel, 1988). As a result, the KBS Member time deposits are ideal for conducting a sequence stratigraphic analysis to determine lake level fluctuations during the Pleistocene. There is a need to understand significant source areas of the KBS Member time deposits together with the occurrence, timing, and influence of the paleoenvironmental change in the KFF (KBS Member) and how these drove biotic evolution and hominin adaptation.

3.2. Research aims and objectives

The main objective of this research is to adopt a novel approach to an investigation through the adoption of framework petrography and paleocurrent analysis to depict sediment provenance of the KBS Member sandstones and the source areas' palaeohydrological conditions during their deposition, providing additional evidence for East Turkana Basin sediment depositional history and stratigraphic controls. This provenance approach shall be coupled with sedimentary facies analysis and sequence stratigraphic modelling to synthesise the occurrence, timing, and quantify the recognised driving forces (climatic, tectonic, and volcanic influences) of lake level fluctuations on palaeoenvironmental changes and palaeogeographic variability across the KFF during the KBS Member time interval. This shall be achieved by yielding a high-resolution geologic palaeoenvironmental reconstruction and a basin analysis model that will serve as the environmental control setting in understanding biotic evolution and hominin adaptation at the onset of the KBS Member time interval.

3.3. Research questions

The following questions are posed to address the objectives of this study:

1. What are the Pleistocene Koobi Fora Formation (KBS Member) lithofacies, bounding surfaces, their correlations, and their order? This will be understood by

adopting sequence stratigraphic modelling and revising the established lithostratigraphy of the Pleistocene Koobi Fora Formation (KBS Member) and its bounding surfaces.

2. What are the Pleistocene palaeoenvironments and their environmental variability in the KBS across the regions?

3. What are KBS Member time deposits' major source areas from which they were primarily derived, and what were the palaeohydrological conditions of the source areas during their deposition, including transport pathways of siliciclastic sediments?

4. What are the long-term contributing factors to the Pleistocene lake-level fluctuations (tectonic, climate, or the interplay of both); their occurrence, timing, and effect on palaeogeographic changes in the KBS across the regions?

5. What is the relation between lake-level fluctuations and the evolutionary succession of the genus *Homo*?

CHAPTER 4: MATERIALS AND METHODOLOGY

This chapter outlines the systematic lithological framework of data collection procedures and methodologies adopted to acquire datasets from the KBS Member-time deposits. It addresses the above-mentioned aims and objectives in Chapter 3. The lithological investigations included identifying and interpreting sedimentary units and sandstone sample collection for sedimentary facies and palaeocurrent analyses, petrography, and sequence stratigraphic modelling. These procedures are elaborated on below.

4.1. Fieldwork

Fieldwork was conducted during the Kenyan cool–dry season, spanning two field seasons in the remote region of the country between June of 2023 and September-October of 2024, which collectively amounted to nineteen fieldwork days. The fieldwork required outcrop observations prior to sample collection; these included lithological variations and sedimentary features, grain size distribution, rock textural characteristics, and mineralogy. Thereafter, the data was recorded and photographed, and sandstone sampling followed.

The sampling of KBS Member sandstones involved a systematic approach of outcrop point selection that covered three Koobi Fora Formation subregions, namely Ileret, Karari, and Koobi Fora (Base Camp), representing both the lower and the upper KBS Member deposits (Figure 1B). These subregions preserve well-documented, extensive outcrops of the KBS Member deposits that allow for this type of study (Brown and Feibel, 1986). Only indurated sandstones were collected to preserve their grain framework and avoid contamination from modern sediments; thus, availability was considered. A total of twenty-nine KBS Member sandstone outcrops were selected: twenty-two from the Ileret subregion, two from the Karari subregion, and five from the Base Camp subregion (Appendix C). These selected outcrops were also used to comprehensively understand the region's sedimentology through the aforementioned

lithological investigations: petrographic, palaeocurrent, sedimentary facies, and sequence stratigraphic analyses.

The equipment used to collect the data included a geological hammer for sampling and exposing fresh sedimentary surfaces for descriptions and interpretations. A hand lens was used to examine the petrography of hand specimens in the field. A Brunton compass was used to record structural features. A Jacob's staff with an Abney Level was used to measure strata thicknesses accurately. Digital photographs of the outcrops with defined lithofacies were also taken to complement field notes. Lastly, a global positioning system (GPS) receiver was used to record the locations of samples collected (including collecting volcanic ash from the KBS Tuff) and mark the stratigraphic sections' locations.

4.2. Sedimentary facies analysis

The term 'facies' denotes observable distinct internal characteristics within a confined body of rock that form under various sedimentation conditions, processes and environments, distinguishing strata or sedimentary beds from others through appearance and composition (Miall, 1996; 2000). Accordingly, facies distinguished based on lithological and petrological characteristics, consisting of similar physical, chemical and biological properties that contribute to their formation, are referred to as 'lithofacies' (Reading, 1986; Miall, 1996; Selley, 1985; Nichols, 2009). Furthermore, persistent lithofacies bundles are classified as 'lithofacies associations' (Nichols, 2009). These associations are defined by dominant lithofacies with standard progression and some minor lithofacies that may or may not complete an association, reflecting how lithofacies coincide in natural depositional environments (Fiebel, 2013).

Since lithofacies associations are genetically regulated by distinct physical, chemical and biological processes within a given depositional environment, they are considered valuable proxies for determining conditions within sedimentary basins during deposition and sedimentation environments through sedimentary facies analysis (Walker, 1997; Reading, 1996; Miall, 2000, 2006; Boggs Jr, 2006; Nichols, 2009). This method requires physical, chemical and biological observations, identifications and

interpretations; these thus aid in reconstructing sedimentary processes and environments to determine provenances of deposits (Nichols, 2009).

When considering the Koobi Fora Region's sedimentary strata, attempts have been proposed to develop a definitive lithofacies scheme to infer its deposits and interpret depositional environments within the formation through sedimentary facies analysis (Bowen, 1974; Burggraf & Vondra 1982). The initial KFF lithofacies classification scheme identified four primary depositional environments: lacustrine, fluvial, deltaic, and alluvial fans (Feibel, 1988; 2013). Due to ongoing research, the scheme was further elaborated, and lacustrine and fluvial variants were identified (Burggraf *et al.,* 1981; White *et al.,* 1981). Burggraf and Vondra (1982) synthesised this lithofacies scheme as a rift-valley sedimentation model. In addition to applying refined lithofacies approaches to the Koobi Fora stratigraphy, Brown and Feibel (1986) re-evaluated the Koobi Fora stratigraphy. Consequently, much of the sedimentary facies analysis employed in this study was initially outlined in a report by Feibel and Brown (1986), which was then refined and expanded by Feibel (1988), Feibel *et al.* (1991), Gathogo (2003), Gathogo and Brown (2006), and Feibel (2013).

In order to interpret depositional settings, lithofacies within a sedimentary sequence must be characterised (Harms *et al.*, 1982). Individual lithofacies presented in this study are delineated following lithofacies patterns introduced by Miall (1977) and a lithofacies classification scheme presented by Feibel (2013), ensuring consistency in the Koobi Fora Formation descriptions and classifications. The Feibel (2013) scheme provides a standard framework for any sedimentological environment in the Koobi Fora Region, and it is only utilised in this study for descriptive and ordering purposes. Additionally, lithofacies units were described based on their dominant lithology, composition, sorting and maturity, bounding surfaces, bedding plane geometry, primary and secondary structures, biogenic characters, palaeocurrent directions, and colour of exposed and fresh sedimentary surfaces using Munsell's geological colour chart (Appendix D). The lithofacies units were further classified using the Wentworth (1922) grain-size scale to determine grain size (Table 1) and Folk's sedimentary detritic rock classification (1954) (Figure 6). These lithofacies were then arranged into sedimentary units, representing lithofacies associations. Lastly, field observations and

descriptions (field notes) were complimented by digital photographs of outcrops with defined lithofacies.

Table 1: *The Wentworth (1922) grain size scale for sediments, with equivalent with phi-units and grain size in mm.*

Millimeters (mm)		Micrometers (µm)	Phi (ϕ)	Wentworth size class	
	4096		-12.0	Boulder	
	256		-8.0	Cobble	Gravel
	64		-6.0	Pebble	
	4		-2.0	Granule	
	2.00		-1.0	Very coarse sand	
	1.00		0.0	Coarse sand	
1/2	0.50	500	1.0	Medium sand	Sand
1/4	0.25	250	2.0	Fine sand	
1/8	0.125	125	3.0	Very fine sand	
1/16	0.0625	63	4.0	Coarse silt	
1/32	0.031	31	5.0	Medium silt	
1/64	0.0156	15.6	6.0	Fine silt	Silt
1/128	0.0078	7.8	7.0	Very fine silt	
1/256	0.0039	3.9	8.0		
	0.00006	0.06	14.0	Clay	Mud

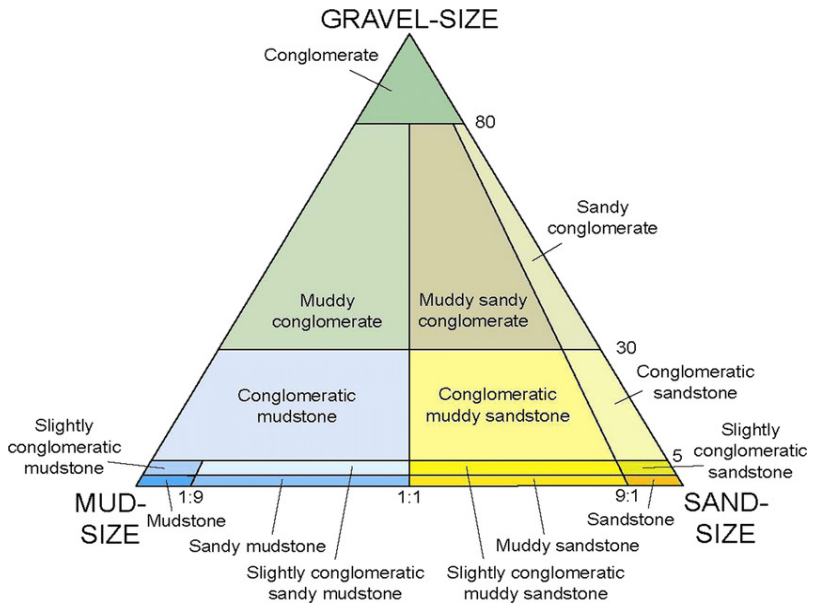

Figure 6: *Terminology of sedimentary rocks based on percentages of sand, mud, and gravel ratio (Folk, 1954).*

4.3. Palaeocurrent analysis

Palaeocurrent analysis is one of the practical methods employed in studying sedimentary basin analysis to delineate sediment dispersal systems and directional flow patterns, identify sediment provenance, and reconstruct basin palaeogeography (Hoque, 1975; Pryor, 1961; Miall, 1996). This analysis is applied with the assumption that directional current vectors point towards palaeo-slopes, where sediment transportation occurs (Pryor, 1961). However, the assumption's validity is rational in some environments due to different sediment depositional systematics (Hoque, 1975).

This study uses the palaeocurrent analysis to determine KBS Member sediment distribution patterns across the formation and infer its source areas (High and Picard, 1974; Miall, 1974; Dasgupta, 2002). A total of three hundred forty-nine (349) unidirectional palaeocurrent indicators generated by the palaeo-flows, within limits of preservation, were identified, and their azimuthal readings were recorded throughout the KBS Member stratigraphic succussion (Ileret, Karari and Base Camp) using a Silva expedition compass clinometer. This data is presented in Appendix E. The azimuthal readings were then analysed and presented as rose diagrams; circular frequency histograms, commonly used for directional data, were refined using the Rose.NET 1.0 (x86) software. Statistic parameters were also applied to supplement the rose diagrams pertaining to trend directions, and these included mean palaeocurrent (*m*), standard deviation (*S.D.*), vector magnitude – flow strength (*V.M.*), and consistency ratio – deviation from mean palaeocurrent vectors (*C.R.*).

4.4. Sandstone petrographic analysis

The twenty-nine collected sandstones were selected to represent the KBS Member lithofacies, particularly fluvial channel lithofacies' (and ~lacustrine lithofacies), as well as lithology variations, grain size distributions, textural characteristics, and mineralogy distributions (Appendix C). These sandstone samples underwent thin-section preparation at Rhodes University (RU). They were cut and polished to acquire ~30 µm-thick thin sections. This preparation required different treatment processes depending on the nature of the sediment samples. Sediment samples were cut using

a diamond-cut blade to acquire flat surface slabs. These sediment samples were dried and embedded in epoxy resin and then were cut, obtaining flat surface slabs. After that, the slabs were polished to have smoother surfaces with a thickness of 30 μm using different grit grades ranging (from coarse to fine), then dried. During the drying process, bubbles might develop in the thin sections due to the embedded epoxy, and those were removed. The final slide thickness of the thin sections was determined by using a petrographic microscope through cross-polarised light to observe interference colours (mostly feldspar and quartz). Once the desired thickness was achieved, a thin layer of epoxy was used to cover the samples, and the sections were ready for petrography.

The petrographic analysis was also conducted at RU using the Leica DM EP Polarizing Microsystem Olympus BX51 microscope equipped with a Leica EC4 digital camera attached to obtain microphotographs of thin sections under both cross-polarised light (XPL) and plane polarised light (PPL). The petrography of each polished thin section was described in terms of grain mineralogy framework, grain size, grain sorting, grain roundness and sphericity, grain-matrix proportion, grain contacts and interactions, cementation type, and maturity. Visual estimation diagrams proposed by Powers (1953) and Compton's classification scheme (1962) were used to estimate roundness and sphericity to classify grain sizes that will infer maturity (Figure 7). The sedimentary grain size nomenclature utilised in this study follows the Udden-Wentworth scale (Udden, 1914; Wentworth, 1922) (Table 1), with reported grain size in Phi (Φ). Additionally, each thin section's porosity proportion was assessed visually using Terry and Chilingar's (1955) guide for porosity estimations (Figure 8).

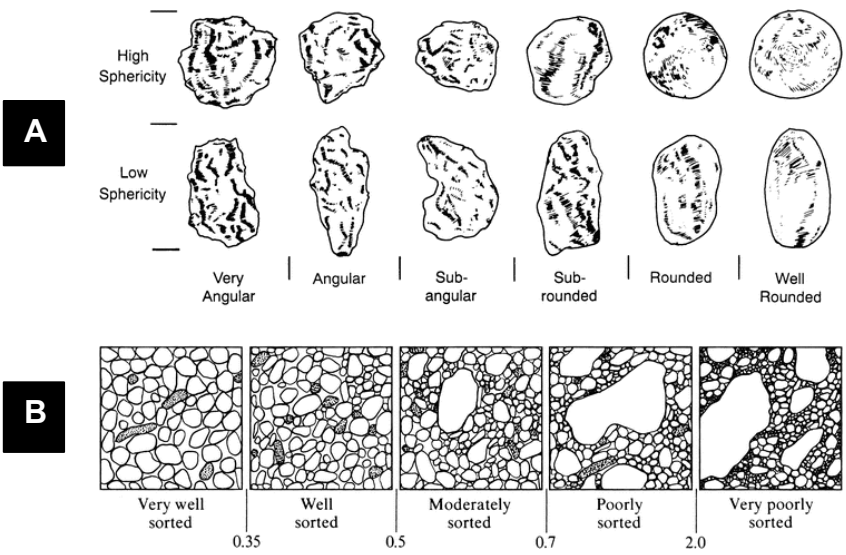

Figure 7: ***(A)*** *Terminology of degree of rounding of detrital grains (Powers, 1953).* ***(B)*** *Classification regarding the degree of sorting (Compton, 1962).*

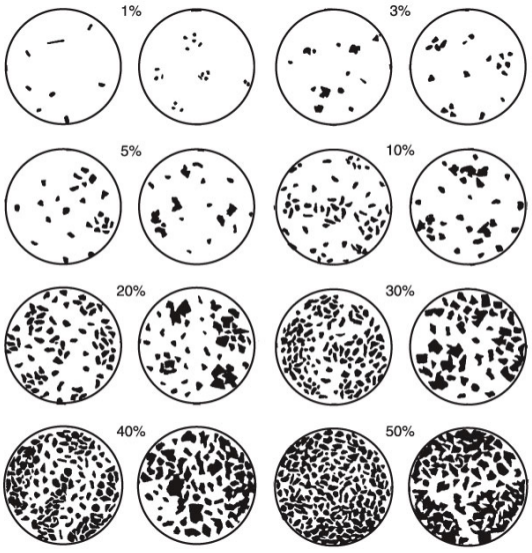

Figure 8: *Comparison chart for porosity estimations in percentages (Terry and Chilingar, 1955).*

The petrographic analysis of each sand sample was conducted by counting 400 points on each thin section under a polarising microscope using the Gazzi-Dickinson method (Gazzi, 1966; Dickinson, 1970; Ingersoll *et al.*, 1984). The sand classification was based on three primary framework components, provided they exceed 10 percent of the bulk section (*QFL*): quartz (*Q*), feldspars (*F*) and lithic fragments (*L*), also following the Dott (1964) classification scheme that was later detailed by Garzanti (2019) (Table 2). Quartz is subdivided into two variants: monocrystalline (*Qm*) and polycrystalline (*Qp*) variations; feldspar is subdivided into two variants: plagioclase (*P*) (albite) and potassium (*K*) (mostly microcline) feldspars; and lastly, lithic fragments are grouped according to their protolith composition as volcanic (*Lv*), metamorphic (*Lm*) and sedimentary (*Ls*) lithics (after Garzanti, 2019). Volcanic lithic fragments are classified as microlithic, felsic and lathwork volcanic lithics. Metamorphic lithic fragments are classified according to the metamorphic rank proposed by Garzanti and Vezzoli (2003). Sedimentary lithic fragments are classified as mudrocks, carbonate lithics, biogenic material from shells and mammalian fossil fragments. Other accessory minerals identified include tabular biotite (most common), chlorite, amphibole, and opaque minerals (hematite). Moreover, this data was further used to interpret the sandstone's sediment provenance (source rocks).

Table 2: *Detrital grain parameters. Modified after Gazzi (1966); Dickinson (1970) and Ingersoll et al. (1984).*

Detrital Grain Parameters	**Counted Detrital Grain Parameters**	**Recalculated Detrital Grain Parameters**
1) Quartz (Q) is sum of:	• *Qm* = monocrystalline quartz • *Qp* = polycrystalline quartz (inc. chert)	*Q = Qm + Qp*
2) Feldspar (*F*) is the sum of:	• *P* = plagioclase feldspar • *K* = potassium feldspar	*F = P + K*
3) Lithic fragments (*L*), sum of:	• *Lv* = volcanic lithics • *Lm* = metamorphic lithics • *Ls* = sedimentary lithics	*L = Lv + Lm + Ls*
(*Q*, *F*, *L* where *Q+F+L* = 100) *QFL%Q = 100Q/(Q + F + L)* *QFL%F = 100F/(Q + F + L)* *QFL%L = 100L/(Q + F + L)*		

Detailed sandstone petrography is essential to investigate sediment provenance and reconstruct palaeogeographic basins' evolution and dynamics (Gómez-Gras *et al.*, 2016). The petrography method used in this study prevents incorrect interpretations of sandstones and allocates clastic detrital sediment to distinct source areas. This methodological approach can further infer sediment transportation, distribution, diagenesis and the interplay of physical and chemical processes (Suttner, 1974; Dickinson *et al.*, 1983; Dickinson, 1985; 1988).

In the East Turkana Basin context, minimal work has been done on investigating sediment provenance (source rocks) through integrated sedimentological approaches, where Quaternary dynamics are considered; these include comprehending intra-basinal sediment provenance in terms of sedimentary processes and fluvial influences within the basin. Previous petrographic studies lack adequate data that describes and interprets the primary provenance of these sediments (*e.g.,* Vondra *et al.*, 1971; Bowen & Vondra, 1973; Bowen, 1974; Findlater, 1976; Vondra and Bowen, 1976; Vondra and Bowen, 1978; Vondra *et al.*, 1978; Vondra and Burggraf, 1978; Burggraf *et al.*, 1981; White *et al.*, 1981; Brown and Cerling, 1982; Burggraf and Vondra, 1982; Cerling and Brown, 1982).

For the abovementioned issue, the framework petrography used in this study will adequately complement other sedimentological analyses highlighted in this chapter to constrain mineralogical patterns, sand dispersal pathways and sediment source of the KBS Member sandstones. This approach will also aid in depicting the region's palaeogeomorphology, determining the source area and depositional sink, palaeohydrological conditions during sediment deposition (palaeoclimatic conditions) over spatial scales, and monitoring sediment composition changes associated with fluvio-lacustrine interactions across the KFF through the multi-proxy datasets.

4.5. Sequence stratigraphy

Sequence stratigraphy is a methodology used to analyse and identify depositional sequences with relatively conformable successions bounded by erosional surfaces or correlative conformities within stratigraphic-time frameworks through local, regional

and interregional correlations in sedimentary basins (Posamentier *et al.*, 1988; Haq, 1991; Allen & Allen, 1990; Martins-Neto & Catuneanu, 2009). Fundamental principles of this methodology were initially proposed for marine sequences within the context of passive-margin settings, neglecting conditions and dynamics of continental rift settings (Vail *et al.*, 1977; Posamentier & Vail, 1988; Posamentier *et al.*, 1988; Martins-Neto & Catuneanu, 2009). Many authors have sought to apply the passive-margin principles to all other tectonic settings, including for lacustrine sequences within the context of continental rift settings, despite distinctions between sequence dynamics between tectonically stable and active basins, and that resulted in several issues and misunderstandings (Keighley *et al.*, 2003; Martins-Neto & Catuneanu, 2009). The primary problem is that standard passive-margin stratigraphic frameworks are driven by sea-level changes, challenging applying the same principles to basins isolated from the ocean (Zavala *et al.*, 2024). In contrast to marine passive-margin systems, stratigraphic frameworks within lacustrine continental rift basins are not directly determined by sea-level fluctuations, rather than by timing and rate of tectonic subsidence regimes and occasional pulses of extension that form sediment accumulation space, as well as local climate, resulting in lake level fluctuations (Martins-Neto & Catuneanu, 2009).

Sedimentary basins in continental rift settings are composed of depositional sequences that display correlations of coeval depositional systems (Van Eeden, 1996). These depositional system correlations are defined by systems tract successions (STS) with stratal geometries demonstrating discrete lithofacies at bounding surfaces, thus displaying depositional cycle completions (Brown & Fisher, 1977; Posamentier *et al.*, 1988; Van Eeden, 1996). Throughout time, these depositional cycles are characterised by two depositional phases: transgression and regression phases (T and R phases), stratigraphically divided into transgressive systems tract (TST) and regressive systems tract (RST), respectively, demonstrating variations in the cyclic nature of lake-level fluctuations and sedimentation rates (Brown & Fisher, 1977; Zavala *et al.*, 2024) (Figure 9). During transgression, lake-level rise (sediment accommodation) surpasses the sedimentation rate, resulting in retrogradation or landward shifts of the shoreline (lake margin) and lithofacies. Conversely, regression is characterised by progradation or lake-ward shoreline shifts and lithofacies, whereby the sedimentation rate surpasses sediment accommodation

(Plint, 1988; Posamentier *et al.*, 1992). These depositional phases (STS) are separated by a maximum flooding surface (MFS), displaying the maximum transgression and marking the upper boundary of the TST when the shoreline reaches its most landward position (Cherry, 2012; Zavala *et al.*, 2024) (Figure 9). Furthermore, these fundamental constituents of STS consist of parasequences and parasequence sets (Van Wagoner *et al.*, 1990). Parasequences are relatively conformable successions of genetically related beds or bed-sets with distinctive stacking patterns bounded by MFS and their correlative surfaces in vertical successions, characterised as parasequence sets (Van Wagoner *et al.*, 1990). The parasequence sets define depositional geometries during phases of relative eustatic fluctuations, allowing stratigraphic correlations through sequence stratigraphy (Cherry, 2012).

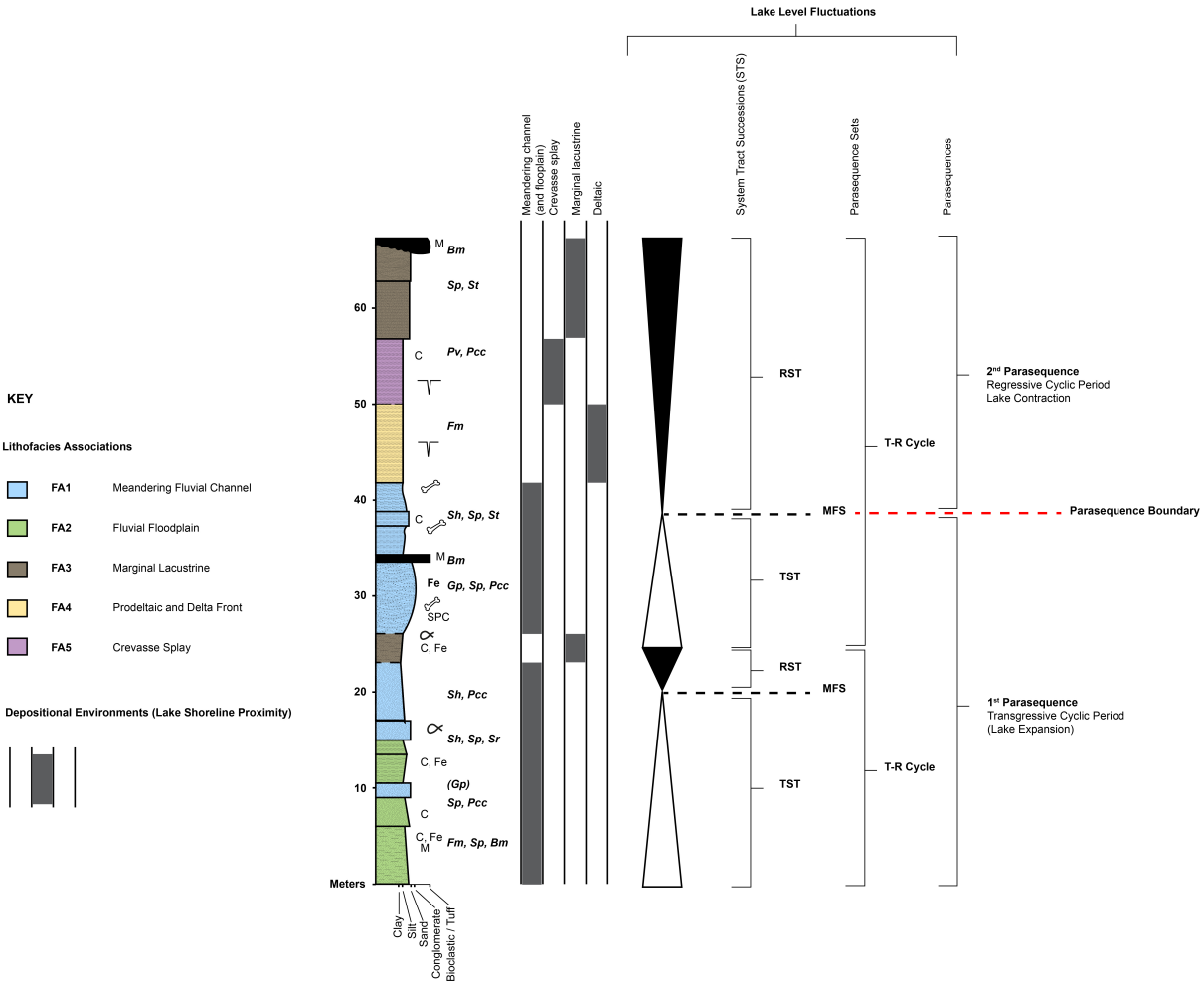

Figure 9*: Composite stratigraphic section of the KBS Member as an illustration demonstrating the origin and internal organisation of a lacustrine continental rift depositional sequence generated during lake-level fluctuations. A high-resolution version of this figure is found in the Appendices section (Appendix F).*

As mentioned above, the KBS Member stratigraphic sequence is interpreted as sedimentary beds of terrigenous clastic, arenaceous bioclastic carbonate and volcaniclastic deposits derived from marginal lacustrine, fluvial and deltaic depositional settings (White *et al.*, 1981; Burggraf *et al.,* 1981; Burggraf & Vondra, 1982; Feibel, 1983; Brown & Feibel, 1986; Gathogo & Brown, 2006; Feibel, 2013). These lithological and depositional setting interpretations are constructively delineated by concepts that serve as fundamentals of sequence stratigraphy (Posamentier *et al.*, 1988). Therefore, understanding the aforementioned continental rift sequence stratigraphic principles allows for high-resolution palaeoenvironmental reconstructions, as this study applies this as a research framework to interpret depositional systems and determine transgressive and regressive sequence trends of Lake Turkana using the KBS Member fluvio-lacustrine deposits, focusing on the interplay between fluvial processes and lake-level fluctuations. This study further incorporates the sequence stratigraphic principles of fluvial systems to infer their sedimentary structures, stacking patterns, and channel morphology in relation to the lake-level fluctuations, providing a detailed understanding of fluvio-lacustrine sedimentary dynamics in continental rift settings.

This was done using spatially correlated geological stratigraphic sections and the KBS Tuff as a bounding marker horizon to produce a lake-level basin fluctuation model for the KBS Member-time interval. Stratigraphic sections drawn during fieldwork were redrawn using the SedLog software to ensure a precise recording of identified depositional trends (Zervas *et al.*, 2009). The stratigraphic sections were then digitised and annotated using the Adobe Illustrator CC software for correlation. All KBS Member stratigraphic sections are represented in Appendix G. After the correlation alignment, primary stratigraphic surfaces, sequence boundaries and MFS were identified and interpreted through sedimentological and stratigraphic parameters, including the sedimentary facies analysis outcomes.

CHAPTER 5: RESULTS

5.1. KBS Member sedimentary facies data

The KBS Member sedimentary sequences provide significant indications of palaeoenvironmental heterogeneity across the Turkana Basin (Feibel, 1988, 2013). Extensive KBS Member deposit descriptions from multiple collection areas were done through sedimentary facies analysis. Eleven lithofacies characterising the KBS Member Pleistocene sedimentary sequences are described, representing five lithofacies associations across the northeastern Turkana Basin.

5.1.1. Lithofacies descriptions and interpretations

Field observations identified eleven distinctive lithofacies characterising the KBS Member-time deposits within the study sites. The predominant lithological components present in the region are fine clastics (*F*) (*i.e.,* muds and silts), sands (*S*), gravels (*G*), pedogenically modified sediments (*P*), and bioclastic sediments (*B*). Table 3 details each lithofacies' descriptions and process interpretations, and Figure 10 presents field photographs of the KBS Member lithofacies encountered in the field during this study.

Table 3: *Individual KBS Member lithofacies classification and descriptions encountered during the study, and their sedimentary characteristics and process interpretations. This table corresponds with Figure 10 below.*

Code	Lithofacies	Description	Process interpretation
Fl	Interlaminated silt and clay	The *Fl*-lithofacies are characterised by finely interbedded or horizontal interlaminated silts and clays, defined by grain size and colour variation. Silt laminations are generally pinkish grey to very light grey (5YR 8/1 to N8) in colour, whereas clays are olive black to medium grey (5Y 2/1 to N5). *Fl*-lithofacies beds are laterally extensive throughout the KBS Member sequence. They occur as tabular or sheet-shaped bodies with a thickness ranging from 0.25 to 4 m until they become obscured by weathered material or grade into *Fm*-lithofacies. They are closely associated with *Fm*-lithofacies and are also often associated with silt to sand-lithofacies (as minor lithofacies). Additionally, *Fl*-lithofacies deposits consist of mammalian fossil hash assemblages, rhizoliths, bioturbation (burrowing) and carbonate nodules. See Figures 10 (A, B and C).	Slow suspension-fallout deposition of silt- and clay-sized grains on a planar surface due to periodic intersects of the water table and surface (Miall, 1977; 2006). Alternatively, during extremely low energy regimes, when weak traction currents transport incoming sediment; however, in higher energy regimes, high-density flows may be significant (Miall, 2006; Feibel, 2013). The close association between *Fl*- and *Fm*-lithofacies is due to the pulsed accumulation of fines (Feibel, 2013).

Fm	Massive mud	The *Fm*-lithofacies are characterised by moderately- to well-sorted massive mud sequences (no sedimentary structures) that appear olive black to medium grey (5Y 2/1 to N5) in colour. *Fm*-lithofacies beds are laterally extensive throughout the KBS Member as lens, sheet- or tabular-shaped bodies with a thickness ranging from 0.25 to 5 m. The beds are either soft or semi-indurated. Additionally, as mentioned above, these lithofacies always occur in close association with *Fl*-lithofacies and sand-lithofacies. These lithofacies deposits consist of fossil hash assemblages, rhizoliths, carbonate nodules, bioturbation (burrowing) and some desiccation cracks. See Figures 10 (B, C, and G). *Note: Mudstones with evident soil overprint are classified as part of the pedogenic lithofacies (P) category – Pv-lithofacies (silt or clay with pedogenic structures); however, they are part of the same lithofacies group as unaltered muds, which are Fm-lithofacies in this case (Feibel, 2013).*	Suspension-fallout deposition of mud-sized grains due to vertical settling as a function of low-density gravity flows from standing pools of water during low-stage channel abandonment with bottom currents (Miall, 1977). Alternatively, periodic high-density gravity underflows of rivers as a result of fair-weather and storm wave bases can be suggested for this lithofacies, representing a high-water table that experienced extensive rapid sedimentation and bioturbation (Rust 1978; Nutz *et al.*, 2020).

Sh	Horizontally bedded silt and/or sandstone	The *Sh*-lithofacies are characterised by horizontally laminated silts to very fine- and fine-grained moderate- to well-sorted sandstones. These have consistent horizontal laminations and streaming or parting lineations that are defined by grain size and colour variations due to the common nature of the sequence. In the field, outcrop surfaces are moderate pink, greyish pink, moderate brown, moderate reddish orange to greyish yellow (5R 7/4, 5R 8/2, 5YR 4/4, 10R 6/6 to 5Y 5/4) in colour. In contrast, fresh surfaces are pale yellowish orange to moderate yellowish green (10YR 8/6 to 5Y 7/6). The *Sh*-lithofacies are the most frequent sand-lithofacies in the KBS Member sequence. Its beds appear as soft or indurated tabular sheets finning upwards, with thicknesses ranging from 0.25 to 4 m. Additionally, the beds frequently have sharp lower-bounding surfaces. Over a few metres, the lithofacies often grade into other sand-lithofacies (laterally and vertically) – occurring in close association with all other sand-lithofacies or occurring between non-sand-lithofacies. The *Sh*-lithofacies deposits consist of mammalian fossil hash assemblages, rhizoliths and bioturbation (burrowing).	Subcritical to supercritical upper plane bed flows; however, the *Sh*-lithofacies can also occur at lower flow velocities at shallower depths (Miall, 2006; Miall, 1977). Additionally, the *Sh*-lithofacies in stable regions are associated with standard depositional rates without sand deposits producing ripples or dunes (*Sr*-lithofacies) (Wang, 2018; Miall, 2006).

		See Figures 10 (D, E, K and O).	
St	Trough cross-bedded sandstone	The *St*-lithofacies is characterised by trough cross-bedded fine- to medium-grained moderately sorted sandstones with occasionally minimal quantities of light olive grey (5Y 5/2) fine silt draping between foresets, defining the troughs. In the field, exposed outcrop surfaces of *St*-lithofacies range from moderate pink, greyish pink, moderate brown, and moderate reddish orange to greyish yellow (5R 7/4, 5R 8/2, 5YR 4/4, 10R 6/6 to 5Y 5/4). In contrast, St-lithofacies fresh surfaces range from pale yellowish orange to moderate yellowish green (10YR 8/6 to 5Y 7/6). *St*-lithofacies sandstones are common throughout the KBS Member sequence with laterally extensive truncated or curved bounding surfaces, with thicknesses ranging from 0.5 to 6 m depending on the bedform magnitude. These sediments are indurated and soft with fining- and coarsening-upward successions defined by angled foresets with planar surfaces separating each bed and preceded by curved laminae, forming shallow 'U' shape geometries.	Migration of three-dimensional sinuous to linguoid crested dunes that experienced lee deposition and stoss erosion under moderate- to high-flow velocities in lower-flow regime conditions – deeper sections of channels where there is fast-flowing water (Miall, 1977). During maximum flooding, troughs are scraped into sedimentary beds and filled by migrating dune-waning flows (Wilson *et al.*, 2014).

		The *St*-lithofacies deposits consist of mammalian fossil hash assemblages, rhizoliths and bioturbation (burrowing). See Figures 10 (F and G).	
Sr	Ripple cross-laminated sandstone	The *Sr*-lithofacies is characterised by ripple cross-bedded fine- to medium-grained moderately to well-sorted sandstones, displaying olive grey (5Y 5/2) silt-draped foresets in greyish pink, pale red, greyish orange pink to very pale orange (5R 8/2, 5R 6/2 or 10R 6/2, 10R 8/2 and 10YR 8/2, respectively) coloured sand in the outcrop, and yellowish grey, pale yellowish green, pale green, greenish grey to medium light grey sand (5Y 8/1, 10GY 7/2, 10G 6/2, 5G 6/1, and N6, respectively) in fresh surfaces. *Sr*-lithofacies beds are laterally extensive throughout the KBS Member sequence. They are as indurated or soft with thickness ranging from 0.5 to 5 m depending on the bedform magnitude, with an upward-fining succession. *Sr*-lithofacies' sedimentary structure is defined by laminae that down-lap onto the surrounding surfaces, producing a laminate with apparent symmetrical and traverse ripples. These lithofacies usually occur with other sand-lithofacies and undergo a	Migration of several asymmetric ripples in lower flow regimes during oscillatory or a combination of oscillatory and unidirectional flows when there are deteriorating flow velocities and channel levels (Wilson *et al.*, 2014; Miall, 2003).

		vertical transition into *St*-lithofacies (rib and furrow structures). *Sr*-lithofacies deposits consist of mammalian fossil assemblages and rhizoliths. See Figures 10 (E, H, I, K, and L); Figure 18 (B).	
Sp	Planar cross-bedded sandstone	The *Sp*-lithofacies are characterised by planar cross-bedded coarse- to medium-grained poorly- to moderately sorted sandstones with shallow angled foresets (~20-30°) and planar surfaces separating each bed. In the field, *Sp*-lithofacies outcrop surfaces are moderate pink, greyish pink, moderate brown, moderate reddish-orange to greyish yellow (5R 7/4, 5R 8/2, 5YR 4/4, 10R 6/6 to 5Y 5/4) in colour, similar to that of *Sh*- and *St*-lithofacies; whereas, *Sp*-lithofacies fresh surfaces are pale yellowish orange to moderate yellow-green (10YR 8/6 to 5Y 7/6) or light to pale brown, very pale orange and pale yellowish brown (5YR 6/4, 5YR 5/2, 10YR 8/2 and 10YR 6/2). *Sp*-lithofacies beds are laterally extensive throughout the KBS Member sequence as both indurated and soft vertically and laterally stacked tabular or wedge-shaped sedimentary	Down-current migration of two-dimensional linear or sinuous dunes as bed load (lee deposition and stoss erosion) under lower flow regimes in deeper channel sections and fast-flowing moderately to low flow velocity conditions (Wilson *et al.*, 2014).

		beds with growth or migration trajectories in the lee-foreset dip direction (down depositional dip direction), coarsening-upward with thickness ranges from 0.5 to 6 m. Additionally, this lithofacies is associated with other sand-lithofacies. *Sp*-lithofacies deposits consist of mammalian fossils, rhizoliths and bioturbation (burrowing). See Figures 10 (J, K, and L); Figure 18 (A)	
Gms	Matrix-supported stratified gravel	The *Gms*-lithofacies are characterised by matrix-supported stratified gravels with a wide grain size range of cobbles and pebbles that are moderately to poorly sorted. However, the overall clast-to-matrix ratio varies in proportion due to the lithofacies' highly varying matrix content, whereby some zones and layers in this lithofacies appear to be clast-supported. The *Gms*-lithofacies are also defined by colour variations due to the common nature of the sequence. In the field, *Gms*-lithofacies outcrop surfaces are pale yellowish orange, moderate yellowish brown to brownish black (10YR 8/6, 10YR 5/4 to 5YR 2/1) in colour. In contrast, fresh surfaces	Turbulent density flows that occasionally result in suspension settling, thus facilitating sediment sorting and mud interbed deposition, under constrained rapidly declining flow regimes due to high-strength debris flow deposition (Miall, 2006; Nutz *et al.*, 2020). Clasts roundness suggests that clast transportation was sustained over long distances in relation to time (Reading, 2009). Additionally, the absence of large-size grains, imbrication and bedding is

		are very pale orange, pale yellowish orange to yellowish grey (10YR 8/2, 10YR 8/6 to 5Y 8/1). *Gms*-lithofacies beds are uncommon in the KBS Member sequence and do not have any sedimentary structures (massive); however, they can be associated with crude planar laminations. Additionally, the beds occur as finning- or coarsening-upwards heterolithic discontinuous units below sand-lithofacies with a thickness ranging from 0.5 to 7 m, forming isolated pods lenses or pods within erosional scours. *Gms*-lithofacies deposits consist of mammalian and fish fossil hash assemblages. See Figures 10 (M).	due to rapid deposition with declining flow velocity (Reading, 2009).
Gp	Planar-cross bedded gravel	The *Gp*-lithofacies are characterised by heterometric clast-supported conglomerates with an average grain size of granule to pebble and a moderate- to poorly sorted grain size distribution. The clasts often have medium to high sphericity and are rounded to sub-rounded. In the field, *Gp*-lithofacies outcrop surfaces are pale yellowish orange, moderate yellowish brown to brownish black (10YR 8/6, 10YR 5/4 to 5YR 2/1) in colour. In contrast,	Bedding formation suggests long-lived, consistent linguoid bars and bar accretion flows (Feibel, 2013; Wilson *et al.*, 2014). Carbonate nodule inclusions from adjacent soils suggest open channels during occasional discharge episodes of substantial magnitudes (Feibel, 2013).

		its fresh surfaces are moderate orange-pink, pale yellowish orange, dark yellowish orange to dusky yellowish brown (5Y 8/4, 10YR 8/6, 10YR 6/6 to 10YR 2/2). *Gp*-lithofacies beds are massive thick tabular or wedge-shaped upward-coarsening stratified sequences in planar or cross-bedded geometry, with a thickness ranging from 0.125 to 4 m. The massive nature of the deposit is a significant feature, and the gain size and shape characteristics of granules or pebbles frequently produce weak or absent stratification. *Gp*-lithofacies deposits comprise mammalian fossil hash assemblages, rhizoliths, and carbonate nodules inclusions. See Figures 10 (N).	
Pcc	Pedogenic carbonate	The *Pcc*-lithofacies are characterised by coarsening-upward massive and very well-sorted homogenous muds with calcareous nodules of varying sizes and shapes (irregular); however, the matrix can be weakly laminated. *Pcc*-lithofacies beds are laterally extensive throughout the KBS Member sequence with a thickness that ranges from 0.125 to 6 m.	These lithofacies are produced by pedogenic processes driven by precipitation of carbonates in soil horizons during fluctuations of water tables in moderate flow regimes (Miall, 2006; Wilson *et al.*, 2014). Additionally,

		In the field, the *Pcc*-lithofacies matrix colour is olive black to medium grey (5Y 2/1 to N5), and the nodules are very pale orange to greyish yellow (10YR 8/2 to 5Y 8/4). The matrix is well-indurated and consists of mammalian fossils, fauna bioturbation, rhizoliths and slicken slides. See Figures 10 (N, O, and P).	extensive bioturbation contributes to the absence of these lithofacies (Miall, 2006).
Pv	Silt or clay with Pedogenic structures	The *Pv*-lithofacies are characterised by fining upwards moderately- to well-sorted massive silts/muds with calcareous nodules, slickensides and desiccation cracks. Its matrix colour varies from dark brown to pale yellowish brown (10R 4/3 to 10R 6/2). *Pv*-lithofacies deposits are semi-indurated, allowing for preferential weathering, and consist of mammalian fossil assemblages and rhizoliths. In addition, *Pv*-lithofacies are associated with mud- and silt/sand-lithofacies. See Figures 10 (G, I, L, and M).	Produced by pedogenic processes in lower sedimentation rates (Kraus, 2002; Muller, 2004; Feibel, 2013). The dark brown deposits can be attributed to high organic content (Smith *et al.*, 2008), and the matrix colour variety indicates soil moisture availability (Kraus, 1999). Precipitation during the soil horizon is significant for carbonate nodule formation (Wilson *et al.*, 2014).

Bm	Molluscan carbonate (Siliceous bioclastic carbonate)	The *Bm*-lithofacies are characterised by skeletal material produced by numerous organisms, specifically mollusca (Bivalvia and Gastropoda) shells. The shell size and colour vary. Bivalvian shells are typically larger than Gastropoda and are either moderate yellowish brown, white, very light grey, or dark grey (10YR 5/4, N9, N8 or N3). The *Bm*-lithofacies beds are laterally extensive throughout the KBS Member sequence with a thickness ranging from 0.125 to 3 m. The beds are lithologically defined by poorly- to moderately sorted wide grain size range packed clast-supported sandstone, packstone or rudstone. Additionally, *Bm*-lithofacies beds are massive and consist of bioturbation (burrowing); however, imbricated and weakly bedded deposits are observed. In the field, *Bm*-lithofacies are usually associated with silt/sand-lithofacies. See Figures 10 (L, P, and Q).	Through bedload or suspension during fluctuating high-energy current conditions (Bowen, 1974; Schieber, 2012).

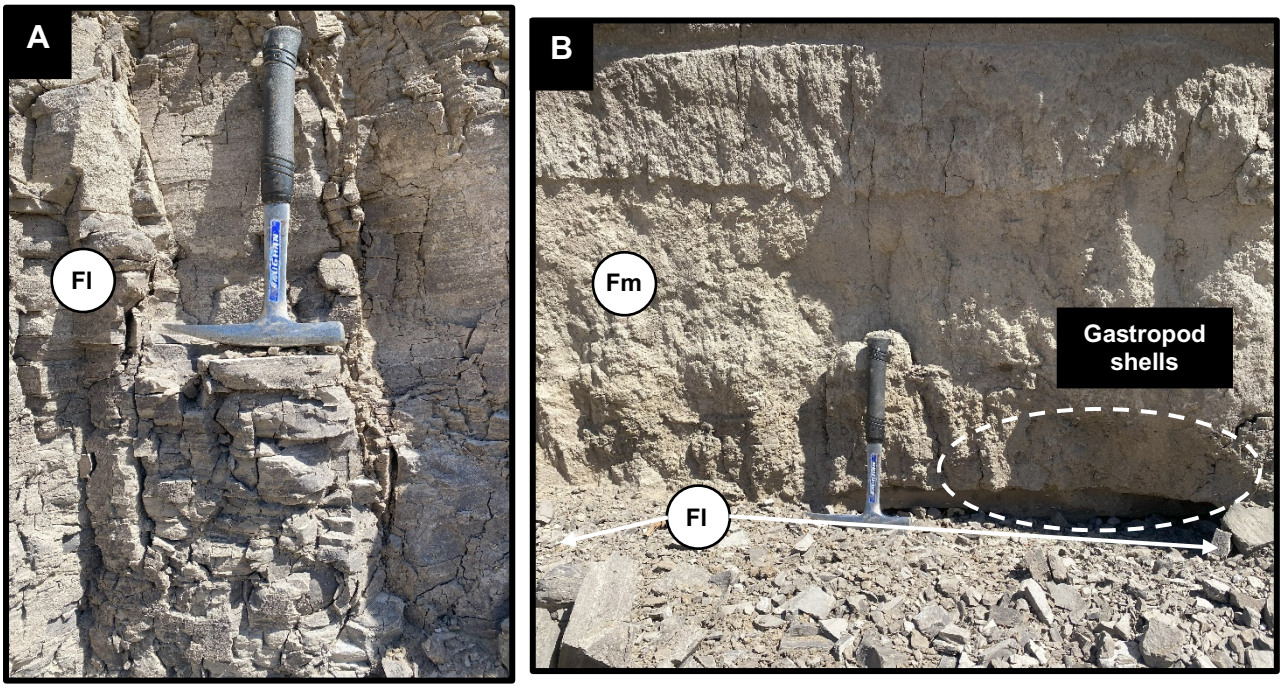

Figure 10: *Representative lithofacies found in the KBS Member of the Koobi Fora Formation.* ***(A)*** *Interlaminated silt and clay (Fl).* ***(B)*** *Massive mud (Fm) with gastropod fossil hash assemblages and collapsed Fl-lithofacies on the surface.* ***(C)*** *Gradational depositional contact between the Fl-lithofacies and the underlying Fm-lithofacies. Photographs A, B, and C were taken and measured at Area 102 in the Base Camp subregion.* ***(D)*** *Horizontally bedded sandstone (Sh) overlying KBS Tuff. The photograph was taken and measured at Area 105 in the Karari subregion.* ***(E)*** *Horizontally bedded sandstone (Sh) overlying reworked KBS Tuff in an erosional depositional contact, with an assemblage of ripple cross-laminated sandstone. The photograph was taken and measured at Area 104 in the Base Camp subregion.* ***(F)*** *Trough cross-bedded sandstone (St). The photograph was taken and measured at Area 9 in the Ileret subregion.* ***(G)*** *St-lithofacies interbedded between Fm-lithofacies in erosional depositional contacts with silt or clay with pedogenic structures (Pv) as minor facies on the overlying bed. The photograph was taken and measured at Area 12 in the Ileret subregion.* ***(H)*** *Ripple cross-laminated sandstone (Sr). The photograph was taken and measured at Area 13 in the Ileret subregion.* ***(I)*** *Sr-lithofacies overlying Pv-facies in an erosional depositional contact. The photograph was taken and measured at Area 10 in the Ileret subregion.* ***(J)*** *Planar cross-bedded sandstone (Sp). The photograph was taken and measured at Area 6A in the Ileret subregion.* ***(K)*** *Sp-lithofacies alongside other sandstone facies (Sr and Sh), consisting of rhizoliths and bioturbation (burrowing). The photograph was taken and measured at Area 10 in the Ileret subregion.* ***(L)*** *Various lithofacies (Sp, Sr, Pv, Bm) in close association overlying a reworked KBS Tuff. The photograph was taken and measured at Area 13 in the Ileret subregion.* ***(M)*** *Matrix-supported stratified gravel (Gms) overlying Pv-lithofacies that overlie reworked KBS Tuff, all in erosional depositional contacts.* ***(N)*** *Planar-cross bedded gravel (Gp) overlying the pedogenic carbonate lithofacies (Pcc) in an erosional depositional contact. Photographs M and N were taken and measured at Area 8A in the Ileret subregion.* ***(O)*** *Pcc-lithofacies with calcareous nodules underlying Sh-lithofacies. The photograph was taken and measured at Area 105 in the Karari subregion.* ***(P)*** *Molluscan carbonate – siliceous bioclastic carbonate (Bm) dominated by bivalve shells, alongside Pcc-lithofacies.* ***(Q)*** *Exposure of the Bm-lithofacies dominated by gastropod shells, alongside Pcc-lithofacies. Photographs P and Q were taken and measured at Area 10 in the Ileret subregion. This figure corresponds with Table 3 above.*

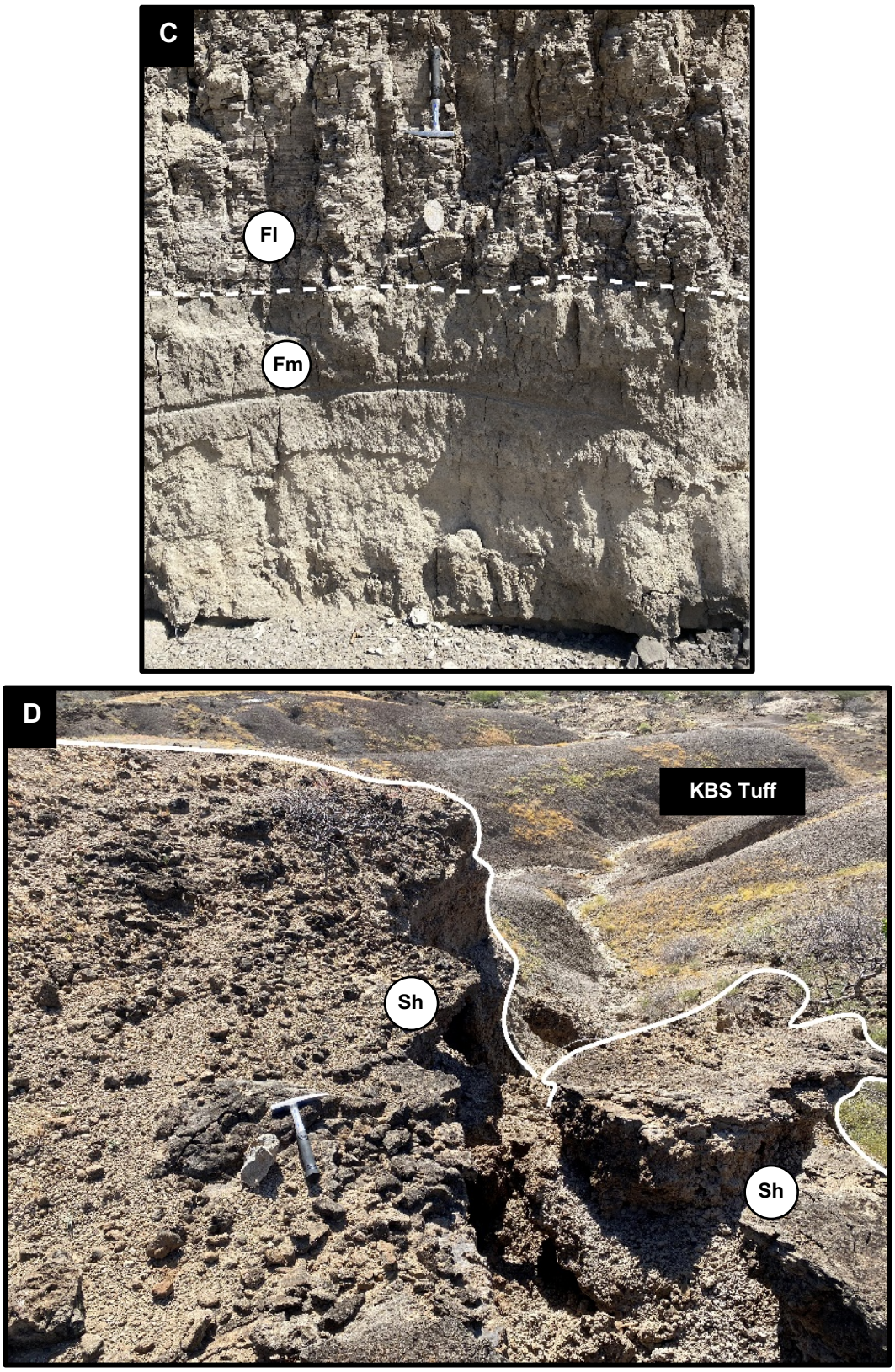

Figure 10**:** *(continued).*

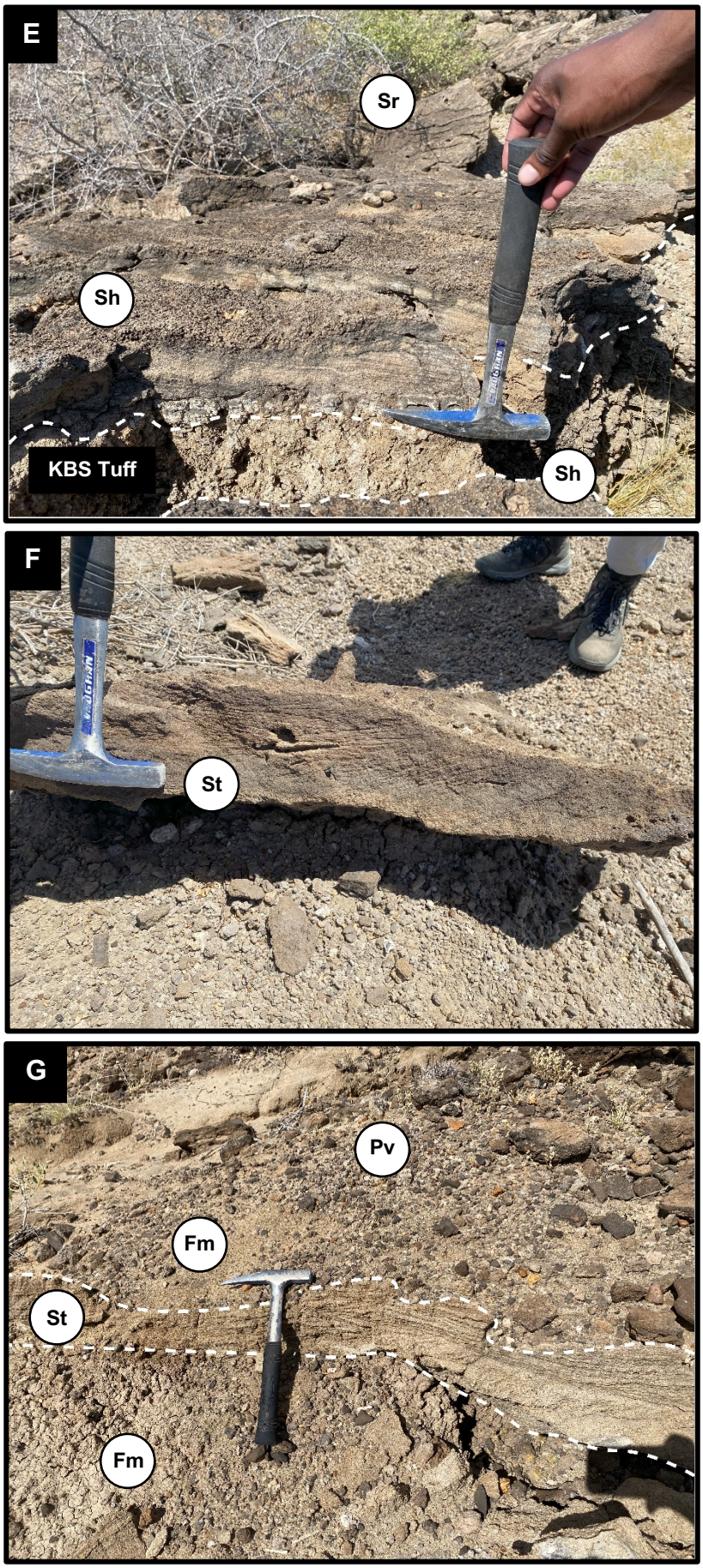

Figure 10: *(continued).*

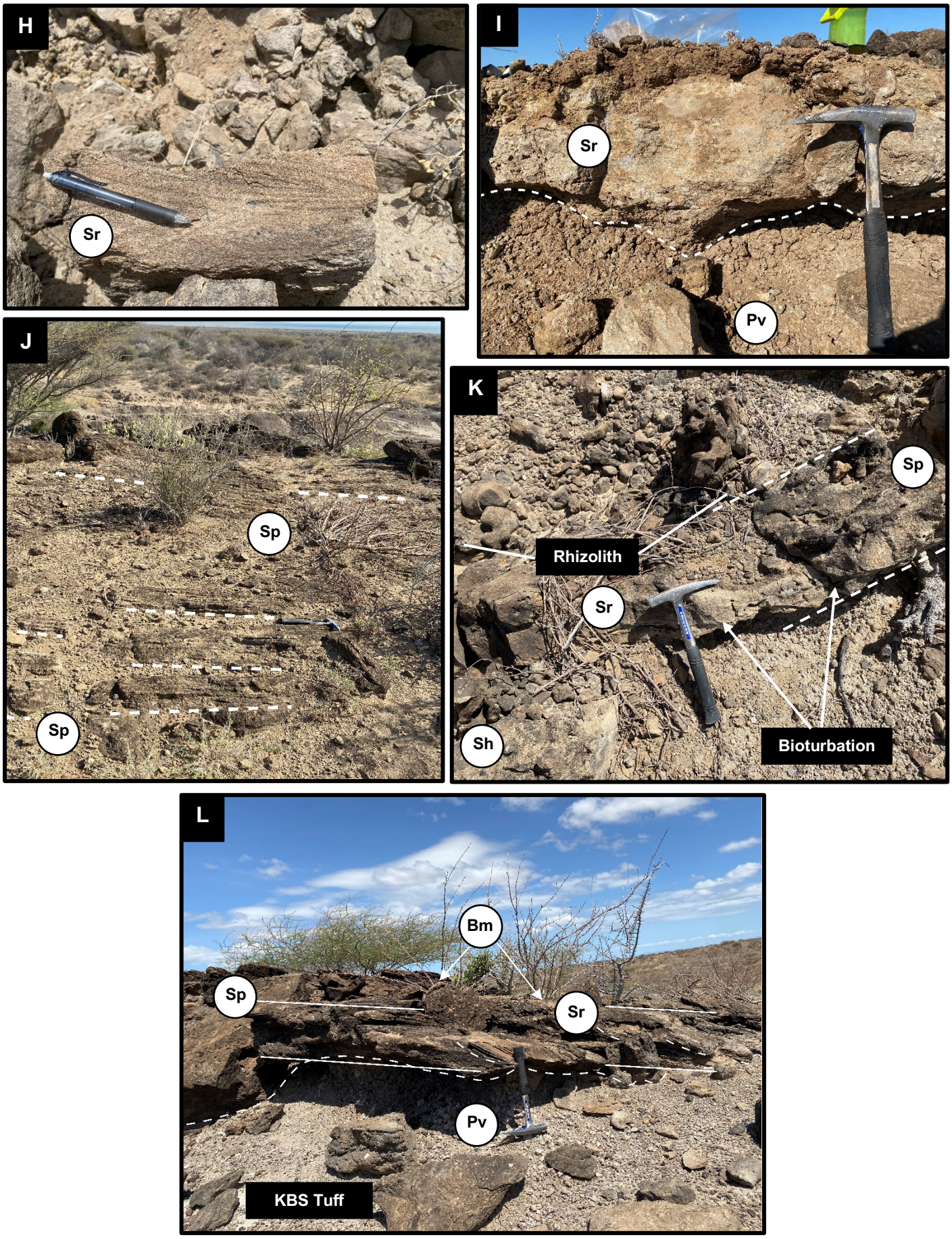

Figure 10: *(continued).*

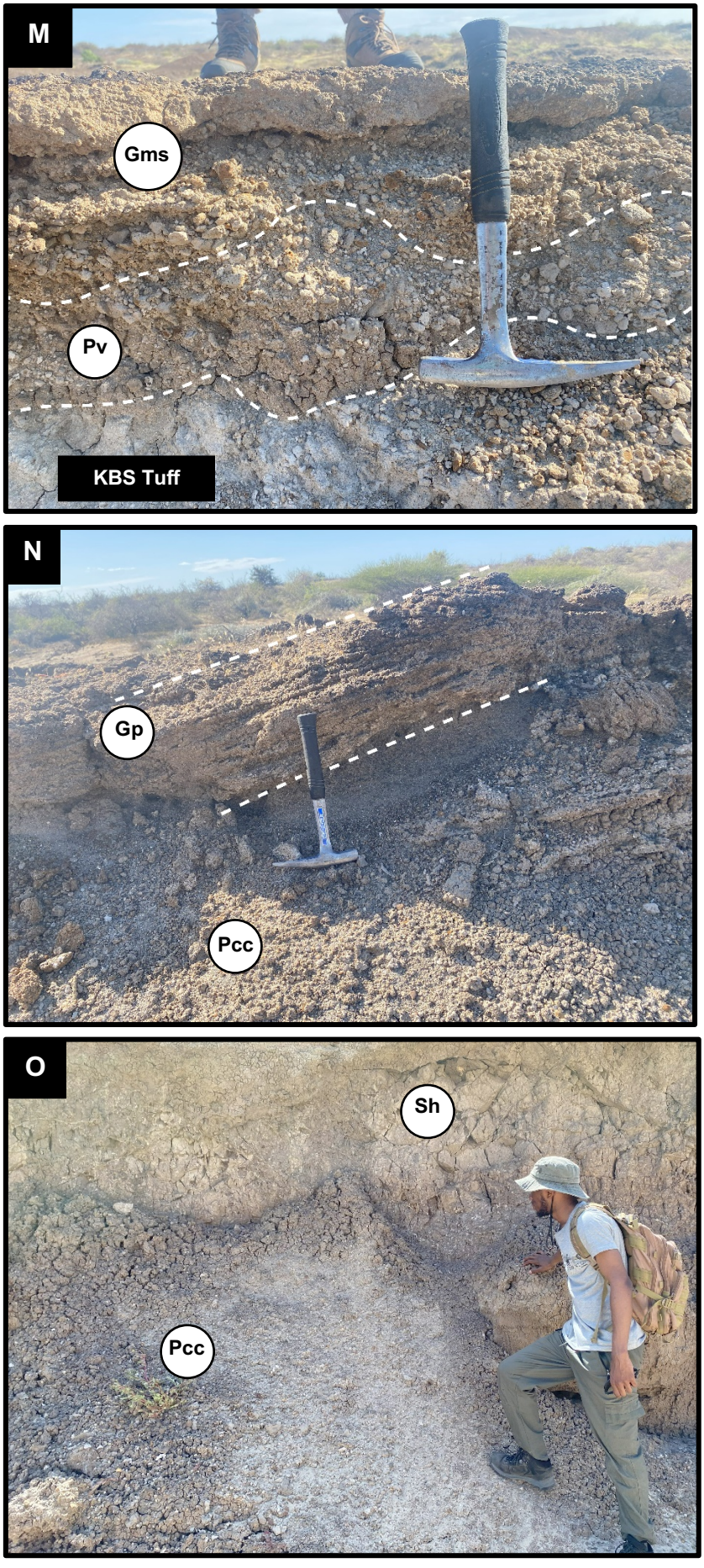

Figure 10: *(continued).*

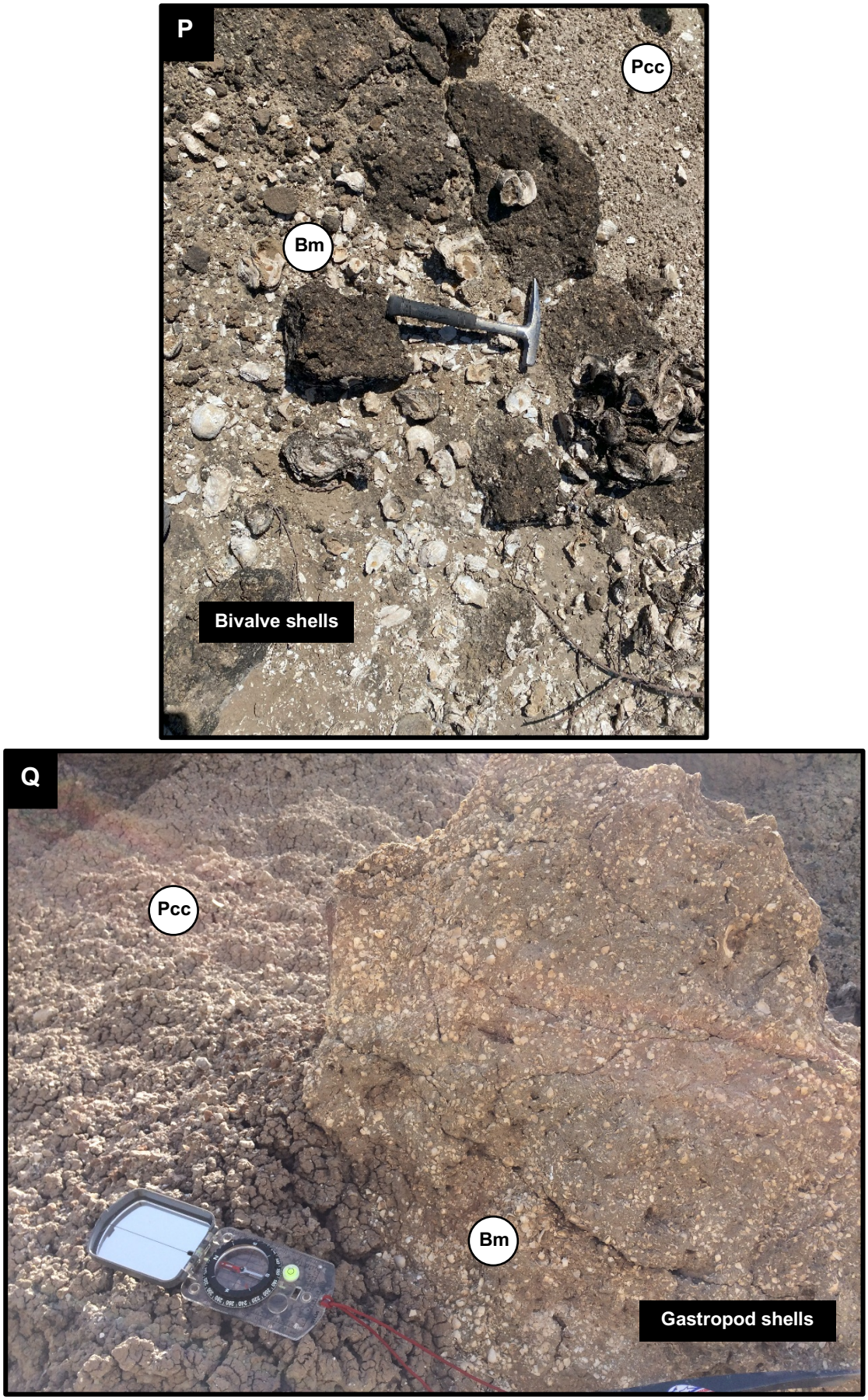

Figure 10: *(continued).*

5.1.2. Lithofacies associations (descriptions and interpretations)

The standardised grouping of lithofacies into lithofacies associations (*FA*) demonstrates a crucial methodologic expansion from identified sedimentary elements to genetically significant sedimentary sequences that characterise palaeo-environmental landscapes (Feibel, 2013). The eleven identified KBS Member lithofacies mentioned in Table 3 are categorised into five *FA* groups; these include meandering fluvial channels (*FA1*), fluvial floodplains (F*A2*), marginal lacustrine (*FA3*), deltas (prodeltaic and delta fronts) (*FA4*) and crevasse splays (*FA5*) (Table 4). The following discussion uses field observations to demonstrate *FA's* distinctive characteristics and interpretations.

Table 4: *Lithofacies associations (FA) applied to the KBS Member, Koobi Fora Formation deposits (after Feibel, 1988; Gathogo and Brown, 2006; Feibel, 2013).*

lithofacies Association Code (FA)	Dominant lithofacies	Minor lithofacies	Palaeoenvironment
FA1	*St, Sp, Sh, Sr*	*Gms, Gp, Bm*	Meandering Fluvial Channel
FA2	*Fm, Pv*	*Pcc*	Fluvial Floodplain
FA3	*Fm, Fl, Bm, Pv*	*Sp, Sr, St*	Marginal Lacustrine
FA4	*Fl, Fm*	*St, Sr*	Prodeltaic and Delta Front
FA5	*Fl, Pv*	*Sr*	Crevasse Splay

5.1.2.1. Fluvial lithofacies associations — FA1 and FA2

Approximately half of the KFF consists of fluvial deposits (Feibel, 1988). These deposits in the KBS Member are classified into two distinct lithofacies associations. The first lithofacies association predominantly comprises coarse- to medium-grained deposits accumulated in fluvial meandering channels (*FA1*). These deposits are common throughout the KBS Member. Fine-grained deposits representing fluvial

floodplain lithofacies association (*FA2*) alongside *FA1* deposits define the second lithofacies association.

5.1.2.1.1. Meandering fluvial channel lithofacies association — FA1

The KBS Member *FA1* depositional sequences start with basal erosional scour surfaces that are approximately 10 to 50 cm, filled by thin lenticular accumulations of gravel lags (mud/clay pebble and granule-sized clasts) that display *Gms*- and *Gp*-lithofacies (Figures 11 and 12). These gravel basal erosional scours predominantly grade into moderately sorted bedded sandstones that are overlain by silts to finer-grained sands (point bar sequence) with upward-finning successions, displaying sand-lithofacies (*St, Sh, Sr,* and *Sp*) and carbonate nodule inclusions (Figures 11 and 12). The upward fining couplets of point bar sequences are observed as being defined by cross-bedding lithofacies that grade into localised laminated lithofacies (Figures 11 and 12). The *FA1* depositional sequences also comprise fragmented bioclastic packstones (*Bivalvia*) (*Bm*-lithofacies) as minor lithofacies. There are also evident stratification features destroyed by bioturbation or truncation in a sequence overlain by the same characterised sequence due to a succeeding channel. In addition, these deposits are further overlain by fine-grained floodplain deposits (*FA2*) or, in the opposite order, defined by erosional surfaces from *FA2* to *FA1* (Figures 11 and 12).

The FA1 depositional sequences are suggested to have been deposited in fluvial meandering rivers with over-bank deposits due to the observed point bar successions (Miall, 1996). This is further supported by palaeocurrent evidence. It is important to note that point bar successions may also develop in low-sinuosity rivers; however, palaeocurrent data show consistent variations in flow directions perpendicular to the point bar lateral accretion surfaces (Figure 19). This pattern is consistent with fluvial meandering rivers (Allen, 1963). The overall clasts of these deposits indicate relatively short transportation periods defined by the degree of clast rounding (angular to subangular) and the gravel lag deposits suggest declining flows on the scour surfaces near the thalweg (Reading, 1996). The observed sedimentary structures represent various fluvial flow regimes and positions in fluvial systems (Reading, 1996).

Carbonates suggest eroded floodplain nodules (Allen, 1964), and the upward fining successions indicate overbank flows of silts and fine-grained sands (Allen, 1964).

5.1.2.1.2. Fluvial floodplain lithofacies association — FA2

FA2 deposits occur abruptly superposed on *FA1* sequences throughout the formation (KBS Member) with varying thicknesses (~10 m) (Figures 11 and 12). These deposits are defined by fine-grained massive silts and clays (*Fm*) with extensive bioturbation, mud cracks, soft sediment deformation, and some colour variations (reds, browns, and greys) in a single subregion and between subregions due to pedogenesis (Figure 12). Additionally, the *FA2* deposits consist of abundant pedogenic alterations (*Pv*) and pedogenic carbonate concretions (*Pcc*) in locally prevalent surface lags (Figures 11 and 12); however, unlike the *FA3* deposits, these deposits lack molluscan bioclastic beds.

The *FA2* sedimentation is primarily driven by avulsion and overbank deposition at slow, constant sedimentation rates (Kraus, 1999; Miall, 2006; Muller, 2004). These deposits' fine-grained nature and sedimentation rate permitted the development of deposits comprising paleosols (Kraus, 1999). Pedogenic carbonate nodules are due to palaeosol precipitation in soil horizons, suggesting seasonal variations in water tables (Mack *et al.*, 1993). In addition, the colour variation of these deposits is due to minerals such as goethite and haematite, which display red colouration, and the brown and grey colouration is due to high organic matter (Smith *et al.*, 2008).

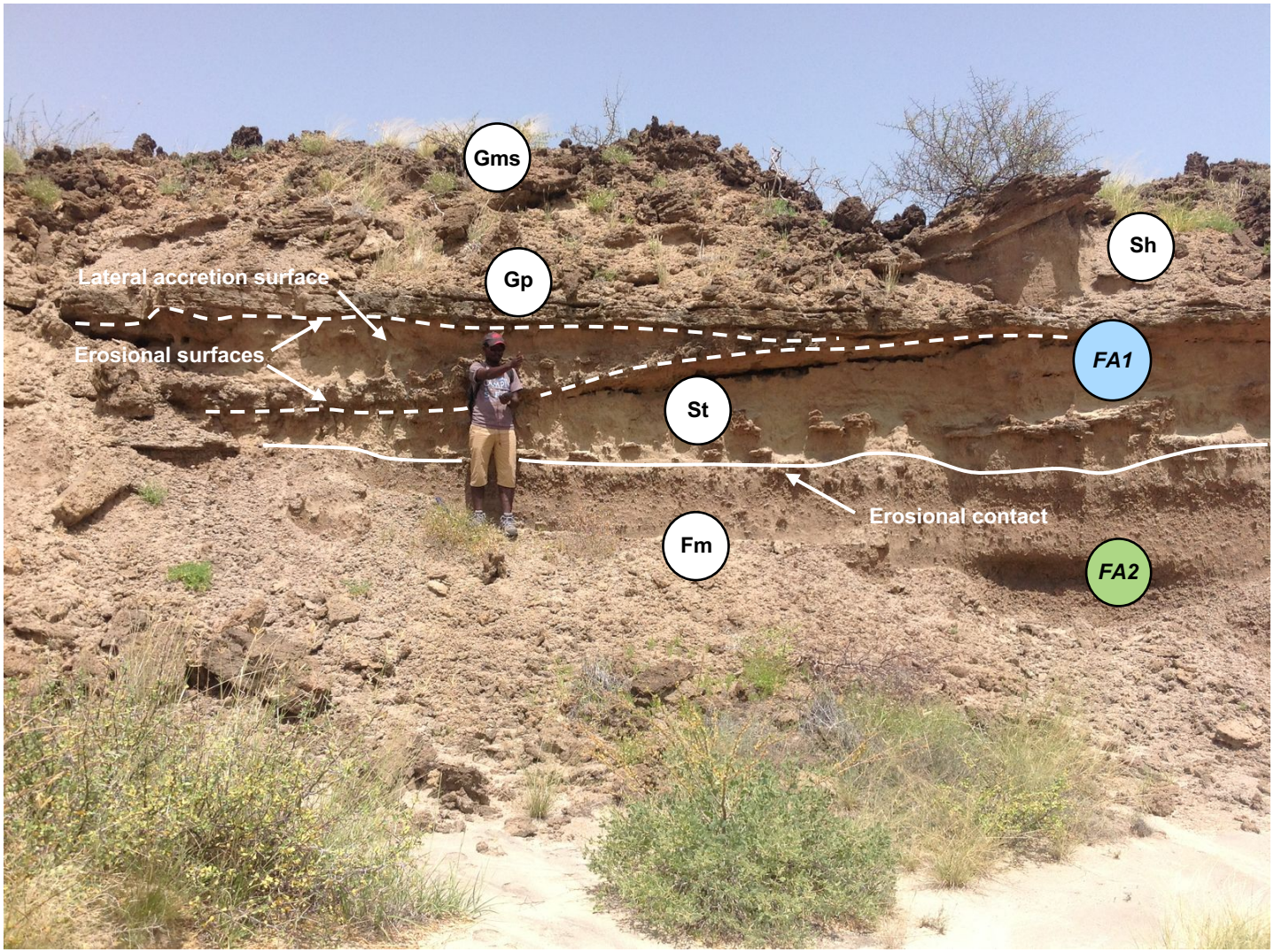

Figure 11: *Example of the KBS meandering fluvial lithofacies association (FA1) from the study locality. The FA1 exposure is defined by lateral accretion with erosive base and upward fining sequence and FA2 underlying an erosional contact of FA1. Scale: 178 cm.*

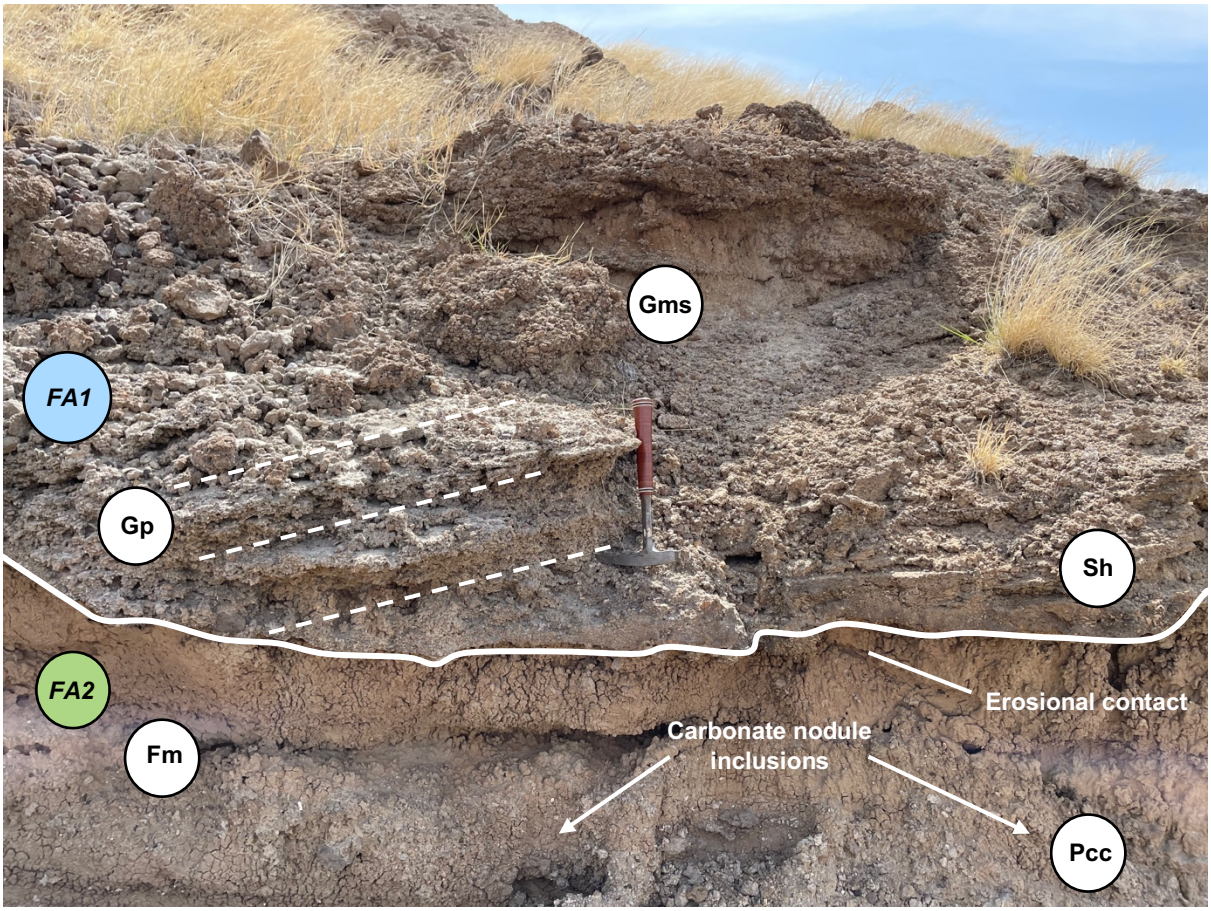

Figure 12: *FA2 pedogenic carbonates in a mudstone (Fm) underlying an erosional contact with FA1 that is defined by Sh, Gp and Gms.*

5.1.2.2. Marginal lacustrine lithofacies association — FA3

Approximately one-third of the KFF is defined by marginal lacustrine lithofacies association deposits (*FA3*) (Fiebel, 2013) with a high degree of arenaceous sediments, both clasts and biogenic material. These arenaceous sediments are demonstrated by a heterolithic assortment of sedimentary sequences, ranging from finer silt interbedded units (rhythmic and arrhythmic interbedding) to coarse-grained moderately to well-sorted sandstones and well-packed bioclastic sandstones (Figures 13 and 14). In the context of KBS Member, the *FA3* deposits are demonstrated by finer lithofacies assemblages (*Fl* and *Fm*), molluscan bioclastic beds (*Bm*), which grade into more arenaceous reworked shoreline sedimentary units with reworked molluscan bioclastic accumulations, locally well-developed pedogenic carbonates (*Pcc*) and pedogenic features as locally prevalent surface lags (*Pv*) (Figure 14). *FA3*

also consist of sandstone units that are characterised by planar lamination (*Sp*), trough cross-bedding (*St*), and ripple cross lamination (*Sr*) with ripple marks that are lenticular on the face profile (Figure 13). In addition, bioturbation that is microbially induced or sand-filled cracks is an additional *FA3* differentiating component.

The frequently close and constant heterogeneous lithofacies and interbedding observed in the *FA3* deposits are suggested to be a result of wave action in relatively high-energy environments to some extent (Fiebel, 2013; Miall, 2003). The well-sorted *FA3* sections and the apparent lenticular ripples imply oscillatory currents (Fiebel, 2013; Miall, 2003), and laminations depict dunes produced by traction currents in nearshore depositional environments (Clifton, 2006). The abundance of molluscan fossil assemblages suggests nearshore palaeoenvironments and the reworked molluscan assemblages suggest moderately high-energy environments, which is also supported by the predominant grain size throughout *FA3* deposits. Bioturbation in these deposits can be attributed to coastal flora or fauna processes (Clifton, 1971; Massari & Parea, 1988; Feibel, 2011; Nutz *et al.*, 2020). The *FA3* deposits have a high carbonate concentration, suggesting biogenic sources or the siliciclastic matrix, resulting in fragmented cementation (Feibel, 2013).

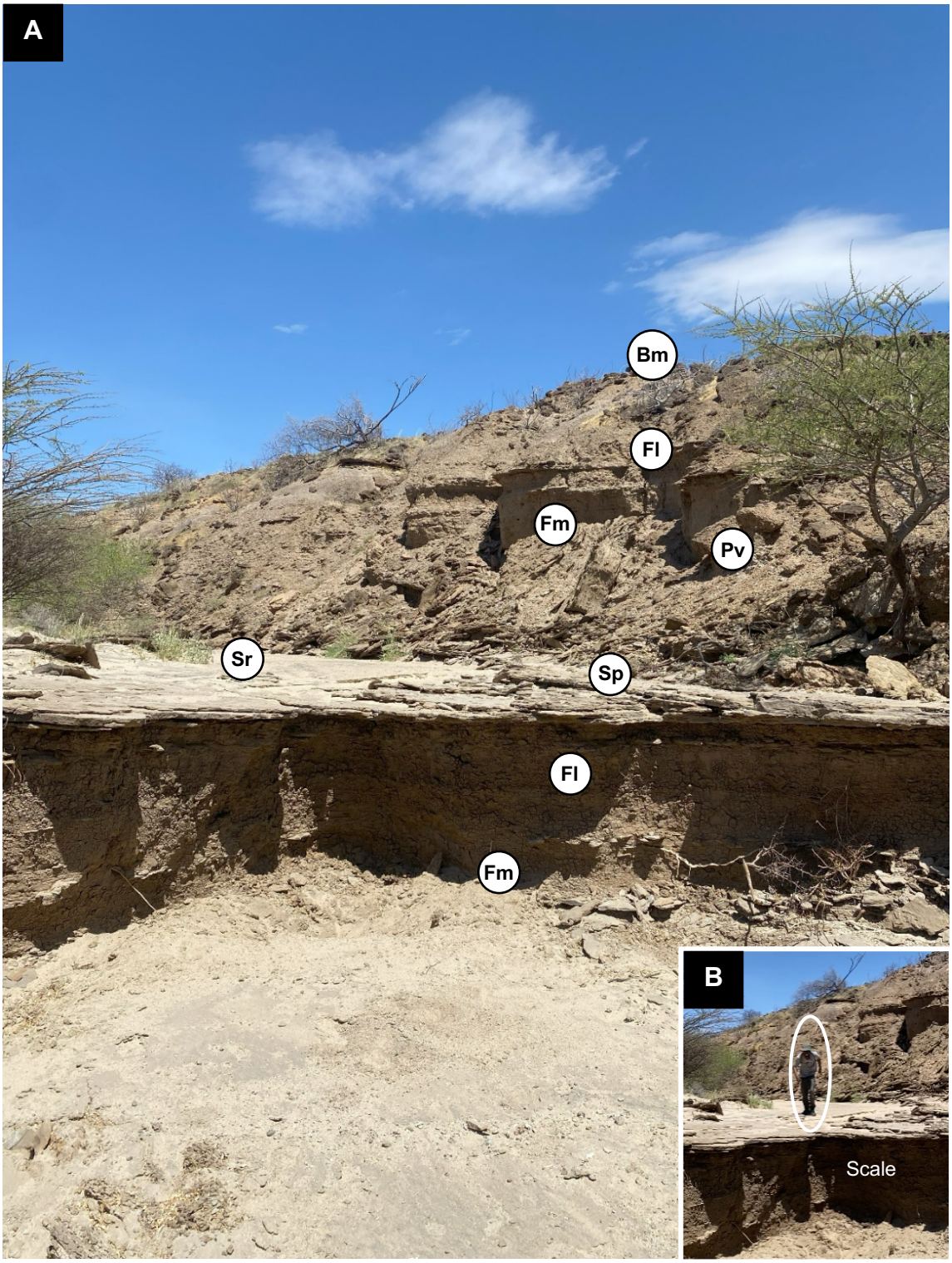

Figure 13: ***(A)*** *Example of the marginal lacustrine lithofacies association (FA3) from study locality. The FA3 is defined by sedimentary sequences that are heterolithic with the exception of well-packed bioclastic sandstones and are distinguished by a heterogeneous assortment of lithofacies.* ***(B)*** *The white circle represents a scale of 172cm.*

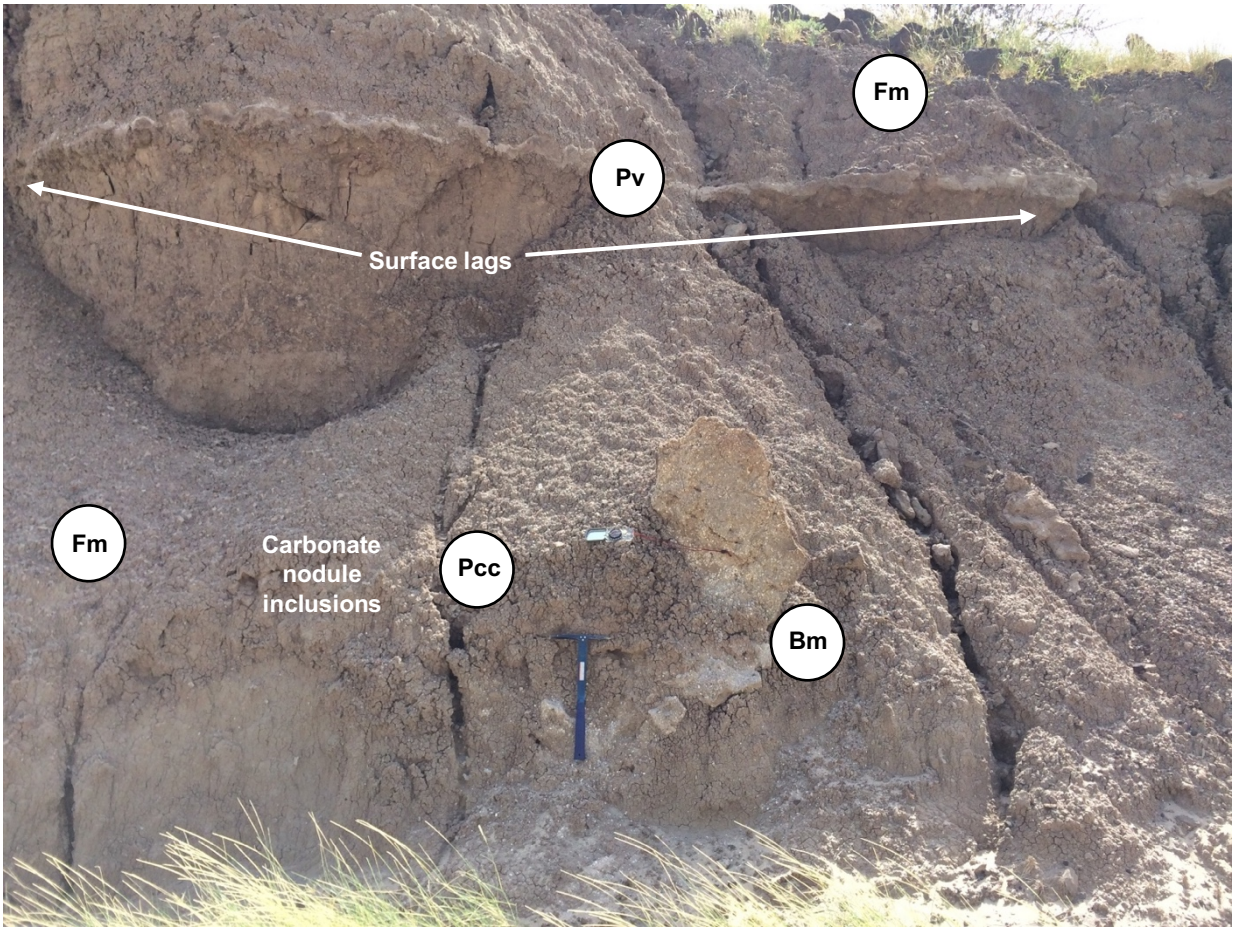

Figure 14: *FA3 outcrop defined by Fm, Pcc, Pv* as locally prevalent surface lags and as carbonate nodule inclusions *and some bioclastic units (Bm) protruding.*

5.1.2.3. Prodeltaic and delta front lithofacies association — FA4

Deltaic lithofacies association deposits (*FA4*) constitute approximately 20 percent of the KFF deposits (Fiebel, 2013), limiting them to the KBS Member time deposits, with thickness exposures ranging from 1–2 m. These deposits display a frequent grain size variation, ranging from fines (muds/sits) to very fine, poorly developed sands. The fine-grained clastic deposits are defined by upward coarsening planar lamination (*Fl*); however, the poorly developed sandy sequences have minor *St*- and *Sr*-lithofacies in upward coarsening thin and invariably planar laminated sand and silt sequence interbeds with mud inclusions (Figure 15). These deposits are overlain by oblique angle deposited sequences with sharp and gradational interlamination contacts, with some evidence of bioturbation. Massive fine-grained sequences (*Fm*) or delta-front

sands with carbonate concretions and desiccation cracks further overlain these laminated sediments. These *Fm* sedimentary units are soft-indurated, with evidence of erosion and weathering, and they also consist of bioturbation (burrows and trails) and some molluscan fossil hash assemblages (Figure 15).

The *FA4* frequent planar laminated fines result from low-energy suspension settling in the wave base of distant offshore settings during wave currents and storm periods (Goodbred and Saito, 2011), suggesting a seasonal detrital clastic material influx (Feibel, 1988). The coarsening upward sequences of fines into sands imply that the fines were deposited on a slope and the sands were deposited during storm events (Reading, 2009). Consequently, the storm events that transported the sand units can also be associated with the observed bioturbation and molluscan fossil hash assemblages (Goodbred and Saito, 2011). The mud inclusions suggest lacustrine delta front avalanching, which is related to shallow water flows (Schwartz, 1982; Neal *et al.*, 2003). Such channels result from the collapse of river effluent or mouth bar, demonstrating lower energy prodeltaic deposits (Johnson & Graham, 2004; Piper *et al.*, 1999; Hodgson, 2009; Fiebel, 2013). In addition, the carbonate inclusions in the sand units are suggested to be from delta front deposits exposed to subaerial conditions during low tides (Reading, 2009).

Figure 15: *Example of the prodeltaic and delta front lithofacies association (FA4) from study locality. The FA4 is defined by fine-grained clastics that are frequently planar laminated (Fl) with weakly developed asymmetrical and wavy lamination in coarser upward-fining units, poorly developed fine sandy sequences (St, Sr) with carbonate grains that are always thin and invariably planar laminated, and sand-silt sequences interbeds that are capped by sands and silts that have been bioturbated or massive fine-grained sequences (Fm) with carbonate concretions and desiccation cracks. Scale: 193 cm.*

5.1.2.4. Crevasse splay lithofacies association — FA5

Observed adjacent to fluvial deposits (*FA1* and *FA2*), the crevasse splay lithofacies association (*FA5*) is a second small-scale lithofacies association variant observed in the KBS Member-time deposits after *FA4*, displaying similar characteristics as the *FA4* deposits. In the field, the *FA5* deposits have a lateral extension of approximately 18 m, defined by thin rippling sand sections (*Sr*) that are coarsening upwards, represented by soft sediment deformation erosive contact, with laminated silts (*Fl*) and clays that display poorly developed pedogenic overprints (*Pv*) (Figure 16). Additionally,

carbonate concretions, desiccation cracks and sparse to intense bioturbation (burrows and trails) are occasionally observed in these deposits.

The *FA5* sedimentary successions provide evidence of rapid localised accumulations in relation to aggradational mud-rich systems (channel avulsion) and fluvial overbank successions (Feibel, 2013; Gulliford *et al.*, 2017). The *Fl*- and *Pv*-lithofacies demonstrate the crevasse splay position during recurring flood episodes on a relatively fixed parent fluvial channel belt (Gulliford *et al.*, 2014). The abundance of *Sr*-lithofacies represents rapid tractional deposition and sediment fallout during unconfined flows with moderate to low concentration in relation to rapid expansion and deposition (Allen, 1973; Gulliford *et al.*, 2014). In addition, the thin rippling sand sections (*Sr*) reflect adjacent fluvial channel avulsion and migration (Reading, 1996). In contrast, the soft sediment deformation erosive contact suggests seasonal flooding and rapid unstable aggradation with unconfined flows in *FA2* settings (Lepre, 2017).

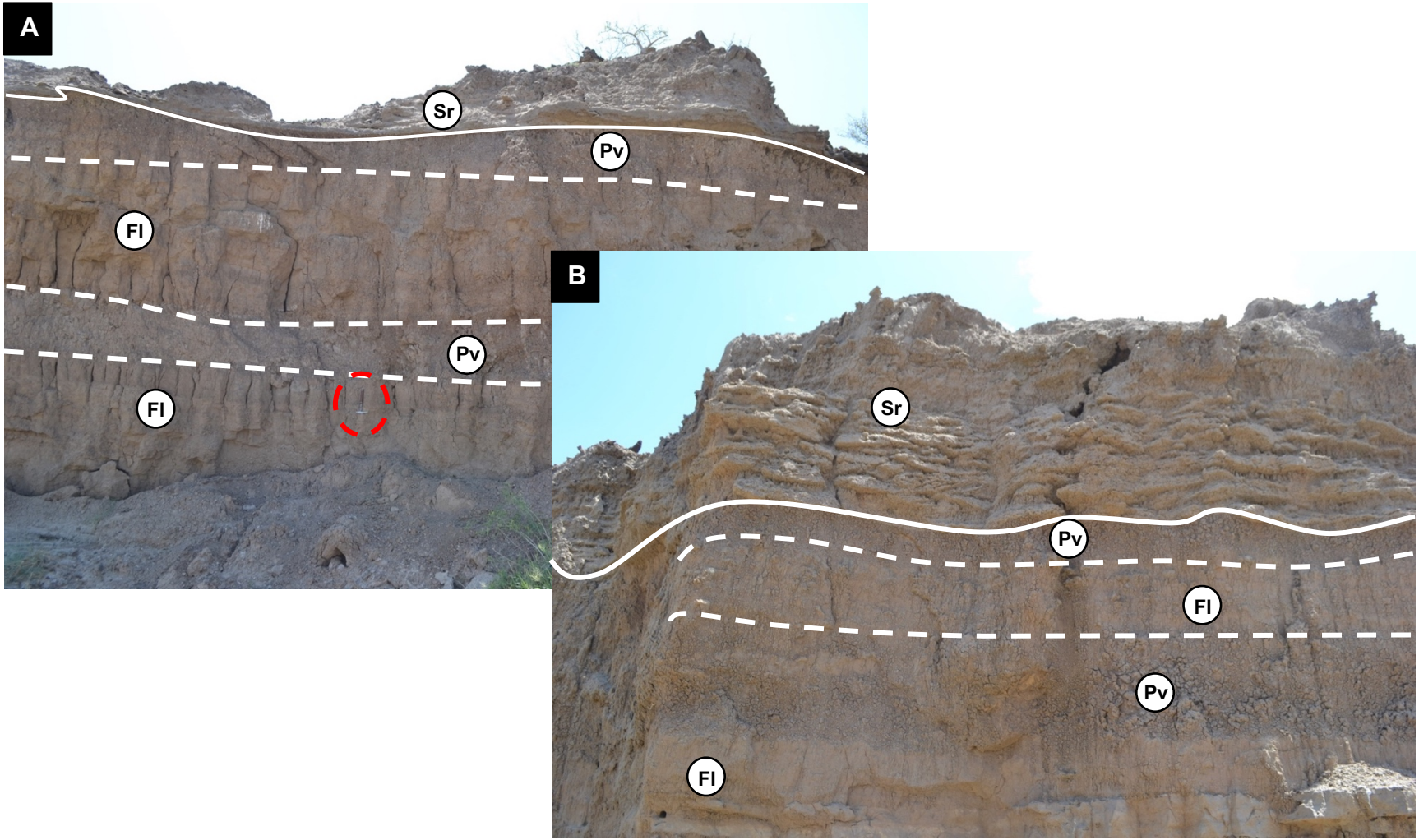

Figure 16: ***(A)*** *Example of the crevasse splay lithofacies association (FA5) from study locality. The FA5 is defined by thin rippling sand sections (Sr) that are coarsening upwards, representing by soft sediment deformation erosive contact, with laminated silts (Fl) and clays that display poorly developed pedogenic overprints (Pv). Geologic hammer (red circle) as scale.* ***(B)*** *A closeup of Figure 16A.*

5.2. Spatial correlation of KBS Member stratigraphic sections

Ten stratigraphic sections were measured and drawn (see Chapters 4.1 and 4.5) for the compassion of lithology, sedimentary structures and fossils, lithofacies, lithofacies association (depositional environments), palaeocurrents, petrography, and stratigraphy. Refer to Appendix G for each measured high-resolution stratigraphic section, with noted positions for rock sample and palaeocurrent reading collections. Descriptions and interpretations for the measured sections are presented in Chapter 6.5 as part of sequence stratigraphic modelling and quantifiable modelling of lake-level fluctuations. The stratigraphic sections were positioned from south to north of the KFF in relation to the modern lake and as well as the palaeolake (Brown & Feibel, 1991) and then spatially correlated using the KBS Tuff as a bounding surface (see Figure 17). Refer to Appendix H for Figure 17 in high resolution.

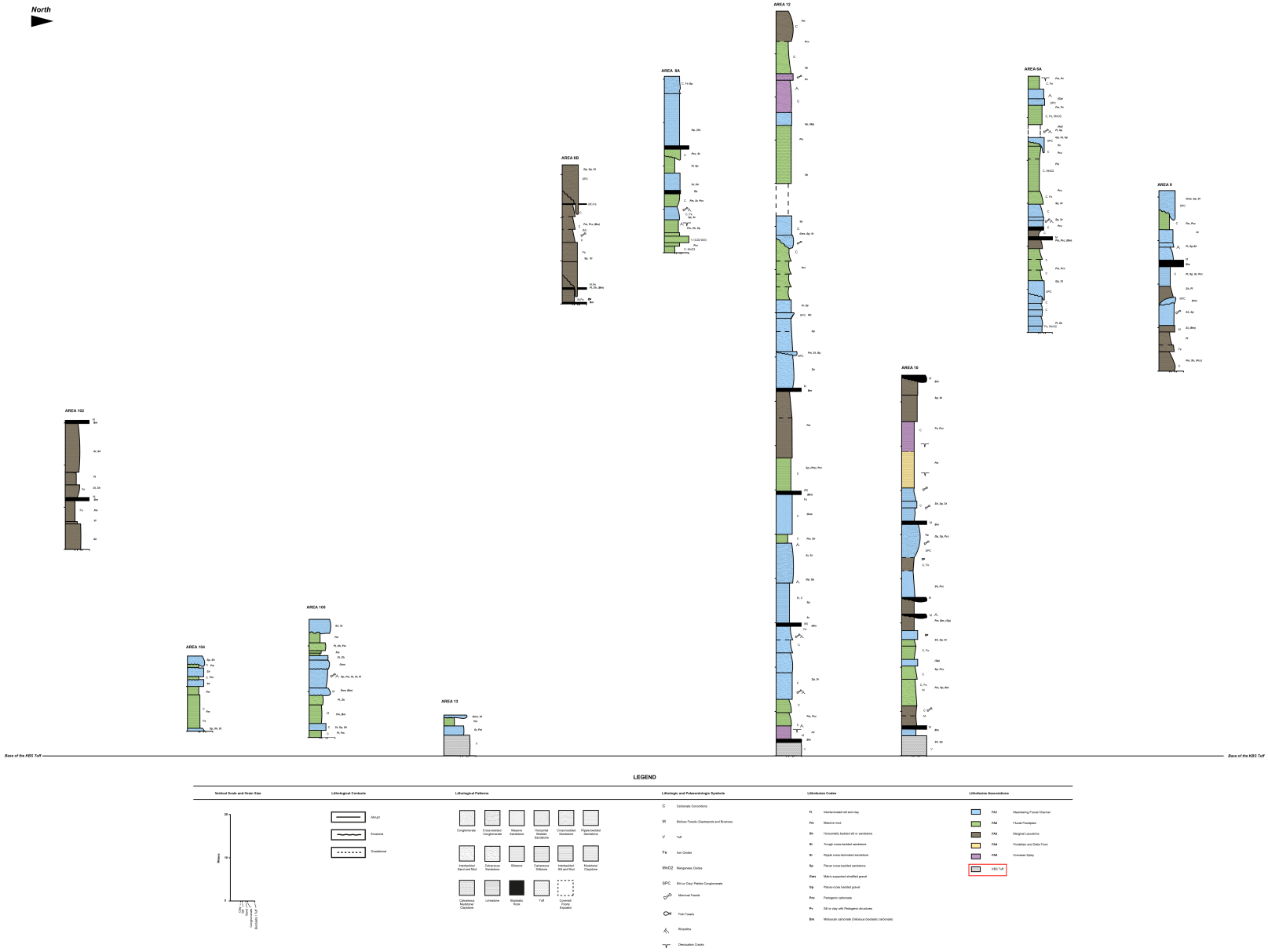

Figure 17: *Spatially correlated (measured) KBS Member stratigraphic sections. See locations in Figure 1B. Lithologies and sedimentary structures allowed the interpretation of five depositional environments. A high-resolution version of this figure is found in the Appendices section (Appendix H).*

5.3. KBS Member palaeocurrent data

Due to abundant KBS Member outcrop exposures with erosion-resistant lithologies, palaeocurrent indicators are well preserved in these deposits. The palaeocurrent vectors in this study were measured from planar cross-bedded and ripple cross-laminated (rib-and-furrow structures) sandstone deposits (Figure 18). These vector measurements are plotted as rose diagrams for all collection areas (Figure 19). Appendix E shows all raw palaeocurrent data collected from the field sites. This data demonstrates unidirectional flows concisely concluded from continental fluvial deposits (Allen, 1964). The data is also presented in Figure 20, reflecting a scatter distribution with differences within the KFF sub-regions and their relative collection areas. These differences are noted and briefly discussed below:

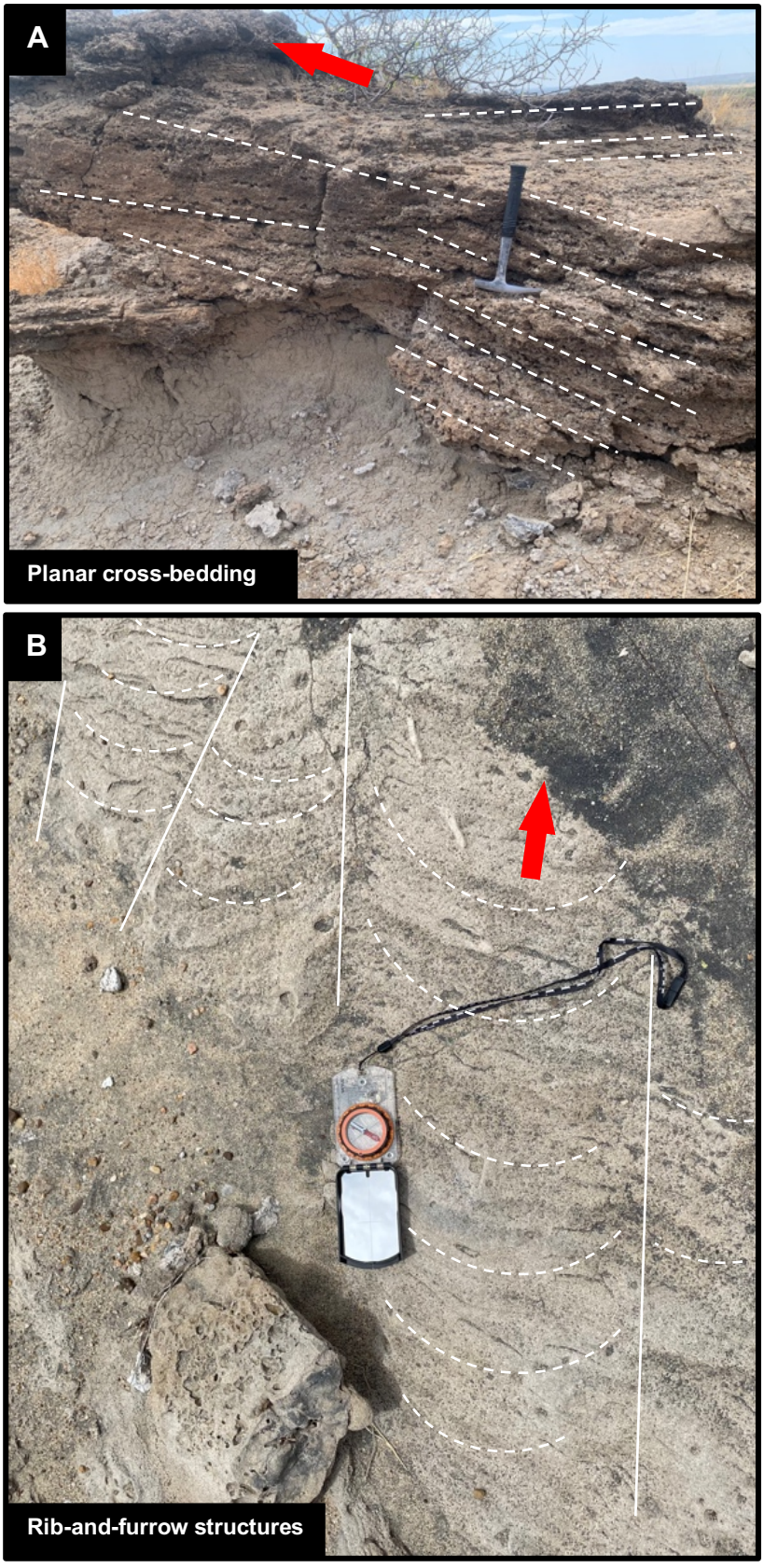

Figure 18: *Examples of KBS Member palaeocurrent indicators observed in the field that were used as vector measurements for palaeocurrent analysis.* ***(A)*** *Planar cross-bedded sandstone deposits.* ***(B)*** *Ripple cross-laminated sandstone deposits, displaying rib-and-furrow structures. Red arrow shows palaeocurret direction.*

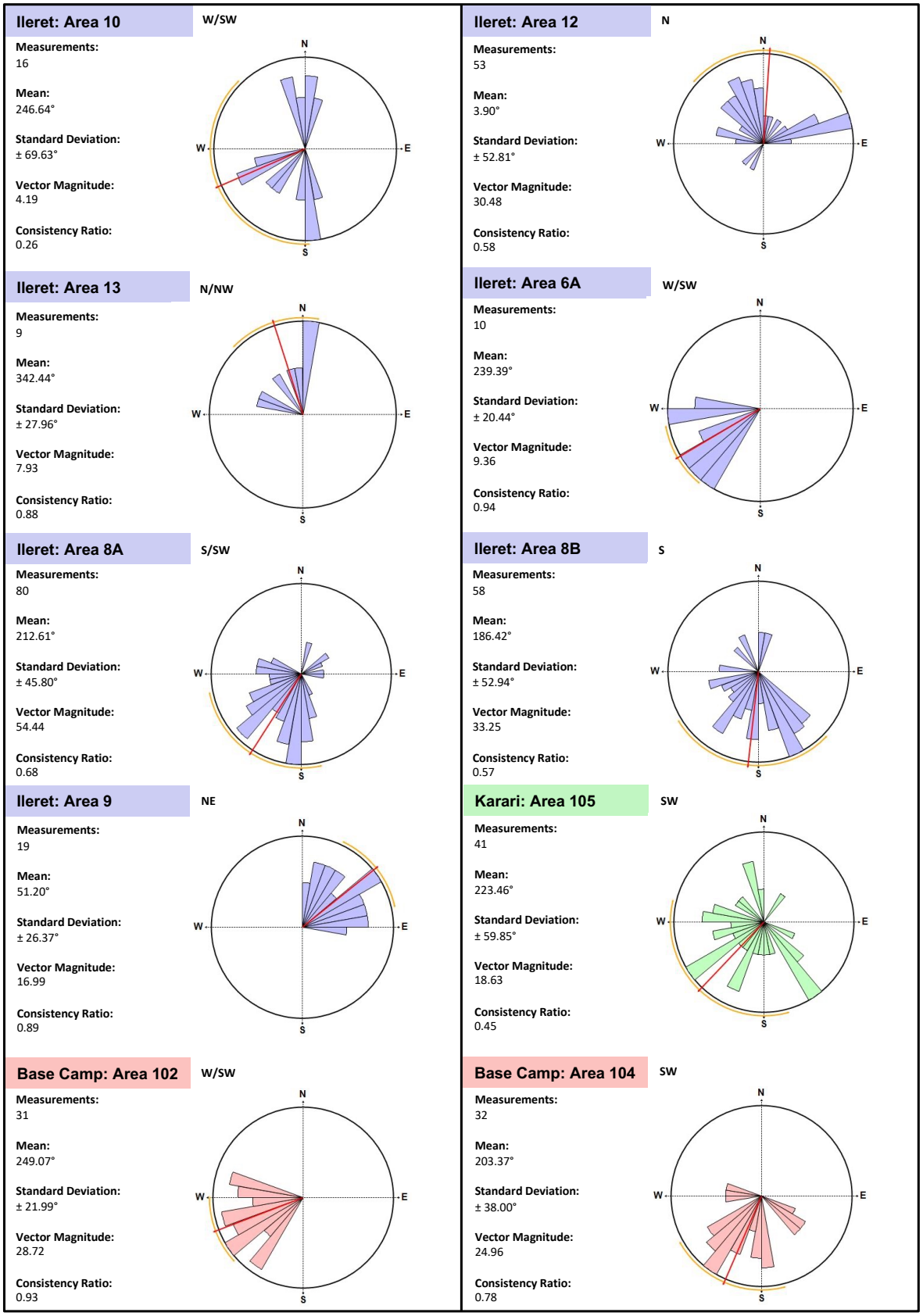

Figure 19: *Rose diagrams showing palaeocurrent directions of the KBS Member palaeo-fluvial systems that were measured in the field. This includes vector mean azimuths and statistical data of the KBS Member deposits within the KFF sub-regions (Ileret, Karari and Base Camp). See Appendix C for comprehensive raw palaeocurrent data.*

5.3.1. Ileret subregion

The Ileret subregion demonstrates distinct palaeocurrent directions defined by various distribution patterns. These readings were acquired from planar cross-bedded sandstone deposits and rib-and-furrow structures (Figure 18; Appendix E). Area 10 yielded sixteen palaeocurrent readings, and Area 6A yielded ten readings—both areas indicating W/SW directions with locality averages of 246.64° and 239.39°, respectively. However, Area 10 displays a high variability unimodal distribution, whereas Area 6A displays a low variability unimodal distribution (Figure 19).

Areas 8A and 8B demonstrate S to SW palaeocurrent direction, obtained from a sum of eighty and fifty-eight palaeocurrent readings, respectively. Area 8A indicates an S/SW direction with an average of 212.61°, whereas Area 8B indicates an S direction with an average of 186.42°. Both areas display a high variability unimodal paleocurrent distribution (Figure 19).

Areas 12, 13 and 9 indicate Northerly (N, N/NW, and NE) directions from a sum of fifty-three, four and nineteen palaeocurrent readings, respectively (Figure 19), all obtained from planar cross-bedded sandstones and rib-and-furrow structures (Figure 18). Area 12 displays a high variability unimodal paleocurrent distribution at a locality average of 3.90°, whereas Areas 13 and 9 display low variability unimodal paleocurrent distributions with averages of 342.44° and 51.20°, respectively (Figure 19).

5.3.2. Karari subregion

The Karari subregion yielded forty-one palaeocurrent readings from Area 105, acquired from planar cross-bedded sandstone deposits and rib-and-furrow structures (Figure 18). The readings indicate a SW palaeocurrent direction with a high variability unimodal distribution, averaging 223.46° (Figure 19; Appendix E).

5.3.3. Base Camp subregion

The Base Camp subregion yielded thirty-one palaeocurrent readings from Area 102 and thirty-two from Area 104, acquired from planar cross-bedded sandstone deposits (Figure 18). Dominantly W to SW readings were obtained, where Area 102 indicates significant W/SW directions with an average of 249.07°, displaying a low viability unimodal paleocurrent distribution, and Area 104 indicates a significant SW direction with an average of 203.37°, demonstrating a high variability unimodal paleocurrent distribution (Figure 19; Appendix E).

5.3.4. KBS Member palaeocurrent summary:

The palaeocurrent vector measurements collected in this study are plotted onto the KFF satellite image (Figure 20). Although the data has a scatter distribution within the KFF sub-regions and their relative collection areas, the average palaeocurrent measurements of the KBS Member sandstones demonstrate an overall unimodal SW palaeo-flow trends; however, in contrast to the other collection areas, Areas 9, 12 and 13 indicate northerly directed palaeo-flows (Figure 20).

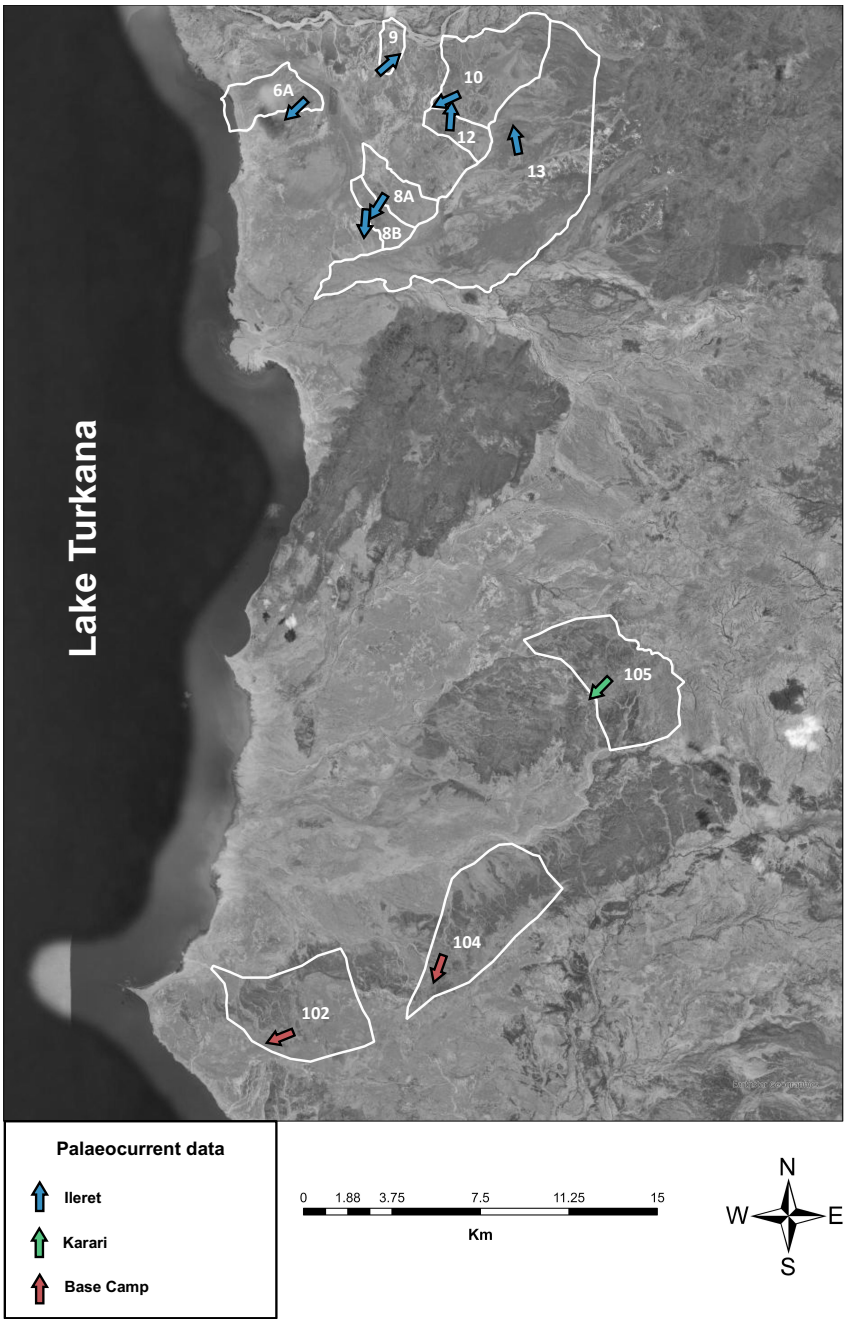

Figure 20: *Map showing mean palaeocurrent vector directions demonstrated by the KFF KBS Member deposits.*

5.4. KBS Member sandstone petrographic data

Sandstone petrography has been proven as an essential tool for investigating provenances of ancient terrigenous deposits, inferring their sediment transportation, distribution, diagenesis and the interplay of physical and chemical processes during deposition, as well as reconstructing the evolution and dynamics of palaeogeographic basins (Suttner, 1974; Dickinson *et al.*, 1983; Dickinson, 1985; 1988; Garzanti, 2016, 2019). This study conducted the petrographic analysis on twenty-nine KBS Member sandstones from various collection areas (Table 5), and the results are presented as follows:

Table 5: *Table showing the study's collection areas and their sub-region locations of samples used for petrographic analysis.*

KFF Sub-Region	Collection Area	KBS Member Sample ID	Latitude	Latitude	Elevation (m)
Ileret	10	BC2301	4.28812	36.30822	420
		BC2303	4.283003	36.31553	432
		BC2304	4.27797	36.31100	434
		BC2305	4.27873	36.31037	438
		BC2306	4.27873	36.31037	443.5
		BC2307	4.28577	36.30742	449
	12	BC2308	4.301310	36.31500	434
		BC2309	4.30064	36.31506	439
		BC2310	4.29538	36.31552	452
	13	BC2311	4.26586	36.33472	411
		BC2313	4.26691	36.33166	429
		BC2314	4.26691	36.33166	436
	6A	BC2316	4.29021	36.24991	411
		BC2317	4.28582	36.25004	418
		BC2318	4.28690	36.25054	424
		BC2319	4.28805	36. 25077	432
	8A	BC2329	4.252609	36.276889	428.3
	8B	BC2331	4.241544	36.278087	414.7
		BC2332	4.241442	36.278405	416.2
	9	BC2333	4.297967	36.278475	423.2
		BC2335	4.295786	36.278044	434
		BC2336	4.295667	36.277962	435.2
Karari	105	BC2320	4.07169	36.36380	451
		BC2322	4.06501	36.36597	515
Base Camp	102	BC2323	3.952371	36.241586	438.3
		BC2324	3.946267	36.246728	433
	104	BC2325	3.959701623	36.30311934	464
		BC2326	3.957175	36.304957	453.1
		BC2328	3.956998	36.304827	455.2

5.4.1. Framework grain mineralogy

Primary observable grains that make sandstones are referred to as 'framework grains', and this study considers these grains as those that fall within the Wentworth (1922) grain size classification scheme's "coarse silt to sand" category (500 to 31 µm in diameter) (Table 1). These grains are further categorised into three primary groups based on their mineralogical compositions, namely, quartz (*Q*), feldspar (*F*), and lithic fragments (*L*). These are noted and briefly discussed below:

5.4.1.1. Quartz (Q)

Quartz is the most prevalent framework grain observed in the thin sections, occurring either as monocrystalline (*Qm*) or polycrystalline grains (*Qp*) (Figure 21). These grains are observed as angular to sub-rounded and display straight to undulose extinctions (Figure 21). Quartz constitutes a proportion between 51–67 percent of the total rock components, with the highest proportion found in the Ileret sub-region (Figures 26 and 27). More than 70 percent of the total quartz observed is *Qm* (Figures 26 and 27), with angular to sub-rounded shapes and either sutured or straight boundaries (Figure 21). These further display straight to undulose extinction, and some grains exhibit internal fracturing. The amount of *Qp* also varies proportionally, constituting less than 30 percent of the total quartz observed (Figures 26 and 27).

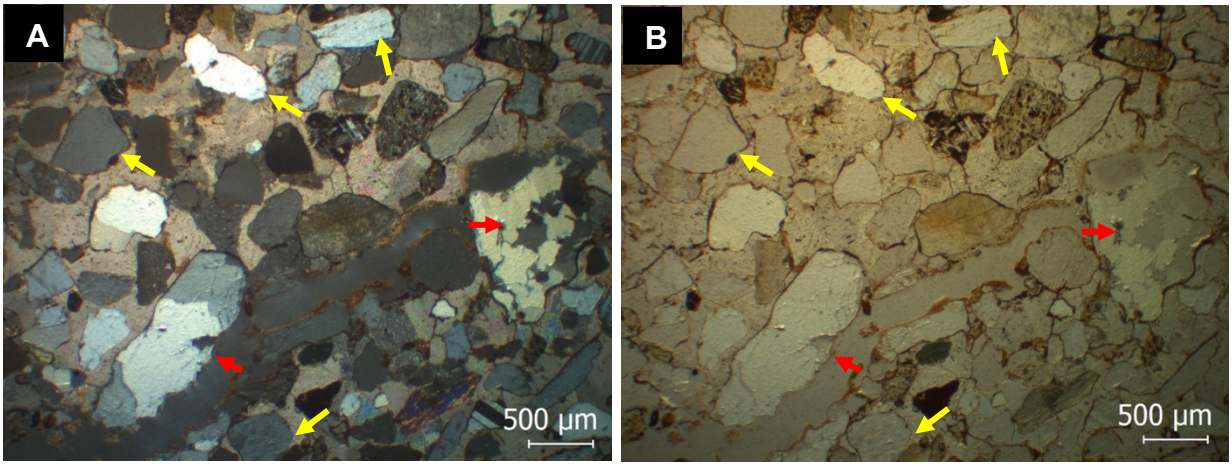

Figure 21: *Photomicrographs showing quartz as primary framework grain mineralogy in the KBS Member sandstones, indicated by arrows; yellow arrows indicate monocrystalline quartz (Qm), whereas the red arrows indicate polycrystalline quartz (Qp).* ***(A)*** *XPL and* ***(B)*** *PPL.*

5.4.1.2. Feldspar (F)

Feldspars are primarily observed as plagioclase (*P*) and potassium (*K*) feldspars (Figure 22), comprising 12–32 percent of the total rock components, with the highest proportion found in the Ileret sub-region (Figures 26 and 27). The *P*-feldspar is present as albite, displaying albite twinning, whereas the *K*-feldspar is primarily as microcline, displaying crosshatch twinning (Figure 22). These grains are sub-angular and are generally larger than those of *Q*, although this is considerably inconsistent throughout the sandstones (Figure 22). In the overall sandstone samples, *P* constitutes more than 60 percent, whereas *K* is less than 40 percent of the feldspar observed in the total rock components (Figures 26 and 27).

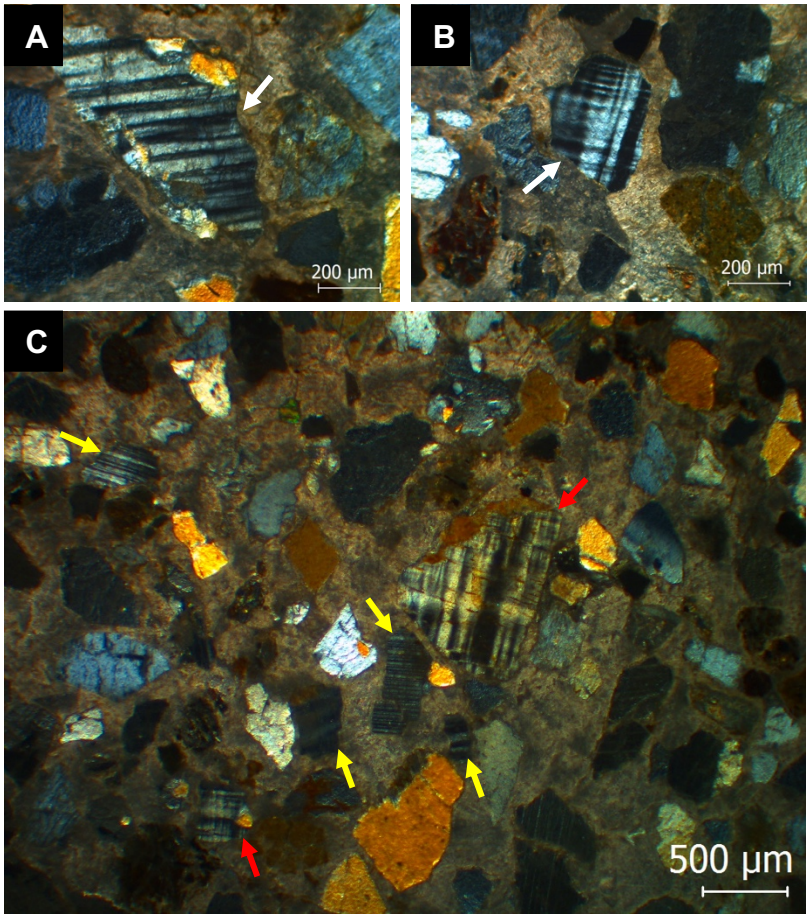

Figure 22: *XPL photomicrographs showing feldspar as primary framework grain mineralogy in the KBS Member sandstones.* ***(A)*** *Plagioclase feldspar (P; albite).* ***(B)*** *Potassium feldspar (K; microcline).* ***(C)*** *The yellow arrows indicate plagioclase feldspar, whereas the red arrows indicate potassium feldspar in the total rock components.*

5.4.1.3. Lithic fragments (L)

The total lithic fragments comprise 13–26 percent of the total rock components throughout the KBS Member sandstones; however, they can occasionally be more prevalent than feldspars (Figures 26 and 27). These fragments represent source rocks that have not disintegrated (Tucker, 2001). They display individual mineral grains that are sub-rounded to sub-angular shapes (Figure 23). The recognised lithic constituents appear to be either volcanic or sedimentary lithics. The volcanic lithic fragments are microlithic volcanics, distinguished by their porphyritic structures and plagioclase crystals, and there are also some felsic volcanics, characterised by their rhyolitic textures. These volcanic lithics are larger than the surrounding grains (Figure 23).

In contrast, the sedimentary lithic fragments are observed as mudrocks and carbonates and are more abundant than volcanic lithics (Figure 23). As a common feature of the sediment matrix, the mudrocks are observed as being spotted, and they are dark brown in both crossed and plane-polarised light with definite boundaries. In contrast, the carbonates are occasionally cement and are observed to have high interference hues (Figure 23). Additionally, another type of lithic fragment observed at low frequencies is chert.

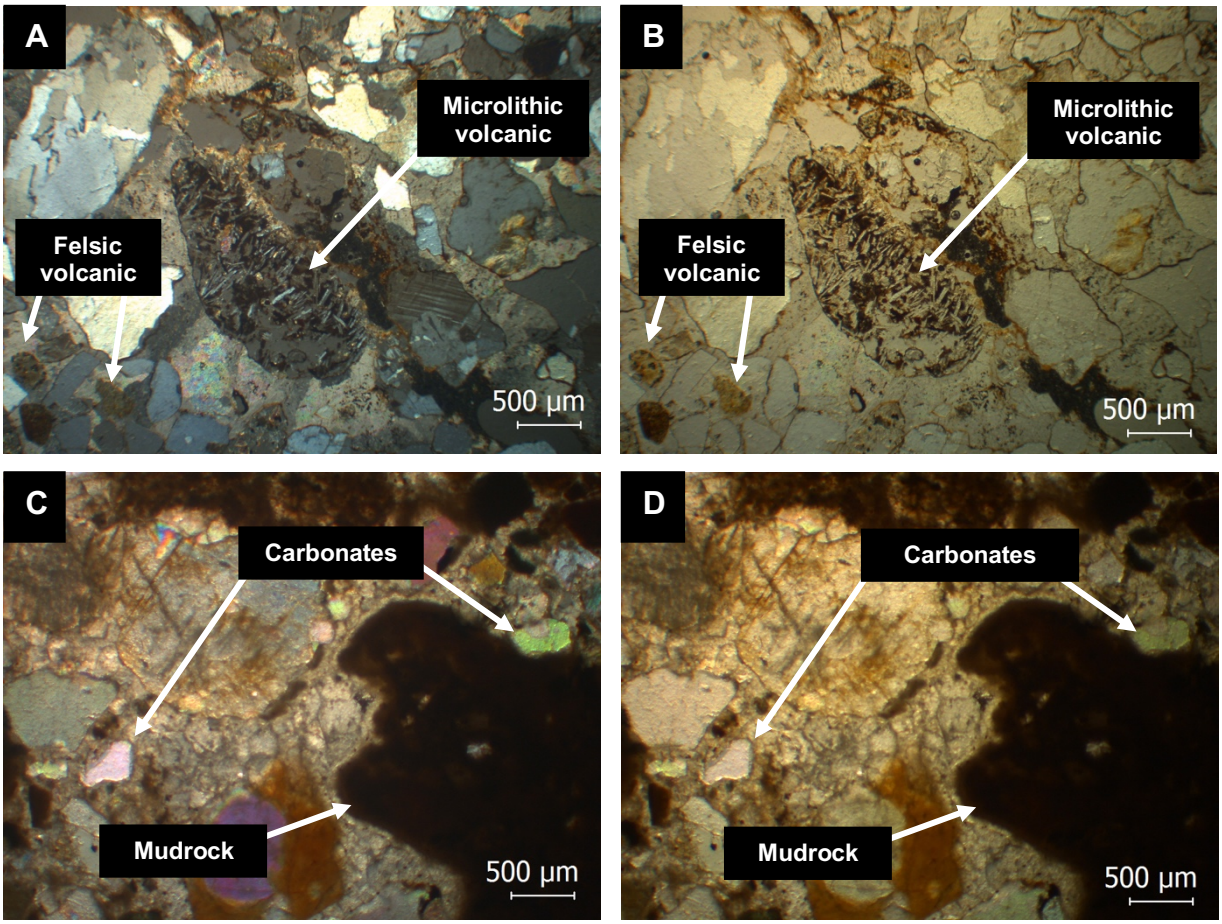

Figure 23: *Photomicrographs showing primary framework grain mineralogy of volcanic lithic fragments **(A)** and **(B)**, and sedimentary lithics **(C)** and **(D)**. Photomicrographs **(A)** and **(C)** are XPL, and photomicrographs **(B)** and **(D)** are PPL, respectively.*

5.4.1.4. Accessory framework minerals

The minor framework grains in the KBS Member sandstones are referred to as accessory mineral grains, with a widely varying abundance throughout the sandstones. The most prevalent minerals are tabular biotite (most common), chlorite, amphibole, and opaque minerals (hematite) (Figure 24).

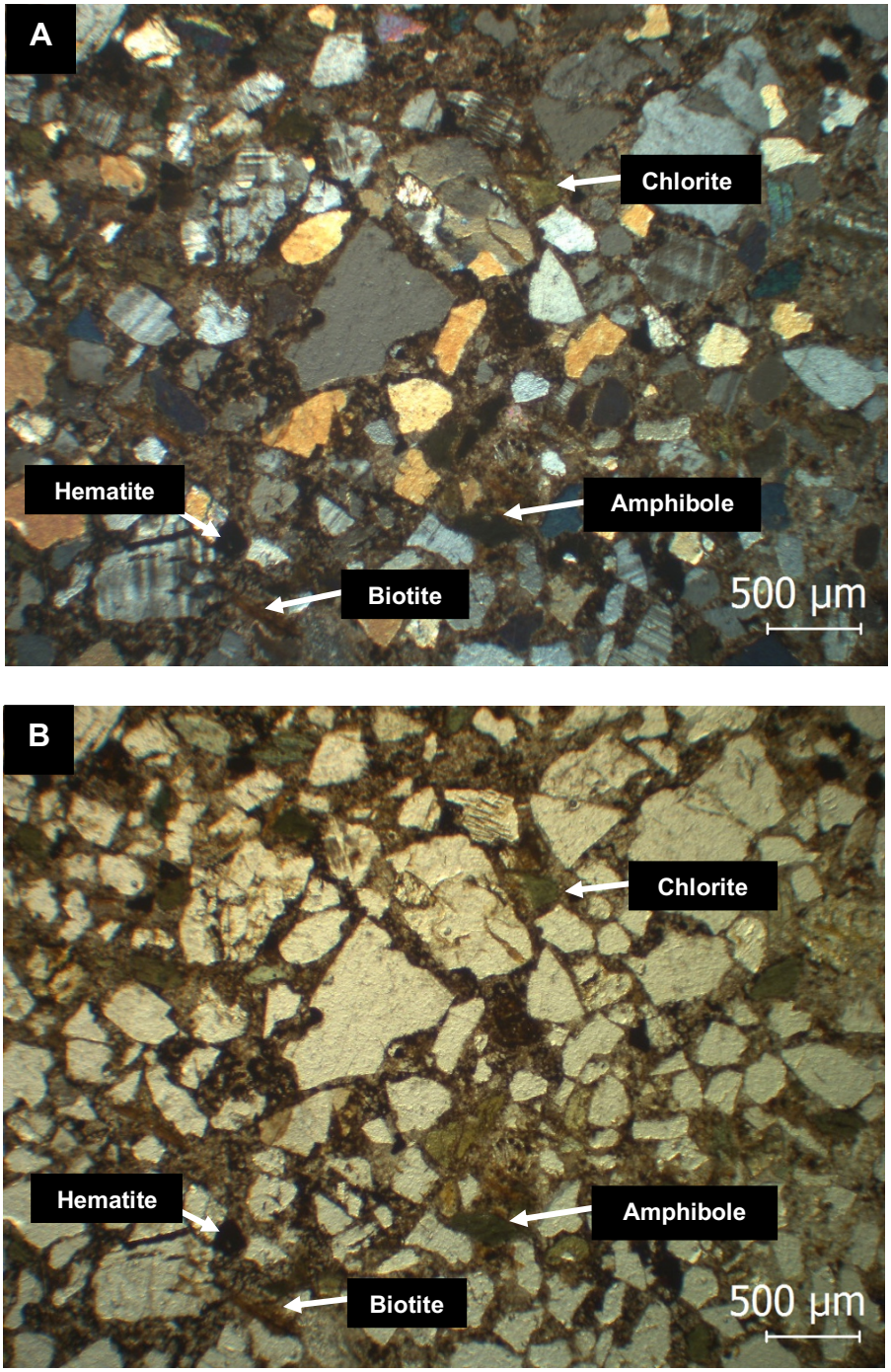

Figure 24: *Photomicrographs showing accessory minerals as primary framework grain mineralogy in the KBS Member sandstones; tabular biotite, chlorite, amphibole, and opaque minerals (hematite).* ***(A)*** *XPL and* ***(B)*** *PPL.*

5.4.2. Matrix proportion, cementation type, porosity, and grain contact (compaction)

The matrix represents the finer fragments filling interstitial spaces between larger framework grains. These fragments include finer-grained tuffaceous material, clastic rock clays, and some calcite, all within the pore space, constituting a proportion of less than 10 percent of the total rock volume (Table 6). The cement is primarily calcitic; however, some sandstones present it as isotropic minerals (Figure 25). These sandstones display porosity ranging from 5–10 percent of the total rock volume (Table 6). Regarding grain compaction, the overall KBS Member sandstone grains demonstrate long contacts, concavo-convex closely packed and tangential contacts, although some are sutured (Figure 25). Notably, these petrographic elements and the sandstone grain size and shape ranges are significant in determining sandstone composition and classification.

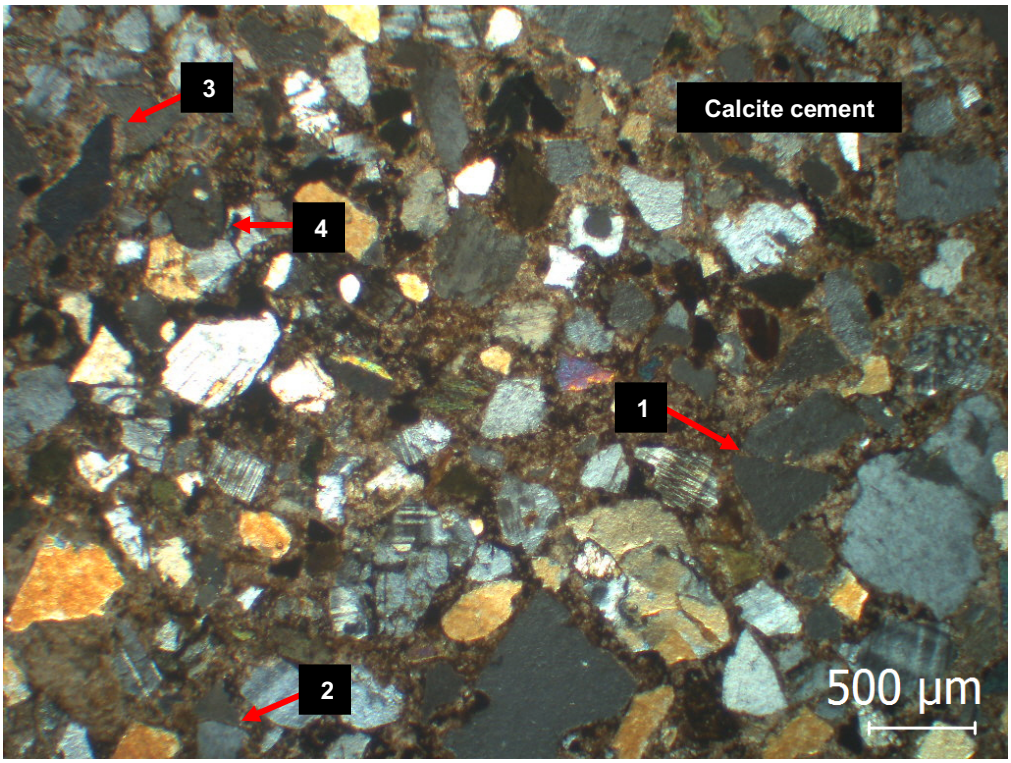

Figure 25: *XPL photomicrographs showing the primarily calcite cement and grain-contact types in the KBS Member sandstones; long contacts (1), concavo-convex closely packed (2), tangential (3), and sutured contacts (4).*

5.4.3. Sandstone classification

The twenty-nine thin sections were characterised and semi-quantitatively analysed through the Gazzi-Dickinson point counting method. This procedure demonstrates component variations in all sections examined. The thin sections were then logged and catalogued according to the locality area, sandstone unit, measured sections, and the collected palaeocurrent data (see Appendix G). The point-counting dataset was used to comprehensively classify the KBS Member sandstones based on the Dott (1964) classification scheme later detailed by Garzanti (2019). This classification scheme is based on relative proportions of principal mineral components: quartz, feldspar, and lithic fragments (*QFL*); and through this, *QFL*-ternary plots were produced to detail the sandstone positions and illustrate variations in the proportions in relation to geographic location and sandstone unit (Figure 26). The results are summarised below.

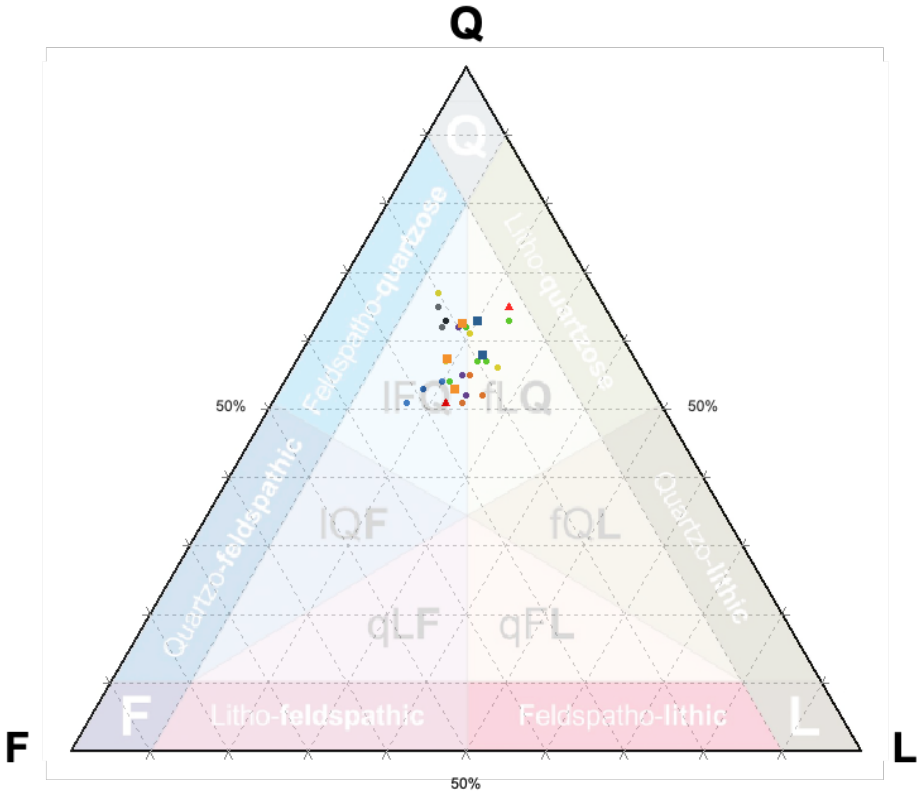

Figure 26: *Ternary diagram (after Garzanti, 2019) for rock classification of the twenty-nine KBS Member sandstones used in this study, together with relevant petrographic parameters. This figure corresponds with Table 6 below.*

Symbol	Collection Area	Sample	*Q* (%)		*F* (%)		*L* (%)	Grain size (μm)	Grain roundness and sphericity	Maturity	Classification
			Qm	*Qp*	*P*	*K*					
●	10 (Ileret subregion)	BC2301	48	9	14	5	24	Medium to very fine sand	Angular to sub-angular	Immature	Feldspatho-litho-quartzose
		BC2303	50	7	16	4	23	Fine sand to coarse silt	Angular to sub-angular	Immature	Feldspatho-litho-quartzose
		BC2304	54	9	10	3	24	Fine sand to coarse silt	Sub-angular to sub-rounded	Immature	Feldspatho-litho-quartzose
		BC2305	43	8	19	7	23	Fine sand to coarse silt	Angular to sub-angular	Immature	Litho-feldspatho-quartzose
		BC2306	56	6	15	4	19	Medium to very fine sand	Angular to sub-angular	Immature	Litho-feldspatho-quartzose
		BC2307	44	10	17	8	21	Medium to very fine sand	Angular to sub-angular	Immature	Litho-feldspatho-quartzose
●	12 (Ileret subregion)	BC2308	46	5	18	7	24	Fine sand to coarse silt	Sub-angular to sub-rounded	Submature	Litho-feldspatho-quartzose
		BC2309	44	8	16	6	26	Fine sand to coarse silt	Sub-angular to sub-rounded	Submature	Feldspatho-litho-quartzose

		BC2310	45	10	14	8	23	Medium sand to coarse silt	Sub-angular to sub-rounded	Submature	Feldspatho-litho-quartzose
●	13 (Ileret subregion)	BC2311	44	10	21	5	20	Fine sand to coarse silt	Sub-angular to sub-rounded	Submature	Litho-feldspatho-quartzose
		BC2313	43	8	26	6	17	Fine sand to coarse silt	Sub-angular to sub-rounded	Submature	Litho-feldspatho-quartzose
		BC2314	45	8	24	5	18	Medium sand to coarse silt	Sub-angular to sub-rounded	Submature	Litho-feldspatho-quartzose
●	6A (Ileret subregion)	BC2316	40	16	12	6	26	Medium to very fine sand	Angular to sub-angular	Immature	Feldspatho-litho-quartzose
		BC2317	48	13	12	7	20	Medium to very fine sand	Angular to sub-angular	Immature	Feldspatho-litho-quartzose
		BC2318	55	12	13	7	13	Medium sand to coarse silt	Angular to sub-angular	Immature	Litho-feldspatho-quartzose
		BC2319	47	10	18	6	19	Medium sand to coarse silt	Angular to sub-angular	Immature	Litho-feldspatho-quartzose
●	8A (Ileret subregion)	BC2329	49	14	14	7	16	Medium sand to coarse silt	Angular to sub-angular	Immature	Litho-feldspatho-quartzose

●	8B (Ileret subregion)	BC2331	52	13	11	10	14	Fine sand to coarse silt	Angular to sub-angular	Immature	Litho-feldspatho-quartzose
		BC2332	51	11	15	7	16	Medium sand to coarse silt	Angular to sub-angular	Immature	Litho-feldspatho-quartzose
●	9 (Ileret subregion)	BC2333	47	8	17	6	22	Fine sand to coarse silt	Sub-angular to sub-rounded	Submature	Litho-feldspatho-quartzose
		BC2335	48	4	18	6	24	Very fine sand to coarse silt	Sub-angular to sub-rounded	Submature	Litho-feldspatho-quartzose
		BC2336	54	8	16	4	18	Medium sand to coarse silt	Sub-angular to sub-rounded	Submature	Litho-feldspatho-quartzose
▲	105 (Karari subregion)	BC2320	60	5	9	3	23	Fine sand to coarse silt	Sub-angular to sub-rounded	Submature	Feldspatho-litho-quartzose
		BC2322	49	2	19	8	22	Medium sand to coarse silt	Sub-angular to sub-rounded	Submature	Litho-feldspatho-quartzose
■	102	BC2323	51	7	14	5	23	Medium sand to coarse silt	Sub-angular to sub-rounded	Submature	Feldspatho-litho-quartzose

	(Base Camp subregion)	BC2324	59	4	13	4	20	Fine sand to coarse silt	Sub-angular to sub-rounded	Submature	Feldspatho-litho-quartzose
	104 (Base Camp subregion)	BC2325	50	3	18	7	22	Medium sand to coarse silt	Sub-angular to sub-rounded	Submature	litho-feldspatho-quartzose
		BC2326	57	5	14	5	19	Medium sand to coarse silt	Sub-angular to sub-rounded	Submature	litho-feldspatho-quartzose
		BC2328	52	6	16	8	18	Fine sand to coarse silt	Sub-angular to sub-rounded	Submature	litho-feldspatho-quartzose

Figure 26: *(continued).*

Table 6: *Additional petrographic parameters, corresponding with Figure 26.*

Collection Area	Sample	Grain sorting	Grain-matrix proportion	Grain porosity
10	BC2301	Poorly sorted	< 5%	< 10%
	BC2303	Poorly sorted	< 5%	< 10%
	BC2304	Moderately to poorly sorted	< 5%	< 10%
	BC2305	Moderately to poorly sorted	< 5%	< 10%
	BC2306	Poorly sorted	< 5%	< 10%
	BC2307	Poorly sorted	< 5%	< 10%
12	BC2308	Moderately sorted	< 5%	< 10%
	BC2309	Moderately sorted	< 5%	< 10%
	BC2310	Moderately sorted	< 5%	< 10%
13	BC2311	Moderately sorted	< 5%	< 10%
	BC2313	Moderately sorted	< 5%	< 10%
	BC2314	Moderately sorted	< 5%	< 10%
6A	BC2316	Poorly sorted	< 5%	< 10%
	BC2317	Moderately to poorly sorted	< 5%	< 10%
	BC2318	Poorly sorted	< 5%	< 10%
	BC2319	Poorly sorted	< 5%	< 10%
8A	BC2329	Moderately to poorly sorted	< 5%	< 10%
8B	BC2331	Poorly sorted	< 5%	< 10%
	BC2332	Poorly sorted	< 5%	< 10%
9	BC2333	Moderately sorted	< 5%	< 10%
	BC2335	Moderately sorted	< 5%	< 10%
	BC2336	Moderately sorted	< 5%	< 10%

105	BC2320	Well to moderately sorted	< 10%	< 5%
	BC2322	Well to moderately sorted	< 10%	< 5%
102	BC2323	Well to moderately sorted	< 10%	< 5%
	BC2324	Well to moderately sorted	< 10%	< 5%
104	BC2325	Well to moderately sorted	< 10%	< 5%
	BC2326	Well to moderately sorted	< 10%	< 5%
	BC2328	Well to moderately sorted	< 10%	< 5%

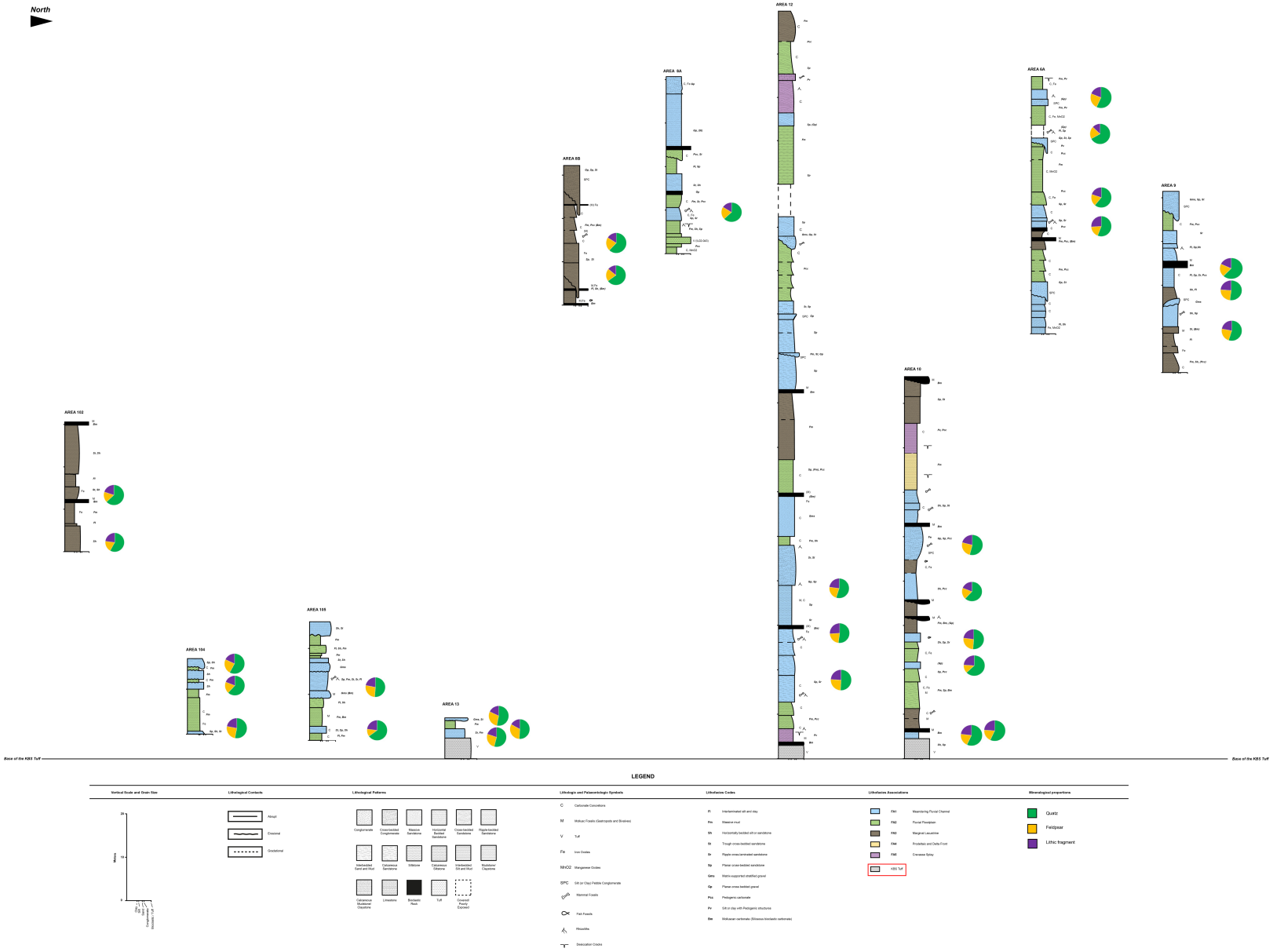

Figure 27: *Spatially correlated (measured) KBS Member stratigraphic sections with QFL mineralogical proportions plotted in positions of sample collection. See Appendix F for high resolution. A high-resolution version of this figure is found in the Appendices section (Appendix I).*

5.4.3.1. Ileret subregion

The Ileret subregion is represented by sandstones in collection areas 10, 12, 13, 6A, 8A, 8B, and 9 (Table 5; Figure 26). These sandstones display some variability. Sandstones from collection areas 13, 8A, 8B and 9 are classified as litho-feldspatho-quartzose, whereas those from collection areas 10, 12 and 6A are classified as both litho-feldspatho-quartzose and feldspatho-litho-quartzose (Figure 26). When considering textural maturity, sandstones collected from areas 12, 13 and 9 are sub-mature compared to the remaining sandstones collected in areas 10, 6A, 8A and 8B, which are immature (Figures 26 and 28).

There is also grain roundness and sphericity variability throughout the subregion, with grains being angular to sub-rounded (Figures 26 and 28). This variability can also be seen in grain sorting, matrix proportions and porosity (Table 6). The general framework grain mineralogy also widely varies, composing 51–67 percent of quartz**,** with *Qm* constituting 71–91 percent and *Qp* constituting 10–29 percent of the total quartz, 13–32 percent of the total feldspars with *P* constituting 63–82 percent and *K* constituting 19–37 percent of the total feldspars and 13–26 percent of lithics of the total rock volumes (Figures 26 and 27). Lithics throughout the subregion are represented by volcanic and sedimentary lithic fragments, as well as biotite, amphibole, chlorite, and opaque minerals (Figures 23 and 24). Additionally, there are some biogenic materials as lithic fragment components; these comprise plant materials, mammalian bones, and, more frequently, molluscan shell fragments, primarily identified as cross sections (Figure 28).

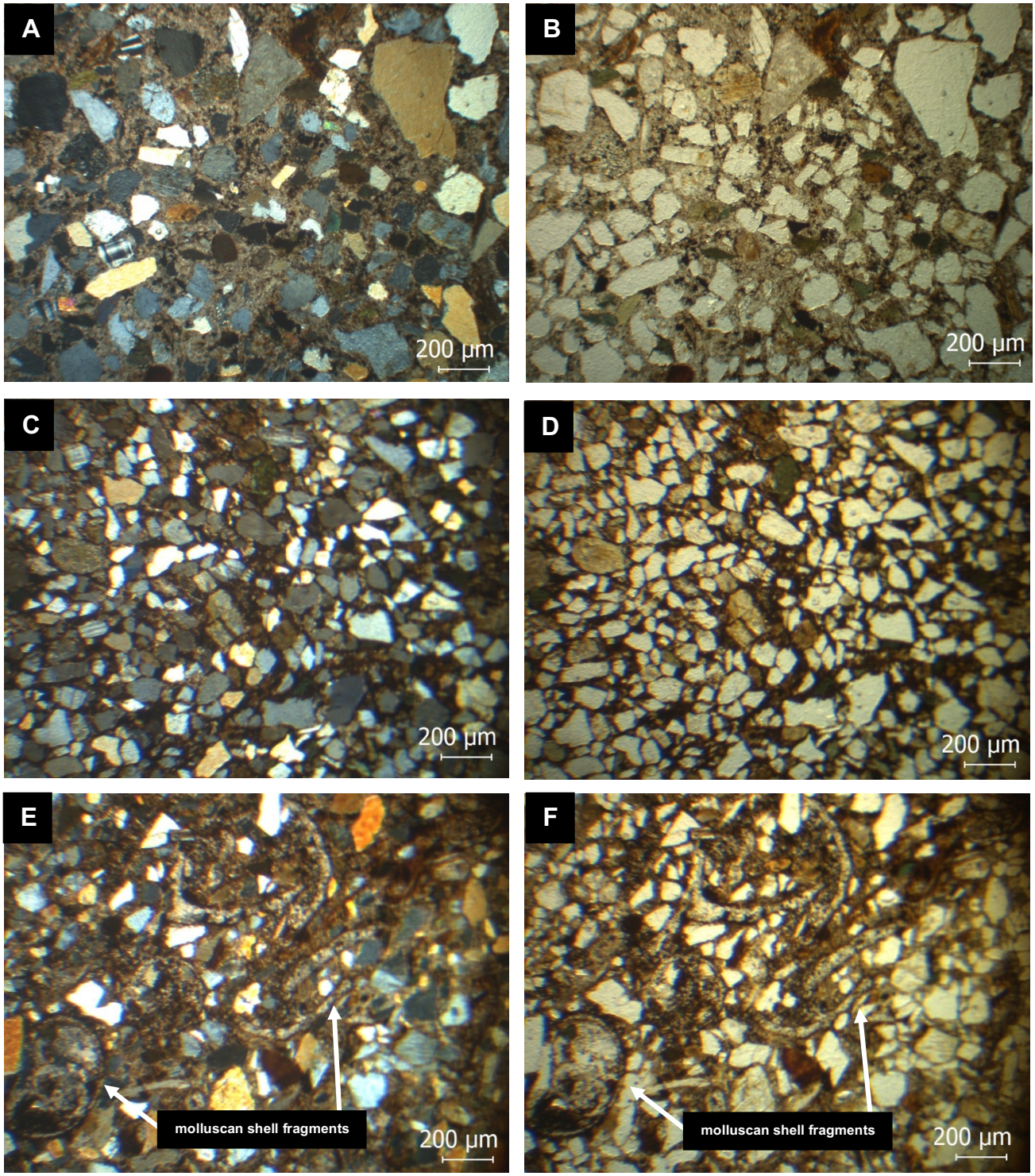

Figure 28: *Thin section photomicrographs showing the Ileret subregion sandstones, represented under XPL (Left) and PPL (Right). Photomicrographs **(A)** and **(B)** represent immature sandstones, and photomicrographs **(C)** and (**D)** represent submature sandstones. Photomicrograph **(E)**and **(F)** represent biogenic materials as lithic fragment components; molluscan shell fragments, identified as cross sections.*

5.4.3.2. Karari subregion

The Karari subregion is presented by sandstones in collection area 105. The sandstones are classified as well to moderately sorted feldspatho-litho-quartzose and litho-feldspatho-quartzose, respectively (Figure 26). Both sandstones are sub-mature and show relatively sub-angular to sub-rounded grains; however, they constitute varying grain sizes and matrix proportions that are less than 10 per cent and porosity that is less than 5 per cent (Figures 26 and 29; Table 6).

The sandstones display mineralogy that is composed of 51–65 percent of quartz, with *Qm* constituting 92–96 percent and *Qp* constituting 4–8 percent of the total quartz, 19–27 percent of the total feldspars with *P* constituting 69–75 percent, and *K* constituting 25–31 percent of the total feldspars and 20–23 percent of lithics of the total rock volumes (Figures 26 and 27). The lithics in both areas are represented by volcanic and sedimentary lithic fragments, biotite, amphibole and opaque minerals (Figures 23 and 24).

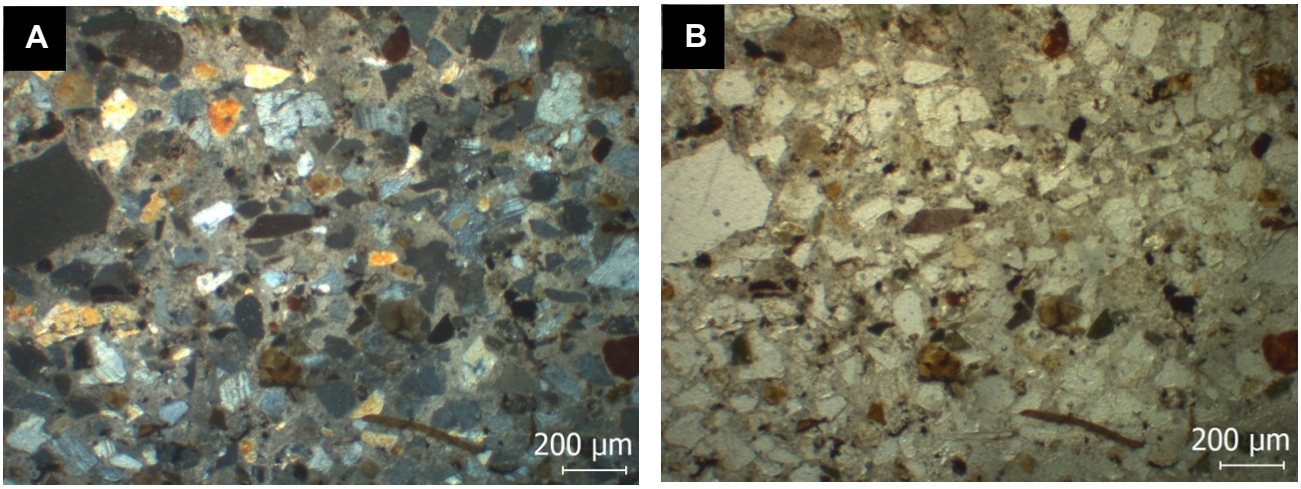

Figure 29: *Thin section photomicrographs showing the Karari subregion sandstone, representing submature sandstone. Under XPL (Left) and PPL (Right).*

5.4.3.3. Base Camp subregion

The Base Camp subregion is represented by sandstones in collection areas 102 and 104 of the KFF. Sandstones from area 102 are classified as feldspatho-litho-quartzose, whereas those from area 104 are classified as litho-feldspatho-quartzose sandstones (Figures 26). This sandstone textural diversity within this subregion can also be defined as moderately sorted sub-mature sediments with grain roundness and sphericity ranging from sub-angular to sub-rounded (Figures 26 and 30). They also vary in grain sizes, with a matrix proportion of less than 10 percent and less than 5 percent porosity (Figures 26 and 30; Table 6). Overall, sandstones from area 102 display mineralogy that is composed of 58–63 percent quartz, with *Qm* constituting 88–94 percent and *Qp* constituting 6–12 percent of the total quartz, 17–19 percent of the total feldspars with *P* constituting 74–76 percent and *K* constituting 24–26 percent of the total feldspars and 20–23 percent of lithics of the total rock volumes (Figures 26 and 27). In contrast, sandstones from area 104 display mineralogy that is composed of 53–62 percent quartz, with *Qm* constituting 90–94 percent and *Qp* constituting 6–10 percent of the total quartz, 19–25 percent of the total feldspars with *P* constituting 67–74 percent and *K* constituting 26–33 percent of the total feldspars and 18–22 percent of lithics of the total rock volumes (Figures 26 and 27). The lithics in both areas are represented by volcanic and sedimentary lithic fragments, biotite, amphibole and opaque minerals (Figures 23 and 24).

5.4.4. KBS Member sandstone petrography summary:

The analysed sandstones vary in grain size, ranging from coarse silt to sand-sized grains cemented by calcite and/or clay cement components throughout the subregions. They also have varying framework-supported textures, consisting of variability in grain roundness and sphericity, ranging from angular to sub-rounded grains, as well as grain sorting that ranges from moderately to poorly sorted.

CHAPTER 6: DISCUSSION

6.1. KBS Member depositional lithofacies and palaeoenvironmental distributions

The emphasis of this study was on understanding the regional stratigraphy and the palaeoenvironmental conditions during KBS Member time interval. Geological stratigraphic sections of the KBS Member with comprehensive lithological descriptions and interpretations were positioned from south to north of the KFF in relation to the modern lake and as well as the palaeolake (Brown and Feibel, 1991), and spatially correlated using the KBS Tuff as the basal bounding surface (Figure 17). The KBS Member sedimentary sequences indicate palaeoenvironmental heterogeneity across the collection areas in relation to the adjacent Lake Turkana, defined by the identified eleven lithofacies and five lithofacies associations. The palaeoenvironmental heterogeneity is prominent across the Turkana Basin, resulting in the complexity of producing a spatially correlation of sedimentary sequences from various localities based on lithological similarities (Gathogo and Brown, 2006; Feibel, 2013). However, this palaeoenvironmental heterogeneity can be attributed to an amalgamation of dynamic factors, including Walther's Law, which defines direct environmental relationships between extensive lateral lithofacies and superimposed sedimentary successions (Middleton, 1973; Feibel, 2003). Other attributing factors include dynamic fluvial meandering systems with associated deltaic and crevasse splay influences, and conclusively lake-level fluctuations over time (Lake Turkana).

The KBS Member stratigraphic sequence is defined by upward-fining, silt to fine-medium sand-grained interbedded detrital clastic and homogeneous detrital clastic deposits with pedogenic carbonate accumulations and some bioclastic depositional units, which are all consistent with low energy regimes in relation to meandering fluvial and near-lacustrine environments, as seen in the correlated sedimentary sections (Figure 17). The observed stratigraphic sequence and palaeoenvironments of the KBS Member in this study align with those documented by other scholars across the formation (Bowen, 1974; Burggraf *et al.,* 1981; White *et al.*, 1981; Burggraf & Vondra, 1982; Feibel, 1983; Brown & Feibel, 1986; Feibel, 1988; Feibel & Brown, 1991; Feibel

et al., 1991; Gathogo, 2003; Gathogo & Brown, 2006; Quinn, 2006; Lepre *et al.*, 2007; Feibel, 2013; Hammond *et al.*, 2021). Nevertheless, this study is the first to comprehensively delineate the KBS Member depositional lithofacies and palaeoenvironmental distribution across the member in space, offering a more comprehensive palaeogeographical interpretation (Figures 31 and 32). This palaeoenvironmental distribution is seen in Figure 31, which illustrates a generalised palaeoenvironmental framework of fluvio-lacustrine interactions across an extensional basin setting resulting from lithofacies association analysis (Table 4). Fluvial meandering streams draining from the north- and east-orientated volcanic highlands played a vital role in the KBS Member sedimentation, as well as the development of minor palaeoenvironments towards and along the lakeshore. These included a series of crevasse splay and prodeltaic and delta front deposits. This produced palaeoenvironmental framework can be correlated with other fluvio-lacustrine rift basin settings. Furthermore, Figure 32 demonstrates a palaeoenvironmental reconstruction of the KBS Member lithofacies association across the KFF, showing depositional evolution of the KBS Member deposits with dominance of fluvial systems presence at 1.87–~1.7 Ma and a dominance of lacustrine presence (Palaeolake Lorenyang) at ~1.7–1.6 Ma. This demonstration is in conjunction with the punctuated regional Turkana Basin palaeogeographic reconstructions established by Brown and Feibel (1991), together with the conducted palaeocurrent directions (see Figure 20), identified KBS Member lithofacies association distribution (see Figure 31), and the produced KBS Member lake level fluctuation model (see Figure 34).

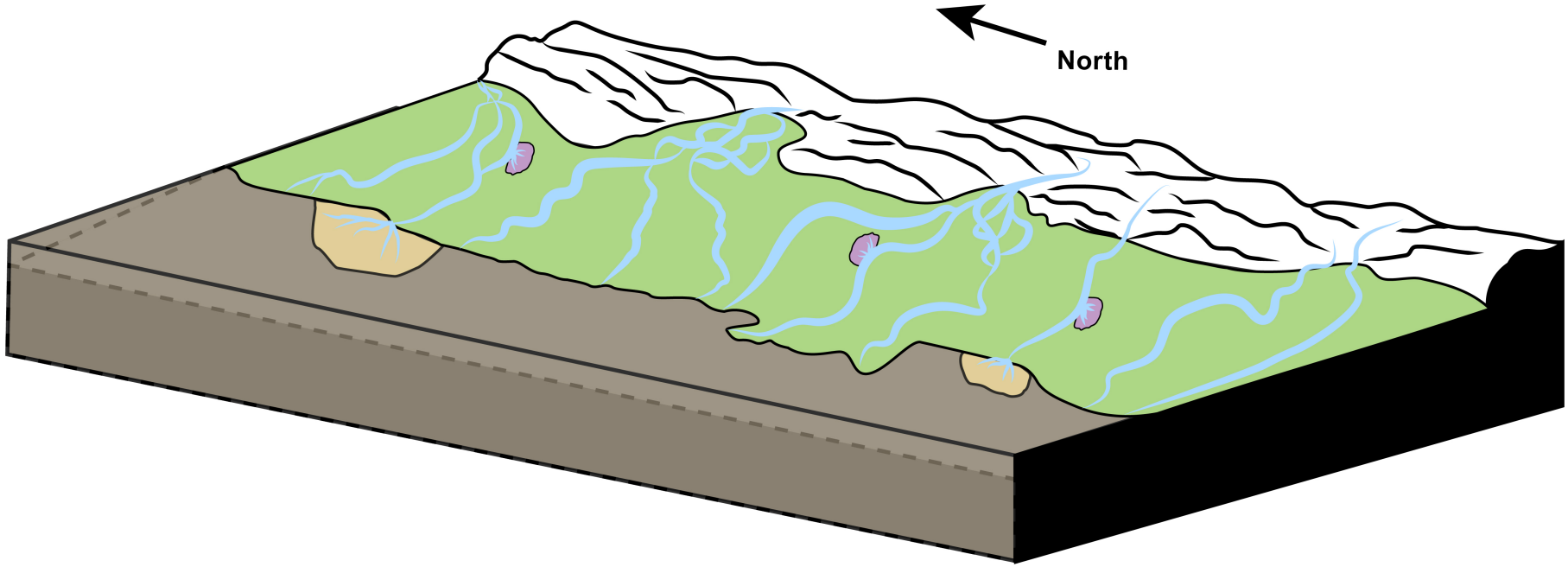

Lithofacies Associations

FA1	Meandering Fluvial Channel	**FA4**	Prodeltaic and Delta Front		Provenance Area
FA2	Fluvial Floodplain	**FA5**	Crevasse Splay		Depositional Base
FA3	Marginal Lacustrine				

Figure 31: *Schematic palaeoenvironmental reconstruction of the KBS Member lithofacies association across the KFF. A high-resolution version of this figure is found in the Appendices section (Appendix J).*

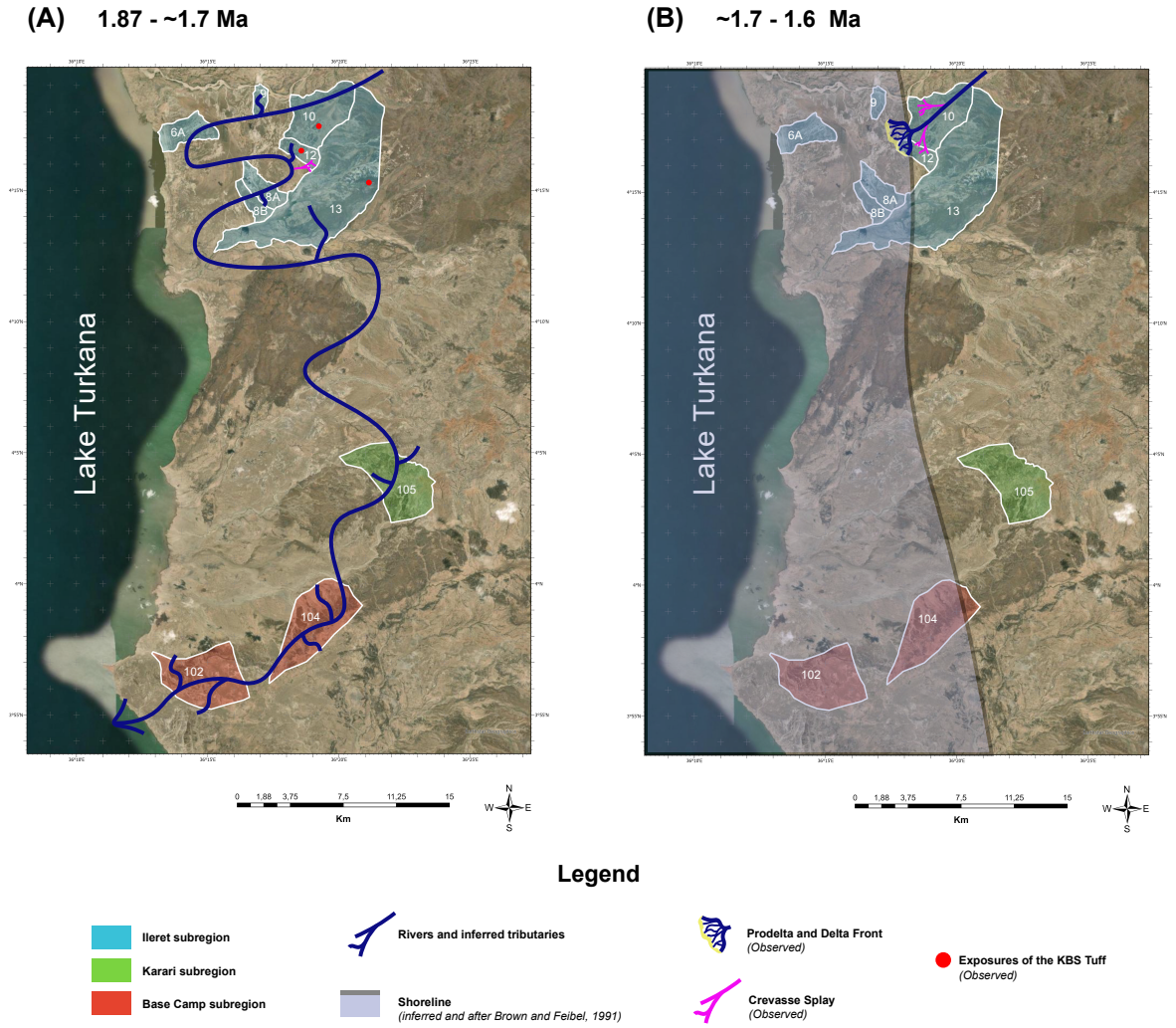

Figure 32: *Schematic palaeoenvironmental reconstruction of the KBS Member lithofacies association across the KFF showing depositional evolution of the KBS Member deposits with dominance of fluvial systems presence at 1.87–~1.7 Ma* ***(A)*** *and a dominance of lacustrine presence (Lake Lorenyang) at ~1.7–1.6 Ma* ***(B)****. The palaeoenvironmental distribution and shoreline are inferred from Brown and Feibel (1991) in accordance with the conducted palaeocurrent directions (see Figure 20), identified KBS Member lithofacies association distribution (see Figure 31), and the produced KBS Member lake level fluctuation model (see Figure 34). Note that the schematic is superimposed on the KFF's modern location and this study's collection areas for orientation. A high-resolution version of this figure is found in the Appendices section (Appendix K).*

6.2. KBS Member fluvial dynamics and morphology

The conducted sedimentary facies analysis of the KBS Member deposits, in association with spatially correlated KBS Member stratigraphic sections, demonstrates a significant predominance of meandering fluvial channel patterns, defined by *FA1* with associated fluvial *FA2* deposits (Figures 17, 31, and 32). This interpretation is consistent with those identified by previous scholars (Behrensmeyer, 1975; Feibel, 1988, 2013; Gathogo & Brown, 2006) across the KFF. However, results from this study delineate this significant fluvial dominance only for the KBS Member time interval.

The marked fluvial predominance is further demonstrated by the radial flow patterns observed in the palaeocurrent data (rose diagrams) (Figure 19). Meandering fluvial systems tend to frequently produce more variable or radial palaeoflow patterns compared to lower sinuosity systems, which is due to channel migration, bend cutoffs, and point-bar accretion surfaces; presenting consistent palaeoflow trends with a laterally migrating meandering system (Allen, 1970; Miall, 1996; Bridge, 2003). This interpretation further supports the observed perpendicular relation between point bar lateral accretion surfaces and the palaeocurrent data (Figure 19). Additionally, this marked fluvial predominance can also be supported by petrographic results. The petrographic data indicate that the examined sandstones comprise poorly to moderately/well sorted, coarse silt to medium sand grain-sized framework mineralogy with angular/sub-angular to sub-rounded grains, which corresponds with stable (low-energy) meandering fluvial systems as opposed to other fluvial systems (Clift *et al.*, 2019). The observed KBS Member petrographic parameters further suggest a more distal stable sediment source, with sediment being transported for longer distances before deposition. Such sediment transportation favours more meandering fluvial channel and floodplain lithofacies association deposits (FA1 and FA2) (Garzanti *et al.*, 2005; Garzanti *et al.*, 2007; Clift *et al.*, 2019; Greenberg & Ganti, 2024).

This dynamic fluvial predominance can be attributed to multiple factors; these include low gradient topography, consistent water discharge (climatic conditions), medium to fine-grained sediment supply (and stabilised riverbanks), and medium to lower sediment load corresponding to water discharge. Consequently, these factors can also be attributed as principal boundary conditions that control fluvial channel morphology

as a function of basin-scale responses to water and sediment supply variations (Harris *et al.*, 2006).

Fluvial dynamics and morphologies during the KBS Member time interval have not been thoroughly examined nor received comprehensive attention in relation to palaeoenvironmental reconstructions within the Turkana Basin. However, as part of brief principal depositional environments during the KBS Member time interval, studies by Feibel (1983), Brown and Feibel (1986), Tindall (1986), Feibel (1988), Feibel *et al.* (1989), Brown and Feibel (1991), Lepre *et al.*, (2007) and Gathogo (2017) do mention that the eastern region of the basin had alternations between marginal lacustrine and primary axial fluvial systems, which is also demonstrated in this study (Figures 17, 31, and 32). These studies further mention that there was a significant sedimentation reduction that took place after 1.75 Ma, when the axial fluvial system was morphologically defined by local ephemeral channels and streams with alluvial systems as types of fluvial morphologies, eroding local sections. This axial channel drainage was attributed to the perennial ancestral Omo River, which gave rise to distributary channel networks and floodplains at the marginal lacustrine settings, resulting in the replacement of subaerial deltaic settings as the primary depositional systems along lacustrine margins and contributed to the infill of Lake Turkana (Feibel, 1988; Brown & Feibel, 1991; Lepre, 2007).

The work done here from lithofacies, palaeocurrent, petrographic, and sequence stratigraphic analyses was used to infer and extend our understanding regarding fluvial dynamics and morphologies as part of palaeoenvironmental reconstruction during the KBS Member depositional period. The results reveal that the deposits can also be primarily interpreted as preserving distributive fluvial systems (DFS); thus, the observed meandering fluvial predominance, which can be attributed to this proposed fluvial morphology (Nichols & Fisher, 2007; Stanistreet & McCarthy, 1993). These fluvial systems are defined as those with a downstream decrease in grain and channel sizes and more unconfined channels from the fluvial apex (Nichols & Fisher, 2007). They are also primarily characterised by splay and delta deposits, attributing to radial flow patterns (Nichols & Fisher, 2007). In general, such fluvial morphology suggests a single river which enters a basin at a point and then extends out onto the alluvial plain, which in this case is the perennial ancestral Omo River, implying more interconnected

amalgamated sand bodies close to the fluvial apex along with small disconnected sand bodies that are laterally spaced apart in floodplain deposits; apex to distal, displaying a system that is characterised by medium sand to fine-grained sediment loads from apex to distal and relatively stable current flows, favouring meandering systems (Nichols & Fisher, 2007; Trendell *et al.*, 2013; Callahan, 2023).

Firstly, petrographic evidence that supports this proposed fluvial morphology during the KBS Member time interval is that there is a decrease in grain size towards the south, from Ileret to Base Camp, implying a northern-orientated apex, as DFS tend to have sand-sized grains at apex and coarser fines in distal (Liu *et al.*, 2024) (Figures 28, 29, and 30). Other petrographic parameters further reinforce this grain size distribution along the KFF's subregions, an increase in grain sorting (poorly to moderately/well), grain roundness and sphericity (angular/sub-angular to sub-rounded), grain-matrix proportion, and maturity towards the south (distal), from Ileret to Base Camp, as these petrographic parameters are consistent with DFS characters (Pourmorad & Jahan, 2021; Nichols & Fisher, 2007) (Figure 26; Table 6). Secondly, as mentioned above, the lithofacies analysis reveals a predominance of the meandering fluvial channel and broad fluvial floodplain lithofacies associations (FA1 and FA2), together with the presence of prodeltaic and delta front (FA4) and crevasse splay (FA5) lithofacies association deposits, which define DFS (Nichols & Fisher, 2007) (Figures 31 and 32). Thirdly, sequence stratigraphy further indicates cyclic deposition patterns, suggesting avulsion episodes common in DFS settings (Martin *et al.*, 2021) (Figure 34). Additionally, palaeocurrent data present radial flow patterns which define DFS. Furthermore, the palaeocurrent data also support the notion that the KBS Member fluvial systems had a north-orientated apex and a south-orientated distal, showing an overall flow direction of south-southwest adjacent to Lake Turkana (Figures 19 and 20). It is crucial to note that the proposed fluvial morphology (DFS) does not refute that the KBS Member time deposits preserve ephemeral channels and alluvial systems, but contends, offering additional perspective and enhancing the fluvial dynamics and morphological interactions already established, suggesting that the axial fluvial system of the perennial ancestral Omo River also had distributive characters during the KBS Member time interval.

6.3. KBS Member sandstone provenance: source mineralogy

The KBS Member sandstone petrography outlined in Chapter 5 provides indications for identifying source rocks. These sandstones can be attributed to two primary source rocks, namely, the Precambrian crystalline basement Ethiopian plutonic igneous and metamorphic rocks east of the basin, as well as the Kenyan Cenozoic volcano-sedimentary rocks, extending north of the basin near the Ethiopian-Kenya border (Mathisen & Vondra, 1983; Mosley, 1993; Davidson *et al.*, 1973). The Precambrian rocks include ultramafic and granitic intrusions, high-grade metamorphism gneisses, and some dykes (Davidson *et al.*, 1973; Mathisen & Vondra, 1983; Dunkelman *et al.*, 1988; McDougall & Watkins, 2006), whereas the Cenozoic rocks consist of extensive flood basalts with interbeds of pyroclastic and salic deposits consisting of associated rocks such as tuffs, basalts, ignimbrites, trachytes, as well as some clastic fluvial sediments (Davidson *et al.*, 1973; Fitch & Miller, 1976).

These mineral sources have been thoroughly described by Mathisen and Vondra (1983) through a provenance framework and mapped geology of the basin, and Mathisen (1977) identified heavy mineral distributions that contribute to both source rocks' mineralogy found in KFF sandstones together with parameters that influence the distribution of specific minerals. Through sandstone petrography conducted for this study, it is evident that both source areas influenced the KBS Member sandstone mineralogy (see below). Nonetheless, the Precambrian rocks, easterly adjacent to the collection areas, are primary attributes of the sandstones' diverse framework grains, compared to the Cenozoic rocks, which can be considered as the secondary mineralogy attributes of the sandstones.

Provenance studies can present relevant information about parent rocks; however, they have limitations, particularly when understanding proportional representations using the point count method (Agyemang *et al.*, 2019). These limitations result from certain chemically instable minerals, for example, feldspars, which are prone to dissolution or replacement during diagenesis as a function of climatic conditions, thus changing the minerals' petrographic provenance signals (Agyemang *et al.*, 2019; Helmold, 1985; Milliken *et al.*, 1989; Critelli & Nilsen, 1996). Consequently, these complications hinder this study from confidently assigning the observed feldspars to their respective parent rocks. Nevertheless, feldspars indicate either igneous or

metamorphic source rocks (Pittman, 1970); therefore, in this case, it can be attributed to the Precambrian crystalline basement Ethiopian plutonic igneous and metamorphic rocks. However, it is crucial to note that feldspars from Precambrian sources are more inclined to have undergone extensive diagenetic alteration and weathering, limiting their preservation potential in the sedimentary record (Weltje & von Eynatten, 2004; Agyemang *et al.*, 2019; Helmold, 1985; Milliken *et al.*, 1989; Critelli & Nilsen, 1996). In contrast, feldspars from Cenozoic sources, which have experienced less weathering, may be overrepresented during the point count method (Weltje & von Eynatten, 2004). This introduces a potential preservation bias toward the primary source area of the feldspar, resulting in the Kenyan Cenozoic volcano-sedimentary rocks not being completely ruled out as the potential source rocks.

Quartz is a relatively abundant and enduring mineral species in sedimentological records, and its abundance suggests felsic sources (Tucker, 2001). The modal analysis of the examined sandstones displays two types of quartz: monocrystalline and polycrystalline quartz (Figure 21). In proportion comparison, the abundance of the monocrystalline quartz exceeds that of the polycrystalline quartz (Figure 26), suggesting a dominance of felsic-rich igneous sources compared to metamorphic sources (Folk, 1974; Tucker, 2001); the probable source rocks in this case are the Precambrian crystalline basement Ethiopian plutonic igneous rocks. This provenance source can also be supported and reinforced by the straight to undulose extinctions displayed by both quartz, indicating high-grade metamorphic and plutonic origins (Bowen, 1974). This generally means that the rocks were derived from the Precambrian basement strained metamorphic rocks associated with dykes.

The observed micas in the thin sections may have originated from schist sources of the Precambrian metamorphic rocks (Mosley, 1993). The observed opaque minerals may represent those that Mathisen (1977) and Mathisen and Vondra (1983) identified, which include ilmenite being the most common, magnetite, goethite and hematite (Figure 24).

The sandstone matrix may result from diagenesis processes during rock disintegration and compression or during transportation and deposition of detrital material with the same framework grains as the sandstones (Nichols, 2009). The cement type observed in these sandstones is calcite, as mentioned above. In this case, the cement would

have been primarily derived from the basement rocks of the Cenozoic volcano-sedimentary rocks. In addition, underlying sediments from stratigraphically older units than the KBS Member (*e.g.,* Burgi Member) that underwent precipitation would be the secondary carbonate source (pedogenic carbonates). These include oncoids, stromatolites and pedogenic carbonates (Hargrave *et al.*, 2014). Another secondary direct source of carbonate precipitation would be the carbonate-rich packstones during weathering processes, resulting in calcite formation (Gierlowski-Kordesch, 2010; Hargrave *et al.*, 2014).

6.4. KBS Member palaeogeography and sediment distribution

Palaeocurrent data has long been a practical method for effectively comprehending sedimentary basin analysis and relations between sediment source and sink, delineating palaeogeography and palaeo-regional slopes (Pryor, 1961; Potter & Pettijohn, 1977; Hoque, 1975; Miall, 1996). Predictions regarding sediment provenance/source areas are determined by understanding the overall sediment dispersal directions (Dickinson, 1985). As previously mentioned, the KBS Member sandstone palaeocurrent data indicate overall south-southwest palaeoflow directions adjacent to Lake Turkana, suggesting a northern-orientated apex, which corresponds with the proposed geographic positions of the KBS Member sandstone mineralogy source areas (north and east of KFF). However, collection areas 9, 12 and 13 indicate northerly palaeoflow directions (Figure 20). Beyond the KBS Member spatial stratigraphic scale, these palaeoflow directions fit into the comprehensive basin-scale palaeogeographic and palaeoenvironmental review of the Turkana Basin between ~1.87 and ~1.6 Ma (KBS Member time interval) in relation to the ancestral Omo River hydrological systems (Brown & Feibel, 1991).

The ancestral Omo River entered the basin, flowing north to south during ~1.87 Ma, and stopped at an axial lake margin (Brown & Feibel, 1991). As the river entered the northern basin, it flowed east-southeast along the northern lake margin before turning south-southwest to the lake's margin due to expansive flood basins that flanked the course of the river (Lepre, 2009) (Figure 33A). This coincides with the obtained south-southwest palaeoflow directions and the overall increase in sandstone maturity from

collection areas 10, 6A, 8A and 8B (Ileret sub-region) to areas 105, 102, and 104 (Karari and Base Camp subregions) (Figures 20 and 26; Table 6).

In contrast, since the palaeoflow directions obtained in collection areas 9, 12 and 13 are different from the overall south-southwest palaeoflow trend, they can be attributed to depositional features of DFS, including prodeltaic and delta front (*FA4*) and crevasse splay (*FA5*). As mentioned above, these depositional features produce radial flow patterns which display various palaeoflow trends that are different from the primary channel flow trend, resulting from multiple channel shifts and changes in hydrodynamic discharge (Slingerland & Smith, 2004; Owen *et al.*, 2004; Weissmann *et al.*, 2010). However, palaeocurrent data are inconclusive in demonstrating the characteristic radial flows; therefore, palaeoflow directions obtained in collection areas 9, 12 and 13 cannot be attributed to DFS depositional features. Consequently, these presented collection areas are geographically adjacent to the proposed northern-orientated apex and consist of sub-mature sandstones (Figure 26; Table 6), supporting the impracticality of this attribution.

Alternatively, according to the basin-scale palaeogeographic and palaeoenvironmental review, the ancestral Omo River receded to the north-northwest (Nile drainage system) during ~1.8 Ma due to Lake Turkana reaching its maximum water level, resulting in a lake level regression (Lepre, 2009; Brown & Feibel, 1991). As a result of lake level fluctuations in the basin, the northeast margin produced multi-threaded channel systems that flowed in the northeast lakeshore (Lepre, 2009) (Figure 33B), supporting the overall obtained northeast palaeoflow directions and sandstone maturity in collection areas 9 and 12 (Figures 20 and 26; Table 6). The review further states that the ancestral Omo River reclaimed the northeast basin during 1.6 Ma and that the lake was extensively infilled, resulting in shallow lake remnants along the basin's north-western margin (Brown & Feibel, 1991; Lepre, 2009; Harris *et al.*, 1988) (Figure 33C), supporting the overall obtained northwest palaeoflow direction and the sandstone maturity in collection area 13 (Figures 20 and 26; Table 6).

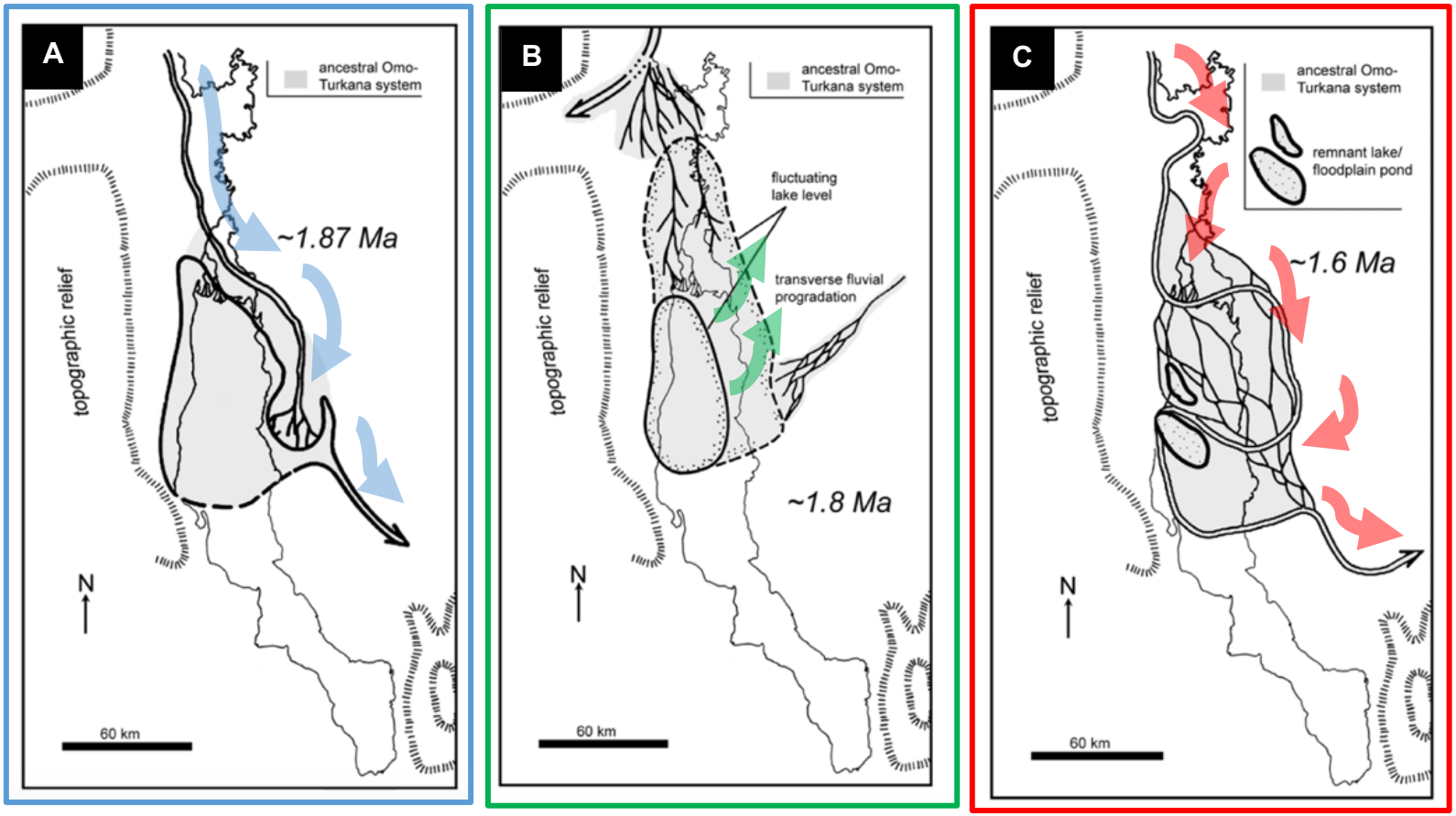

Figure 33: *Paleogeographic map of the ancestral Omo-Turkana river system from:* ***(A)*** *Around 1.87 Ma. The blue arrows indicate the Omo River entering the basin flowing from N towards SSE before turning SSW towards the lake due to extensive flood basins that flanked the course of the river.* ***(B)*** *Around 1.8 Ma. The green arrows indicate when the lake reached its maximum water level, resulting in water moving inland (lake level regression).* ***(C)*** *Around 1.6 Ma. The red arrows indicate when the river reclaimed the NE basin and that the lake was extensively infilled, changing the course of the river. Acquired and modified after Brown and Feibel (1991) and Lepre (2009).*

6.5. Sequence stratigraphic modelling

Through time and space, lake level fluctuations serve as essential archives for continental palaeoenvironmental reconstruction studies as well as a reference for interpreting atmospheric circulations and palaeohydrology constructs to infer regional and global palaeoclimate change and tectonic dynamics (Digerfeldt *et al.*, 2007; Dearing, 2013). Sedimentary records assess probable correlations and differentiations between climatic and tectonic influences, achieved through sequence stratigraphic modelling and quantifiable modelling of lake-level fluctuations.

The analysis of vertically stacking of the KBS Member lithological successions though spatial correlation of stratigraphic sections, in accordance with descriptions and interpretations of the KBS Member lithofacies (Table 3; Figure 10) as well as their depositional environments (*FA1–FA5*) (Table 4; Figures 11–16) as a subject of sequence stratigraphy, has been proposed to develop a lake-level fluctuation model (Figure 34). Referencing a broader sequence-scale resolution (low-frequency), the model delineates two well-defined parasequences depicting two distinct low-frequency palaeolake transgression and regression sequences (cyclic periods) that are defined by parasequence sets which display T-R cyclicity (TSTs and RSTs) from the KBS Member in KFF during the Pleistocene, despite the discontinuous nature of the KBS Member outcrop exposures (Figure 34). Significantly, at such a scale, the parasequence boundary surface is defined by a major MFS, marking the apex of lake transgression and the beginning of lake regression lithofacies.

The two defined parasequences are primarily bounded by the KBS Tuff as a bounding surface (at the base) and as well as the position of the Okote Tuff (at the top); which is not presented on the model due to the discontinuous exposures of these deposits, overall, providing a coherent stratigraphic marker for spatial correlation of the geographically disparate KBS Member stratigraphic sections. The lower parasequence, directly above the KBS Tuff, displays a retrogradational stacking pattern (progressive deepening succession) dominated by *FA1* and *FA2* deposits, indicative of lake expansions and rising water levels towards the parasequence boundary surface (Figure 34). In contrast, the upper parasequence displays a progradational stacking pattern (shallowing succession), dominated by *FA3* deposits, as the lake contracted prior to the deposition of the Okote Tuff (Figure 34).

Considered together, these two proposed KBS Member parasequences capture low-frequency depositional cycles (Figure 34). Presenting them at the sequence scale provides a robust stratigraphic framework for correlating discontinuous exposures, constraining their positions relative to the bounding tuffs, and palaeoenvironmental interpretation of the interplay between climatic, tectonic, and volcanic controls on the lake-level fluctuations and the KBS Member deposition during the Pleistocene.

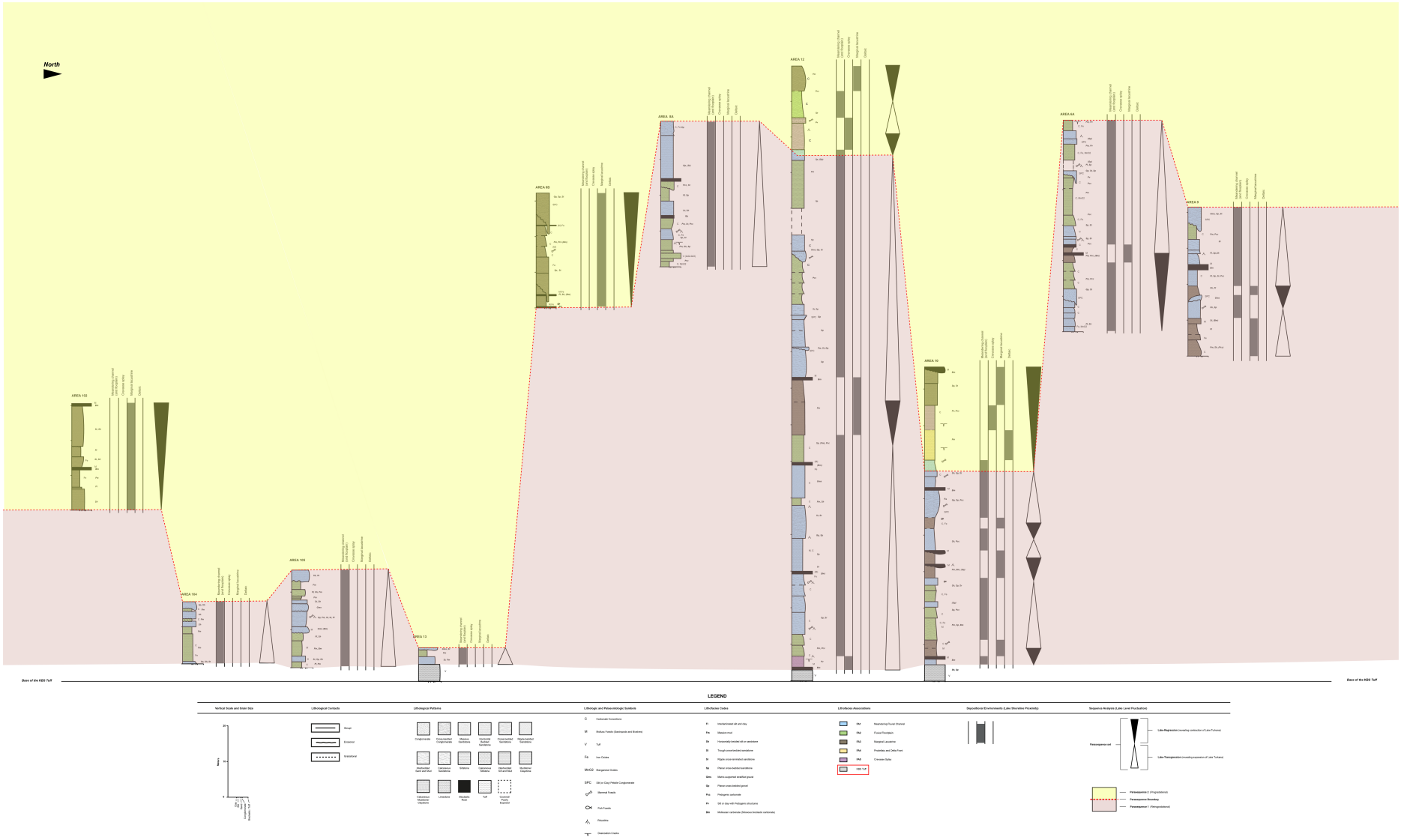

Figure 34: *Lake level fluctuation model for the KBS Member time-deposits indicating two parasequences, reflecting two low-frequency transgression-regression (T-R) cyclic periods due to Lake Turkana's water level fluctuations. The KBS Tuff is used as a sequence boundary surface. The stratigraphic sections are positioned from south to north of the KFF. A high-resolution version of this figure is found in the Appendices section (Appendix L).*

6.5.1. KBS Member time interval parasequences

6.5.1.1. Lower Parasequence: Palaeolake transgressive cyclic period (FA1 and FA2 dominated)

The lower parasequence from the bounding marker horizon (KBS Tuff) reflects a palaeolake retrogradational period primarily defined by *FA1* and *FA2* deposits and some minor *FA3* and *FA5* deposits (Figure 34). Directly overlaying the KBS Tuff, the succession of the KBS Member deposits begins with *FA1* and *FA2* deposits (collection areas 104, 105 and 13) and bioclastic sandstone deposits that are overlain by *FA5* and *FA3* deposits in collection areas 12 and 10, respectively (Figure 34).

Stratigraphic sections from collection areas 104, 105 and 13 display a parasequence set that records well-defined transgression cycles (TSTs) represented by *FA1* and *FA2* sequence alternation (Figure 34). In the stratigraphic section from collection area 104, the *FA1* deposits are overlain by 9.8 m thick *FA2* deposits that are further overlain by alternating sequences of *FA1* (2 m thick) and *FA2* (0.5 m thick) deposits (Figure 34). Similarly, in stratigraphic sections from collection areas 105 and 13, the *FA1* and *FA2* sequence alternation is apparent, beginning with *FA2* deposits (1.3 m thick) in collection area 105 and *FA1* deposits (2 m thick) in collection area 13, 4.5 m above the KBS Tuff. The *FA1* deposits range from 1.3–6 m thick, and *FA2* deposits range from 3.6–8 m thick (Figure 34). Additionally, a stratigraphic section from collection area 8 represents the *FA1* and *FA2* sequence alternation with silicious bioclastic carbonate deposits in the upper section of the KBS Member. This succession is defined by *FA1 deposits* (2–6 m thick) and *FA2* deposits (2–7 m thick).

In contrast, this is not the case for stratigraphic sections from collection areas 12, 10, 6A and 9. They consist of traces of *FA3* deposits and reveal multiple parasequence sets representing multiple T-R cycles (TSTs and RSTs) (Figure 34). Furthermore, in contrast to the stratigraphic section from collection area 8A, other upper KBS Member successions (collection areas 6A and 9) from this transgressive cyclic period demonstrate sequence alternations of *FA1*, *FA2* and *FA3* deposits and some bioclastic carbonate deposits (Figure 34). The stratigraphic section from collection area 6A displays two parasequence sets, revealing regression (RST) and transgression (TST)

cycles, respectively. However, the stratigraphic section from collection area 9 also has two parasequence sets, revealing T-R and transgression (TST) cycles, respectively (Figure 34).

Stratigraphic sections from collection areas 12 and 10 are defined by an amalgamation of depositional environments (*FA1*, *FA2*, *FA3*, *FA4* and *FA5*), directly overlaying the KBS Tuff (Figure 34). The stratigraphic section from collection area 12 displays three parasequence sets revealing three T-R cycles; nonetheless, the first two parasequence sets are within the transgressive cyclic period, except for the regression period (RST) of the second T-R cycle, which falls within the regressive cyclic period (upper parasequence) (Figure 34). In contrast, the stratigraphic section from collection area 10 displays four parasequence sets that reveal a regression cycle (RST) and three T-R cycles; the last parasequence set's regression period (RST) falls within regressive cyclic period (upper parasequence) (Figure 34). Additionally, the transitions between these two-lake level fluctuation cyclic periods in collection areas 12 and 10 successions are marked at ~134 m and ~57 m above the KBS Tuff, respectively.

6.5.1.2. Upper Parasequence: Palaeolake regressive cyclic period (FA3 dominated)

In contrast to the lower parasequence, the upper parasequence reflects a palaeolake progradational period (regressive cyclic period) primarily marked by *FA3* deposits and some minor *FA1*, *FA2*, *FA4* and *FA5* deposits (Figure 34). Directly above the parasequence boundary (from the lower parasequence), stratigraphic sections from collection areas 102 and 8B are defined by *FA3* deposits with silicious bioclastic carbonate deposits, displaying a parasequence set recording well-defined regression cycles (RSTs) (Figure 34).

In stratigraphic sections from collection areas 12 and 10, the parasequence boundary begins with *FA1* deposits that display a lake-level fluctuations transition from the lower to the upper parasequence. In collection area 12, the *FA1* deposits are overlain by minor *FA1*(4 m thick) deposits that are overlain by *FA5* (10 m thick), *FA2* (7 m thick) and *FA3* (6 m thick) deposits, revealing two parasequence sets that are defined by a

regression cycle (RST) and a T-R cycle, respectively (Figure 34). In contrast, the stratigraphic sections from collection area 10 preserve a parasequence set that records well-defined regression cycle (RST), demonstrated by a transition from *FA1* to *FA4* deposits (8 m thick) that are overlain by *FA5* (6 m thick) and *FA3* (10 m thick) deposits, as well as bioclastic carbonate deposits (1 m thick) (Figure 34).

6.5.2. Lake level fluctuations (Origin of the T-R cyclic periods)

The observed KBS Member palaeoenvironmental heterogeneity is primarily influenced by fluvial systems together with lake level fluctuations of the adjacent Lake Turkana during the Pleistocene period, as mentioned above. Through sequence stratigraphic modelling, the produced lake-level basin fluctuation model reveals that the KFF (KBS Member) experienced two low-frequency transgressive-regressive cyclic periods that are delineated by two established parasequences. The lower parasequence from the KBS Tuff reflects a palaeolake retrogradational period, whereas the upper parasequence reflects a palaeolake progradational period (see Figure 34).

Lake level fluctuations act as significant indicators of lacustrine water budget changes, changes in catchment area evaporation rates or changes in the physiography of the basin (Nutz *et al.*, 2017). These alterations in lake levels can result from complex interactions between various external factors, including climate and tectonism (and volcanism). The Turkana Basin lake level fluctuation controlling factors have been up for discussion for decades. According to some scholars, climatic conditions are proposed as the fundamental controlling factors of the fluctuations (Trauth *et al.*, 2005, 2007; Maslin & Trauth, 2009; Maslin *et al.*, 2014; Nutz *et al.*, 2020). In comparison, other scholars have suggested that local tectonism and volcanism are the fundamental control factors, with minor climate influence (Feibel, 1988; Brown & Feibel, 1991; Bruhn *et al.*, 2011; Lupien *et al.*, 2018; Boës *et al.*, 2019). Overall, the Pleistocene Lake Turkana level fluctuations and the KBS Member geographic and temporal variability palaeoenvironmental framework can be attributed to these aforementioned controlling factors.

6.5.2.1. Climatic-related factors

Climatic-related factors are considered one of the most influential drivers of modern and ancient lake-level fluctuations (Tiercelin, 1990; Harrison & Digerfeldt, 1993; Carroll & Bohacs, 1999; Lepre, 2007; Magny *et al.*, 2007; Shuman *et al.*, 2009; Nutz *et al.*, 2017; Nutz *et al.*, 2020). In the case of basins in eastern Africa (Turkana Basin), these factors include the ratio of evaporation and precipitation across water bodies, water and sediment transportation rates, and sediment deposition regimes in catchment areas, all as functions of fluctuating monsoon rainfall systems (Gasse, 2006; Lepre, 2007). Differentiating heating between marine and terrestrial regions defines these rainfall systems, which induce moisture-rich oceanic air landward convection (McGregor & Nieuwolt, 1998).

The occurrence of fluctuating monsoonal rainfall systems in basins in eastern Africa is primarily due to Northern Hemisphere summer movements during an elliptical orbital insolation, which are functions of fluctuating precession (mostly), orbital eccentricity and obliquity (Prell & Kutzbach, 1987; Clement *et al.*, 2004; Lepre, 2007). Superimposed on these elliptical orbital insolation effects are the Northern Hemisphere glaciation influences and the Intertropical Convergence Zone (ITCZ) annual latitudinal shifts, which supply moisture from the Atlantic and Indian Oceans, resulting in high seasonality (Lourens *et al.*, 1996; Peter, 2004; Lepre, 2007; Levin *et al.*, 2009; Nicholson, 2017).

As mentioned above, the KBS Member lake-level fluctuation model delineates two parasequences reflecting palaeolake retrogradational and progradational periods, demonstrating cyclic patterns in climate change, wet and dry environmental conditions, respectively, which may have influenced the ancestral Omo River runoff through the KFF (Figure 34). This model coincides with the global eccentricity cycles compared to Omo-Turkana Basin pelagic lakes and tectonic episodes presented by Gathogo (2017) and Raynolds (2024), which reveal a decline in eccentricity during the KBS Member time interval (1.87–1.6 Ma), with having a maximum eccentricity between 1.85 and 1.83 Ma and a drastic decline around ~1.7 Ma, suggesting wetter climatic conditions followed by drier conditions, respectively (Figures 32 and 35A), thus further confirming the time span of the two identified T-R cyclic periods. The model also corresponds well with the regional climatic proxy record from the

Mediterranean Sea as compared with the geological record in the Omo-Turkana Basin, also presented by Gathogo (2017) (Figure 35B).

In addition, based on sedimentary and stratigraphic evidence, *Fl*-lithofacies and desiccation cracks observed in prodeltaic and delta front (*FA4*), and crevasse splay (*FA5*) related deposits imply low-amplitude changes with moisture and sedimentary variations occurring with high-low frequencies, which can be attributed to fluctuating monsoonal rainfall systems (Lepre *et al.*, 2007). These palaeoclimatic changes are applicable as functions of shifting weather patterns and episodic and short-term processes such as seasonal and annual sediment transportation and deposition variations (Lepre *et al.*, 2007). Contrarily, the produced lake-level model presents stratigraphic variations in lithofacies palaeoenvironments defined by the observed parasequences, suggesting higher-amplitude sedimentary and hydrological fluctuations, occurring at a relatively low frequency. The identified corresponding lake level fluctuations suggest that the region experienced lake-level transgression and regression cycles, reflecting cyclic wetter and drier climatic conditions, respectively (Lepre *et al.*, 2007) (Figures 32, 34, and 35B).

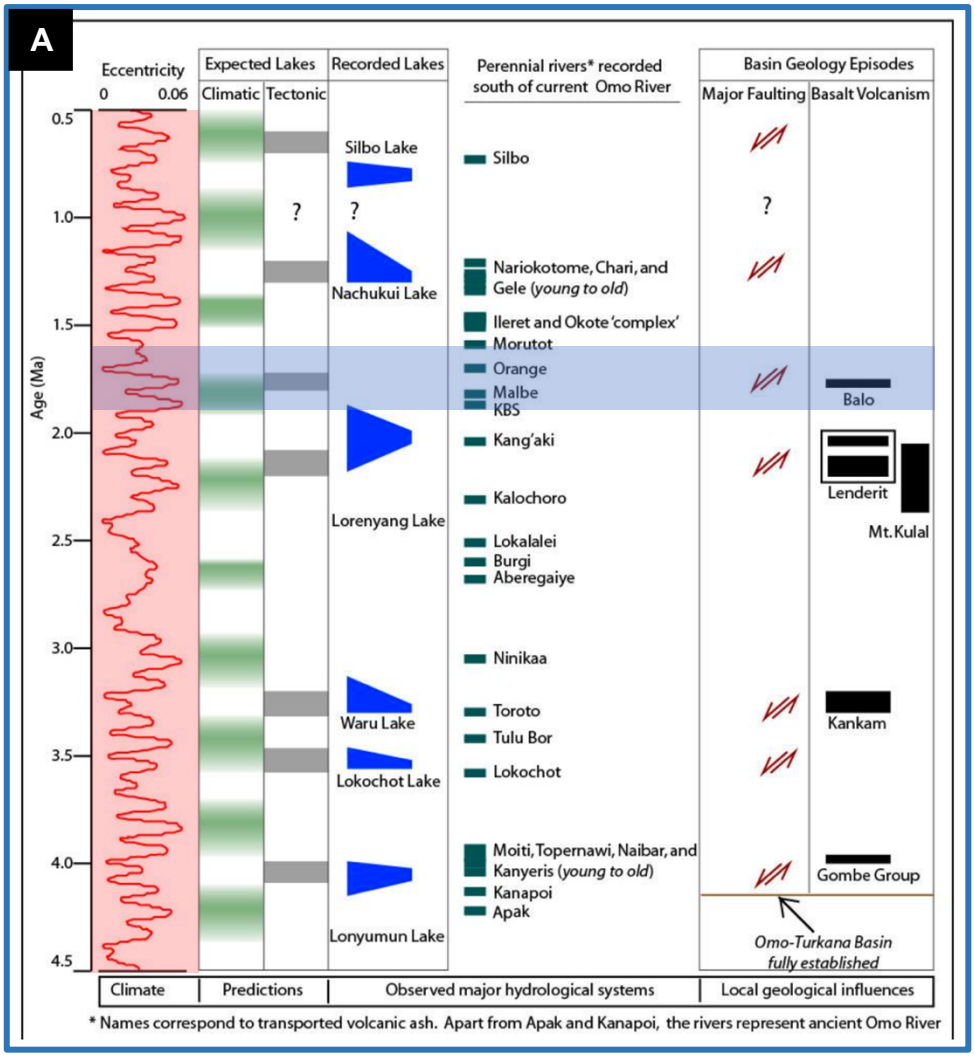

Figure 35: ***(A)*** *Overview diagram illustrating the timing of global eccentricity cycles (eccentricity), shaded in red, in association with the KBS Member time interval (1.87–1.6 Ma), shaded in blue, as well as pelagic lakes and tectonic episodes in the Omo-Turkana Basin. Acquired and modified after Gathogo (2017).* ***(B)*** *KBS Member time interval (1.87–1.60 Ma) climate proxy records based on marine deposits from the Mediterranean Sea in association with the eccentricity cycles in Figure 35A. the estimated palaeolake level fluctuation periods are indicated. Acquired and modified after Gathogo (2017). This figure is in accordance with the produced lake level model presented in Figure 34.*

As highlighted above, fluctuating monsoon rainfall systems are the primary climate-controlling factors for modern and ancient lake-level changes; this can also be confirmed by the QFL ternary diagram plotting the position of KBS Member sandstones during petrographic analysis. The produced plotting position for these ancient sediments coincides with that of Garzanti (2016) on East African Rift (EAR) modern sediments in relation to climate-related weathering, denoting that the East African Rift Basins experience intermediate to tropical dry seasons (Figure 36). These climatic seasons can be defined by extensive wet and dry conditions, which are suitable conditions for environmental physical and chemical processes that affect the relative durability of detrital minerals, as well as a diagenetic bias for quartzose to lithic sediment clastics and feldspatho-quartzose to quartzo-feldspathic sands in East African Rift settings (Garzanti, 2016; Garzanti *et al.*, 2013), supporting the overall hypothesis that the KFF experienced high seasonality which then influenced lake level fluctuations during the KBS Member time interval. Additionally, the produced KBS Member lake-level fluctuation model corresponds with the period of high humidity, as previously mentioned in the literature (Feibel, 1988, 2011; Trauth *et al.*, 2005; Lepre, 2007; Maslin *et al.*, 2014; Potts & Faith, 2015; Gathogo, 2017).

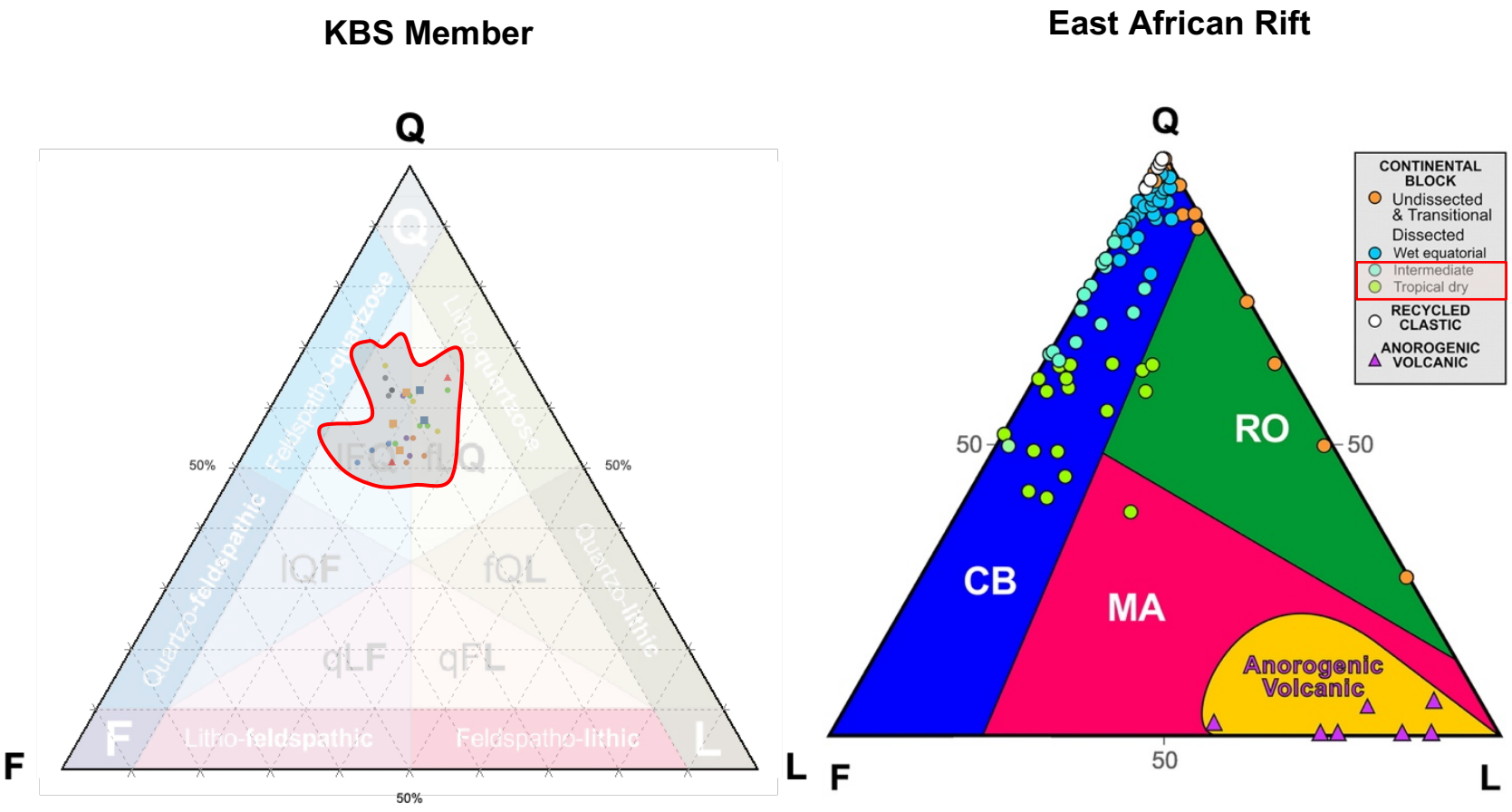

Figure 36: *KBS Member sandstone QFL ternary diagram coinciding with that of Garzanti (2016) on East African Rift modern sediments in relation to climate-related weathering, denoting that the East African Rift Basins experience intermediate to tropical dry seasons. Acquired and modified after Garzanti (2016).*

6.5.2.2. Tectonic-related factors

The significance of tectonism and volcanism as controlling factors for lake level fluctuations and the formation of lacustrine basin sedimentary sequences is often obscured by climatic-related controlling factors (Carroll & Bohacs, 1999). Tectonic controlling factors in settings of eastern Africa can be demonstrated by spatial fault distributions and tectonic movements associated with basin geometries and structures, substantially influencing lake level fluctuations, lacustrine sedimentology and stratigraphy (Tiercelin, 1990; Cohen *et al.*, 1997; Morley *et al.*, 2000). These parameters are evident in the KBS Member outcrops as major faults and disconformities, which may have exposed the basement source rocks which contributed to the framework grain mineralogy of the KBS Member sandstones or may have geographically altered the angularity of the region during the KBS Member time interval. This basin physiography alteration might have favoured fluvial catchment (source area and sediment distribution), where the ancestral Omo River, coming in from the north, entered the basin, allowing drastic outlet position alterations that contributed to the lake water balance fluctuations. This basin physiography alteration and the fluvial influence can be further supported by the tephra fluvial deposits observed during fieldwork in KBS Member sequences, suggesting periods of explosive volcanism in Ethiopia and the fluvial transportation of volcanic ash into the basin (Figures 10E, 10L, and 10M).

The main tectonic episode associated with volcanism during the KBS Member time interval was the local extrusion of the Balo Basalt at the south end of the Turkana rift segment (1.79 ± 0.02 Ma) (Gathogo *et al.*, 2008; Bruhn *et al.*, 2011; Gathogo, 2017; Boës, 2019) which occurred between 1.79 and 1.75 Ma, as part of the Paleolake Lorenyang phase which spanned between ~2.1 and ~1.3 Ma (Feibel, 2011; Nutz *et al.*, 2020; Cohen *et al.*, 2023). The Balo Basalt volcanism event closed off the Omo-Turkana outflow sill to the Indian Ocean (Cohen *et al.*, 2023), narrowing the depositional area and depositional cessation (Figure 35A). During this episode, ephemeral channels resulted in increased extensive erosion and lacustrine conditions diminished, suggesting that this tectonic episode may have produced a large and deep accommodation volume along a narrow zone within the axial centre of the basin, which

is now under Lake Turkana, that the ancestral Omo River may not have been able to fill rapidly (Gathogo, 2017).

A study by Boës *et al.* (2019) suggests that during this eruption, the Paleolake Turkana changed from being endorheic to exorheic due to the river outflow cut-offs with the Indian Ocean during the insolation/eccentricity maxima at 1.9–1.8 Ma, resulting to a palaeolake retrogradational period (lake level rise), and the opening of a new temporary outflow sill toward the west and the Mediterranean Sea. The study further mentions that according to stable isotope records (δ18O and δ13C) of fossil bivalve shells, the Paleolake Turkana was indeed temporarily exorheic around 1.9 Ma (Vonhof *et al.*, 2013), and at around 1.7 Ma, the new temporary outflow sill was cut off by a lake level fall and the Omo-Turkana outflow sill to the Indian Ocean was blocked by the Balo eruption event, resulting to a palaeolake progragadtional period. Furthermore, a study by Nutz *et al.* (2020) demonstrates that the Paleolake Lorenyang phase coincides with the Omo Valley's most significant negative shift in $\delta^{13}C$ isotopic values, suggesting an increase in precipitation on the Ethiopian Highlands, which influenced the ancestral Omo River discharge. Moreover, findings from these studies coincide with the produced lake level fluctuation model and the timing of the proposed palaeoclimatic conditions (Figures 34 and 35B).

However, the evidence presented is partially insufficient to support tectonism and volcanism as primary contributors to the KBS Member lake-level fluctuations. Therefore, it is feasible to conclude that tectonism and volcanism had minor influences on the KBS Member lake-level fluctuations compared to climatic-related conditions. However, it is crucial to note that they both played a vital role in the reorganisation of the ancestral Omo River course outflow systems and modulation responses of Palaeolake Turkana to climatic-related factors during the Pleistocene (Watkins, 1986; Haileab *et al.*, 2004; Gathogo *et al.*, 2008; Opdyke *et al.*, 2010; Bruhn *et al.*, 2011; Boës *et al.*, 2019; Nutz *et al.*, 2020).

6.5.3. Palaeonvironmnetal conditions and lake level fluctuations across the basin during the KBS Member time interval.

A recent study by Nutz *et al.* (2017) adopted sequence stratigraphy as a tool to represent the reconstruction of paleo-Lake Turkana levels, providing a comprehensive record of lake level fluctuations and palaeohydrology for Lake Turkana between 1.95 and 1.72 Ma (humid period), using the Nachukui Formation, northwest of Turkana Basin, as a study area. Based on sedimentary facies, sequence stratigraphic, bathymetry change and shoreline migration analyses, this study identified one long-term R-T cycle defined by five higher-frequency cycles of lake level fluctuations between 1.87 and 1.76 Ma (within the KBS Member time interval), appointing the origins of these T-R cyclic periods to orbital forcings, and further concluding that the region experienced relatively dry conditions and low climatic variability between 1.87 and 1.76 Ma (Nutz *et al.*, 2017). However, in contrast to the Nutz *et al.* (2017) study, this investigation strongly suggests that the eastern margin of the basin (KFF) experienced wetter conditions between 1.87 to ~1.7 Ma and drier conditions from ~1.7 until 1.6 Ma, all defined by high climatic variability (seasonality) (Figures 34 and 35B). This notable spatial variability, together with paleoenvironmental climatic condition disparity between the Nachukui and the Koobi Fora Formations throughout the same time interval, can be attributed to tectonic and geomorphological factors which may have influenced the hydrology of both formations during the KBS Member time interval.

This observed hydrological configuration can be supported by the palaeocurrent data from this study, which corresponds with the overall basin-scale palaeogeography review of Turkana Basin during the KBS Member time interval, as mentioned above, suggesting wetter conditions between 1.87 and 1.8 Ma compared to the western margin of the basin. Additionally, this observed hydrological configuration is further supported by the higher sapropel contents between 1.87 and ~1.7 Ma in KFF, as presented by Gathogo (2017), suggesting high local humidity and water inflow. Overall, this spatial variability and paleoenvironmental climatic condition disparity between the Nachukui and the Koobi Fora Formations can be secondarily supported by the Turkana-Omo rift magnetostratigraphic and sedimentological evidence presented by Lepre (2014). This study concludes that Lake Turkana expanded

asynchronously in the rift as a result of drainage network volcano-tectonic influences, which resulted in variations in depositional slopes or topographic elevations throughout the formations at times of flooding, proving a plausible explanation for hydrologic restrictions and lacustrine basin interactions through volcano-tectonic factors (Lepre, 2014).

6.5.4. Lake level fluctuation and environmental change on human evolution

The abundance of documented records of hominin fossils discovered in eastern Africa is one of the most significant sources of palaeoecological data, particularly those from the Pleistocene interval (Bobe, 2011). The KFF Pleistocene period signifies the *Paranthropus* evolution; the first emergence of the genus *Homo*, and the increase in mammalian diversity in eastern Africa (Bobe, 2011). Within this context, the presented KBS Member palaeoenvironmental heterogeneity and the two lake level fluctuation cycles suggest that hominins had access to various habitats in the northeast Turkana Basin.

Pedogenic carbonate isotope records from the Omo Group (including the KFF) reflect regional climatic changes and local biological heterogeneity, including the expansion of grasslands in floodplain environments and increased aridity during the Pliocene and Pleistocene (from ~4 Ma) (Cerling *et al.*, 1988; Levin *et al.*, 2004; Wynn, 2004; Quinn *et al.*, 2007; Levin *et al.*, 2011). These records demonstrate periods of intense aridity, resulting to a significant vegetation transition from C_3 biomass proportion to more open C_4 grassland (Bobe & Behrensmeyer, 2004; Wynn, 2004; Fernández & Vrba, 2006, Bobe, 2011; Joordens *et al.*, 2011; Lupien *et al.*, 2018; Lupien *et al.*, 2020). After ~2 Ma, this vegetation transition coincides with Lake Lorenyang's drainage, which resulted in varying water balance and vegetation across various tectonic settings and depositional environments (Levin *et al.*, 2011). Subsequently, this Lake Lorenyang phase also coincides with the produced KBS Member lake level fluctuation model (~1.87–1.6 Ma), as attributed above; the broader palaeoenvironmental instability phase.

This palaeoenvironmental instability phase is well demonstrated by the produced KBS Member lake level fluctuation model, with the lower parasequence reflecting lake expansion and retrogradational stacking pattern, and the upper parasequence recording lake contraction and progradational stacking patterns (Figure 34). These parasequences imply alternating wet and dry phases, as mentioned above, concluding that the lake margin was not a stable setting because when lake levels contract, habitats and faunal resources are reduced, and when lake levels expand, habitats and faunal resources reshape again (Trauth *et al.*, 2005; Levin, 2015; Nutz *et al.*, 2020). Such environmental conditions are the primary selection pressures on hominins, rather than long-term directional trends (Levin, 2015), meaning the KBS Member lake level fluctuations would have forced hominins to adapt to shifting water source and food availability mosaics.

During the noted transgression period, wetland and lake margins may have provided more resources and supported herbivorous populations, whereas during the regression period, the instability would have pushed the hominins toward more reliable, perennial sources such as rivers and floodplains (Potts, 1998; Bobe & Behrensmeyer, 2004; Levin, 2015). This landscape instability is a fundamental constraint that led to the rise in adaptation of open habitats, ecosystem heterogeneity, and diversity, as mentioned, which influenced the turnover of hominins (human lineage); variations from quadrupedal primates, depicting the Homo species' adaptation and evolution during the extinction of other hominin lineages (Jolly, 1970). Additionally, this landscape instability would have promoted flexibility in subsistence strategies together with habitat use, as well as mobility, fostering the development of adaptive traits that distinguish early Homo species (Potts, 1998; 2012; Levin, 2015). Thus, the presented KBS Member palaeoenvironmental heterogeneity and the identified lake level fluctuation cycles significantly influenced the evolution of hominins (genus Homo) and their cultural development; archaeological material (stone tools) in eastern Africa (Antón & Swisher, 2004; Kimbel *et al.*, 1996).

Furthermore, the mentioned palaeoenvironmental instabilities, being the primary selection pressures on hominin adaptations, are further supported by archaeological and palaeontological investigations. As highlighted above, the KBS excavations, which occurred from 1969 to 1972, yielded in situ artefacts as well as faunal remains,

suggesting hominin butchering of macro-mammals (Harris & Isaac, 1976; Isaac, 1976; Leakey & Leakey, 1978; Isaac, 1997; Braun & Harris, 2009). In the context of sequence stratigraphy, these excavation sites occur within the same depositional intervals represented in the fluctuation model (Figure 34), suggesting that hominin subsistence was directly tied to the noted lake level fluctuation phases.

CHAPTER 7: CONCLUSION

Comprehensive sedimentological, sedimentary facies, palaeocurrent, petrographic, and sequence stratigraphic studies have been conducted in the Pleistocene north-eastern Turkana Basin (Koobi Fora Formation) deposits. The KBS Member deposits (1.87–1.6 Ma) were examined to contribute to a better understanding of these deposits, including their lithofacies, depositional environments, and sediment provenance (source areas). Palaeohydrological conditions during deposition were also examined, and a lake-level basin fluctuation model of the Koobi Fora Formation during the KBS Member time interval was produced. Additionally, the effects of climatic, tectonic, and volcanic influences on the palaeogeography of the fossil record and lake level fluctuations during the Pleistocene were quantified. The main conclusions of this study are:

- The KBS Member sedimentary sequences indicate an extensive palaeoenvironmental heterogeneity across the formation, defined by eleven lithofacies and five lithofacies associations, which document four distinct palaeoenvironments: meandering fluvial channels (with associated fluvial floodplains), marginal lacustrine, prodeltaic and delta front environments, as well as crevasse splays.
- The KBS Member deposit demonstrates a significant predominance of meandering fluvial channel patterns, defined by *FA1* with associated fluvial *FA2* deposits.
- Due to study area limitations, assessing the fluvial morphology was challenging; however, limited evidence suggests the presence of distributive fluvial systems (DFS). It is crucial to note that the proposed fluvial morphology (DFS) does not refute that the KBS Member time deposits preserve ephemeral channels and alluvial systems, but contends, offering additional perspective and enhancing the fluvial dynamics and morphological interactions, suggesting that the axial fluvial system of the perennial ancestral Omo River also had distributive characters during the KBS Member time interval.

- The KBS Member sandstones can be attributed to two primary source rocks: The Precambrian crystalline basement Ethiopian plutonic igneous and metamorphic rocks, east of the basin, as well as the Kenyan Cenozoic volcano-sedimentary rocks, which extend north of the basin near the Ethiopian-Kenyan border.

- Palaeocurrent data indicate overall south-southwest palaeoflow directions adjacent to Lake Turkana, which suggests a northern-orientated apex. However, some collection areas indicate northerly palaeoflow directions. These presented palaeoflow directions correspond with the comprehensive basin-scale palaeogeography review of Turkana Basin between ~1.87 and ~1.6 Ma (KBS Member time interval) in relation to paleoenvironments and ancestral Omo River fluvial dispersal hypotheses.

- The KBS Member lake-level fluctuation model delineates two well-defined parasequences. These parasequences reflect two low-frequency transgressive-regressive cyclic periods. The lower parasequence, from the KBS Tuff, reflects a palaeolake retrogradational period, whereas the upper parasequence reflects a palaeolake progradational period. Nevertheless, this study is the first to comprehensively delineate the KBS Member depositional lithofacies and palaeoenvironmental distribution across the KFF, offering a more precise understanding of the palaeoenvironmental heterogeneity of the KBS Member.

- The lake fluctuations are primarily attributed to climatic-related factors, which are influenced by monsoonal rainfall systems as a function of Northern Hemisphere summer movements during an elliptical orbital insolation due to fluctuating precession (mostly), orbital eccentricity, and obliquity, as well as tectonic and volcanic instabilities. However, tectonism and volcanism had a minor influence on the KBS Member lake-level fluctuations compared to climatic-related conditions.

- The produced KBS Member lake-level fluctuation model corresponds to the period of high humidity during the KBS Member time interval, as previously mentioned in the literature. However, it is crucial to note that there is spatial variability and paleoenvironmental climatic condition disparity across the different formations of the basin, suggesting that Lake Turkana expanded asynchronously in the rift as a result of drainage network volcano-tectonic influences, which resulted in variations

in depositional slopes or topographic elevations throughout the formations at times of flooding, proving a plausible explanation for hydrologic restrictions and lacustrine basin interactions through volcano-tectonic factors.

- The Lake Turkana fluctuations contributed significantly to the evolution of Pleistocene hominins in the northeast Turkana Basin by developing and expanding open habitats, promoting ecosystem heterogeneity, and spatial negentropy during the substantial grassland expansion periods in East Africa, which then influenced the turnover of hominins (human lineage). Therefore, Pleistocene hominin evolution was driven by diachronic and synchronic climatic instabilities, as well as habitat heterogeneity.

This multifaceted approach will improve our understanding of the KBS Member depositional history and stratigraphic controls. The produced basin analysis model with high-resolution multiscalar palaeoenvironmental reconstruction of the landscape, together with the lake level fluctuation recognised driving forces (climate change and tectonism) in the palaeogeography of the fossil record, will serve as the environmental control setting in understanding the evolutionary succession of the genus *Homo* at the onset of the Pleistocene.

REFERENCES

Agyemang, P. C. O., Roberts, E. M., Downie, B., & Sertich, J. J. (2019). Sedimentary provenance and maximum depositional age analysis of the Cretaceous? Lapur and Muruanachok sandstones (Turkana Grits), Turkana Basin, Kenya. Geological Magazine, 156(8), 1334-1356.

Allen, J. R. L. (1963). The classification of cross-stratified units. With notes on their origin. *Sedimentology, 2*(2), 93-114.

Allen, J. R. L. (1964). A review of the origin and characteristics of recent alluvial sediments. *Sedimentology*, *5*(2), 89-191.

Allen, J. R. L. (1973). A classification of climbing-ripple cross-lamination. *Journal of the Geological Society*, *129*(5), 537-541.

Allen, J. R. L. (1983). Studies in fluviatile sedimentation: bars, bar-complexes and sandstone sheets (low-sinuosity braided streams) in the Brownstones (L. Devonian), Welsh Borders. *Sedimentary Geology*, *33*(4), 237-293.

Allen, P. H., & Allen, I. R. (1990). *Basin Analysis - Principles and Applications*. Oxford: Blackwell Scientific Publications, 451.

Alexeev, V. P. (1986). *The origin of the human race.* Moscow: Progress Publishers.

Amajor, L. C. (1987). Paleocurrent, petrography and provenance analyses of the Ajali sandstone (upper cretaceous), southeastern Benue Trough, Nigeria. *Sedimentary Geology*, *54*(1-2), 47-60.

Antón, S. C., & Swisher, C. C. (2004). Early dispersals of *Homo* from Africa. *Annual Review of Anthropology*, *33*(1), 271-296.

Arambourg, C., & Wolff, R. G. (1969). New paleontological data on the age of the “Gres du Lubur” (Turkana Grits) west of Lake Rodolphe. Proceedings of the Geological Society of France, 6, 190-202.

Aranha, R. D. J. (2015). *Factors controlling the composition and lithofacies characteristics of the Paleoproterozoic Bar River Formation, Huronian Supergroup*. London, Ontario: The University of Western Ontario (MSc Dissertation) [pdf].

Avery, S. (2010). *Hydrological impacts of Ethiopia's Omo Basin on Kenya's Lake Turkana water levels and fisheries*. Tunis: African Development Bank.

Baker, B. T., & Wohlenberg, J. (1971). Structure and evolution of the Kenya Rift Valley. *Nature*, *229*(5286), 538-542.

Baker, M. A., Stocking, R. A., & Meehan, J. P. (1972). Thermal relationship between tympanic membrane and hypothalamus in conscious cat and monkey. *Journal of Applied Physiology*, *32*(6), 739-742.

Baldes, M. J., Raynolds, R. G., & Feibel, C. S. (2024). The Upper Burgi Unconformity: A major hiatus in the fossiliferous Koobi Fora formation identified in area 116, east Turkana, Kenya. *Journal of African Earth Sciences*, *210*, 105135.

Beck, C. C., Berke, M., Feibel, C. S., Foerster, V., Olaka, L., Roberts, H. M., Scholz, C. A., Cantner, K., Noren, A., Kiptoo, G. M., Muirhead, J., & The Deep Drilling in the Turkana Basin (DDTB) project team. (2024). ICDP workshop on the Deep Drilling in the Turkana Basin project: exploring the link between environmental factors and hominin evolution over the past 4 Myr. *Scientific Drilling*, *33*, 93-108.

Behrensmeyer, A. K., & Laporte, L. F. (1981). Footprints of a Pleistocene hominid in northern Kenya. *Nature*, *289*(5794), 167-169.

Behrensmeyer, A. K., Todd, N. E., Potts, R., & McBrinn, G. E. (1997). Late Pliocene faunal turnover in the Turkana basin, Kenya and Ethiopia. *Science*, *278*(5343), 1589-1594.

Behrensmeyer, A. K., Potts, R., & Deino, A. (2018). The Oltulelei Formation of the southern Kenyan Rift Valley: A chronicle of rapid landscape transformation over the last 500 ky. *GSA Bulletin*, *130*(9-10), 1474-1492.

Beverly, E. J., Lukens, W. E., & Stinchcomb, G. E. (2018). Paleopedology as a tool for reconstructing paleoenvironments and paleoecology. *In* Croft, D. A., Su, D. F., &

Simpson, S. W. (Eds.), *Methods in paleoecology: Reconstructing Cenozoic terrestrial environments and ecological communities*. Gewerbestrasse: Spinger Nature Switzerland, 151-183.

Bishop, W. W., & Miller, J. A. (Eds.). (1972). *Calibration of Hominoid Evolution: Recent Advances in Isotopic and Other Dating Methods Applicable to the Origin of Man*. Edinburgh: Scottish Academic Press.

Blumenschine, R. J., Masao, F. T., & Stanistreet, I. G. (2009). Changes in hominin transport of stone for Oldowan tools across the eastern Olduvai Basin during lowermost Bed II times. *In* Schick, K. D., & Toth, N. P. (Ed). *The cutting edge: New approaches to the archaeology of human origins*. Pennsylvania: Stone Age Institute Press, 1-15.

Bobe, R. (2006). The evolution of arid ecosystems in eastern Africa. *Journal of Arid Environments*, *66*(3), 564-584.

Bobe, R. (2011). Fossil mammals and paleoenvironments in the Omo-Turkana Basin. *Evolutionary Anthropology: Issues, News, and Reviews*, *20*(6), 254-263.

Bobe, R., & Behrensmeyer, A. K. (2004). The expansion of grassland ecosystems in Africa in relation to mammalian evolution and the origin of the genus Homo. *Palaeogeography, Palaeoclimatology, Palaeoecology*, *207*(3-4), 399-420.

Bobe, R., & Leakey, M. G. (2009). Ecology of Plio-Pleistocene mammals in the Omo—Turkana Basin and the emergence of Homo. In *The First Humans–Origin and Early Evolution of the Genus Homo: Contributions from the Third Stony Brook Human Evolution Symposium and Workshop October 3–October 7, 2006* (pp. 173-184). Springer Netherlands.

Bobe, R., Behrensmeyer, A., Leakey, M., & Mbua, E. The Turkana Database: an archive of vertebrate evolution in East Africa. Evol. Anthropol. 20, 256 (2011).

Bobe, R., & Carvalho, S. (2019). Hominin diversity and high environmental variability in the Okote Member, Koobi Fora Formation, Kenya. *Journal of Human Evolution*, *126*, 91-105.

Bobe, R., d'Oliveira Coelho, J., Carvalho, S., & Leakey, M. (2022). Early hominins and paleoecology of the Koobi Fora Formation, Lake Turkana Basin, Kenya. *African paleoecology and human evolution*.

Boës, X., Prat, S., Arrighi, V., Feibel, C., Haileab, B., Lewis, J., & Harmand, S. (2019). Lake-level changes and hominin occupations in the arid Turkana basin during volcanic closure of the Omo River outflows to the Indian Ocean. *Quaternary Research*, *91*(2), 892-909.

Boggs Jr, S. (2006). *Principles of Sedimentology and Stratigraphy (4th Edition).* New Jersey: Pearson Prentice Hall, 662.

Boone, S. C., Kohn, B. P., Gleadow, A. J., Morley, C. K., Seiler, C., & Foster, D. A. (2019). Birth of the East African Rift System: Nucleation of magmatism and strain in the Turkana Depression. *Geology*, *47*(9), 886-890.

Bosworth, W. (1992). Mesozoic and early Tertiary rift tectonics in East Africa. *Tectonophysics*, *209*(1-4), 115-137.

Bosworth, W., & Morley, C. K. (1994). Structural and stratigraphic evolution of the Anza rift, Kenya. *Tectonophysics*, *236*(1-4), 93-115.

Bowen, B. E. (1974). *The geology of the Upper-Cenozoic sediments in the East Rudolf Embayment of the Lake Rudolf Basin, Kenya*. Ames: Iowa State University (PhD Dissertation) [pdf].

Bowen, B. E., & Vondra, C. F. (1973). Stratigraphical Relationships of the Plio-Pleistocene Deposits, East Rudolf, Kenya. *Nature*, *242*(5397), 391-393.

Braun, D. R., Rogers, M. J., Harris, J. W., & Walker, S. J. (2008). Landscape-scale variation in hominin tool use: evidence from the developed Oldowan. *Journal of Human Evolution*, *55*(6), 1053-1063.

Braun, D. R., & Harris, J. W. (2009). Plio-Pleistocene technological variation: a view from the KBS Mbr., Koobi Fora formation. *In* Schick, K. D., & Toth, N. P. (Ed). *The cutting edge: New approaches to the archaeology of human origins*. Pennsylvania: Stone Age Institute Press, 17-32.

Braun, D. R., Harris, J. W., & Maina, D. N. (2009). Oldowan raw material procurement and use: evidence from the Koobi Fora Formation. *Archaeometry*, *51*(1), 26-42.

Braun, D. R., Harris, J. W., Levin, N. E., McCoy J. T., Herries, A. I. R., Bamford M. K., Bishop, L. C., Richmond, B. G., & Kibunjia, M. (2010). Early hominin diet included diverse terrestrial and aquatic animals 1.95 Ma in East Turkana, Kenya. *Proceedings of the National Academy of Sciences*, *107*(22), 10002-10007.

Breecker, D. O., Sharp, Z. D., & McFadden, L. D. (2009). Seasonal bias in the formation and stable isotopic composition of pedogenic carbonate in modern soils from central New Mexico, USA. *Geological Society of America Bulletin*, *121*(3-4), 630-640.

Bristow, C. S., Skelly R. L., & Ethridge F. G. (1999). Crevasse splays from the rapidly aggrading, sand-bed, braided Niobrara River, Nebraska: effect of base-level rise. *Sedimentology*, *46*(6), 1029-1047.

Brown, F. H. (1995). The potential of the Turkana Basin for paleoclimatic reconstruction in East Africa. *Paleoclimate and evolution with emphasis on human origins. Yale University Press, New Haven*, 319-330.

Brown, F. H., & Cerling, T. E. (1982). Stratigraphical significance of the Tulu Bor tuff of the Koobi Fora formation. *Nature*, *299*(5880), 212-215.

Brown, F. H., & Feibel, C. S. (1985). Stratigraphical notes on the Okote Tuff Complex at Koobi Fora, Kenya. *Nature*, *316*(6031), 794-797.

Brown, F. H., & Feibel, C. S. (1986). Revision of lithostratigraphic nomenclature in the Koobi Fora region, Kenya. *Journal of the Geological Society*, *143*(2), 297-310.

Brown, F. H., & Feibel, C. S. (1991). Stratigraphy, depositional environments and palaeogeography of the Koobi Fora Formation. *Koobi Fora research project*, *3*, 1-30.

Brown, F. H., Haileab, B., & McDougall, I. (2006). Sequence of tuffs between the KBS Tuff and the Chari Tuff in the Turkana Basin, Kenya and Ethiopia. *Journal of the Geological Society*, *163*(1), 185-204.

Brown Jr, L. F., & Fisher, W. L. (1977). Seismic-stratigraphic interpretation of depositional systems: examples from brazilian rift and pull-apart basins. In Payton, C.

E. (Ed.), Seismic Stratigraphy – Applications to Hydrocarbon Exploration. American Association of Petroleum Geologists Memoir 26, 213-248.

Bruhn, R. L., Brown, F. H., Gathogo, P. N., & Haileab, B. (2011). Pliocene volcano-tectonics and paleogeography of the Turkana Basin, Kenya and Ethiopia. *Journal of African Earth Sciences*, *59*(2-3), 295-312.

Buck, W. R. (1991). Modes of continental lithospheric extension. *Journal of Geophysical Research: Solid Earth*, *96*(B12), 20161-20178.

Bunn, H. T. (1981). Archaeological evidence for meat-eating by Plio-Pleistocene hominids from Koobi Fora and Olduvai Gorge. *Nature*, *291*(5816), 574-577.

Bunn, H. T. (1994). Early Pleistocene hominid foraging strategies along the ancestral Omo River at Koobi Fora, Kenya. *Journal of Human evolution*, *27*(1-3), 247-266.

Bunn, H. T. (1997). The Bone Assemblages from the Excavated Sites. *In* Isaac, G. L. (Ed.), *Koobi Fora Research Project, vol. 5: Plio-Pleistocene Archaeology.* Oxford: Clarendon Press, 402-459.

Burggraf Jr, D. R., & Vondra, C. F. (1982). Rift valley facies and paleoenvironments: an example from the East African rift system of Kenya and southern Ethiopia. *Zeitschrift für Geomorphologie. Supplementband Stuttgart*, *42*, 43-73.

Burggraf Jr, D. R., White, H., Frank, H. J., & Vondra, C. F. (1981). The rift valley setting: Implications for hominid habitats, East Turkana, Kenya, Part II. *In* Rapp, G. R., & Vondra, C. F. (Eds.), *Hominid Sites, Their Paleoenvironmental Settings*. *AAAS Selected Symposium, 63*, 115-147.

Callahan, E. (2023). Depositional History and Provenance Analysis of the Permian-Aged Garber Sandstone, Central Oklahoma. Norman: Graduate College-University of Oklahoma (MSc Dissertation) [pdf].

Cane, M. A., & Molnar, P. (2001). Closing of the Indonesian seaway as a precursor to east African aridification around 3–4 million years ago. *Nature*, *411*(6834), 157-162.

Carr, C. J. (2017). *River basin development* and *human rights in Eastern Africa – A policy crossroads*. Gewerbestrasse: Springer Nature.

Carroll, A. R., & Bohacs, K. M. (1999). Stratigraphic classification of ancient lakes: Balancing tectonic and climatic controls. *Geology*, *27*(2), 99-102.

Catuneanu, O. (2006). *Principles of Sequence Stratigraphy*. Amsterdam: Elsevier.

Catuneanu, O. (2019). Model-independent sequence stratigraphy. *Earth-science reviews*, *188*, 312-388.

Catuneanu, O., Abreu, V., Bhattacharya, J. P., Blum, M. D., Dalrymple, R. W., Eriksson, P. G., Fielding, C. R., Fisher, W. L., Galloway, W. E., Gibling, M. R., Giles, K. A., Holbrook, J. M., Jordan, R., Kendall, C. G. StC., Macurda, B., Martinsen, O. J., Miall, A. D., Neal, J. E., Nummedal, D., Pomar Posamentier, L. H. W., Pratt, B. R., Sarg, J. F., Shanley, K. W., Steel, R.J., Strasser, A., Tucker, M. E., & Winker, C. (2009). Towards the standardisation of sequence stratigraphy. *Earth-science reviews, 92* (1- 2), 1-29.

Catuneanu, O., Galloway, W. E., Kendall, C. G. S. C., Miall, A. D., Posamentier, H. W., Strasser, A., & Tucker, M. E. (2011). Sequence stratigraphy: methodology and nomenclature. Newsletters on stratigraphy, 44, 173-245.

Cerling, T. E. (1992). Development of grasslands and savannas in East Africa during the Neogene. *Palaeogeography, Palaeoclimatology, Palaeoecology*, *97*(3), 241-247.

Cerling, T. E., & Powers, D. W. (1977). Paleorifting between the Gregory and Ethiopian rifts. *Geology*, *5*(7), 441-444.

Cerling, T. E., Cerling, B. W., Curtis, G. H., Drake, R. E., & Brown, F. H. (1979). Preliminary correlations between the Koobi Fora and Shungura Formations, East Africa. *Nature*, *279*(5709), 118-121.

Cerling, T. E., & Brown, F. H. (1982). Tuffaceous marker horizons in the Koobi Fora region and the Lower Omo Valley. *Nature*, *299*(5880), 216-221.

Cerling, T. E., Bowman, J. R., & O'Neil, J. R. (1988). An isotopic study of a fluvial-lacustrine sequence: the Plio-Pleistocene Koobi Fora sequence, East Africa. *Palaeogeography, palaeoclimatology, palaeoecology*, *63*(4), 335-356.

Cherry, S. (2012). *Sequence Stratigraphy and Depositional Systems of the Mansfield Sand, Upper Atoka Formation, Arkoma Basin, Arkansas*. Arkansas: University of Arkansas (MSc Dissertation) [pdf].

Clement, A. C., Hall, A., & Broccoli, A. J. (2004). The importance of precessional signals in the tropical climate. *Climate Dynamics*, *22*, 327-341.

Clift, P. D., Olson, E. D., Lechnowskyj, A., Moran, M. G., Barbato, A., & Lorenzo, J. M. (2019). Grain-size variability within a mega-scale point-bar system, False River, Louisiana. Sedimentology, 66(2), 408-434.

Clifton, H. E. (1971). Orientation of empty pelecypod shells and shell fragments in quiet water. *Journal of Sedimentary Research, 41*(3), 671-682.

Clifton, H. E. (2006). A re-examination of facies models for clastic shorelines. *In* Posamentier, H. W., & Walker, R. G. (Eds.), *Facies Models Revisited*, *84*, 293-337. SEPM Special Publication.

Cohen, A. S., Lezzar, K. E., Tiercelin, J. J., & Soreghan, M. (1997). New palaeogeographic and lake-level reconstructions of Lake Tanganyika: Implications for tectonic, climatic and biological evolution in a rift lake. *Basin research*, *9*(2), 107-132.

Cohen, A. S., Manobianco, J., Dettman, D. L., Black, B. A., Beck, C., Feibel, C. S., & Vonhof, H. (2023). Seasonality and lake water temperature inferred from the geochemistry and sclerochronology of quaternary freshwater bivalves from the Turkana Basin, Ethiopia and Kenya. *Quaternary Science Reviews*, *317*, 108284.

Compton, R. R. (1962). Manual of field geology. *Soil Science*, *93*(4), 295.

Craig, H., & Gordon, L. I. (1965). *Deuterium and oxygen 18 variations in the ocean and the marine atmosphere*. Laboratorio di geologia nucleare.

Crete, L. (2021). *Dietary ecology of mixed-feeding antelopes in the Omo-Turkana basin during the Plio-Pleistocene: a tool to investigate hominin palaeo-environments*. Poole: Bournemouth University (PhD Dissertation) [pdf].

Critelli, S., & Nilsen, T. H. (1996). Petrology and diagenesis of the Eocene Butano sandstone, La Honda basin, California. The Journal of Geology, 104(3), 295-315.

Curtis, G. H. (1975). Improvements in potassium-argon dating: 1962-1975. *World archaeology*, *7*(2), 198-209.

Dasgupta, P. (2002). Determination of paleocurrent direction from oblique sections of trough cross-stratification – A precise approach. *Journal of Sedimentary Research*, *72*(1), 217-219.

Day, M. H., Leakey, R. E. F., Walker, A. C., & Wood, B. A. (1976). New hominids from East Turkana, Kenya. *American Journal of Physical Anthropology*, *45*(3), 369-435.

Dearing, J. A. (2013). Why Future Earth needs lake sediment studies. *Journal of Paleolimnology, 49*, 537-545.

Delagnes, A., & Roche, H. (2005). Late Pliocene hominid knapping skills: the case of Lokalalei 2C, West Turkana, Kenya. *Journal of Human Evolution, 48*, 435-472.

de Heinzelin, J. (1983). *In* The Omo Group (Ed.), *Koninklijk Museum voor Midden-Afrika*. Geologische Wetenschappen, Tervuren.

deMenocal, P. B. (1995). Plio-pleistocene African climate. *Science*, *270*(5233), 53-59.

Dickinson, W. R. (1970). Interpreting detrital modes of graywacke and arkose. *Journal of Sedimentary Research*, *40*(2), 695-707.

Dickinson, W. R. (1985). Interpreting provenance relations from detrital modes of sandstones. *In* Reidel, D. (Ed.), *Provenance of arenites*, 333-361. Dordrecht: Springer Netherlands.

Dickinson, W. R. (1985). Interpreting provenance relations from detrital modes of sandstones. *In* Zuffa, G. G. (Ed.), Provenance of arenites. Dordrecht: Springer Netherlands, 333-361.

Dickinson, W. R. (1988). Provenance and sediment dispersal in relation to paleotectonics and paleogeography of sedimentary basins. *In* Kleinspehm, K. L., &

Paola, C. (Eds.), *New perspectives in basin analysis*, New York: Springer New York, 3-25.

Dickinson, W. R., Beard, L. S., Brakenridge, G. R., Erjavec, J. L., Ferguson, R. C., Inman, K. F., & Ryberg, P. T. (1983). Provenance of North American Phanerozoic sandstones in relation to tectonic setting. *Geological Society of America Bulletin*, *94*(2), 222-235.

Digerfeldt, G., Sandgren, P., & Olsson, S. (2007). Reconstruction of Holocene lake-level changes in Lake Xinias, central Greece. *The Holocene*, *17*(3), 361-367.

Dondeyne, S., Kangi, G., Rosier, I., Kassa, H., & Van Orshoven, J. (2024). Climate, Water and Land Use of the Omo-Turkana Basin: Opportunities and Challenges for Sound Natural Resources Management. *Proceedings of the Royal Academy of Overseas Sciences*, *2024*(2), 73-94.

Dott, R. H. (1964). Wacke, graywacke and matrix; what approach to immature sandstone classification? Journal of Sedimentary Research, 34(3), 625-632.

Drake, R. E., Curtis, G. H., Cerling, T. E., Cerling, B. W., & Hampel, J. (1980). KBS Tuff dating and geochronology of tuffaceous sediments in the Koobi Fora and Shungura Formations, East Africa. *Nature*, *283*(5745), 368-372.

Dunkelman, T. J., Karson, J. A., & Rosendahl, B. R. (1988). Structural style of the Turkana rift, Kenya. Geology, 16(3), 258-261.

Dunkelman, T. J., Rosendahl, B. R., & Karson, J. A. (1989). Structure and stratigraphy of the Turkana rift from seismic reflection data. *Journal of African Earth Sciences, 8*, 489-510.

Ebinger, C. J., & Ibrahim, A. (1994). Multiple episodes of rifting in Central and East Africa: A re-evaluation of gravity data. *Geologische Rundschau*, *83*(4), 689-702.

Ebinger, C. J., Yemane, T., Harding, D. J., Tesfaye, S., Kelley, S., & Rex, D. C. (2000). Rift deflection, migration, and propagation: Linkage of the Ethiopian and Eastern rifts, Africa. *Geological Society of America Bulletin*, *112*(2), 163-176.

Enos, P., Scholle, P. A., Bebout, D. G., & Moore, C. H. (1983). Carbonate depositional environments. *AAPG Memoir*, *33*, 507-538.

Farrell, K. M. (1987). Sedimentology and facies architecture of overbank deposits of the Mississippi River, False River region, Louisiana. *In* Ethridge, F. G., Flores, R. M., & Harvey, M. D. (Eds.), *Recent Developments in Fluvial Sedimentology, 39.* SEPM Society for Sedimentary Geology.

Fazzini, M., Bisci, C., and Billi, P. (2015). The climate of Ethiopia. *L*and*scapes* and *l*and*forms of Ethiopia*, 65-87.

Feibel, C. S. (1983). *Stratigraphy and Paleoenvironments of the Koobi Fora Formation along the Western Koobi Fora Ridge, East Turkana, Kenya*. Ames: Iowa State University (MSc Dissertation) [pdf].

Feibel, C.S. (1988). *Paleoenvironments of the Koobi Fora Formation Turkana Basin, Northern Kenya.* Salt Lake City: University of Utah (PhD Dissertation) [pdf].

Feibel, C. S. (1994). Freshwater stingrays from the Plio-Pleistocene of the Turkana Basin, Kenya and Ethiopia. *Lethaia* 26,359–366.

Feibel, C. S. (2003). Stratigraphy and depositional setting of the Pliocene Kanapoi Formation, lower Kerio valley, Kenya. *Contributions in Science, 498*, 9-20.

Feibel, C. S. (2011). A geological history of the Turkana Basin. *Evolutionary Anthropology: Issues, News, and Reviews*, *20*(6), 206-216.

Feibel, C. S. (2013). Facies Analysis and Plio-Pleistocene Paleoecology. *In* Sponheimer, M., Lee-Thorp, J. A., Reed, K. E., & Ungar, P. (Eds.), *Early Hominin Paleoecology*. University Press of Colorado, 35-58.

Feibel, C. S., & Brown, F. H. (1986). *Depositional history of the Koobi Fora Formation, northern Kenya*. *In* Proceedings of the Second Conference on the Geology of Kenya.

Feibel, C. S., Brown, F. H., & McDougall, I. (1989). Stratigraphic context of fossil hominids from the Omo group deposits: Northern Turkana Basin, Kenya and Ethiopia. *American Journal of Physical Anthropology*, *78*(4), 595-622.

Feibel, C. S., Harris, J. M., & Brown, F. H. (1991). Palaeoenvironmental context for the late Neogene of the Turkana Basin. *Koobi Fora research project*, *3*, 321-370.

Fernández, M. H., & Vrba, E. S. (2006). Plio-Pleistocene climatic change in the Turkana Basin (East Africa): evidence from large mammal faunas. *Journal of Human Evolution*, *50*(6), 595-626.

Findlater, I. C. (1976). Tuffs and the recognition of isochronous mapping units in the East Rudolf succession. *In* Coppens, Y., Howell, F. C., Isaac, G. LI., & Leakey, R. E. F. (Eds.), *Earliest Man and Environments in the Lake Rudolf Basin.* Chicago: University of Chicago Press, 94-104.

Fitch, F. J., & Miller, J. A. (1970). Radioisotopic age determination of Lake Rudolf Artefact Site. *Nature, Land*. 226, 226-228.

Fitch, F. J., Hooker, P. J., & Miller, J. A. (1976). 40Ar/39Ar dating of the KBS tuff in Koobi Fora formation, East Rudolf, Kenya. *Nature*, *263*(5580), 740-744.

Folk, R. L. (1954). The distinction between grain size and mineral composition in sedimentary-rock nomenclature. *The Journal of Geology*, *62*(4), 344-359.

Folk, R. (1974). Petrology of Sedimentary Rocks. Austin: Hemphill.

Folk, R. L. (1980). *Petrology of sedimentary rocks*. Austin: Hemphill publishing company.

Fortelius, M., Žliobaitė, I., Kaya, F., Bibi, F., Bobe, R., Leakey, L., and Werdelin, L. (2016). An ecometric analysis of the fossil mammal record of the Turkana Basin. *Philosophical Transactions of the Royal Society B: Biological Sciences*, *371*(1698), 20150232.

Frostick, L. E., & Reid, I. (1990). Structural control of sedimentation patterns and implication for the economic potential of the East African Rift basins. *Journal of African Earth Sciences (and the Middle East)*, *10*(1-2), 307-318.

Furman, T., Bryce, J. G., Karson, J., & Iotti, A. (2004). East African Rift System (EARS) plume structure: insights from Quaternary mafic lavas of Turkana, Kenya. *Journal of Petrology*, *45*(5), 1069-1088.

Furman, T., Kaleta, K. M., Bryce, J. G., & Hanan, B. B. (2006). Tertiary mafic lavas of Turkana, Kenya: constraints on East African plume structure and the occurrence of high-μ volcanism in Africa. *Journal of Petrology*, *47*(6), 1221-1244.

Garzanti, E. (2016). From static to dynamic provenance analysis—Sedimentary petrology upgraded. *Sedimentary Geology*, *336*, 3-13.

Garzanti, E. (2019). Petrographic classification of sand and sandstone. *Earth-science reviews*, *192*, 545-563.

Garzanti, E., & Vezzoli, G. (2003). A classification of metamorphic grains in sands based on their composition and grade. *Journal of Sedimentary Research*, *73*(5), 830-837.

Garzanti, E., Vezzoli, G., Andò, S., Paparella, P., & Clift, P. D. (2005). Petrology of Indus River sands: a key to interpret erosion history of the Western Himalayan Syntaxis. *Earth and Planetary Science Letters*, *229*(3-4), 287-302.

Garzanti, E., Vezzoli, G., Andò, S., Lavé, J., Attal, M., France-Lanord, C., & DeCelles, P. (2007). Quantifying sand provenance and erosion (Marsyandi river, Nepal Himalaya). *Earth and Planetary Science Letters*, *258*(3-4), 500-515.

Garzanti, E., Padoan, M., Andò, S., Resentini, A., Vezzoli, G., & Lustrino, M. (2013). Weathering and relative durability of detrital minerals in equatorial climate: sand petrology and geochemistry in the East African Rift. The Journal of Geology, 121(6), 547-580.

Gasse, F. (2006). Climate and hydrological changes in tropical Africa during the past million years. *Comptes rendus PALEVOL*, 5(1-2), 35-43.

Gathogo, N. P. (2003). *Stratigraphy and paleoenvironments of the Koobi Fora Formation of the Ileret Area, Northern Kenya*. Salt Lake City: University of Utah (MSc Dissertation) [pdf].

Gathogo, N. P. (2017). *Geology of the Omo-Turkana Basin of Eastern Africa: Tectonics and climate in the evolution in a Piocene and Pleistocene sequence*. Salt Lake City: University of Utah (PhD Dissertation) [pdf].

Gathogo, N. P., & Brown, F. H. (2006). Stratigraphy of the Koobi Fora Formation (Pliocene and Pleistocene) in the Ileret region of northern Kenya. *Journal of African Earth Sciences*, 45, 369-390.

Gathogo, N. P., Brown, F. H., & McDougall, I. (2008). Stratigraphy of the Koobi Fora Formation (Pliocene and Pleistocene) in the Loiyangalani region of northern Kenya. *Journal of African Earth Sciences*, *51*(5), 277-297.

Gazzi, P. (1966). Le arenarie del flysch sopracretaceo dell'Appennio modenese: correlazioni con il flysch di Monghidero. *Mineralogica et Petrographica Acta*, *12*, 69-97.

Gierlowski-Kordesch, E. H. (2010). Lacustrine carbonates. *Developments in sedimentology*, *61*, 1-101.

Gleadow, A. J. W. (1980). Fission track age of the KBS Tuff and associated hominid remains in northern Kenya. *Nature*, *284*(5753), 225-230.

Gómez-Gras, D., Roigé, M., Fondevilla, V., Oms, O., Boya, S., & Remacha, E. (2016). Provenance constraints on the Tremp Formation paleogeography (southern Pyrenees): Ebro Massif vs Pyrenees sources. *Cretaceous Research*, *57*, 414-427.

Goodbred Jr, S. L., & Saito, Y. (2011). Tide-dominated deltas. In Principles of tidal sedimentology. *Springer Netherlands*, 129-149.

Greenberg, E., & Ganti, V. (2024). The pace of global river meandering influenced by fluvial sediment supply. Earth and Planetary Science Letters, 634, 118674.

Groves, C. P., & Mazák, V. (1975). An approach to the taxonomy of the Hominidae: Gracile Villafranchian Hominids of Africa. Caspos Mineral Geology, 20, 225-247.

Gulliford, A. R., Flint, S. S., & Hodgson, D. M. (2014). Testing applicability of models of distributive fluvial systems or trunk rivers in ephemeral systems: Reconstructing 3-D fluvial architecture in the Beaufort Group, South Africa. *Journal of Sedimentary Research*, *84*(12), 1147-1169.

Gulliford, A. R., Flint, S. S., & Hodgson, D. M. (2017). Crevasse splay processes and deposits in an ancient distributive fluvial system: the lower Beaufort Group, South Africa. *Sedimentary Geology*, *358*, 1-18.

Haileab, B., Brown, F. H., McDougall, I. A. N., & Gathogo, P. N. (2004). Gombe Group basalts and initiation of Pliocene deposition in the Turkana depression, northern Kenya and southern Ethiopia. *Geological Magazine*, *141*(1), 41-53.

Hailemichael, M., Aronson, J. L., Savin, S., Tevesz, M. J., & Carter, J. G. (2002). $\delta^{18}O$ in mollusk shells from Pliocene Lake Hadar and modern Ethiopian lakes: Implications for history of the Ethiopian monsoon. *Palaeogeography, Palaeoclimatology, Palaeoecology*, *186*(1-2), 81-99.

Hakala, S. E. (2012). *Distribution of mammalian fauna during the early Pleistocene of the Koobi Fora formation, East Turkana, Kenya*. Georgia: University of Georgia (Msc Dissertation) [pdf].

Hammond, A. S., Mavuso, S. S., Biernat, M., Braun, D. R., Jinnah, Z., Kuo, S., Melaku, S., Wemanya, S. N., Ndiema, E. K., Patterson, D. B., & Uno, K. T. (2021). New hominin remains and revised context from the earliest *Homo erectus* locality in East Turkana, Kenya. *Nature Communications*, *12*(1), 1939.

Haq, B. U. (1991). Sequence stratigraphy, sea-level change, and significance for the deep sea. *Sedimentation, Tectonics and Eustasy: Sea-Level Changes at Active Margins*, 1-39.

Hargrave, J. E., Hicks, M. K., & Scholz, C. A. (2014). Lacustrine carbonates from Lake Turkana, Kenya: a depositional model of carbonates in an extensional basin. *Journal of Sedimentary Research*, *84*(3), 224-237.

Harmand, S., Lewis, J. E., Feibel, C. S., Lepre, C. J., Prat, S., Lenoble, A., ... & Roche, H. (2015). 3.3-million-year-old stone tools from Lomekwi 3, West Turkana, Kenya. *Nature*, *521*(7552), 310-315.

Harms, J. C., Southard J. B., & Walker, R. G. (1982). Structures and sequences in clastic rocks. *Society of Economic Paleontologists and Mineralogists, 9,* 4-19.

Harris, J.W. (1972). In: Kenya, N.M.o. (Ed.), *Field Notes on the 1972 Season at Koobi Fora*. Nairobi, Kenya.

Harris, J. W., & Isaac, G. (1976). The Karari industry: early Pleistocene archaeological evidence from the terrain east of Lake Turkana, Kenya. *Nature*, *262*(5564), 102-107.

Harris, J. M., Brown, F. H., & Leakey, M. G. (1988). Stratigraphy and paleontology of Pliocene and Pleistocene localities west of Lake Turkana, Kenya. *Contributions in Science Community Science Natural History Museum of Los Angeles, 399*, 1-128.

Harris, J. M., Brown, F. H., Leakey, M. G., Walker, A. C., & Leakey, R. E. (1988). Pliocene and Pleistocene hominid-bearing sites from west of Lake Turkana, Kenya. *Science*, *239*(4835), 27-33.

Harris, J. W. K., Leakey, M. G., & Brown, F. H. (2006). A brief history of research at Koobi Fora, northern Kenya. *Ethnohistory*, 53(*1*), 35-69.

Harrison, S. P., & Digerfeldt, G. (1993). European lakes as palaeohydrological and palaeoclimatic indicators. *Quaternary Science Reviews*, *12*(4), 233-248.

Harrison, T., & Harris, E. E. (1996). Plio-pleistocene cercopithecids from Kanam East, western Kenya. *Journal of Human Evolution*, *30*(6), 539-561.

Hay, R. L. (1980). The KBS tuff controversy may be ended. *Nature, 284*(5755), 401-401.

Helmold, K. P. (1985). Provenance of feldspathic sandstones—The effect of diagenesis on provenance interpretations: A review. Provenance of arenites, 139-163.

Hein, F. J., & Walker, R. G. (1977). Bar evolution and development of stratification in the gravelly, braided, Kicking Horse River, British Columbia. *Canadian Journal of Earth Sciences*, *14*(4), 562-570.

High, L. R., & Picard, M. D. (1974). Reliability of cross-stratification types as paleocurrent indicators in fluvial rocks. *Journal of Sedimentary Research*, *44*(1), 158-168.

Hillhouse, J. W., Ndombi, J. W. M., Cox, A., and Brock, A. (1977). Additional results on palaeomagnetic stratigraphy of the Koobi Fora Formation, east of Lake Turkana (Lake Rudolf), Kenya. *Nature*, *265*(5593), 411-415.

Hodbod, J., Stevenson, E. G., Akall, G., Akuja, T., Angelei, I., Bedasso, E. A., & Tebbs, E. (2019). Social-ecological change in the Omo-Turkana basin: A synthesis of current developments. *Ambio*, *48*, 1099-1115.

Hoque, M. (1975). Paleocurrent and paleoslope – A case study. *Palaeogeography, Palaeoclimatology, Palaeoecology*, *17*(1), 77-85.

Hsieh, J. C., Chadwick, O. A., Kelly, E. F., & Savin, S. M. (1998). Oxygen isotopic composition of soil water: quantifying evaporation and transpiration. *Geoderma*, *82*(1-3), 269-293.

Hurford, A. J., Gleadow, A. J. W., & Naeser, C. W. (1976). Fission-track dating of pumice from the KBS Tuff, East Rudolf, Kenya. *Nature*, *263*(5580), 738-740.

Ilgar, A., & Nemec, W. (2005). Early Miocene lacustrine deposits and sequence stratigraphy of the Ermenek Basin, Central Taurides, Turkey. *Sedimentary Geology*, *173*(1-4), 233-275.

Ingersoll, R. V., Bullard, T. F., Ford, R. L., Grimm, J. P., Pickle, J. D., & Sares, S. W. (1984). The effect of grain size on detrital modes: a test of the Gazzi-Dickinson point-counting method. *Journal of Sedimentary Research*, *54*(1), 103-116.

Isaac, G. L. (1976). East Africa as a source of fossil evidence for human evolution. *Human Origins: Perspectives on Human Evolution, 3,* 121-137.

Isaac, G. L. (1978). The Harvey Lecture series, 1977-1978. Food sharing and human evolution: archaeological evidence from the Plio-Pleistocene of east Africa. *Journal of Anthropological Research*, *34*(3), 311-325.

Isaac, G. L. (1997). *Koobi Fora Research Project (5th Volume): Plio-Pleistocene Archaeology*. New York: Clarendon Press.

Isaac, G. L., Leakey, R.E.F., & Behrensmeyer, A.K. (1971). Archeological traces of early hominid activities, East of Lake Rudolf, Kenya. *Science, 173*, 1129–1134.

Isaac, G. L., & Behrensmeyer, A. K. (1997). Geological context and palaeoenvironments. *Koobi Fora Research Project*, *5*, 12-70.

Jolly, C. J. (1970). The Seed-Eaters: A New Model of Hominid Differentiation Based on a Baboon Analogy. *Man, 5*(1), 5-26.

Joordens, J. C., Vonhof, H. B., Feibel, C. S., Lourens, L. J., Dupont-Nivet, G., van der Lubbe, J. H., & Kroon, D. (2011). An astronomically-tuned climate framework for hominins in the Turkana Basin. *Earth and Planetary Science Letters*, *307*(1-2), 1-8.

Keeley, L. H., & Toth, N. (1981). Microwear polishes on early stone tools from Koobi Fora, Kenya. *Nature, 293*(5832), 464-465.

Keighley, D., Flint, S., Howell, J., & Moscariello, A. (2003). Sequence stratigraphy in lacustrine basins: a model for part of the Green River Formation (Eocene), southwest Uinta Basin, Utah, USA. *Journal of Sedimentary Research*, *73*(6), 987-1006.

Kidney, C. L. (2012). *Pliocene stratigraphy and geology of the northeastern Ileret region, Kenya*. Salt Lake City: The University of Utah: (Msc Dissertation) [pdf].

Kim, S. T., & O'Neil, J. R. (1997). Equilibrium and nonequilibrium oxygen isotope effects in synthetic carbonates. *Geochimica et cosmochimica acta*, *61*(16), 3461-3475.

Kimbel, W. H. (1988). Identification of a partial cranium of Australopithecus afarensis from the Koobi Fora Formation, Kenya. *Journal of Human Evolution*, *17*(7), 647-656.

Kimbel, W. H., Walter, R. C., Johanson, D. C., Reed, K. E., Aronson, J. L., Assefa, Z., and Smith, P. E. (1996). Late Pliocene *Homo* and Oldowan tools from the Hadar Formation (Kada Hadar Member), Ethiopia. *Journal of human evolution*, *31*(6), 549-561.

Kolding, J. (1992). A summary of Lake Turkana: an ever-changing mixed environment. *Internationale Vereinigung für Theoretische und Angew*and*te Limnologie: Mitteilungen*, *23*(1), 25-35.

Kraus, M. J. (1999). Paleosols in clastic sedimentary rocks: their geologic applications. *Earth-Science Reviews, 47*(1-2), 41-70.

Kraus, M. J. (2002). Basin-scale changes in floodplain paleosols: implications for interpreting alluvial architecture. *Journal of Sedimentary Research*, *72*(4), 500-509.

Lavin, J. (2010). *Palaeoecology of the KBS Member of the Koobi Fora Formation: Implications for Pleistocene Hominin Behaviour*. Cape Town: University of Cape Town (MSc Dissertation) [pdf].

Leakey, L. S., Tobias, P. V., & Napier, J. R. (1964). A new species of the genus Homo from Olduvai Gorge. *Nature*, *202*(4927), 7-9.

Leakey, M. D. (1970). New hominid remains and early artefacts from northern Kenya: Early artefacts from the Koobi Fora area. *Nature*, *226*(5242), 228-230.

Leakey, M. D. (1976). *Olduvai Gorge*, III Cambridge: Cambridge University Press.

Leakey, M. G., & Leakey, R. F. (1978). *Koobi Fora Research Project (1st Volume): The Fossil Hominids and An Introduction to Their Context, 1968-1974*. Oxford: Clarendon.

Leakey, M. G., Feibel, C. S., McDougall, I., & Walker, A. (1995). New four-million-year-old hominid species from Kanapoi and Allia Bay, Kenya. Nature, 376(6541), 565-571.

Leakey, M. G., Spoor, F., Dean, M. C., Feibel, C. S., Antón, S. C., Kiarie, C., & Leakey, L. N. (2012). New fossils from Koobi Fora in northern Kenya confirm taxonomic diversity in early Homo. *Nature*, *488*(7410), 201-204.

Leakey, M. G., Spoor, F., Brown, F. H., Gathogo, P. N., Kiarie, C., Leakey, L. N., & McDougall, I. (2001). New hominin genus from eastern Africa shows diverse middle Pliocene lineages. Nature 410, 433-40.

Leakey, R. E. F. (1973). Further evidence of lower pleistocene hominids from East Rudolf, North Kenya, 1972. *Nature*, *242*(5394), 170-173.

Leakey, R. E. F., Behrensmeyer, A. K., Fitch, F. J., Miller, J. A., & Leakey, M. D. (1970). New hominid remains and early artifacts from northern Kenya. *Nature*, 266, 223-230.

Lepre, C. J. (2009). *Plio-pleistocene stratigraphy and paleogeography for Hominin remains from areas 130 and 133, Koobi fora, Kenya*. New Jersey: Rutgers, The State University of New Jersey (PhD Dissertation) [pdf].

Lepre, C. J. (2014). Early Pleistocene lake formation and hominin origins in the Turkana–Omo rift. *Quaternary Science Reviews*, *102*, 181-191.

Lepre, C. J. (2017). Crevasse-splay and associated depositional environments of the hominin-bearing lower Okote Member, Koobi Fora Formation (Plio-Pleistocene), Kenya. *The Depositional Record*, *3*(2), 161-186.

Lepre, C. J., Quinn, R. L., Joordens, J. C. A., Swisher, C. C., & Feibel, C. S. (2007). Plio-Pleistocene facies environments from the KBS Member, Koobi Fora Formation: implications for climate controls on the development of lake-margin hominin habitats in the northeast Turkana Basin (northwest Kenya). *Journal of Human Evolution, 53*, 504-514.

Lepre, C. J., & Kent, D. V. (2010). New magnetostratigraphy for the Olduvai Subchron in the Koobi Fora Formation, northwest Kenya, with implications for early Homo. *Earth and Planetary Science Letters*, *290*(3-4), 362-374.

Lepre, C. J., Roche, H., Kent, D. V., Harmand, S., Quinn, R. L., Brugal, J. P., Texier, P. J., & Feibel, C. S. (2011). An earlier origin for the Acheulian. *Nature*, *477*, 82-85.

Lepre, C. J., & Quinn, R. L. (2022). Aridification and orbital forcing of eastern African climate during the Plio-Pleistocene. *Global and Planetary Change*, *208*, 103684.

Levin, N. E. (2008). *Isotopic Records of Plio-Pleistocene Climate and Environments in Eastern Africa*. Salt Lake City: University of Utah (PhD Dissertation) [pdf].

Levin, N. E., Quade, J., Simpson, S. W., Semaw, S., & Rogers, M. (2004). Isotopic evidence for Plio–Pleistocene environmental change at Gona, Ethiopia. *Earth and Planetary Science Letters*, *219*(1-2), 93-110.

Levin, N. E., Zipser, E. J., & Cerling, T. E. (2009). Isotopic composition of waters from Ethiopia and Kenya: Insights into moisture sources for eastern Africa. *Journal of Geophysical Research: Atmospheres*, *114*(D23).

Levin, N. E., Brown, F. H., Behrensmeyer, A. K., Bobe, R., & Cerling, T. E. (2011). Paleosol carbonates from the Omo Group: Isotopic records of local and regional environmental change in East Africa. *Palaeogeography, Palaeoclimatology, Palaeoecology*, *307*(1-4), 75-89.

Liu, J., Zhang, C., Zhang, X., Zhu, R., & Shaohua, Z. (2024). Fluvial fan sedimentary characteristics of distributive fluvial system. *Scientific Reports*, *14*(1), 21329.

Liu, X., Madsen, D., & Zhang, X. (2021). The driving forces underlying spatiotemporal lake extent changes in the inner Tibetan Plateau during the Holocene. *Frontiers in Earth Science*, *9*, 685928.

Lourens, L. J., Antonarakou, A., Hilgen, F. J., Van Hoof, A. A. M., Vergnaud-Grazzini, C., & Zachariasse, W. J. (1996). Evaluation of the Plio-Pleistocene astronomical timescale. *Paleoceanography*, *11*(4), 391-413.

Lupien, R. L., Russell, J. M., Feibel, C., Beck, C., Castañeda, I., Deino, A., & Cohen, A. S. (2018). A leaf wax biomarker record of early Pleistocene hydroclimate from West Turkana, Kenya. *Quaternary Science Reviews*, *186*, 225-235.

Lupien, R. L., Russell, J. M., Grove, M., Beck, C. C., Feibel, C. S., & Cohen, A. S. (2020). Abrupt climate change and its influences on hominin evolution during the early Pleistocene in the Turkana Basin, Kenya. *Quaternary Science Reviews*, *245*, 106531.

Mack, G. H., James, W. C., & Monger, H. C. (1993). Classification of paleosols. *Geological society of America bulletin*, *105*(2), 129-136.

MacLatchy, L., De Silva, J.M., Sanders, W. J., & Wood, B. (2010). Hominini. *Werdelin and Sanders,* 471-540.

Magny, M., Vannière, B., de Beaulieu, J. L., Bégeot, C., Heiri, O., Millet, L., Peyron, O., & Walter-Simonnet, A. V. (2007). Early-Holocene climatic oscillations recorded by lake-level fluctuations in west-central Europe and in central Italy. *Quaternary Science Reviews*, *26*(15-16), 1951-1964.

Maguire, P. K. H., Keller, G. R., Klemperer, S. L., Mackenzie, G. D., Keranen, K., Harder, S., & Amha, M. (2006). Crustal structure of the northern Main Ethiopian Rift

from the EAGLE controlled-source survey; a snapshot of incipient lithospheric break-up. *Geological Society, London, Special Publications*, *259*(1), 269-292.

Martin, B., Owen, A., Nichols, G. J., Hartley, A. J., & Williams, R. D. (2021). Quantifying downstream, vertical and lateral variation in fluvial deposits: implications from the Huesca Distributive Fluvial System. *Frontiers in Earth Science*, *8*, 564017.

Martins-Neto, M. A., & Catuneanu, O. (2010). Rift sequence stratigraphy. *Marine and Petroleum Geology*, *27*(1), 247-253.

Maslin, M. A., & Christensen, B. (2007). Tectonics, orbital forcing, global climate change, and human evolution in Africa: introduction to the African paleoclimate special volume. *Journal of human evolution*, *53*(5), 443-464.

Maslin, M. A., & Trauth, M. H. (2009). Plio-Pleistocene East African pulsed climate variability and its influence on early human evolution. *In* Grine, F. E., Leakey, R. E., & Fleagle, J. G. (Eds.), *The First Humans: Origins of the Genus Homo*. New York: Springer, 151-158.

Maslin, M. A., Brierley, C. M., Milner, A. M., Shultz, S., Trauth, M. H., & Wilson, K. E. (2014). East African climate pulses and early human evolution. *Quaternary Science Reviews*, *101*, 1-17.

Massari, F., & Parea, G. C. (1988). Progradational gravel beach sequences in moderate- to high-energy, microtidal marine environments. *Sedimentology, 35*, 881-913.

Mathisen, M. E. (1977*). A provenance and environmental analysis of the Plio-Pleistocene sediments in the East Turkana Basin, Lake Turkana, Kenya*. Ames: Iowa State University of Science and Technology (PhD Dissertation) [pdf].

Mathisen, M. E., & Vondra, C. F. (1983). Provenance of the Plio-Pleistocene sediments in the East Turkana basin, northern Kenya. *Palaeogeography, palaeoclimatology, palaeoecology*, *44*(1-2), 141-168.

McDougall, I. (1985). K-Ar and $^{40}Ar/^{39}Ar$ dating of the hominid-bearing Pliocene-Pleistocene sequence at Koobi Fora, Lake Turkana, northern Kenya. *Geological Society of America Bulletin*, *96*(2), 159-175.

McDougall, I., Maier, R., Sutherland-Hawkes, P., & Gleadow, A. J. W. (1980). K–Ar age estimate for the KBS Tuff, East Turkana, Kenya. *Nature*, *284*(5753), 230-234.

McDougall, I., & Brown, F. H. (2006). Precise $^{40}Ar/^{39}Ar$ geochronology for the upper Koobi Fora Formation, Turkana basin, northern Kenya. *Journal of the Geological Society*, *163*(1), 205-220.

McDougall, I., & Brown, F. H. (2008). Geochronology of the pre-KBS tuff sequence, Omo Group, Turkana Basin. *Journal of the Geological Society*, *165*(2), 549-562.

McGregor, G. R., & Nieuwolt, S. (1998). *Tropical climatology—an introduction to the climates of the low latitudes*. Hoboken: John Wiley.

McKee, E. D., Crosby, E. T., & Berryhill, H. L. (1967). Flood deposits, Bijou Creek, Colorado. *Journal of Sedimentary Research*, *37*(3), 829-851.

Mechie, J., Keller, G. R., Prodehl, C., Khan, M. A., & Gaciri, S. J. (1997). A model for the structure, composition and evolution of the Kenya rift. *Tectonophysics*, *278*(1-4), 95-119.

Miall, A. D. (1974). Paleocurrent analysis of alluvial sediments; a discussion of directional variance and vector magnitude. *Journal of Sedimentary Research*, *44*(4), 1174-1185.

Miall, A. D. (1977). A review of the braided-river depositional environment. *Earth-Science Reviews*, *13*(1), 1-62.

Miall, A. D. (1996). Methods of architectural-element analysis. *The geology of fluvial deposits: sedimentary facies, basin analysis, and petroleum geology*, 75-98.

Miall, A. D. (1996). *The Geology of Fluvial Deposits: Sedimentary Facies, Basin Analysis and Petroleum Geology*. Berlin: Springer-Verlag.

Miall, A. D. (2000). *Principles of sedimentary basin analysis* (3rd Edition). Berlin: Springer-Verlag.

Miall, A. D. (2006). *The Geology of Fluvial Deposits*. Berlin: Springer-Verlag.

Middleton, G. V. (1973). Johannes Walther's law of the correlation of facies. *Geological Society of America Bulletin, 84*(3), 979-988.

Milliken, K. L., McBride, E. F., & Land, L. S. (1989). Numerical assessment of dissolution versus replacement in the subsurface destruction of detrital feldspars, Oligocene Frio Formation, South Texas. *Journal of Sedimentary Research, 59*(5), 740-757.

Morley, C. K., Wescott, W. A., Stone, D. M., Harper, R. M., Wigger, S. T., & Karanja, F. M. (1992). Tectonic evolution of the northern Kenyan Rift. *Journal of the Geological Society*, *149*(3), 333-348.

Morley, C. K., Wescott, W. A., Stone, D. M., Harper, R. M., Wigger, S. T., Day, R. A., Karanja, F. M. (1999). Geology and geophysics of the western Turkana basins, Kenya. *In*: Morley, C. K. (Ed.), *Geoscience of Rift Systems—Evolution of East Africa*. AAPG Studies Geolog, 44, 19-54.

Morley, C. K., Vanhauwaert, P., & De Batist, M. (2000). Evidence for high-frequency cyclic fault activity from high-resolution seismic reflection survey, Rukwa Rift, Tanzania. *Journal of the Geological Society*, *157*(5), 983-994.

Mosley, P. N. (1993). Geological evolution of the late Proterozoic “Mozambique Belt” of Kenya. Tectonophysics, 221(2), 223-250.

Muller, R., Nystuen, J. P., & Wright, V. P. (2004). Pedogenic mud aggregates and paleosol development in ancient dryland river systems: criteria for interpreting alluvial mudrock origin and floodplain dynamics. *Journal of Sedimentary Research, 74*(4), 537-551.

Neal, A., Richards, J., & Pye, K. (2003). Sedimentology of coarse-clastic beach-ridge deposits, Essex, southeast England. *Sedimentary Geology, 162*, 167-198.

Nichols, G. (2009). *Sedimentology and Stratigraphy (2nd Edition).* West Sussex: Wiley-Blackwell, 419.

Nichols, G. (2009). *Sedimentology and Stratigraphy*. Oxford: Wiley-Blackwell, 419.

Nichols, G. J., & Fisher, J. A. (2007). Processes, facies and architecture of fluvial distributary system deposits. *Sedimentary geology, 195*(1-2), 75-90.

Nicholson, S. (2016). The Turkana low-level jet: Mean climatology and association with regional aridity. *International Journal of Climatology*, *36*(6), 2598-2614.

Nicholson, S. E. (2017). Climate and climatic variability of rainfall over eastern Africa. *Reviews of Geophysics*, *55*(3), 590-635.

Nicholson, S. E. (2018). The ITCZ and the seasonal cycle over equatorial Africa. *Bulletin of the American Meteorological Society*, *99*(2), 337-348.

Nutz, A., Schuster, M., Boës, X., & Rubino, J. L. (2017). Orbitally-driven evolution of Lake Turkana (Turkana Depression, Kenya, EARS) between 1.95 and 1.72 Ma: A sequence stratigraphy perspective. *Journal of African Earth Sciences*, *125*, 230-243.

Nutz, A., Schuster, M., Barboni, D., Gassier, G., Van Bocxlaer, B., Robin, C., Ragon, T., Ghienne, J., & Rubino, J. (2020). Plio-Pleistocene sedimentation in West Turkana (Turkana Depression, Kenya, East African Rift System): Paleolake fluctuations, paleolandscapes and controlling factors. *Earth-Science Reviews*, *211*, 103415.

O'Brien, K., Patterson, D. B., Biernat, M. D., Braun, D. R., Cerling, T. E., McGrosky, A., & Faith, J. T. (2020). Ungulate turnover in the Koobi Fora Formation: Spatial and temporal variation in the Early Pleistocene. *Journal of African Earth Sciences*, *161*, 103658.

Olago, D. O., & Odada, E. O. (2000). An inter-basinal comparison of the sedimentology of Late Holocene to recent sediments in the Rift Valley, Lake Turkana, Kenya. *Journal of African Earth Sciences*, *31*(2), 237-252.

Olsen, P. E., Kent, D. V., Cornet, B., Witte, W. K., & Schlische, R. W. (1996). High-resolution stratigraphy of the Newark rift basin (early Mesozoic, eastern North America). *Geological Society of America Bulletin*, *108*(1), 40-77.

Opdyke, N. D., Kent, D. V., Huang, K., Foster, D. A., & Patel, J. P. (2010). Equatorial paleomagnetic time-averaged field results from 0–5 Ma lavas from Kenya and the latitudinal variation of angular dispersion. *Geochemistry, Geophysics, Geosystems*, *11*(5).

Owen, A., Nichols, G. J., Hartley, A. J., & Weissmann, G. S. (2017). Vertical trends within the prograding Salt Wash distributive fluvial system, SW United States. *Basin Research*, *29*(1), 64-80.

Patterson, D. B. (2016). *Ecosystem Evolution and Hominin Ecology between 2.0 and 1.4 Ma at East Turkana, Northern Kenya*. Washington: George Washington University (PhD Dissertation) [pdf].

Patterson, D. B., Braun, D. R., Allen, K., Barr, W. A., Behrensmeyer, A. K., Biernat, M., & Bobe, R. (2019). Comparative isotopic evidence from East Turkana supports a dietary shift within the genus Homo. *Nature ecology & evolution*, *3*(7), 1048-1056.

Peter, B. D. (2004). African climate change and faunal evolution during the Pliocene–Pleistocene. *Earth and Planetary Science Letters*, *220*(1-2), 3-24.

Pettijohn, F. J., Potter, P. E., & Siever, R. (1987). Introduction and source materials. *Sand and sandstone*, 1-21.

Phillips, D., Matchan, E. L., Gleadow, A. J. W., Brown, F. H., McDougall, I., Cerling, T. E., Leakey, M. G., Hergt, J. M., & Leakey, L. N. (2023). $^{40}Ar/^{39}Ar$ eruption ages of Turkana Basin tuffs: millennial-scale resolution constrains palaeoclimate proxy tuning models and hominin fossil ages. *Journal of the Geological Society*, *180*(4), jgs2022-171.

Pittman, E. D. (1970). Plagioclase feldspar as an indicator of provenance in sedimentary rocks. *Journal of Sedimentary Research*, *40*(2).

Plint, A. (1988). Sharp-based shoreface sequences and "Offshore Bars" In the Cardium Formation of Alberta: Their Relationship to Relative Changes in Sea Level. *In* Wilgus, C. K., Hastings, B. S., Kendall, C. G. St. C., Posamentier, H. W., Ross, C. A., & Van Wagoner, J. C (Eds.), *Sea Level Changes – An Integrated Approach, 42*. SEPM Special Publication.

Pobiner, B. L., Rogers, M. J., Monahan, C. M., & Harris, J. W. (2008). New evidence for hominin carcass processing strategies at 1.5 Ma, Koobi Fora, Kenya. *Journal of Human Evolution*, *55*(1), 103-130.

Posamentier, H. W., & Vail, G. P. (1988). Eustatic controls on clastic deposition II – sequence and systems tract models. *In* Wilgus, C. K., Hastings, B. S., Kendall, C. G., Posamentier, H. W., Ross, C. A., & Van Wagoner, J. C. (Eds.), *Sea Level Changes – an Integrated Approach, 42*. SEPM Special Publication, 125-154.

Posamentier, H. W., Allen, G. P., James, D. P., & Tesson, M. (1992). Forced regressions in a sequence stratigraphic framework: concepts, examples, and exploration significance. *AAPG bulletin*, *76*(11), 1687-1709.

Posarnentier, H. W., & Allen, G. P. (1999). *Siliciclastic sequence stratigraphy – concepts and applications*. SEPM Society for Sedimentary Geology.

Potter, P.E., & Pettijohn, F.J. (1977). *Paleocurrents and basin analysis (2nd Edition)*. Berlin: Springer-Verlag, 425.

Potts, R. (1998). Environmental hypotheses of hominin evolution. *American Journal of Physical Anthropology: The Official Publication of the American Association of Physical Anthropologists*, *107*(27), 93-136.

Potts, R. (2012). Environmental and behavioral evidence pertaining to the evolution of early Homo. *Current Anthropology, 53*(S6), S299-S317.

Potts, R., & Faith, J. T. (2015). Alternating high and low climate variability: the context of natural selection and speciation in Plio-Pleistocene hominin evolution. *Journal of Human Evolution, 87*, 5-20.

Pourmorad, S., & Jahan, S. (2021). A Model for Comprehensive Studies of Alluvial Fan Deposits: A Case Study at Ramhormoz Mega-Fan in Southwest Iran. *Advances in Applied Science Research*, *12*(3), 14.

Powers, M. C. (1953). A new roundness scale for sedimentary particles. *Journal of Sedimentary Petrology, 23*, 117-119.

Pratt, D. J., Greenway, P. J., & Gwynne, M. D. (1966). A classification of East African rangeland, with an appendix on terminology. *Journal of applied ecology*, 369-382.

Prell, W. L., & Kutzbach, J. E. (1987). Monsoon variability over the past 150,000 years. *Journal of Geophysical Research: Atmospheres*, *92*(D7), 8411-8425.

Pryor, W. A. (1961). Sand trends and paleoslope in Illinois Basin and Mississippi embayment, in Geometry of sandstone bodies. *American Association* of *Petroleum Geologists*, 119-133.

Quade, J., & Levin, N. E. (2013). East African hominid paleoecology: Isotopic evidence from paleosols. *Early hominin paleoecology*, 59-102.

Quinn, R. L. (2006). *Stable isotopic evidence for Plio-Pleistocene hominin paleoenvironments of the Koobi Fora formation, Turkana Basin, northern Kenya*. Rutgers The State University of New Jersey, School of Graduate Studies.

Quinn, R. L., Lepre, C. J., Wright, J. D., & Feibel, C. S. (2007). Paleogeographic variations of pedogenic carbonate $\delta^{13}C$ values from Koobi Fora, Kenya: implications for floral compositions of Plio-Pleistocene hominin environments. *Journal of Human Evolution*, *53*(5), 560-573.

Quinn, R. L., Lewis, J., Brugal, J. P., Lepre, C. J., Trifonov, A., & Harmand, S. (2021). Influences of dietary niche expansion and Pliocene environmental changes on the origins of stone tool making. *Palaeogeography, Palaeoclimatology, Palaeoecology*, *562*, 110074.

Ragon, T., Nutz, A., Schuster, M., Ghienne, J. F., Ruffet, G., & Rubino, J. L. (2019). Evolution of the northern Turkana Depression (East African Rift System, Kenya) during the Cenozoic rifting: New insights from the Ekitale Basin (28-25.5 Ma). *Geological Journal*, *54*(6), 3468-3488.

Rannikko, J., Žliobaitė, I., & Fortelius, M. (2017). Relative abundances and palaeoecology of four suid genera in the Turkana Basin, Kenya, during the late Miocene to Pleistocene. *Palaeogeography, Palaeoclimatology, Palaeoecology*, *487*, 187-193.

Raynolds, R. G. (2024). Time mapping in the Turkana Basin, Kenya: Applied Mapping Tools. *Journal of African Earth Sciences*, 105296.

Reading, H. G. (1996). *Sedimentary Environments: process, facies and stratigraphy*. Blackwell Science.

Reading, H. G. (Ed.). (2009). *Sedimentary environments: processes, facies and stratigraphy*. John Wiley and Sons.

Reading, H. G., & Levell, B. K. (1996). Chapter 2: Controls on the sedimentary rock record. *In* Reading, H. G. (Ed.), *Sedimentary Environments: Processes, Facies ad Stratigraphy (3rd Edition).* Oxford: Blackwell Science Ltd., Blackwell Publishing, 5-36.

Renaut, R. W., & Owen, R. B. (2023). The Turkana Basin. In *The Kenya Rift Lakes: Modern and Ancient: Limnology and Limnogeology of Tropical Lakes in a Continental Rift*. Berlin, Heidelberg: Springer Berlin Heidelberg, 631-691.

Roche, H., Delagnes, A., Brugal, J. P., Feibel, C., Kibunjia, M., Mourre, V., and Texier, P. J. (1999). Early hominid stone tool production and technical skill 2.34 Myr ago in West Turkana, Kenya. *Nature*, *399*, 57-60.

Roche, H., Brugal, J. P., Delagnes, A., Feibel, C., Harmand, S., Kibunjia, M., & Texier, P. J. (2003). Les sites archéologiques plio-pléistocènes de la formation de Nachukui, Ouest-Turkana, Kenya: bilan synthétique 1997-2001. *Comptes Rendus Palevol*, *2*(8), 663-673.

Rogers, M. J., Feibel, C. S., & Harris, J. W. K. (1994). Changing patterns of land use by Plio-Pleistocene hominids in the Lake Turkana Basin. *Journal of Human Evolution*, 27, 139-158.

Rooney, T. O., Wallace, P. J., Muirhead, J. D., Chiasera, B., Steiner, R. A., Girard, G., & Karson, J. A. (2022). Transition to magma-driven rifting in the South Turkana Basin, Kenya: Part 2. *Journal of the Geological Society*, *179*(6), 2021-160.

Rozanski, K., Araguás-Araguás, L., & Gonfiantini, R. (1993). Isotopic patterns in modern global precipitation. *Climate change in continental isotopic records*, *78*, 1-36.

Rust, B. R. (1978). A classification of alluvial channel systems. *In* Miall A. D. (Ed.), *Fluvial Sedimentology*. Canadian Society of Petroleum Geologists: Calgary, Canada, 5, 187-198.

Schick, K. D. (1987). Modeling the formation of early stone age artefact concentrations. *Journal of human evolution, 16*, 789-807.

Schieber, J. (2012). *Flume Experiments with Carbonate Muds and Their Relevance for the Micrite Problem and the Deposition of Ancient Carbonates*. Long Beach, California: AAPG Annual Meeting, Abstract Search and Discovery article #90142.

Schwartz, R. K. (1982). Broken Early Cretaceous foreland basin in southwestern Montana: sedimentation related to tectonism. *In* Powers, R. B. (Ed.), *Geologic studies of the Cordilleran thrust belt: Denver*. Rocky Mountain Association of Geologists, 159-183.

Selley, R. C. (1985). *Ancient Sedimentary Environments: And their sub-surface diagnosis*. Boston: Springer US.

Shuman, B., Henderson, A. K., Colman, S. M., Stone, J. R., Fritz, S. C., Stevens, L. R., Power, M. J., & Whitlock, C. (2009). Holocene lake-level trends in the Rocky Mountains, USA. *Quaternary Science Reviews*, *28*(19-20), 1861-1879.

Sier, M. J., Langereis, C. G., Dupont-Nivet, G., Feibel, C. S., Joordens, J. C., van Der Lubbe, J. H., & Cohen, A. (2017). The top of the Olduvai Subchron in a high-resolution magnetostratigraphy from the West Turkana core WTK13, hominin sites and Paleolakes Drilling Project (HSPDP). *Quaternary Geochronology*, *42*, 117-129.

Sikes, N. E., & Ashley, G. M. (2007). Stable isotopes of pedogenic carbonates as indicators of paleoecology in the Plio-Pleistocene (upper Bed I), western margin of the Olduvai Basin, Tanzania. *Journal of Human Evolution*, *53*(5), 574-594.

Slingerland, R., & Smith, N. D. (2004). River avulsions and their deposits. *Annual Review of Earth and Planetary Sciences, 32*(1), 257-285.

Smith, J. J., Hasiotis, S. T., Kraus, M. J., & Woody, D. T. (2008). Relationship of floodplain ichnocoenoses to paleopedology, paleohydrology, and paleoclimate in the

Willwood Formation, Wyoming, during the Paleocene-Eocene Thermal Maximum. *Palaios, 23*(10), 683-699.

Smith. N. D., Cross, T. A., Dufficy, J. P., & Clough, S. R. (1989). Anatomy of an avulsion. *Sedimentology, 36*, 1-23.

Spoor, F., Leakey, M. G., Gathogo, P. N., Brown, F. H., Antón, S. C., McDougall, I., & Leakey, L. N. (2007). Implications of new early Homo fossils from Ileret, east of Lake Turkana, Kenya. *Nature*, *448*(7154), 688-691.

Squire, O. J. (2012). *Examining atmospheric dust deposition and its effects on alpine lakes in the Uinta Mountains, Utah*. Utah: The University of Western Ontario (MSc Dissertation) [pdf].

Stanistreet, I. G., & McCarthy, T. S. (1993). The Okavango Fan and the classification of subaerial fan systems. Sedimentary geology, 85(1-4), 115-133.

Stanley, S. M. (1995). Climatic forcing and the origin of the human genus. *In* Stanley, S. M (Ed.), *Effects of past global change on life*. Washington, DC: National Academy Press, 233-243.

Suttner, L. J. (1974). Sedimentary petrographic provinces: an evaluation. *In* Ross, C. A. (Ed.), *Paleogeographic Provinces and Provinciality*. SEPM Special Publication, *21*, 75-84.

Tanner, L. H. (2002). Borate formation in a perennial lacustrine setting: Miocene–Pliocene furnace creek formation, Death Valley, California, USA. Sedimentary Geology, 148(1-2), 259-273.

Tanner, L. H. (2010). Continental carbonates as indicators of paleoclimate. Developments in Sedimentology, 62, 179-214.

Terry, R. D., & Chilingar, G. V. (1955). Summary of" Concerning some additional aids in studying sedimentary formations," by MS Shvetsov. *Journal of Sedimentary Research*, *25*(3), 229-234.

Thuo, P. (2009). *Stratigraphic, petrographic and diagenetic evaluation of Cretaceous-Paleogene potential reservoir sandstones of Western Turkana, Kenya: implications on*

the petroleum potential of Northwestern Kenya. Brest: Université de Bretagne (PhD Dissertation) [pdf].

Tiercelin, J. J. (1990). Rift-basin sedimentation: responses to climate, tectonism and volcanism. Examples of the East African Rift. *Journal of African Earth Sciences (and the Middle East)*, *10*(1-2), 283-305.

Tindall, K.W. (1986). *Stratigraphy and paleoenvironments of the Koobi Fora Formation along the eastern Koobi Fora Ridge, East Turkana, Kenya*. Ames: Iowa State University (MSc Dissertation) [pdf].

Trauth, M. H., Maslin, M. A., Deino, A., & Strecker, M. R. (2005). Late cenozoic moisture history of East Africa. *Science*, *309*(5743), 2051-2053.

Trauth, M. H., Maslin, M. A., Deino, A. L., Strecker, M. R., Bergner, A. G., & Dühnforth, M. (2007). High-and low-latitude forcing of Plio-Pleistocene East African climate and human evolution. *Journal of Human Evolution*, *53*(5), 475-486.

Trendell, A. M., Atchley, S. C., & Nordt, L. C. (2013). Facies analysis of a probable large-fluvial-fan depositional system: the Upper Triassic Chinle Formation at Petrified Forest National Park, Arizona, USA. Journal of Sedimentary Research, 83(10), 873-895.

Tucker, M. E. (2001). Sedimentary Petrology. Oxford: Blackwell.

Tylmann, W., Pędziszewska, A., Żarczyński, M., Latałowa, M., & Zolitschka, B. (2024). Lake level fluctuations and varve preservation – The sediment record from Lake Suminko (Poland) reflects European paleoclimatic changes. *Quaternary Science Reviews*, *339*, 108854.

Udden, J. A. (1914). Mechanical composition of clastic sediments. *Geological Society of America Bulletin, 25*, 655-744.

Vail, P. R. (1977). Seismic stratigraphy and global changes of sea level. *Memoir of the American Association of Petroleum Geologists*, *26*, 49-50.

Van Eeden, J. (1996). *Basin analysis and sequence stratigraphy: a review, with a short account of its applicability and utility for the exploration of auriferous placers in the Witwatersrand Basin*. Grahamstown: Rhodes University (PhD Dissertation) [pdf].

Van Wagoner, J. C., Mitchum, R. M., Campion, K. M., & Rahmanian, V. D. (1990). Siliciclastic sequence stratigraphy in well logs, cores, and outcrops: concepts for high-resolution correlation of time and facies. *American Association* of Petroleum Geologists Methods in Exploration Series, 7, 55.

Vetel, W., & Le Gall, B. (2006). Dynamics of prolonged continental extension in magmatic rifts: the Turkana Rift case study (North Kenya). *Geological Society, London, Special Publications*, *259*(1), 209-233.

Villaseñor, A., Uno, K. T., Kinyanjui, R. N., Behrensmeyer, A. K., Bobe, R., Advokaat, E. L., & Braun, D. R. (2023). Pliocene hominins from East Turkana were associated with mesic environments in a semiarid basin. *Journal of Human Evolution*, *180*, 103385.

Vondra, C. F., Johnson, G. D., Behrensmeyer, A. K., & Bowen, B. E. (1971). Preliminary stratigraphical studies of the East Rudolf basin, Kenya. *Nature*, 231, 245-248.

Vondra, C. F., & Bowen, B. E. (1976). Plio-Pleistocene deposits and environments, East Rudolf, Kenya. *Earliest Man and Environments in the Lake Rudolf Basin*, 79-93.

Vondra, C. F., & Burggraf Jr, D. R. (1977). Fluvial facies of the Plio-Pleistocene Koobi Fora Formation, Karari Ridge, East Lake Turkana, Kenya. *In* Miall, A. D. (Ed.), *Fluvial Sedimentology (5th Volume)*. Canadian Society of Petroleum Geologists Memoir, 511-529.

Vondra, C. F., & Bowen, B. E. (1978). Stratigraphy, sedimentary facies and paleoenvironments, East Lake Turkana, Kenya. *Geological Society, London, Special Publications*, *6*(1), 395-414.

Vondra, C. F., Burggraf Jr, D. R., & White, H. J. (1978). The Plio-Pleistocene, sediments, environments, and chronology along the Karari escarpment, East Turkana, Kenya. *Transactions of the Nebraska Academy of Sciences*, *6*, 19-34.

Vonhof, H. B., Joordens, J. C., Noback, M. L., van der Lubbe, J. H., Feibel, C. S., & Kroon, D. (2013). Environmental and climatic control on seasonal stable isotope variation of freshwater molluscan bivalves in the Turkana Basin (Kenya). *Palaeogeography, Palaeoclimatology, Palaeoecology*, *383*, 16-26.

Vrba, E. S., Denton, G. H., Partridge, T. C., & Burckle, L. H. (Eds.). (1995). *Paleoclimate and evolution, with emphasis on human origins*. Yale University Press.

Walker, R. G. (1997). Facies and Facies Models. General Introduction. *In* Walker, R. G., & James, N. P. (Eds.), *Facies Models: Response to Sea Level Change*. St. John's, Newfoundland: GEOText 1, Geological Association of Canada, 1-14.

Walter, H. (1970). *Vegetation zones and climate.* Stuttgart: Eugen Ulmer.

Wang, Z., Zhu, X., Wu, Z., Liu, F., Liang, B., He, Y., & Huang, F. (2018). Experiment research on geometry and evolution characteristics of sand wave bedforms generated by waves and currents. In *IOP Conference Series: Earth and Environmental Science, 171*(1), 012002.

Watkins, R. T. (1986). Volcano-tectonic control on sedimentation in the Koobi Fora sedimentary basin, Lake Turkana. *Geological Society, London, Special Publications, 25*(1), 85-95.

Weissmann, G. S., Hartley, A. J., Nichols, G. J., Scuderi, L. A., Olson, M., Buehler, H., & Banteah, R. (2010). Fluvial form in modern continental sedimentary basins: distributive fluvial systems. *Geology*, *38*(1), 39-42.

Weltje, G. J., & von Eynatten, H. (2004). Quantitative provenance analysis of sediments: review and outlook. *Sedimentary geology*, 171(1-4), 1-11.

Wentworth, C. K. (1922). A scale of grade and class terms for clastic sediments. *Journal of Geology*, *30*, 377-394.

White, H., Burggraf Jr, D. R., Bainbridge, R. B., & Vondra, C. F. (1981). The rift valley setting: Implications for hominid habitats, East Turkana, Kenya, Part I. *In* Rapp, G. R., & Vondra, C. F. (Eds.), *Hominid Sites, Their Paleoenvironmental Settings, 63*. AAAS Selected Symposium, 57-113.

White, T. D., & Harris, J. M. (1977). Suid evolution and correlation of African hominid localities. *Science*, *198*(4312), 13-21.

Wilson, K. E., Maslin, M. A., Leng, M. J., Kingston, J. D., Deino, A. L., Edgar, R. K., & Mackay, A. W. (2014). East African lake evidence for Pliocene millennial-scale climate variability. *Geology*, *42*, 955-958.

Withjack, M. O., Schlische, R. W., & Olsen, P.E. (2002). Rift basin structure and its inf luence on sedimentary systems. *In* Renaut, R. W., & Ashley, G. M. (Eds.), *Sedimentation in Continental Rifts, 73*. SEPM Special Publication, 57-81.

WoldeGabriel, G., Hart, W. K., Katoh, S., Beyene, Y., & Suwa, G. (2005). Correlation of Plio–Pleistocene Tephra in Ethiopian and Kenyan rift basins: Temporal calibration of geological features and hominid fossil records. *Journal of Volcanology and Geothermal Research*, *147*(1-2), 81-108.

Wood, B. A. (1991). The evolution of Homo erectus: By G. Philip Rightmire (1990). Cambridge: Cambridge University Press. xii+ 260 pp.£ 32· 50/$44· 50. ISBN 0-521-30880-1. *Journal of Human Evolution*, *21*(6), 491-494.

Wood, B. A. (1991). *Koobi Fora Research Project (4th Volume): Hominid Cranial Remains from Koobi Fora*. Oxford: Clarendon.

Wood, B. A. (1992). Origin and evolution of the genus Homo. *Nature*, *355*(6363), 783-790.

Wood, B. A. (1996). Human evolution. *Bioessays*, *18*(12), 945-954.

Wood, B. A. (2009). Where does the genus Homo begin, and how would we know? In The First Humans-Origin and Early Evolution of the Genus Homo: Contributions from the Third Stony Brook Human Evolution Symposium and Workshop October 3-October 7, 2006. *Springer*, 17-28.

Wood, B. A., & Strait, D. (2004). Patterns of resource use in early Homo and Paranthropus. *Journal of Human Evolution, 46*(2), 119-162.

Wood, B. A., & Baker, J. (2011). Evolution in the genus Homo. *Annual Review of Ecology, Evolution, and Systematics,* 42, 47-69.

Wood, B. A., & Leakey, M. (2011). The Omo-Turkana Basin fossil hominins and their contribution to our understanding of human evolution in Africa. Evolutionary Anthropology. *Issues, News, and Reviews, 20*(6), 264-292.

Wynn, J. G. (1998). *Paleopedological characteristics associated with intervals of environmental change from the Neogene Turkana Basin, Northern Kenya*. Salt Lake City: University of Utah (PhD Dissertation) [pdf].

Wynn, J. G. (2000). Paleosols, stable carbon isotopes, and paleoenvironmental interpretation of Kanapoi, Northern Kenya. *Journal of Human Evolution*, *39*(4), 411-432.

Wynn, J. G. (2004). Influence of Plio-Pleistocene aridification on human evolution: Evidence from paleosols of the Turkana Basin, Kenya. *American Journal of Physical Anthropology: The Official Publication of the American Association of Physical Anthropologists*, *123*(2), 106-118.

Wynn, J. G., & Feibel, C. S. (1995). Paleoclimatic implications of vertisols within the Koobi Fora Formation, Turkana Basin, Northern Kenya. *Journal of Undergraduate Research and Scholarly Excellence*, *6*, 33-42.

Yost, C. L., Lupien, R. L., Beck, C., Feibel, C. S., Archer, S. R., & Cohen, A. S. (2021). Orbital influence on precipitation, fire, and grass community composition from 1.87 to 1.38 Ma in the Turkana Basin, Kenya. *Frontiers in Earth Science*, *9*, 568646.

Yuretich, R. F. (1979). Modern sediments and sedimentary processes in Lake Rudolf (Lake Turkana) eastern rift valley, Kenya. *Sedimentology*, *26*(3), 313-331.

Zavala, C., Liu, H. Q., Li, X. B., Trobbiani, V., Li, Y., Arcuri, M., & Zorzano, A. (2024). High-frequency lacustrine sequence stratigraphy of clastic lakes: lessons from ancient successions. *Journal of Palaeogeography.*

APPENDICES

Appendix A: High resolution map of **(A)** Digital elevation model (DEM) map showing the East African Turkana Basin, Kenya, with the Koobi Fora (Red Box), Nachukui and Shungura Formations. The DEM data was acquired from the World Resources Institute. **(B)** Satellite image of the Koobi Fora Region (formation) with Lake Turkana in the western end of the image, showing the formations' subregions and collection areas (represented by white numerals) from which the KBS Member sandstone and supplemented datasets were derived: Ileret (Blue), Karari (Green) and Base Camp (Red) subregions.

Appendix B: High resolution map showing the geological setting of the Turkana Basin. **(A)** Position of the Turkana Basin within the East African Rift System (EARS), between the Ethiopian and Kenyan domal uplifts. **(B)** Geological map of the Turkana Basin compiled from Ragon *et al.* (2019), Nutz *et al.* (2020), and Renault and Owen (2023). The study area is located east of the Northern Lake Basin (Koobi Fora Formation); shown by a red block, together with the palaeomargin of Lake Lorenyang (2–1.6 Ma) in reference to the present Lake Turkana; shown by the navy-blue dotted lines, after Brown and Feibel (1991). **(C)** Stratigraphic and geologic chart of the Turkana Basin; after Renault and Owen (2023).

Appendix C: Database of KBS Member sandstones collected during field work. Collector: Bukho Charles (BC).

Appendix D: Munsell's geological colour chart. Retrieved from:

https://www.vawaterwellassociation.org/wp-content/uploads/2014/05/Munsell-sample-from-the-munsell-website-CIPA00011_599.pdf

Appendix E: Palaeocurrent data collected during field work.

Appendix F: Composite stratigraphic section of the KBS Member as an illustration demonstrating the origin and internal organisation of a lacustrine continental rift depositional sequence generated during lake-level fluctuations.

Appendix G: High resolution stratigraphic sections with noted positions for rock sample and palaeocurrent reading collections (Arranged form South to North).

Appendix H: High resolution spatial correlation of KBS Member stratigraphic sections (Arranged form South to North).

Appendix I: High resolution spatial correlation of KBS Member stratigraphic sections with QFL mineralogical proportions (Arranged form South to North).

Appendix J: High resolution schematic palaeoenvironmental reconstruction of the KBS Member lithofacies association across the KFF

Appendix K: High resolution schematic palaeoenvironmental reconstruction of the KBS Member lithofacies association across the KFF showing depositional evolution of the KBS Member deposits with dominance of fluvial systems presence at 1.87–~Ma **(A)** and a dominance of lacustrine presence (Lake Lorenyang) at ~1.7–1.6 Ma **(B)**. The palaeoenvironmental distribution and shoreline are inferred from Brown and Feibel (1991) in accordance with the conducted palaeocurrent directions (see Figure 20), identified KBS Member lithofacies association distribution (see Figure 31), and the produced KBS Member lake level fluctuation model (see Figure 34). Note that the schematic is superimposed on the KFF's modern location and this study's collection areas for orientation.

Appendix L: High resolution lake level fluctuation model for the KBS Member time-deposits (Arranged form South to North).

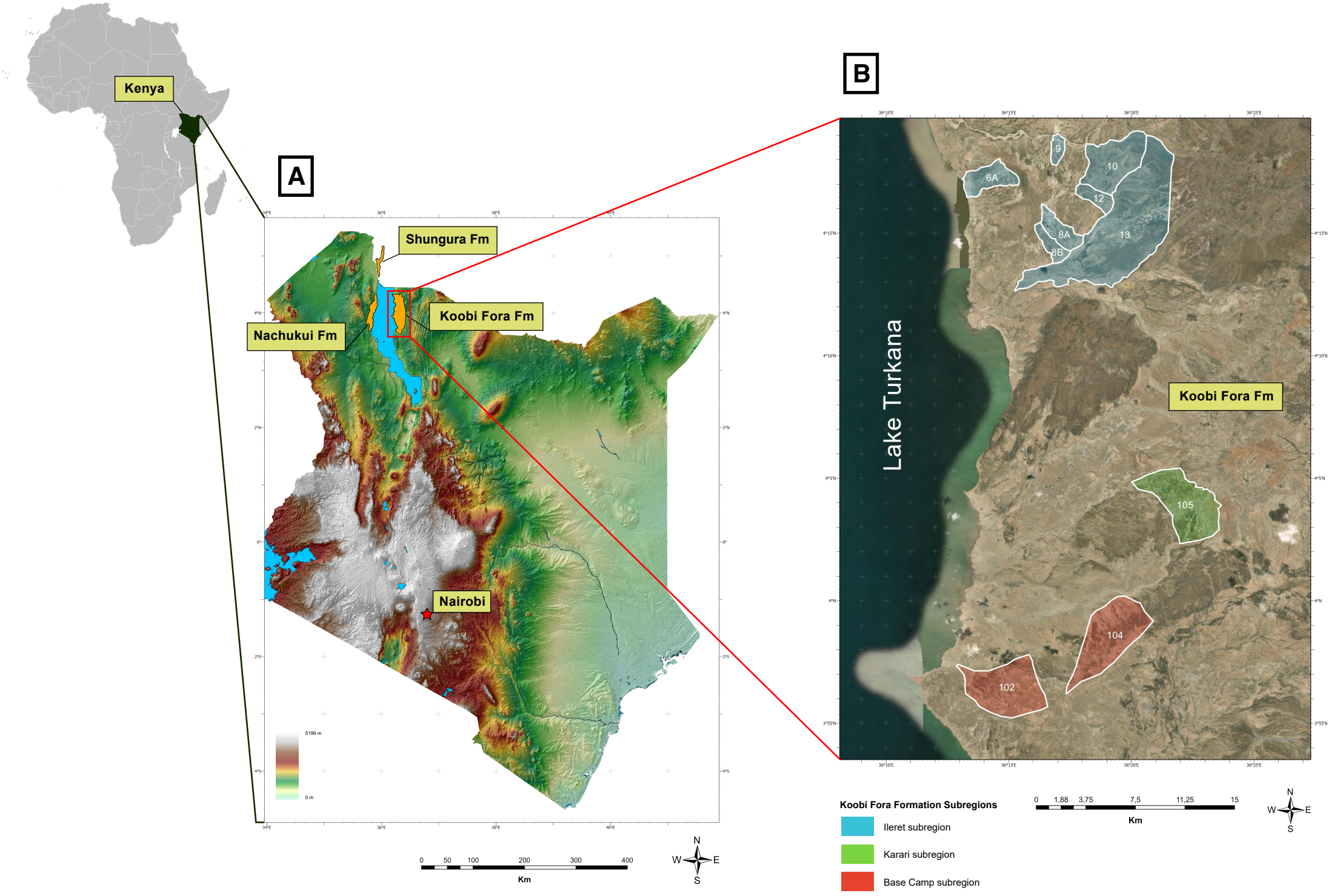
Kenya
A
Shungura Fm
Koobi Fora Fm
Nachukui Fm
Nairobi
5199 m
0 m
0 50 100 200 300 400
Km
N
W
E
S
B
Lake Turkana
Koobi Fora Fm
9
10
6A
12
8A
13
8B
105
104
102
Koobi Fora Formation Subregions
Ileret subregion
Karari subregion
Base Camp subregion
0 1,88 3,75 7,5 11,25 15
Km
N
W
E
S

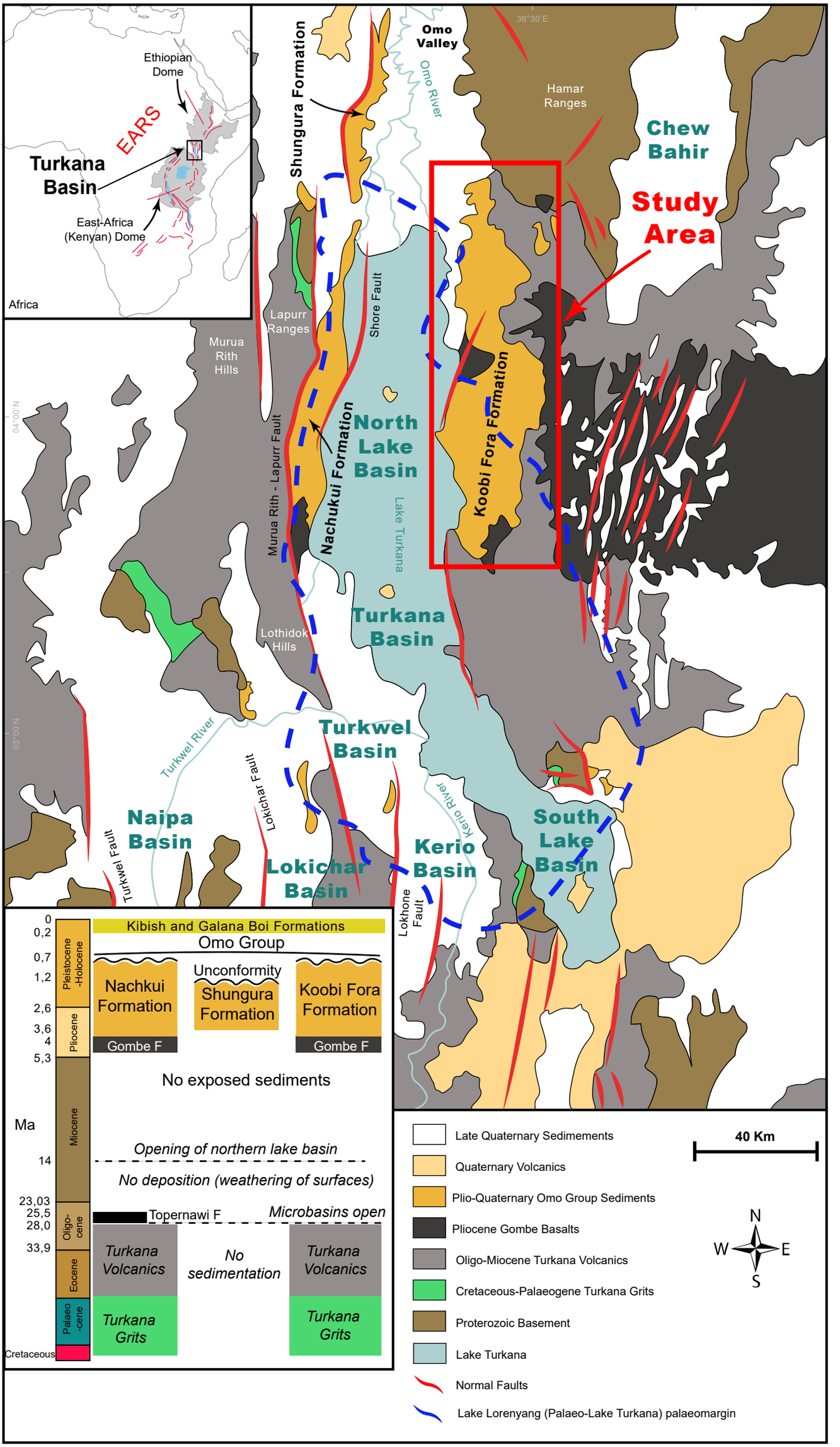
Ethiopian Dome
EARS
Turkana Basin
East-Africa (Kenyan) Dome
Africa
Shungura Formation
Omo Valley
Omo River
36°30'E
Hamar Ranges
Chew Bahir
Study Area
Lapurr Ranges
Shore Fault
Murua Rith Hills
Murua Rith - Lapurr Fault
Nachukui Formation
North Lake Basin
Koobi Fora Formation
Lake Turkana
Turkana Basin
Lothidok Hills
Turkwel River
Turkwel Basin
Lokichar Fault
Kerio River
Naipa Basin
Turkwel Fault
Lokichar Basin
Kerio Basin
South Lake Basin
Lokhone Fault
04°00'N
03°00'N
Kibish and Galana Boi Formations
Omo Group
Nachkui Formation
Unconformity
Shungura Formation
Koobi Fora Formation
Gombe F
Gombe F
No exposed sediments
Opening of northern lake basin
No deposition (weathering of surfaces)
Topernawi F
Microbasins open
Turkana Volcanics
No sedimentation
Turkana Volcanics
Turkana Grits
Turkana Grits
Ma
0
0,2
0,7
1,2
2,6
3,6
4
5,3
14
23,03
25,5
28,0
33,9
Pleistocene -Holocene
Pliocene
Miocene
Oligo-cene
Eocene
Palaeo -cene
Cretaceous
Late Quaternary Sedimements
Quaternary Volcanics
Plio-Quaternary Omo Group Sediments
Pliocene Gombe Basalts
Oligo-Miocene Turkana Volcanics
Cretaceous-Palaeogene Turkana Grits
Proterozoic Basement
Lake Turkana
Normal Faults
Lake Lorenyang (Palaeo-Lake Turkana) palaeomargin
40 Km
N
W
E
S

Appendix C: *Database of KBS Member sandstones collected during field work. Collector: Bukho Charles (BC).*

Field number	Collection method	Collector	Date (M/D/Y)	Collection material	Chronology 1	Chronology 2	Lat	Long	Collecting area	Context	Analysis	Notes
BC2301	Surface Collection	BC	6/03/2023	Sample (Micromorph)	Pleistocene	KBS Mbr	4.28812	36.30822	10	Sand	Petrography	Sandstone, 1m above the KBS Tuff, Sr
BC2303	Surface Collection	BC	6/03/2023	Sample (Micromorph)	Pleistocene	KBS Mbr	4.283003	36.31553	10	Sand	Petrography	Sandstone, right above the KBS Tuff, with gastropods and bivalves as a top unit
BC2304	Surface Collection	BC	6/03/2023	Sample (Micromorph)	Pleistocene	KBS Mbr	4.27797	36.31100	10	Sand	Petrography	Sandstone, 1st SS (conglomeritic) above KBS Tuff, Sh
BC2305	Surface Collection	BC	6/03/2023	Sample (Micromorph)	Pleistocene	KBS Mbr	4.27873	36.31037	10	Sand	Petrography	Sandstone, 2nd SS above the KBS Tuff,St, Sp, Sh,, Rhizoliths
BC2306	Surface Collection	BC	6/03/2023	Sample (Micromorph)	Pleistocene	KBS Mbr	4.27873	36.31037	10	Sand	Petrography	Sandstone, 3rd SS above the KBS Tuff
BC2307	Surface Collection	BC	6/03/2023	Sample (Micromorph)	Pleistocene	KBS Mbr	4.28577	36.30742	10	Sand	Petrography	Sandstone, 4th above the KBS Tuff
BC2308	Surface Collection	BC	6/03/2023	Sample (Micromorph)	Pleistocene	KBS Mbr	4.301310	36.31500	12	Sand	Petrography	Sandstone, 5th above the KBS Tuff, near Elephant site
BC2309	Surface Collection	BC	6/03/2023	Sample (Micromorph)	Pleistocene	KBS Mbr	4.30064	36.31506	12	Sand	Petrography	Sandstone, 6th above the KBS Tuff, sandy pack-mollusc bed, gastropods and bioturbation (? Delta/Coast), way-up (top) has tape
BC2310	Surface Collection	BC	6/03/2023	Sample (Micromorph)	Pleistocene	KBS Mbr	4.29538	36.31552	12	Sand	Petrography	Sandstone, 7th above the KBS Tuff, Bioclastic SS, fossiliferous: Mammalian and gastropods (and bioturbation), Compare to [BC2309]
BC2311	Surface Collection	BC	6/04/2023	Sample (Micromorph)	Pleistocene	KBS Mbr	4.26586	36.33472	13	Sand	Petrography	"Far Site", 1st SS above KBS Tuff, Fault: down-thrown fault side
BC2313	Surface Collection	BC	6/04/2023	Sample (Micromorph)	Pleistocene	KBS Mbr	4.26691	36.33166	13	Sand	Petrography	"Ichnofossil", burrowing SS, 2m above KBS Tuff (1st SS)
BC2314	Surface Collection	BC	6/04/2023	Sample (Micromorph)	Pleistocene	KBS Mbr	4.26691	36.33166	13	Sand	Petrography	2nd SS above KBS Tuff
BC2316	Surface Collection	BC	6/04/2023	Sample (Micromorph)	Pleistocene	KBS Mbr	4.29021	36.24991	6A	Sand	Petrography	Conglomeratic bioclastic SS (Mollusc-pack bed), Upper KBS Mbr, fish and mammal fossils
BC2317	Surface Collection	BC	6/04/2023	Sample (Micromorph)	Pleistocene	KBS Mbr	4.28582	36.25004	6A	Sand	Petrography	SS, Sp, Upper KBS Mbr
BC2318	Surface Collection	BC	6/04/2023	Sample (Micromorph)	Pleistocene	KBS Mbr	4.28690	36.25054	6A	Sand	Petrography	SS, Upper KBS Mbr, fish and mammal fossils
BC2319	Surface Collection	BC	6/04/2023	Sample (Micromorph)	Pleistocene	KBS Mbr	4.28805	36. 25077	6A	Sand	Petrography	SS, Upper KBS Mbr
BC2320	Surface Collection	BC	6/05/2023	Sample (Micromorph)	Pleistocene	KBS Mbr	4.07169	36.36380	105	Sand	Petrography	1st SS above KBS Tuff, 2m thick, horizontal lamination
BC2322	Surface Collection	BC	6/05/2023	Sample (Micromorph)	Pleistocene	KBS Mbr	4.06501	36.36597	105	Sand	Petrography	3rd SS above KBS Tuff
BC2323	Surface Collection	BC	6/06/2023	Sample (Micromorph)	Pleistocene	KBS Mbr	3.952371	36.241586	102	Sand	Petrography	40m above KBS Tuff
BC2324	Surface Collection	BC	6/06/2023	Sample (Micromorph)	Pleistocene	KBS Mbr	3.946267	36.246728	102	Sand	Petrography	55m above KBS Tuff, St, Sh
BC2325	Surface Collection	BC	6/06/2023	Sample (Micromorph)	Pleistocene	KBS Mbr	3.959701623	36.30311934	104	Sand	Petrography	SS, GaJj17 site
BC2326	Surface Collection	BC	6/06/2023	Sample (Micromorph)	Pleistocene	KBS Mbr	3.957175	36.304957	104	Sand	Petrography	1st SS above KBS Tuff

BC2328	Surface Collection	BC	6/06/2023	Sample (Micromorph)	Pleistocene	KBS Mbr	3.956998	36.304827	104	Sand	Petrography	3rd SS above KBS Tuff
BC2329	Surface Collection	BC	6/07/2023	Sample (Micromorph)	Pleistocene	KBS Mbr	4.252609	36.276889	8A	Sand	Petrography	SS above KBS (Conlgomeritic), "Francis Fossil Hill"/"Butchery Site", Mammal and Fish Fossil
BC2331	Surface Collection	BC	6/07/2023	Sample (Micromorph)	Pleistocene	KBS Mbr	4.241544	36.278087	8B	Sand	Petrography	SS, 4m above the gastropod unit (Mollusc bed), Upper KBS Mbr
BC2332	Surface Collection	BC	6/07/2023	Sample (Micromorph)	Pleistocene	KBS Mbr	4.241442	36.278405	8B	Sand	Petrography	SS, 4m above [BC2331] Upper KBS Mbr, mammalian fossil, conglomeritic
BC2333	Surface Collection	BC	6/07/2023	Sample (Micromorph)	Pleistocene	KBS Mbr	4.297967	36.278475	9	Sand	Petrography	SS, above Red-sands, Sp, Sh, St, mammal fossils
BC2335	Surface Collection	BC	6/07/2023	Sample (Micromorph)	Pleistocene	KBS Mbr	4.295786	36.278044	9	Sand	Petrography	SS, Sh, St
BC2336	Surface Collection	BC	6/07/2023	Sample (Micromorph)	Pleistocene	KBS Mbr	4.295667	36.277962	9	Sand	Petrography	SS

Appendix D: Munsell's geological colour chart. Retrieved from https://www.vawaterwellassociation.org/wp-content/uploads/2014/05/Munsell-sample-from-the-munsell-website-CIPA00011_599.pdf

5Y 4/4 Moderate Olive Brown	5Y 3/2 Olive Gray	10Y 8/2 Pale Greenish Yellow	10Y 7/4 Moderate Greenish Yellow	10Y 6/2 Pale Olive	10Y 6/6 Dark Greenish Yellow
10Y 5/4 Light Olive	10Y 4/2 Grayish Olive	5GY 7/2 Grayish Yellow Green	5GY 7/4 Moderate Yellow Green	5GY 5/2 Dusky Yellow Green	5GY 3/2 Grayish Olive Green
10GY 7/2 Pale Yellowish Green	10GY 6/4 Moderate Yellowish Green	10GY 5/2 Grayish Green	10GY 4/4 Dark Yellowish Green	10GY 3/2 Dusky Yellowish Green	
5G 7/2 Pale Green	5G 7/4 Light Green	5G 6/6 Brilliant Green	5G 5/2 Moderate Yellow Green	5G 5/6 Moderate Green	5G 3/2 Dusky Green
10G 8/2 Very Pale Green	10G 6/2 Pale Green	10G 4/2 Grayish Green	5BG 7/2 Pale Blue Green	5BG 6/6 Light Blue Green	5BG 5/2 Grayish Blue Green
5BG 4/6 Moderate Blue Green	5BG 3/2 Dusky Blue Green	5B 8/2 Very Pale Blue	5B 7/6 Light Blue	5B 6/2 Pale Blue	5B 5/6 Moderate Blue
5PB 7/2 Pale Blue	5PB 5/2 Grayish Blue	5PB 3/2 Dusky Blue	5P 6/2 Pale Purple	5P 4/2 Grayish Purple	5P 2/2 Very Dusky Purple

Appendix D: *(continued).*

5RP 8/2 Pale Pink	5RP 6/2 Pale Red Purple	5RP 4/2 Grayish Red Purple	5RP 2/2 Very Dusky Purple		
5B 9/1 Bluish White	5G 8/1 Light Greenish Gray	5GY 8/1 Light Greenish Gray	5Y 8/1 Yellowish Gray	5YR 8/1 Pinkish Gray	5B 7/1 Light Bluish Gray
5YR 6/1 Light Brownish Gray	5Y 6/1 Light Olive Gray	5G 6/1 Greenish Gray	5GY 6/1 Greenish Gray	5B 5/1 Medium Bluish Gray	5G 4/1 Dark Greenish Gray
5GY 4/1 Dark Greenish Gray	5Y 4/1 Olive Gray	5YR 4/1 Brownish Gray	5G 2/1 Greenish Black	5GY 2/1 Greenish Black	5Y 2/1 Olive Black
5YR 2/1 Brownish Black					
N9 White	N8 Very Light Gray	N7 Light Gray	N6 Medium Light Gray	N5 Medium Gray	N4 Medium Dark Gray
N3 Dark Gray	N2 Grayish Black	N1 Black			

Appendix D: *(continued).*

Appendix E: *Palaeocurrent data collected during field work*

Collection area	Lat	Long	Indicator type	Lithofacies	Indicator orientation	Mean palaeocurrent direction
10	4.2881575	36.30817	Planar cross-bedding	*Sp*	188° S 172° S 169° S 171° S 216° SW 179° S 350° N 256° N 3° N 15° N 348° N 3° N 352° N 248° W 223° SW 242° SW	W/SW
12	4.295556	36.315833	Planar cross-bedding and Ripple cross-lamination (rib-and-furrow structures)	*Sp*; *Sr*	290° W 287° W 282° W 226° SW 209° SW 272° W 344° N 338° N 340° N 3° N 13° N 36° NE 351° N 355° N 317° NW 324° NW 314° NW 314° NW 317° NW 326° NW 334° NW 345° N 338° N	N

					310° NW 322° NW 322° NW 343° N 341° N 346° N 347° N 354° N 76° E 74° E 88° E 69° E 61° NE 76° E 78° E 335° NW 332° NW 337° N 359° N 76° E 73° E 74° E 75° E 68° E 71° E 78° E 67° E 59° NE 66° NE 71° E	
13	4.26691	36.33166	Ripple cross-lamination (rib-and-furrow structures)	*Sr*	7° N 298° NW 290° W 2° N 346° N 10° N 324° NW 353° N 3° N	N/NW
6A	4.28582	36.25004	Planar cross-bedding	*Sp*	275° W 261° W 228° SW	W/SW

					268° W	
					225° W	
					215° SW	
					231° SW	
					214° SW	
					245° SW	
					234° SW	
8A	4.249722	36.280278	Planar cross-bedding and Ripple cross-lamination (rib-and-furrow structures)	*Sp*; *Sr*	289° W	S/SW
					287° W	
					292° W	
					300° NW	
					249° W	
					234° SW	
					222° SW	
					224° SW	
					231° SW	
					226° SW	
					228° SW	
					236° SW	
					238° SW	
					210° SW	
					232° SW	
					216° SW	
					260° W	
					228° SW	
					199° S	
					228° SW	
					206° SW	
					228° SW	
					206° SW	
					272° W	
					232° SW	
					241° SW	
					217° SW	
					55° NE	
					70° E	
					248° W	
					226° SW	
					253° W	
					243° SW	
					223° SW	
					241° SW	

					229° SW	
					183° S	
					59° NE	
					91° E	
					167° S	
					155° SE	
					167° S	
					178° S	
					196° S	
					219° SW	
					190° S	
					175° S	
					177° S	
					279° W	
					264° W	
					267° W	
					288° W	
					271° W	
					200° S	
					194° S	
					188° S	
					192° S	
					195° S	
					189° S	
					186° S	
					191° S	
					183° S	
					168° S	
					187° S	
					195° S	
					190° S	
					185° S	
					177° S	
					175° S	
					175° S	
					183° S	
					187° S	
					202° S	
					184° S	
					179° S	
					189° S	
					18° N	

					15° N	
					230° SW	
					85° E	
8B	4.243889	36.273889	Planar cross-bedding and Ripple cross-lamination (rib-and-furrow structures)	*Sp*; *Sr*	144° SE 158° S 164° S 153° SE 152° SE 230° SW 219° SW 218° SW 223° SW 138° SE 139° SE 192° S 211° SW 140° SE 215° SW 201° S 189° S 190° S 142° SE 272° W 137° SE 272° W 18° N 17° N 317° NW 210° SW 143° SE 183° S 143° SE 154° SE 159° S 174° S 213° SW 189° S 154° SE 183° S 214° SW 209° SW 194° S	S

					7° N 337° N 337° N 158° S 162° S 168° S 254° W 249° W 252° W 258° W 149° SE 237° SW 153° SE 163° S 155° SE 147° SE 249° W 140° SE 9° N	
9	4.295667	36.277962	Planar cross-bedding	*Sp*	33° NE 22° N 32° N 44° NE 56° NE 9° N 74° E 56° NE 25° NE 13° N 14° N 77° E 90° E 96° NE 62° NE 90° E 55° NE 55° NE 70° E	NE
105	4.071690	36.36380	Planar cross-bedding and Ripple cross-lamination	*Sp; Sr*	347° N 348° N 347° N 356° N	SW

			(rib-and-furrow structures)		32° NE 175° S 192° S 205° SW 203° SW 149° SE 147° SE 142° SE 219° SW 115° SE 138° SE 187° S 313° NW 273° W 302° NW 289° W 274° W 246° SW 260° W 253° W 288° W 275° W 150° SE 165° S 205° SW 203° SW 207° SW 233° SW 233° SW 233° SW 233° SW 239° SW 232° SW 229° SW 242° SW 140° SE 146° SE 144° SE	
102	3.930738	36.24501	Ripple cross-lamination (rib-and-furrow structures)	*Sr*	250° W 239° SW 249° W 238° SW	W/SW

					212° SW 232° SW 220° SW 252° W 258° W 257° W 228° SW 219° SW 246° SW 246° SW 257° W 236° SW 238° SW 284° W 281° W 281° W 285° W 279° W 278° W 270° W 274° W 256° W 266° W 214° SW 226° SW 235° SW 216° W	
104	3.928275	36.243089	Planar cross-bedding	*Sp*	274° W 284° W 261° W 229° SW 227° SW 224° SW 189° S 126° SW 214° SW 215° SW 230° SW 183° S 177° S 201° S 213° SW	SW

					179° S	
					210° SW	
					216° SW	
					236° SW	
					236° SW	
					235° SW	
					176° S	
					199° S	
					188° S	
					220° SW	
					120° SE	
					130° SE	
					135° SE	
					139° SE	

KEY

Lithofacies Associations

- **FA1** Meandering Fluvial Channel
- **FA2** Fluvial Floodplain
- **FA3** Marginal Lacustrine
- **FA4** Prodeltaic and Delta Front
- **FA5** Crevasse Splay

Depositional Environments (Lake Shoreline Proximity)

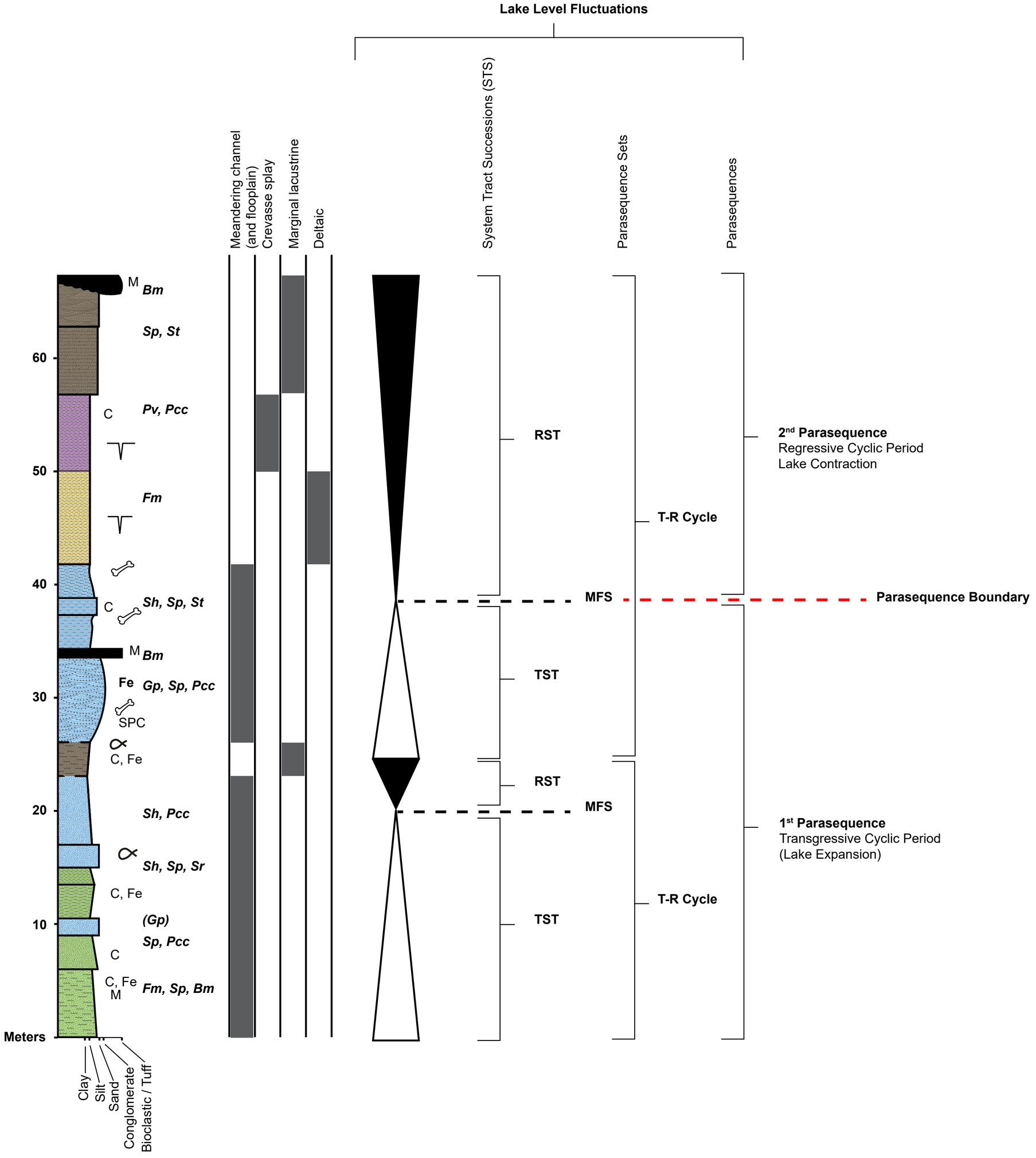

AREA 102

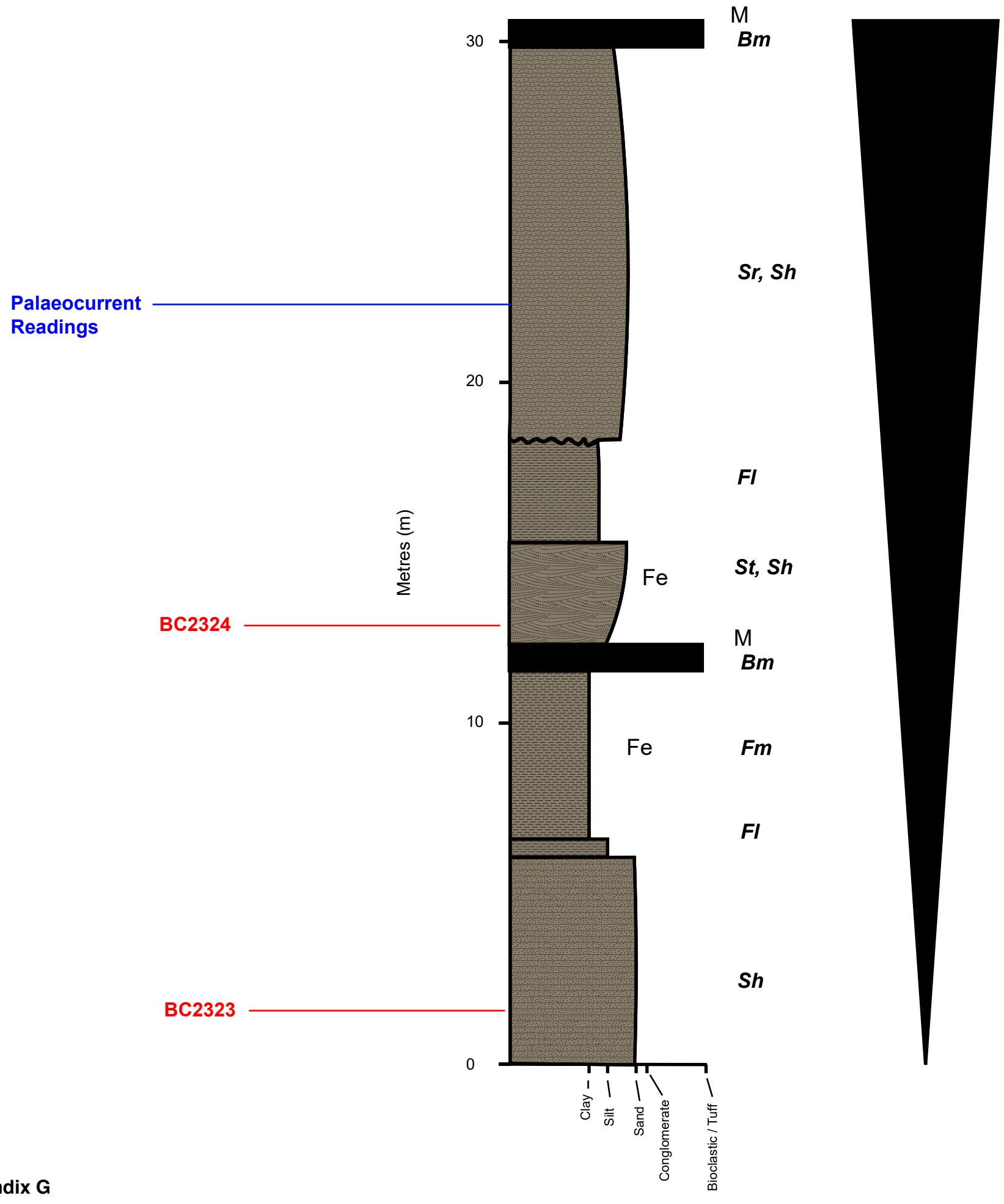

Appendix G

AREA 104

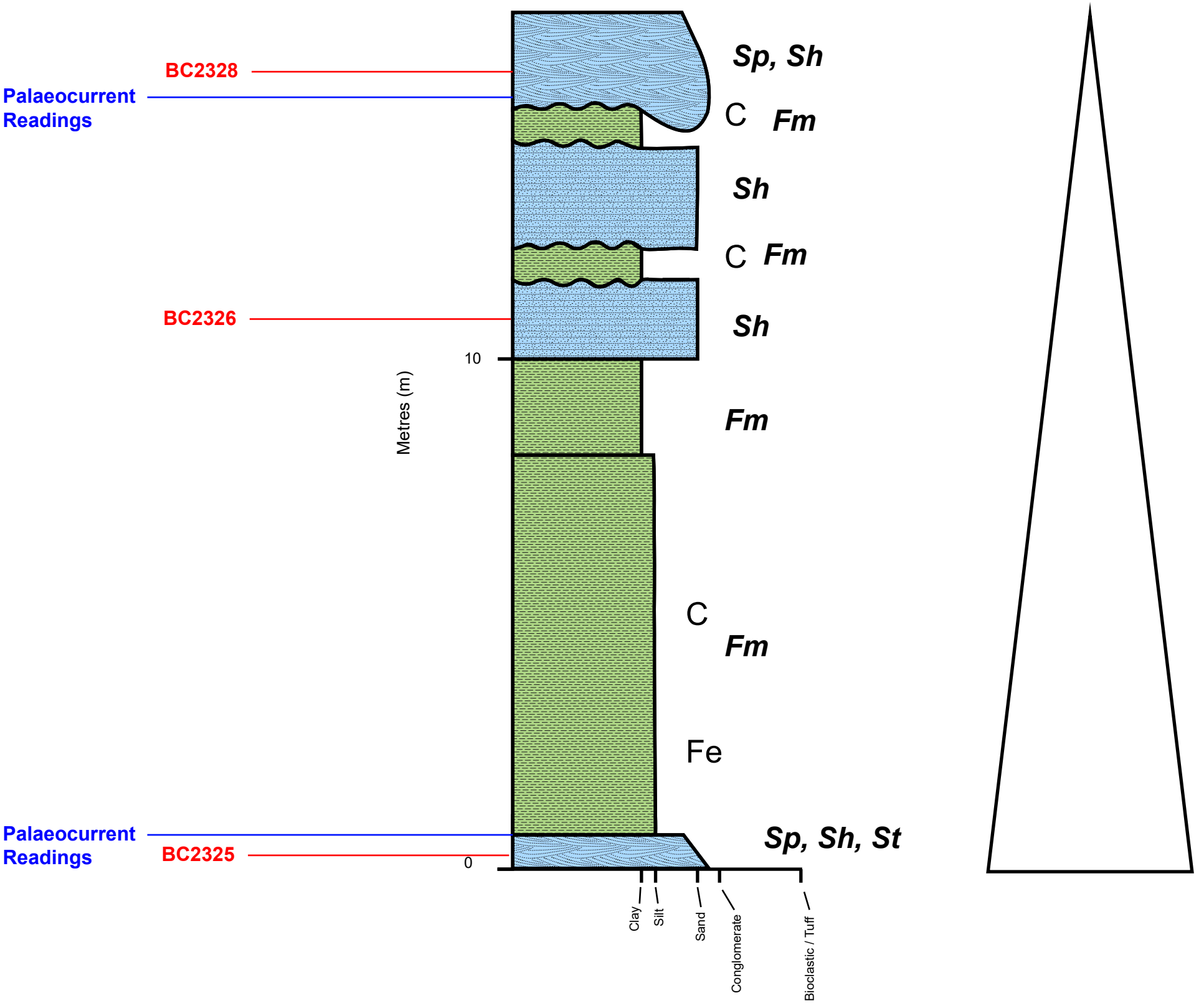
BC2328
Palaeocurrent Readings
BC2326
BC2325
Palaeocurrent Readings
Metres (m)
10
0
Sp, Sh
C
Fm
Sh
C
Fm
Sh
Fm
C
Fm
Fe
Sp, Sh, St
Clay
Silt
Sand
Conglomerate
Bioclastic / Tuff

AREA 105

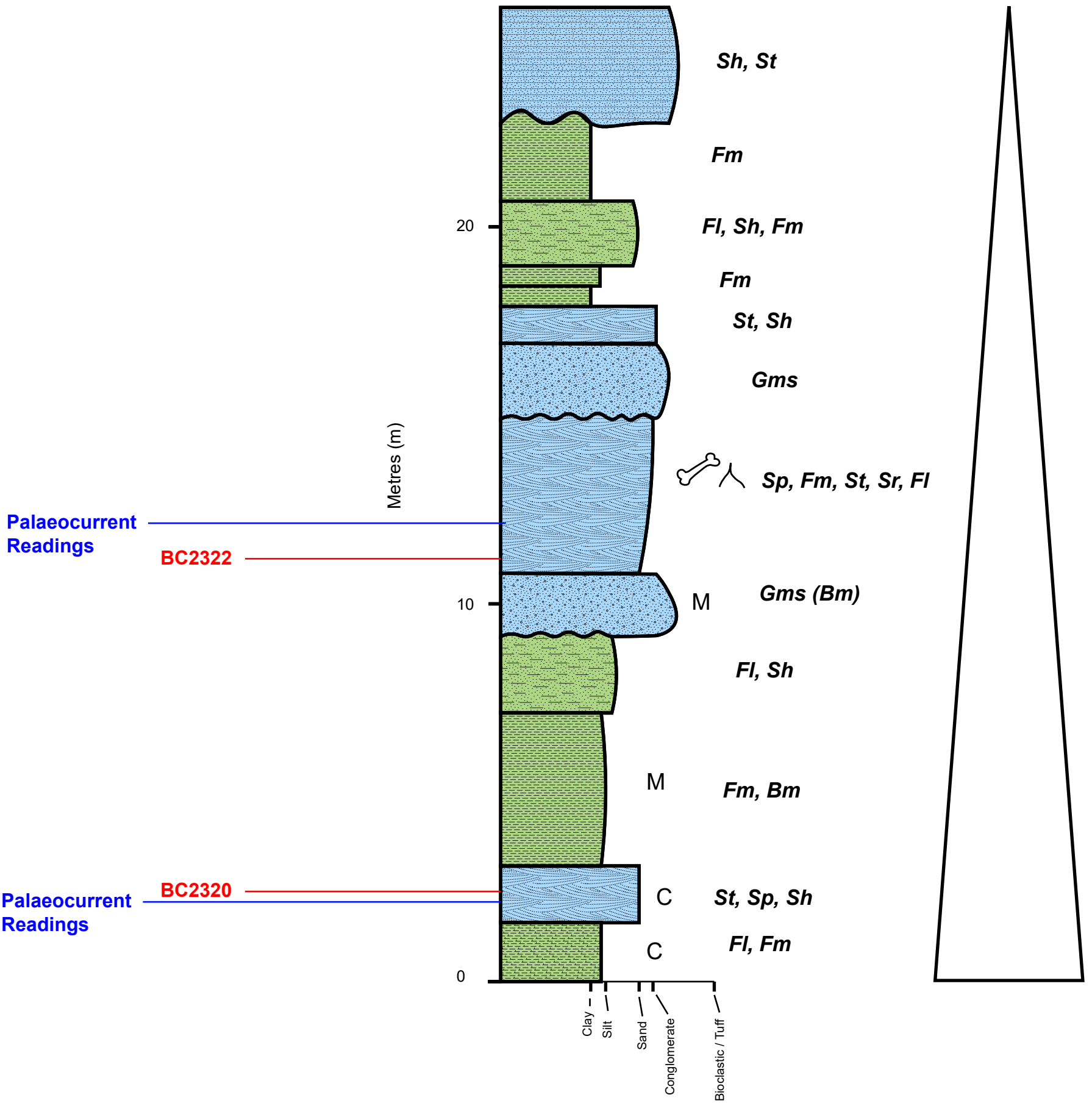

Appendix G

AREA 13

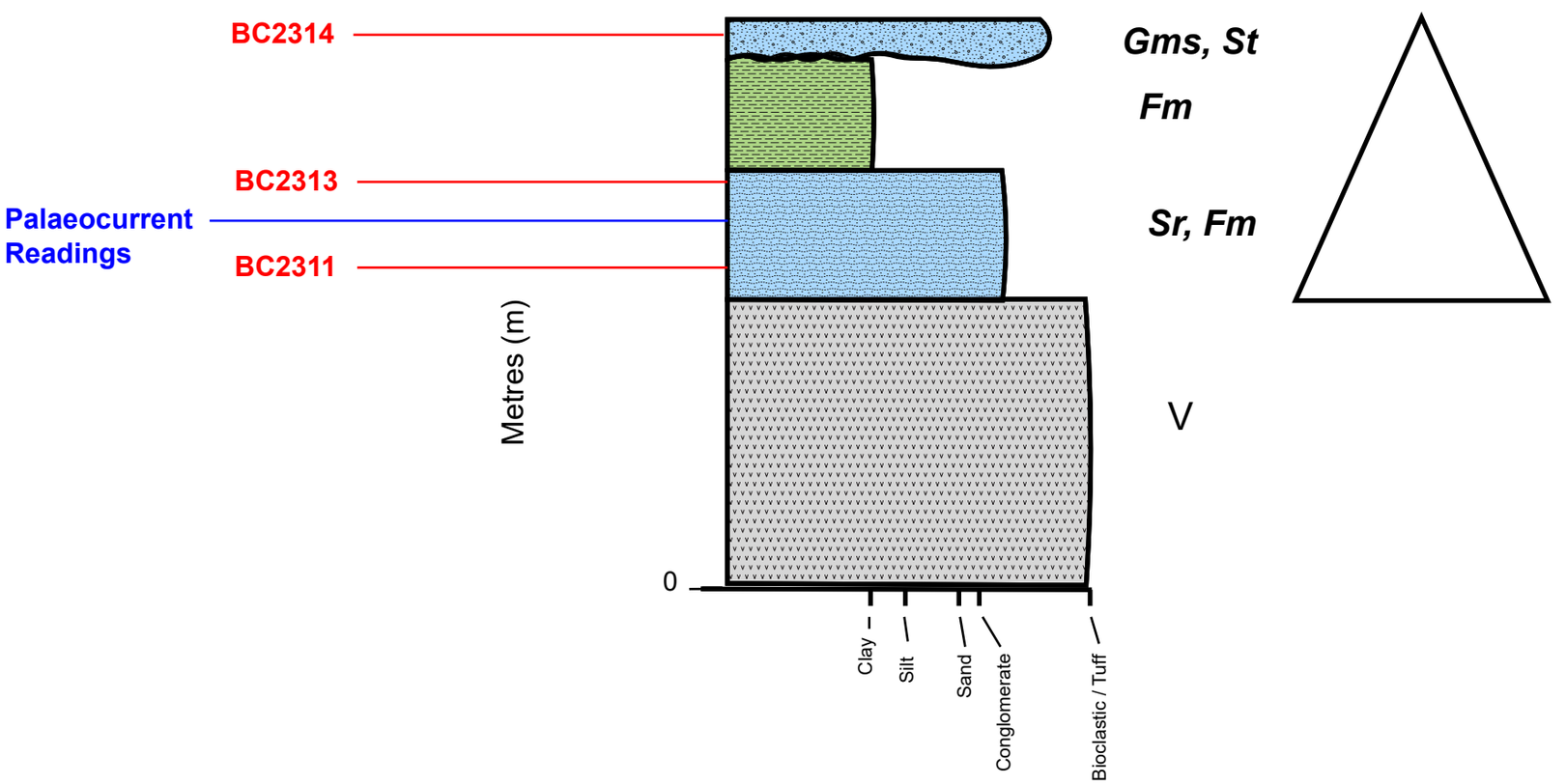

Appendix G

AREA 8B

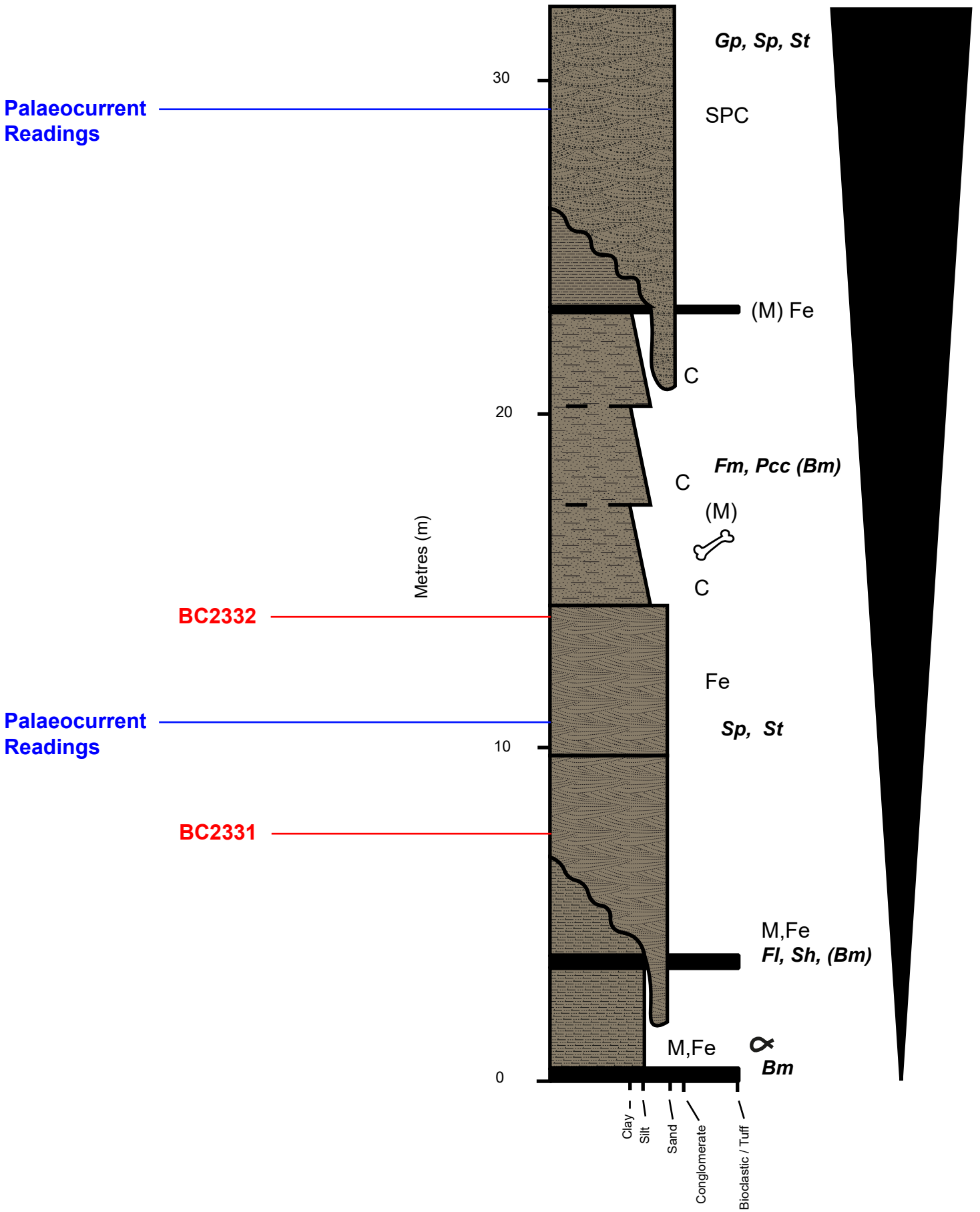

Appendix G

AREA 8A

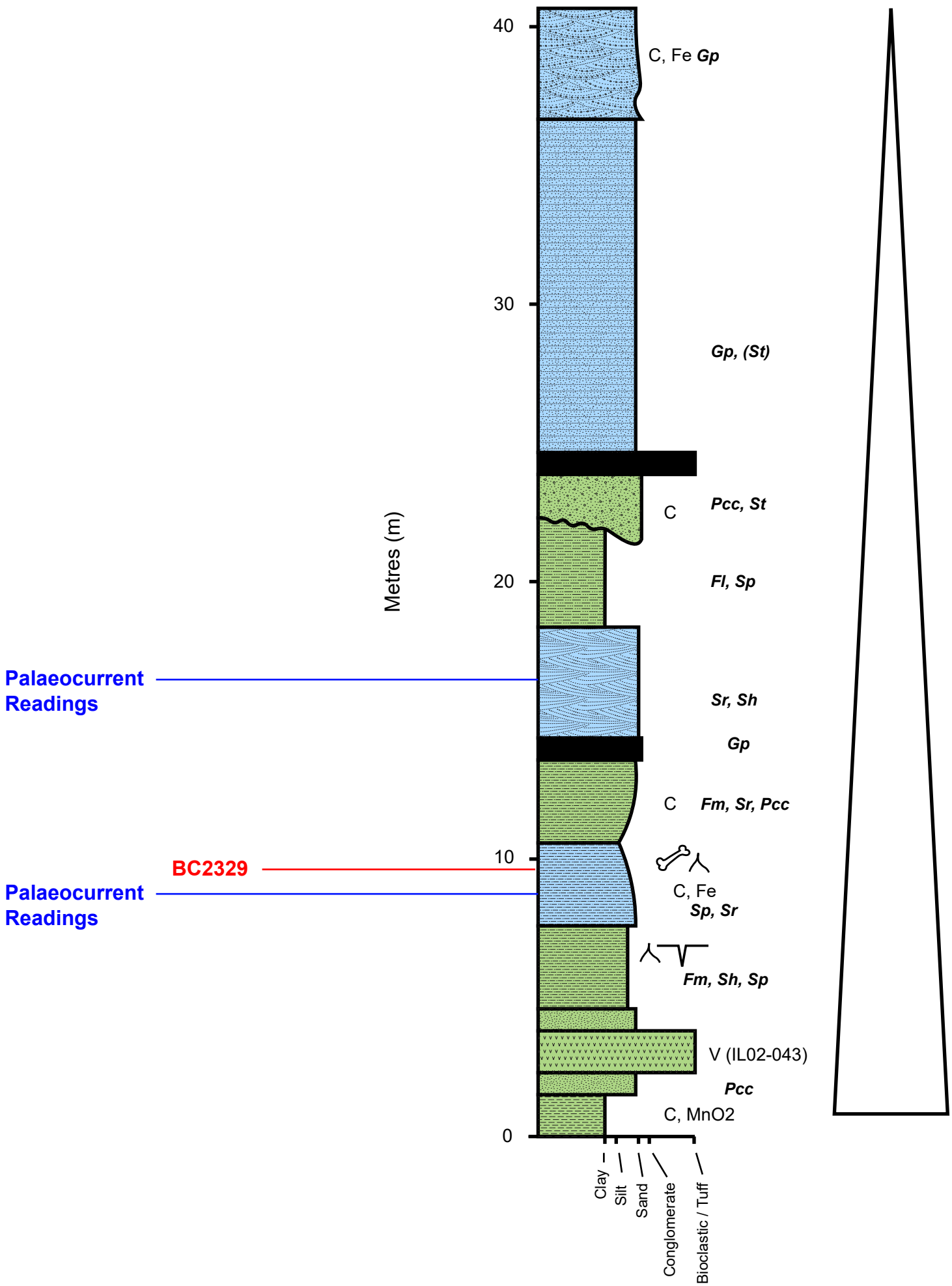

Appendix G

AREA 12

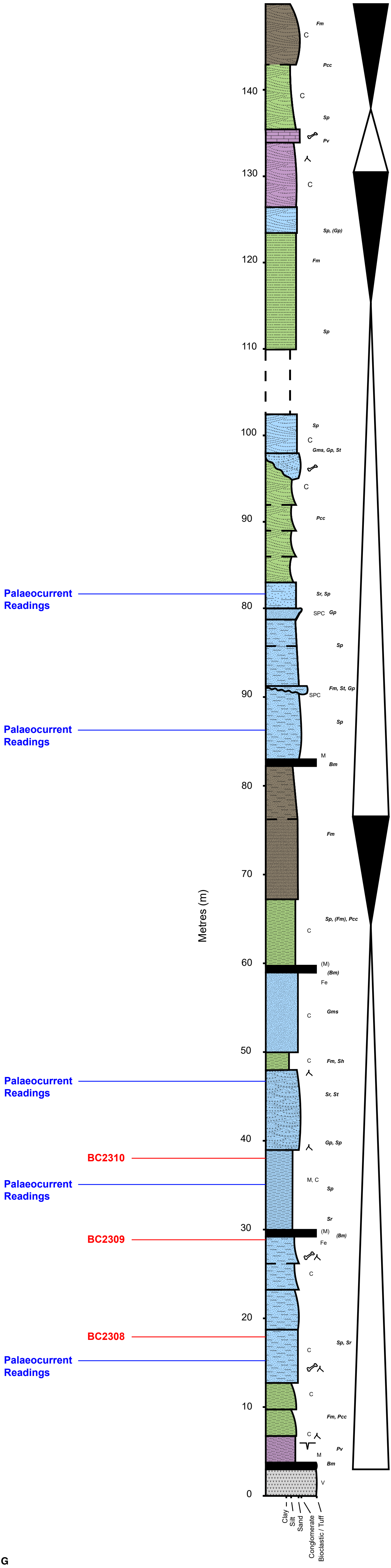

Appendix G

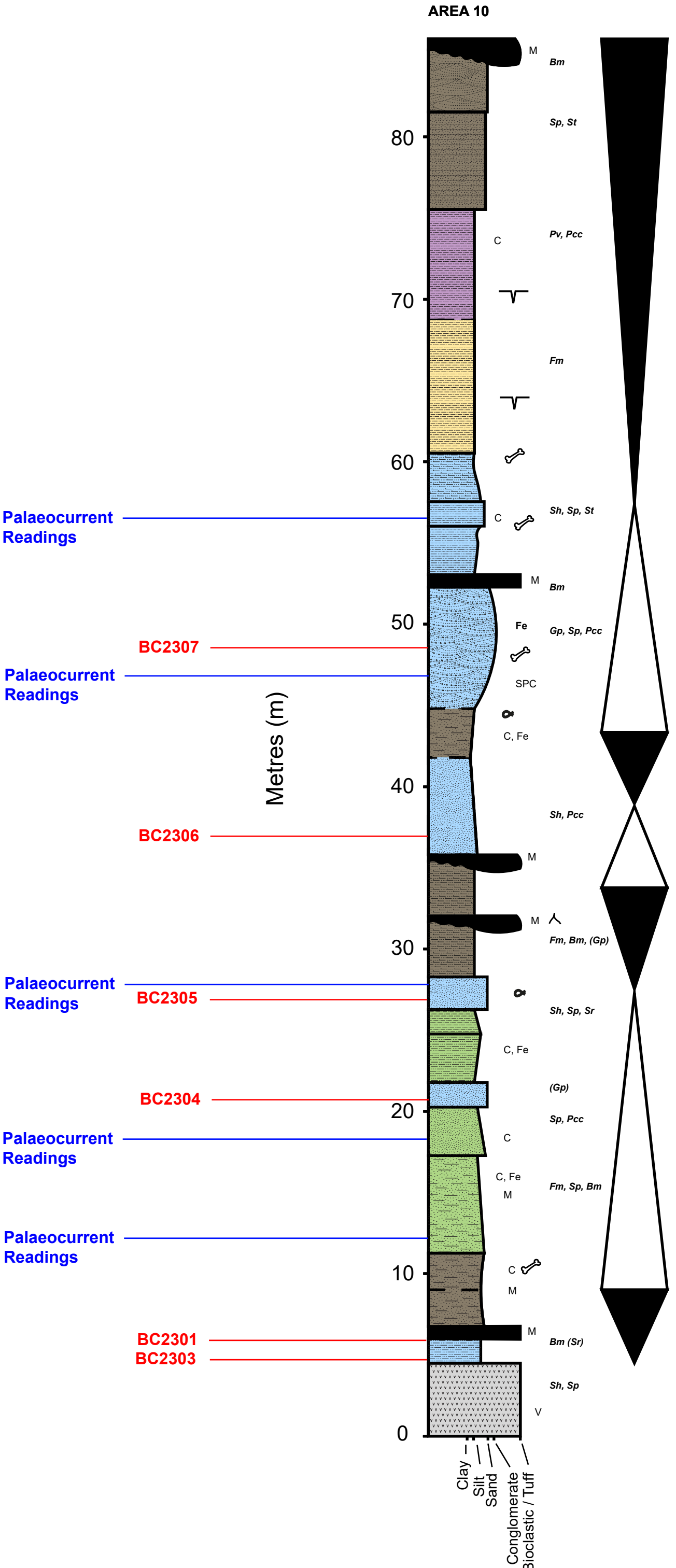
AREA 10
Metres (m)
80
70
60
50
40
30
20
10
0
M
Bm
Sp, St
C
Pv, Pcc
Fm
C
Sh, Sp, St
M
Bm
Fe
Gp, Sp, Pcc
SPC
C, Fe
Sh, Pcc
M
M
Fm, Bm, (Gp)
Sh, Sp, Sr
C, Fe
(Gp)
Sp, Pcc
C
C, Fe
M
Fm, Sp, Bm
C
M
M
Bm (Sr)
Sh, Sp
V
Clay
Silt
Sand
Conglomerate
Bioclastic / Tuff
Palaeocurrent Readings
BC2307
Palaeocurrent Readings
BC2306
Palaeocurrent Readings
BC2305
BC2304
Palaeocurrent Readings
Palaeocurrent Readings
BC2301
BC2303

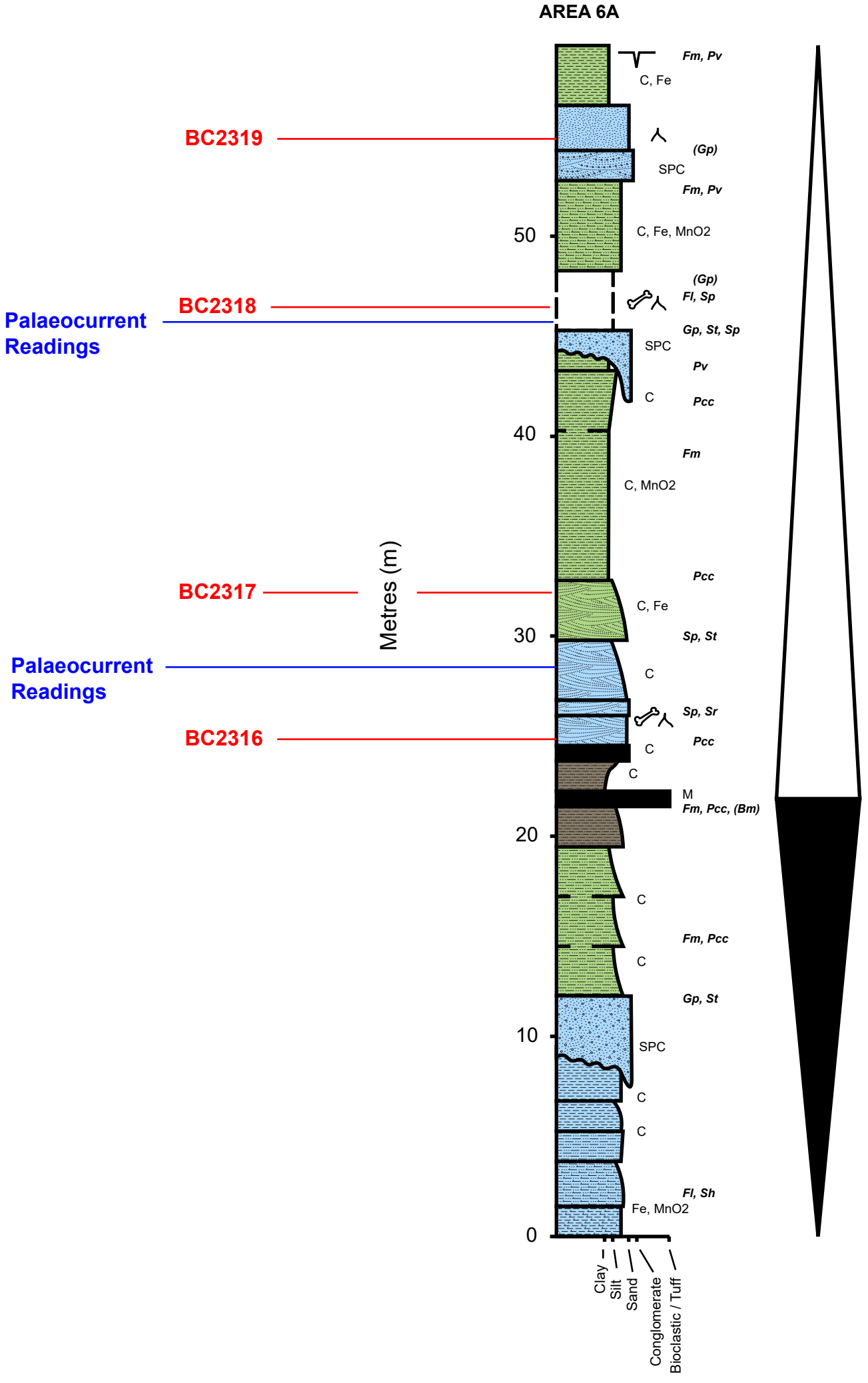
AREA 6A
BC2319
BC2318
Palaeocurrent Readings
BC2317
Palaeocurrent Readings
BC2316
Metres (m)
50
40
30
20
10
0
Fm, Pv
C, Fe
(Gp)
SPC
Fm, Pv
C, Fe, MnO2
(Gp)
Fl, Sp
Gp, St, Sp
SPC
Pv
C
Pcc
Fm
C, MnO2
Pcc
C, Fe
Sp, St
C
Sp, Sr
Pcc
C
C
M
Fm, Pcc, (Bm)
C
Fm, Pcc
C
Gp, St
SPC
C
C
Fl, Sh
Fe, MnO2
Clay
Silt
Sand
Conglomerate
Bioclastic / Tuff

Appendix G

AREA 9

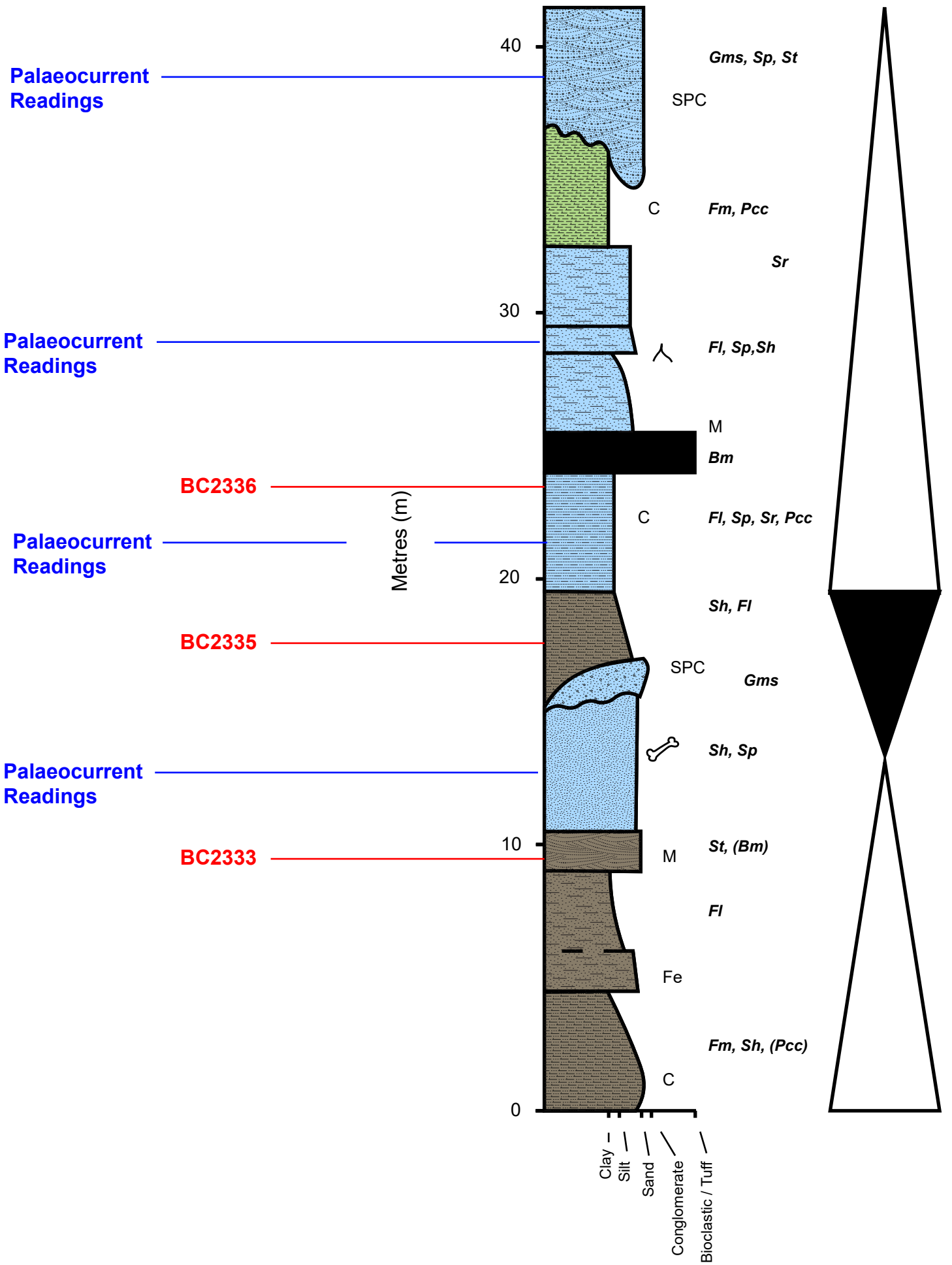

Appendix G

North

AREA 102

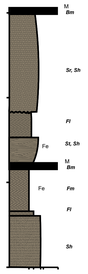

AREA 104

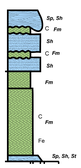

AREA 105

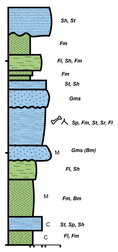

AREA 13

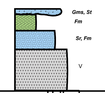

AREA 8B

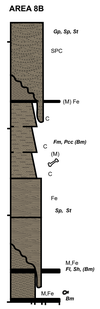

AREA 8A

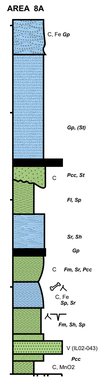

AREA 12

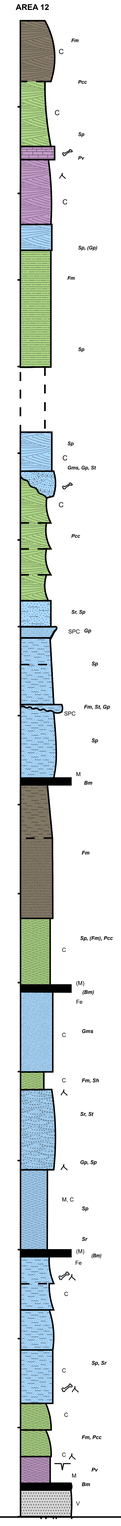

AREA 10

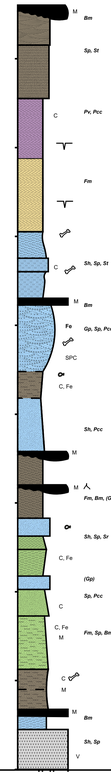

AREA 6A

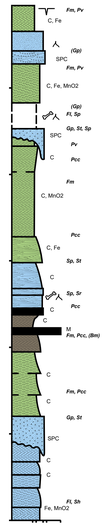

AREA 9

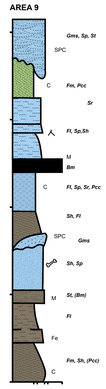

Base of the KBS Tuff

Base of the KBS Tuff

LEGEND

Vertical Scale and Grain Size

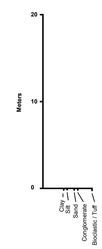

Lithological Contacts

- Abrupt
- Erosional
- Gradational

Lithological Patterns

- Conglomerate
- Cross-bedded Conglomerate
- Massive Sandstone
- Horizontal Bedded Sandstone
- Cross-bedded Sandstone
- Ripple-bedded Sandstone
- Interbedded Sand and Mud
- Calcareous Sandstone
- Siltstone
- Calcareous Siltstone
- Interbedded Silt and Mud
- Mudstone/ Claystone
- Calcareous Mudstone/ Claystone
- Limestone
- Bioclastic Rock
- Tuff
- Covered/ Poorly Exposed

Lithologic and Palaeontologic Symbols

- C — Carbonate Concretions
- M — Mollusc Fossils (Gastropods and Bivalves)
- V — Tuff
- Fe — Iron Oxides
- MnO2 — Manganese Oxides
- SPC — Silt (or Clay) Pebble Conglomerate
- Mammal Fossils
- Fish Fossils
- Rhizoliths
- Desiccation Cracks

Lithofacies Codes

- **Fl** — Interlaminated silt and clay
- **Fm** — Massive mud
- **Sh** — Horizontally bedded silt or sandstone
- **St** — Trough cross-bedded sandstone
- **Sr** — Ripple cross-laminated sandstone
- **Sp** — Planar cross-bedded sandstone
- **Gms** — Matrix-supported stratified gravel
- **Gp** — Planar-cross bedded gravel
- **Pcc** — Pedogenic carbonate
- **Pv** — Silt or clay with Pedogenic structures
- **Bm** — Molluscan carbonate (Siliceous bioclastic carbonate)

Lithofacies Associations

- **FA1** — Meandering Fluvial Channel
- **FA2** — Fluvial Floodplain
- **FA3** — Marginal Lacustrine
- **FA4** — Prodeltaic and Delta Front
- **FA5** — Crevasse Splay
- KBS Tuff

Appendix H

North

AREA 102

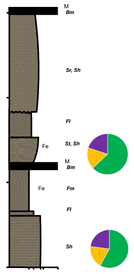

AREA 104

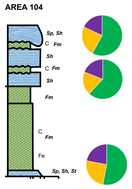

AREA 105

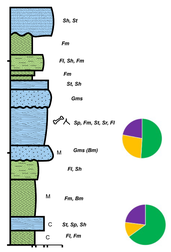

AREA 13

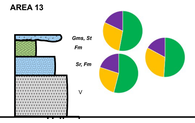

AREA 8B

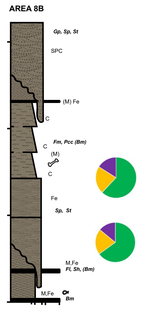

AREA 8A

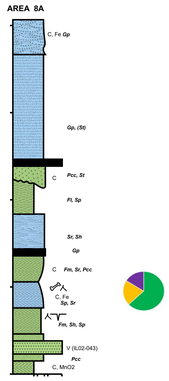

AREA 12

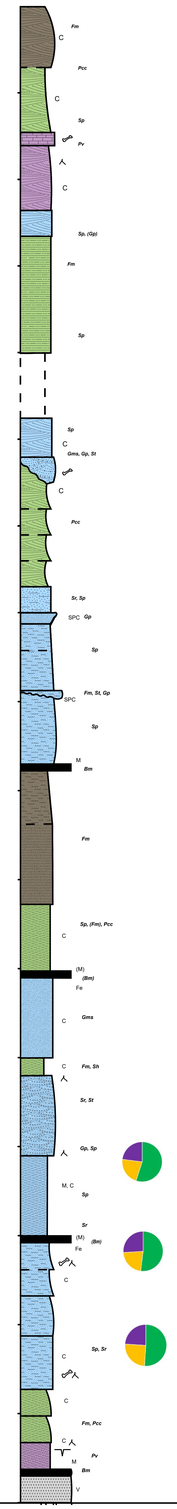

AREA 10

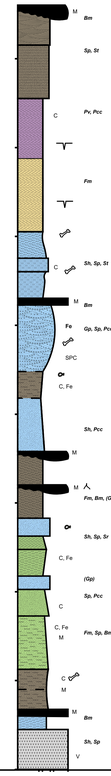

AREA 6A

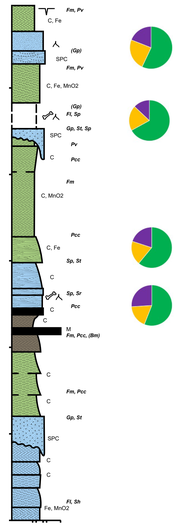

AREA 9

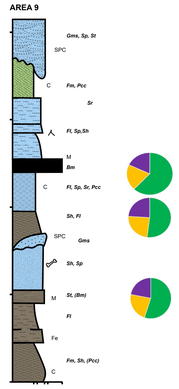

Base of the KBS Tuff

Base of the KBS Tuff

LEGEND

Vertical Scale and Grain Size

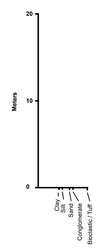

Lithological Contacts

- Abrupt
- Erosional
- Gradational

Lithological Patterns

- Conglomerate
- Cross-bedded Conglomerate
- Massive Sandstone
- Horizontal Bedded Sandstone
- Cross-bedded Sandstone
- Ripple-bedded Sandstone
- Interbedded Sand and Mud
- Calcareous Sandstone
- Siltstone
- Calcareous Siltstone
- Interbedded Silt and Mud
- Mudstone/ Claystone
- Calcareous Mudstone/ Claystone
- Limestone
- Bioclastic Rock
- Tuff
- Covered/ Poorly Exposed

Lithologic and Palaeontologic Symbols

- C — Carbonate Concretions
- M — Mollusc Fossils (Gastropods and Bivalves)
- V — Tuff
- Fe — Iron Oxides
- MnO2 — Manganese Oxides
- SPC — Silt (or Clay) Pebble Conglomerate
- Mammal Fossils
- Fish Fossils
- Rhizoliths
- Desiccation Cracks

Lithofacies Codes

Fl	Interlaminated silt and clay
Fm	Massive mud
Sh	Horizontally bedded silt or sandstone
St	Trough cross-bedded sandstone
Sr	Ripple cross-laminated sandstone
Sp	Planar cross-bedded sandstone
Gms	Matrix-supported stratified gravel
Gp	Planar-cross bedded gravel
Pcc	Pedogenic carbonate
Pv	Silt or clay with Pedogenic structures
Bm	Molluscan carbonate (Siliceous bioclastic carbonate)

Lithofacies Associations

FA1	Meandering Fluvial Channel
FA2	Fluvial Floodplain
FA3	Marginal Lacustrine
FA4	Prodeltaic and Delta Front
FA5	Crevasse Splay
	KBS Tuff

Mineralogical proportions

- Quatz
- Feldpsar
- Lithic fragment

Appendix I

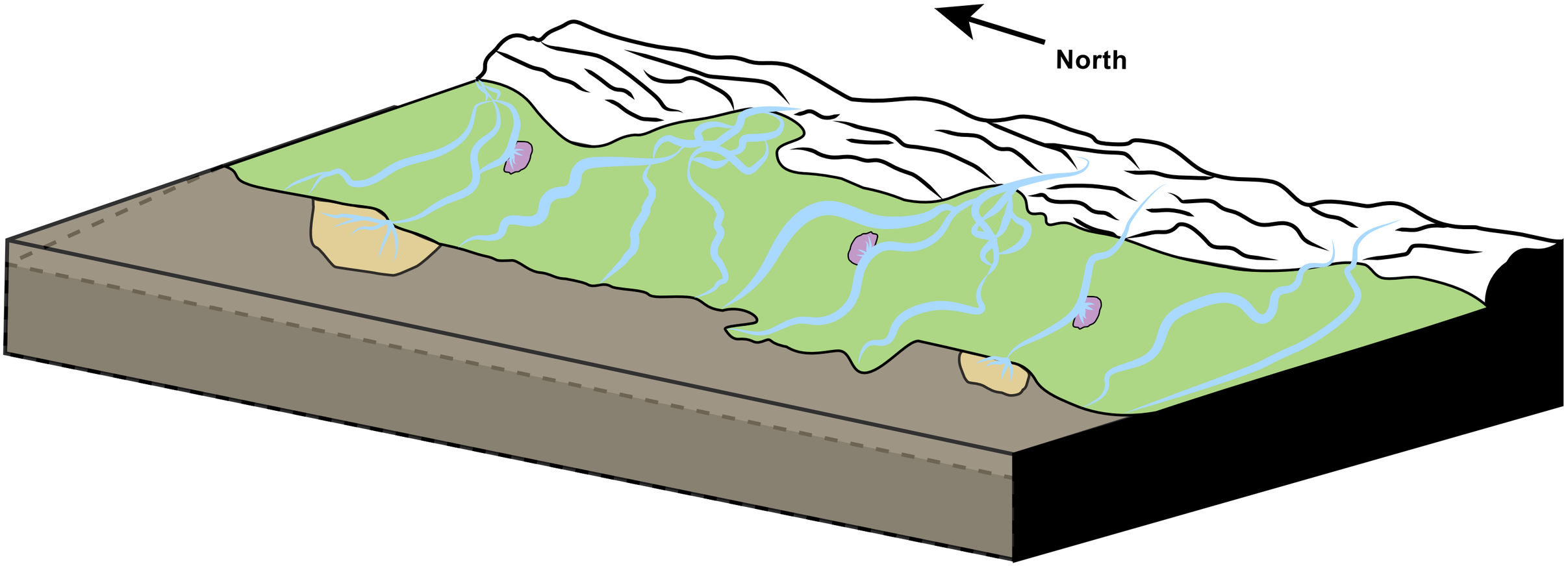

Lithofacies Associations

FA1 Meandering Fluvial Channel

FA2 Fluvial Floodplain

FA3 Marginal Lacustrine

FA4 Prodeltaic and Delta Front

FA5 Crevasse Splay

Provenance Area

Depositional Base

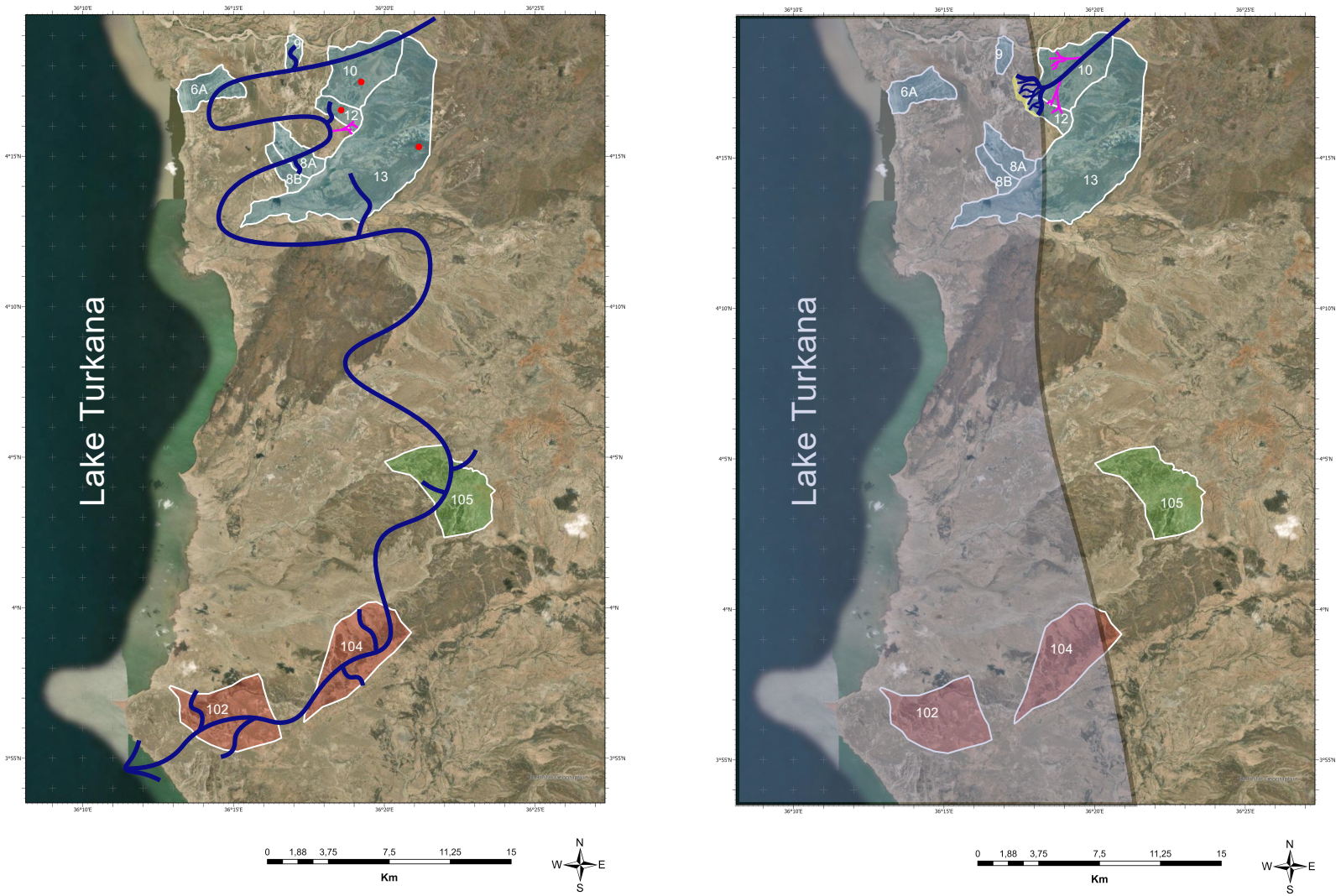
(A) 1.87 - ~1.7 Ma
(B) ~1.7 - 1.6 Ma
Lake Turkana
Lake Turkana
9
10
12
6A
8A
8B
13
105
104
102
0 1,88 3,75 7,5 11,25 15
Km
N
W
E
S
Legend
Ileret subregion
Karari subregion
Base Camp subregion
Rivers and inferred tributaries
Shoreline
(inferred and after Brown and Feibel, 1991)
Prodelta and Delta Front
(Observed)
Crevasse Splay
(Observed)
Exposures of the KBS Tuff
(Observed)

North

AREA 102

AREA 104

AREA 105

AREA 13

AREA 8B

AREA 8A

AREA 12

AREA 10

AREA 6A

AREA 9

Meandering channel (and floodplain)

Crevasse splay

Marginal lacustrine

Deltaic

Base of the KBS Tuff

LEGEND

Vertical Scale and Grain Size

Metres: 20, 10, 0

Clay, Silt, Sand, Conglomerate, Bioclastic / Tuff

Lithological Contacts

Abrupt

Erosional

Gradational

Lithological Patterns

Conglomerate; Cross-bedded Conglomerate; Massive Sandstone; Horizontal Bedded Sandstone; Cross-bedded Sandstone; Ripple-bedded Sandstone; Interbedded Sand and Mud; Calcareous Sandstone; Siltstone; Calcareous Siltstone; Interbedded Silt and Mud; Mudstone/ Claystone; Calcareous Mudstone/ Claystone; Limestone; Bioclastic Rock; Tuff; Covered/ Poorly Exposed

Lithologic and Palaeontologic Symbols

C — Carbonate Concretions

M — Mollusc Fossils (Gastropods and Bivalves)

V — Tuff

Fe — Iron Oxides

MnO2 — Manganese Oxides

SPC — Silt (or Clay) Pebble Conglomerate

Mammal Fossils

Fish Fossils

Rhizoliths

Desiccation Cracks

Lithofacies Codes

Fl — Interlaminated silt and clay

Fm — Massive mud

Sh — Horizontally bedded silt or sandstone

St — Trough cross-bedded sandstone

Sr — Ripple cross-laminated sandstone

Sp — Planar cross-bedded sandstone

Gms — Matrix-supported stratified gravel

Gp — Planar-cross bedded gravel

Pcc — Pedogenic carbonate

Pv — Silt or clay with Pedogenic structures

Bm — Molluscan carbonate (Siliceous bioclastic carbonate)

Lithofacies Associations

FA1 — Meandering Fluvial Channel

FA2 — Fluvial Floodplain

FA3 — Marginal Lacustrine

FA4 — Prodeltaic and Delta Front

FA5 — Crevasse Spley

KBS Tuff

Depositional Environments (Lake Shoreline Proximity)

Sequence Analysis (Lake Level Fluctuation)

Parasequence set

Lake-Regression (revealing contraction of Lake Turkana)

Lake-Transgression (revealing expansion of Lake Turkana)

Parasequence 2 (Progradational)

Parasequence Boundary

Parasequence 1 (Retrogradational)